Identification of myeloid proliferation niches in bone marrow

By

Vanessa Lopez Reyes

A thesis submitted to the University of Ottawa in partial fulfillment of the requirements for the Master's in Science degree in Cellular and Molecular Medicine

Department of Cellular and Molecular Medicine

Faculty of Medicine

University of Ottawa

Ottawa, Ontario, Canada

January 2026

Abstract

Unlike most other tissues found in land vertebrates, the bone marrow (BM) has unique characteristics: It is a soft, gelatinous tissue in which cells are freely moving and distributed in a seemingly random manner. In terms of cell components, the BM houses a wide variety of cell types, especially those of the hematopoietic system. These include the hematopoietic stem cells (HSCs), the hematopoietic progenitor stem cells (HPSCs) and all types of downstream myeloid and lymphoid cells. Cells from the myeloid lineage represents the most frequent cell types in the BM, and include billions of red blood cells and platelets, as well as cells from the innate immune system.

The BM is located inside the cavities of some of the strongest tissues in the body, the skeletal bones. These are composed of connective tissue rich in mesenchymal cells (osteoblast-lineage cells, chondrogenic cells, marrow stromal cells, stromal fibroblasts, endothelial cells and perivascular cells) and complex extracellular matrix (ECM) components. Hence, the biophysical peculiarities of the bone-BM ecosystem have made studying the in situ hematopoietic anatomy and its physiological spatio-temporal cell dynamics quite challenging.

Our group has developed strategies for analyzing entire bone units and their components. These strategies have been optimized and used to preserve the BM of postnatal mice. This enables the present study to focus on the in situ exploration of the spatial niches of the BM.

The aims of this study were therefore to characterize the spatial distribution of proliferative hematopoietic-myelopoietic progenitors with respect to their niche; and analyze the inferred communication networks between bone and BM cells using single-cell transcriptomics in silico.

First, a proliferation-labelling assay was performed on unperturbed mice. Second, the femurs were collected, processed, and stained using immunofluorescence (IF) targeting markers to distinguish between niche-specific cells and the hematopoietic cells of interest. Third, femur sections were imaged to collect 3D spatial Bone-BM data. Fourth, image cytometry was used to compute the relevant spatial variables of the selected markers and random distributions. Finally, integration and cell communication networks were inferred using publicly available BM single-cell transcriptomic datasets.

My results reveal a novel mapping of proliferative myeloid-Gr1+ cells, distributed among privileged BM regions characterized by trabecular bone (TB). These cells preferentially locate at cell-contact distance to the BM-vasculature and at 10-cells distance to the osteogenic niche in a non-random fashion. I used a comprehensive integrated scRNA-seq dataset to identify and infer cell communication networks between niche and GMPs-neutrophils, with relevant reported functions identified through the secreted signaling communication context.

This work ultimately advanced the efforts to reach a comprehensive understanding of the unperturbed proliferative myeloid niches in the post-natal BM of mouse femurs.

Acknowledgments

I would like to dedicate this thesis to the most wonderful people I have had the fortune to meet, learn from, and share experiences with.

Firstly, I would like to thank my supervisor, Dr. Daniel Coutu. Dan, your trust in my achievements and potential has been one of the greatest catalysts in my life. Today, I can confidently say that this whole experience has changed me forever and taught me the crucial academic, professional and ethical foundations of the scientific endeavor. Thank you for your role as supervisor, mentor and friend.

To my colleagues in the Coutu Lab: Medjie, Spencer and Baha. Thank you for your warm welcome and connections. As a queer international student, I was filled with doubts. However, getting to know you, learning from you and sharing our academic journeys inspired me every day. Sharing our friendship has also warmed my heart amidst the loneliness that comes with being an international student in a different country.

To my friends at the OHRI and TOH: Morgan, Sarah, Devansh and Emille. Thank you for your smiles, conversations, reassurances and advice. I have never felt so confident in a workplace before. Thank you for providing such a welcoming environment.

To the sweetest and most wonderful people I have had the blessing of meeting here in Canada: thank you for showing me that I am not a stranger and that I can find a home among you. Zendra, Abi, Fil and Will, thank you for opening your hearts to me. Thank you for reminding me that I am more than just a student, and that I am not just a 'temporary' presence. I am also a partner and a friend worthy of your trust. You have reminded me of my creativity, my strengths, my happiness, my dreams, and of the promise of a future worth fighting for. You have made me feel like a whole person who deserves to be seen and cared for.

To Eliana, my partner on this journey from the very beginning, thank you for being there all these years. Seeing what you have overcome has been the key inspiration behind my desire to explore new frontiers.

Finally, I would like to thank my family — my core, my everything and my home. Mamá y Papá, despite all the odds you have had to overcome in your lives, you have given us life, education, dignity, love and unwavering support. Fernando and Albert, thank you my siblings for trusting me and sharing this life's journey with me, even through the hard times. Rest in peace, little Frank. To the rest of my family, thank you for your trust and unconditional love.

Thank you.

Table of contents

List of figures

List of tables

List of abbreviations

A	
AB	Antibody
AC	Articular cartilage
ACAN	Aggrecan
ACKR1	Atypical Chemokine Receptor 1
ACVS	Animal Care and Veterinary Service
AF	Autofluorescence
ALP	Alkaline phosphatase
AML	Acute myeloid leukemia
ANOVA	Analysis of Variance
APP	Amyloid Precursor Protein
ATP	Adenosine triphosphate
B	
BGLAP	Bone Gamma-Carboxyglutamate Protein
BM	Bone marrow
BMECs	Bone marrow endothelial cells
C	
CAR-cells	CXCL12-Abundant articular cells
CB	Cortical bone
CD	Cluster of differentiation
CDPs	Common dendritic progenitor
CFUs	Colony forming units' assay

cKO	Conditional knockout
CLPs	Common lymphoid progenitor
CML	Chronic myeloid leukemia
CMPs	Common myeloid progenitor
Col1a1/2	Collagen type I alpha chain 1/2
Col2a1	Collagen type 2 alpha chain 1
Col22a1	Collagen type XXII alpha chain 1
Cre	Cre recombinase
CRU	Competitive repopulation unit
CXCL12	C-X-C motif chemokine ligand 12
CXCR4	CXC-chemokine receptor 4
D	
DB	Database
DCs	Dendritic Cells
DE	Differential expression
DMSO	DMSO
DNA	Deoxyribonucleic acid
E	
ECM	Extracellular matrix
ECs	Endothelial cells
EDTA	Ethylenediaminetetraacetic acid
EdU	5-ethynyl-2'-deoxyuridine
EGF	Epidermal growth factor

Em	Emission
EMCN	Endomucin
Ex	Excitation
F	
FACS	Fluorescence activated cell sorting flow cytometry
G	
G-CSF	Granulocyte-colony stimulatory factor
GEO	Gene Expression Omnibus
GFP	Green Fluorescent Protein
GM-CSF	Granulocyte and monocyte-colony stimulatory factor
GMPs	Granulocyte-monocyte progenitors
Gfi1	Growth factor-independent 1
GP	Growth plate
GPCs	Growth plate chondrocytes
GRN	Progranulin
H	
HPSCs	Hematopoietic progenitor stem cells
HPs	Hypertrophic chondrocytes
HSCs	Hematopoietic stem cells
HyD	Hybrid detector
HZ	Hypertrophic zone
I	
ICAM	Intercellular adhesion molecule 1

IF	Immunofluorescence
IGF	Insulin-like growth factor
IGFBP	Insulin-like growth factor binding protein
IL	Interleukin
IP	Intraperitoneal
IRF8	Interferon regulatory factor-8
ITGAM/L	Integrin Subunit Alpha L/M
ITGB	Integrin subunit beta
K	
K.o.	Knockout
L	
Lepr	Leptin receptor cells
Lin	Lineage
LSK	Lin-Sca-1+c-Kit+ cells
M	
MAC-1	Macrophage-1 antigen/CD11b
MHC	Major Histocompatibility Complex
MDPs	Monocyte-dendritic progenitor cells
MDS	Myelodysplastic syndrome
MEPs	Megakaryocyte-erythrocyte progenitor cells
MIF	Migration inhibitory factor
MicroCT	Micro-computed tomography
MK	Midkine

MM	Multiple Myeloma
mRNA	Messenger RNA
mSCF	Membrane bound-Stem cell factor
MSCs	Mesenchymal stem cells
N	
NG2	Neural/glial antigen 2
NGF	Nerve growth factor
NK	Natural killer cells
ns	Not significant
O	
O/N	Overnight
OC	Osteocalcin
OPN	Osteopontin
Osx	Osterix
P	
PBS	Phosphate-Buffered Saline
PCA	Principal Component Analysis
PDPN	Podoplanin
PECAM-1	Platelet Endothelial Cell Adhesion Molecule-1
PFA	Paraformaldehyde
PLAU/uPA	Urokinase plasminogen activator
PMNs	Poly-morpho nuclear cells
PMT	Photomultiplier tube

PTN	Pleiotrophin
PZ	Proliferative zone
R	
RDs	Random dots
RNA	Ribonucleic acid
RZ	Resting zone
S	
Sca-1	Stem cell antigen-1
SCANVI	Single-cell ANnotation
SCF	Stem cell factor
SCVI	Single-Cell Variational Inference tools
SD	Standard deviation
SDF-1	Stromal cell-derived factor 1
SECs	Sinusoidal endothelial cells
SEL(E/P)	Selectin E/P
SIRP	Signal regulatory proteins
SOPs	Standard Operating Procedures
SPP1	Secreted phosphoprotein 1
scRNA-seq	Single-cell RNA sequencing
T	
Tagln	Transgelin
TBS	Tris-Buffered Saline
TFs	Transcription Factors

TGFb	Transforming Growth Factor-beta
THBS	Thrombospondin
U	
ULM	Unweighted linear model
UMAP	Uniform Manifold Approximation and Projection
V	
VTN	Vitronectin
VWF	von Willebrand factor
W	
W.o.	Weeks old
Y	
Y.o.	Years old

Chapter 1: Quantitative approaches to study native bone marrow hematopoietic niches

The BM is a key tissue in mammalian organisms that is responsible for producing all the cell types of circulating blood, known as the hematopoietic system. This system involves two lineages: myeloid-derived and lymphoid-derived cells[1]. Consisting of billions of cells constantly being replenished, the hematopoietic system has one of the most robust and extensive proliferative capacity, as it contains stem cells with remarkable self-renewing and multipotent functions. Downstream of hematopoietic stem cells (HSCs) are hematopoietic stem/progenitor cells (HSPCs) primed towards specific lineages, and their respective oligopotent progenitor cells that generate either red blood cells, innate immune cells, and adaptive immune cells[1]. These ultimately give rise to a wide range of mature cells that enter circulation, including erythrocytes, platelets, macrophages, neutrophils, basophils, eosinophils, dendritic cells, mast cells, natural killer (NK) cells, immature lymphoid B cells and lymphoid T cell precursors[1]. Furthermore, the BM impressively produces all of these cell types in a finely tuned, coordinated fashion, capable of maintaining consistent physiological cell proportions under unperturbed conditions, while also capable to adapt cell frequencies according to the needs during pathological conditions[2–4].

Compared to most tissues, the BM has unique characteristics: It is a non-solid/soft tissue that lacks a readily distinguishable and defined anatomical shape, where cells reside in a seemingly non-specific/homogeneous spatial arrangement, making its micro- and macro-states a spatially indeterminate and dynamic system[5,6]. Meanwhile, the BM is located inside the bone units of the skeletal system, filling the enclosures of these solid tissues with drastic contrasting features, as the bones are amongst the strongest tissues in the organism, with mechanical weight-bearing functions, and with specific cell and ECMs compositions distributed in discrete, consistent and well-characterized locations[6,7].

Remarkably, despite differences in size, location and developmental origin among bone units, the composition and activity of the BM remain consistent: Multipotent and self-renewing HSCs in low frequencies and in a quiescent state, followed by a larger proportion of oligopotent-committed myeloid and lymphoid HPSCs and their downstream hierarchical cell identities[8]. These identities span across diverse differentiation and maturation stages, up to their respective cell state prior to full maturation and circulation release to perform their physiological functions[1,8,9]. Hence, the hematopoietic potential is dynamic and adaptable, receiving and interpreting signals from its

bone microenvironment as well as systemic signaling revealing either homeostatic or stress conditions requiring adaptative hematopoietic measures.

Within the hematopoietic lineages, the myeloid cells represent the greatest variety and frequency of cells, as they possess the most remarkable oligopotent potential in producing the red blood cells and the innate immune system, representing the first line of defense and the most dynamically active cells present in circulation[9]. These cells perform functions ranging from oxygen and nutrient transportation, systemic immune scanning, stress and pro/anti-inflammatory response, coagulation, phagocytosis, and initial antigen collection, processing and presentation to induce lymphoid responses, and inflammation resolution ultimately leading to tissue repair and healing[10].

The bone tissue is formed by cells of mesenchymal origin, comprised mostly of osteogenic cells (osteoblasts and osteocytes) and chondrogenic cells (articular and growth plate chondrocytes). The bone and BM are also rich in stromal cells (also called mesenchymal stromal cells or mesenchymal stem cells, MSCs), endothelial cells, perivascular cells, adipocytes (in an age dependent manner), and neurons[11].

Historically, the endothelial, osteoblastic, stromal and MSCs have been closely investigated and revealed that they provide both the environmental infrastructure necessary for bio-mechanical functions such as adhesion, migration, release and arrest; and the basic functional signaling allowing for hematopoiesis, together forming the micro-environment known as the 'hematopoietic niche'[11]. Nonetheless, several mechanisms regulating and coordinating such complex processes remain to be characterized, especially regarding spatial, cellular, and molecular interactions between BM niches and hematopoietic/myeloid cells in situ.

1.1 The Bone Marrow niche, background

The study of the BM as the blood forming source stems back from the 19th century when, according to the new cellular theory of life, 'precursor cells' were theorized to be the origin of the cells present in the blood[12,13]. Since then, the notion of stem cells was formalized in experiments studying HSCs and their capacity for clonal expansion and repopulation to restore the entire blood system after irradiation and BM transplantation[14,15].

The development of cell sorting techniques such as fluorescence activated cell sorting flow cytometry (FACS) made it possible to isolate HSCs with self-renewal properties to near purity as tested by single-cell transplantations capable of restoring hematopoietic functions[16]. This revealed that the hematopoietic induction and function depend directly on the complex and unique signaling in the environment where the BM resides, the hematopoietic microenvironment[17]. This, defined by the non-hematopoietic stromal cells coexisting with the BM.

The conceptualization of the microenvironmental niche was introduced in 1978 by Ray Schofield, who studied the "immortal behavior" of BM cells from either young or old mice, both of which, when transplanted into W/Wv mice (mast cell-deficient mice by mutation in the Kit gene), were capable of restoring hematopoiesis indefinitely[18]. Schofield concluded that cells with the ultimate stemness capacity must reside in the BM as fixed progenitors, otherwise removal from their BM niche results in loss of “immortality”[18]. The formulation of the hematopoietic niche concept required three features: 1) discrete anatomical locations within the BM microenvironment; 2) defined units formed by sets of actively interacting cells that provide HSC maintenance; and 3) a scaffold that provides active cell attachment as the main mechanical stimulus for HSC stemness, meaning that active detachment would result in differentiation and fate decision into myeloid or lymphoid lineages[18]. Hence, niches are specialized micro-environments in discrete anatomical locations providing the stimuli necessary for inducing cellular functions.

Since then, the study of the cell dynamics responsible for the complex hematopoietic process was achieved through in vivo and in vitro studies, these strategies aiming to understand the BM functions either by recreating or directly studying the hematopoietic niche in situ[19–26]. However, most of these attempts have focused mostly on BM transplantation to study how HSCs act upon reinsertion in their bone niche (in conditional knockout mice, for instance) and analysis using FACS, or by means of imaging of thin cryosections, ultimately disrupting the native tissue architecture and lacking 3D spatial information[21,23,25–29].

The study of the BM using imaging approaches has historically been technically challenging. Part of the difficulties lie in the biomechanical contrasts between the solid and hard bone matrix and the soft marrow, which makes sectioning difficult. Autofluorescence and the random organization of BM cells, which require whole organ imaging to effectively identify the cells of interest. There is also a need for complex marker combinations to identify cell types based

on specific surface proteins and to optimize multiplexing strategies. The complex organization of BM niches (e.g. BM vasculature) and the time-consuming tissue processing, staining and 3D/optical clearing also present challenges. For this reason, the understanding of the BM's in situ spatio-temporal homeostasis remains poorly understood.

1.2 Myeloid lineages and granulopoiesis

The myeloid lineage generates progenitors and mature blood cells, as well as the immune cells known to make up the innate immunity[30–32]. On the other hand, the lymphoid lineage in the BM produces mostly long-lived cells capable of registering and collecting the immune memory of the adaptive immunity and their progenitors[31,32].

With the addition of scRNAseq and lineage tracing analyses, it has been possible to extend the understanding of the differentiation pathways from in vitro and transplant protocols[30–36]. Myelopoiesis is initiated once the common myeloid progenitors (CMPs) are derived from HPSCs, these oligopotent CMPs can differentiate in megakaryocyte-erythrocyte progenitors (MEPs), monocyte-dendritic cell progenitors (MDPs), and granulocyte-monocyte progenitors (GMPs). MDPs follow the Gfi1-low monocyte progenitor route, resulting in Ly6C-high/low monocytes and common dendritic cell progenitors (CDPs), the latter producing dendritic cells[37]. In the case of GMPs, they follow the Gfi1-high monocyte progenitor and granulocyte progenitors (GMPs) pathways, resulting in monocytes, and poly-morpho nuclear (PMNs) cells also known as granulocytes (neutrophils, basophils and eosinophils)[8,37–39]. Finally, the MEPs produce the megakaryocyte and erythroid progenitor cells, the former responsible of platelet production, the latter responsible for mature red blood cells[8].

1.3 The hematopoietic and myelopoietic niche

Several cell types and molecules have been proposed to be integral to the BM hematopoietic niche. Molecules such as CXCL12, Stem Cell Factor (SCF/KitL), IL-7, and osteopontin (OPN) have all been shown through knockout experiments to play a role in maintaining hematopoiesis[40–45]. Similarly, several cell types have been postulated to be integral to the BM niche: osteoblasts, marrow stromal cells (CXCL12-abundant reticular cells/CAR – and/or LepR+ stromal cells), adipocytes, pericytes-smooth muscle cells, endothelial cells (arteriolar or sinusoidal), neurons, as well as non-myelinating Schwann cells[40,46–54]. Experiments where these

cell types are manipulated or ablated all result in defective hematopoiesis[41,43,55]. However, no study so far has been able to demonstrate that HSCs self-renew in a specific niche in situ, in close spatial relationship with specific cell types or molecules. The same holds for more committed progenitors (CMPs, GMPs, MEPs), where the precise anatomical location and cellular/molecular composition of their proliferation and differentiation niches remain unknown. An intriguing theory is that there might not be a single niche for each of these stem/progenitor cell types, but rather multiple niches with progenitor cells mobilizing between them constantly.

So far, early attempts to define the in situ hematopoietic regulator proposed the endosteum-osteoblast system, postulated following in vitro studies, and the competitive repopulation unit (CRU) assays[22,29,46,47]. While these techniques poorly conserved the native tissue organization, the introduction of further immunostaining approaches, confocal imaging and tissue processing revealed that the osteoblastic niche was not the exclusive niche capable of inducing hematopoiesis, as HSCs and HSPCs were located scattered across the BM and in proximity of vascular sinusoids and peri-vascular BM arterioles[28,40,56–58].

This switching of paradigm towards a vascular sinusoidal-based niche perspective has been derived by emphasizing the cell source of key chemokines responsible to induce quiescence exit from HSCs, while inducing specific cell adhesion-migration stimuli[59–61]. Nonetheless, despite the fact that perisinusoidal and periarteriolar endothelial cells actively produce crucial cytokines for hematopoiesis maintenance, this niche poses several questions, such as the fact that these sinusoidal and arteriolar networks are both virtually and practically so abundant throughout the bone and BM that it is consequently not possible for HSCs and other progenitor cell populations to be at a significant distance considered distal to them[60,62,63]. Other criticism questions the lack of matched proportions between the vascular niche and HSCs, if the extensive vascularity represents their niche, why are these HSCs so scarce? Moreover, the factors produced by BM vascularity are also expressed by other major cell types, notably osteoblasts and stromal cells[46–48,64]. This leads to biased interpretations of the effects of niches, either inductive or stochastic, there is a clear need to thoroughly map the BM and its niche architecture.

The knowledge regarding the regulation of myelopoiesis in specialized BM niches is less clear. The consensus to date is that the induction of HSCs and myeloid progenitors is mediated by niche cells that express HSC-proliferative growth factors and chemokines[38,41,65,66]. The most

relevant and well-described inductive elements in unperturbed conditions identified so far are KitL (SCF), CXCL12, Gfi1, G-CSF and GM-CSF, which promotes and regulates the myeloid differentiation through different mechanisms[8,66–68]. Meanwhile, the BM-non hematopoietic cells that produce these factors and build up these niches' functions have largely been confirmed to consist mostly of vascular and osteogenic cells[67,69,70].

Factors such as SCF bind to the Kit receptor on HSCs and HPSCs-myeloid progenitors, while CXCL12 targets the CXC-chemokine receptor 4 (CXCR4) also present in HSCs and myeloid progenitors. Deletion of any of these two factors leads to depletion of HSCs and myelopoietic disruption[40,41]. Despite their historically well-known functions, several questions remain regarding the mechanisms employed to induce these effects at niche-level.

Meanwhile, inflammatory stimuli resulting from pathogenic agents and stress induce a wide variety of systemic expression of interleukins such as IL-6 and IL-17 to directly induce the proliferation and release of myeloid-immune cells, represented mostly by neutrophils and monocytes[71,72]. These inflammatory signaling impact the niche populations and induce the release of further stimulatory and growth factors, such as GM-CSF, G-CSF, and fibroblast growth factors 1 and 2[66,71,73]. These systemic stimuli promoting the production of innate immune cells to react to such stress conditions is known as 'emergency granulopoiesis'.

Based on the functions of these factors, it is assumed that the myeloid-inductive niche should comprise cells that can produce these factors locally, the deletion of which induces the depletion of the hematopoietic-myeloid system.

Research into the cell source of these factors has explored their niche functions, revealing further heterogeneity of BM stromal cells with hematopoietic-myelopoietic inductive competence, as is the case with CAR cells. CAR cells, which are abundant in CXCL12, are mostly vascular-sinusoidal and perivascular cells derived from mesenchymal populations, followed by adipocytes and osteoblasts to a lesser extent[40,41,45,70,74]. Related cells expressing the LepR usually represent MSCs with differentiation potential into bone and stromal cell types[75].

Beyond the induction of proliferation and cell cycle entry, further myelopoietic induction functions rely on the acquisition of cell mobility functions dependant on adhesive and migratory signals of the niche. Research on HSC mobilization has shown that sinusoidal endothelial cells

(SECs) are the most relevant niche cells regulating these migratory functions with specific HSCs and myeloid mechanisms. For example, impaired *EphnB4* expression and interaction with *EphrinB2* on the surface of HSCs results in reduced HSC mobilization and a reduction in myeloid subsets[76]. Similarly, the binding dynamics of CXCL12-CXCR4 dictate the homing capacity of HSCs and HSPCs, meanwhile for granulocyte-neutrophil cells this interaction dictates cell mobility arrest/retention to the niche, which prevents further release and terminal maturation[40,77].

Furthermore, the osteogenic niche also displays relevant niche-adhesive roles, as demonstrated by *Dicer1* deletion in the osteogenic compartment (*Dicer1* floxed alleles under transcriptional control of *Osterix* expressing osteoprogenitors), an RNase III endonuclease responsible of miRNA biogenesis, a transcriptional machinery necessary for lineage definition; leading to loss of osteocalcin (OC)-expressing osteoblasts and mesenchymal-osteoprogenitors, impairing HSC adhesion-mobilization, aberrant proliferation and further myeloid differentiation disruption to the point of producing myelodysplastic conditions[55,78].

These reveal critical and complex functions of specialized niches in BM homeostasis and further concepts of niche-disruption related to myeloid leukemias.

1.3.1 Myelopoietic niche under pathological conditions

Among the hematopoietic-myelopoietic research exploring the effects and functions of the BM niche upon the inductive proliferative stimuli, one of the fields that have provided a robust set of findings is the research focused on malignant-leukemic diseases, especially those focused on myeloid leukemias.

Studies on acute myeloid leukemia (AML), myelodysplastic syndrome (MDS), multiple myeloma (MM) and chronic myeloid leukemia (CML) are increasingly providing relevant information on how niche alterations by means of inflammatory signals, and proteolytic-remodeling dynamics of the osteogenic, endosteal-sinusoidal vascular and sympathetic neuronal niches impacts and promotes myelopoietic induction[79–85].

One of the most notable disruptions to the osteoblastic niche is the severe impairment of trabecular bone. Cases involving AML result in disruption and loss of trabeculae, as revealed by microCT techniques. It is inferred that disruption to the osteogenic niche removes myeloid regulatory stimuli and avoids inflammatory signaling, enabling the leukemic permissive

pathological environment to evade the immune system[80,86]. Meanwhile, the BM vascular niche is also severely impaired under AML, as studies have shown that increased leakage and pathological permeability impair the vascular network, inducing leukemic-friendly environments that promote malignant growth due to metabolic adaptations[79,82].

1.3.2 Myelopoiesis approach on regenerative medicine

Finally, given the growing interest in regenerative medicine and ageing research, studies have observed drastic changes in the BM composition over time, with disruption to the heterogeneous BM niches and their specialized regulatory functions.

In general, MSC niches show increasing impairment of osteogenic potential, leading to an adipogenic bias resulting in accumulation of BM adipocytes known as yellow marrow, increasingly occupying major proportions compared to the hematopoietic BM. In contrast, the hematopoietic-BM known as red marrow, also experiences a multipotential impairment, as it becomes biased towards myelopoiesis with age. This results in a decrease in lymphopoietic potential and marked overall niche changes within the sinusoidal vasculature and neuronal innervation. The former is increasingly impaired by downregulation of endothelial Notch signaling and loss of Endomucin+CD31^{high} vessels. The latter shows loss of b3-adrenergic neurons. Notably, the diameter of sinusoidal vessels increases inversely with the number of ECs with age [69,87–91].

Moreover, ageing also induces extensive cell intrinsic changes with regards to telomere shortening and dysfunction, which, in combination of inflammatory cytokines such as G-CSF, impairs further the lymphoid potential, as demonstrated by telomerase knockout mouse models. Which impairs the BM stromal populations, in particular, the osteoblastic compartment[92].

For regenerative medicine approaches, one of the most relevant findings emphasizing the importance of BM-specific age-related niche composition were obtained from HSCs transplanted from mice of different ages. Young-mice's HSCs transplanted into aged recipients exhibited similar age-related impairments, while aged-mice's HSCs transplanted into young recipients showed recovered multipotent characteristics and increased engraftment [93–95]. This crucial finding is the core proof that the BM niches and their changing-remodeling dynamics are sufficient to impact by means of induction or suppression the entire hematopoietic system, while these quiescent HSCs keep their intrinsic multipotent features. With regards to myelopoiesis in specific,

the loss of osteogenic potential among mesenchymal stromal cells leads to believe that there are crucial specialized osteogenic cells that act as key myeloid regulatory niche elements, crucial for maintaining a homeostatic myeloid-lymphoid ratio. Hence, niches not only act as inductive elements but regulatory as well.

This compendium of evidence demonstrates that the in vivo hematopoietic-myelopoietic functions under both homeostatic and pathological conditions are not cell-autonomous, but rather dependent on the signaling at systemic and niche scales, where the former is reactive to inflammatory and stress conditions while the latter provides a homeostatic-basal stimuli. A dysfunctional niche can alter HSC-HPSCs and myeloid functions, impair multipotency by means of myelopoietic bias under malignant conditions and the aged phenotype. However, there is currently a lack of crucial knowledge in terms of the robust and comprehensive characterization of the detailed spatial-temporal baseline of the in situ niche architecture associated with hematopoietic, myelopoietic and lymphopoietic functions.

1.3.3 Granulopoietic-neutrophilic niche and signaling

Stemming from GMPs, neutrophils are the most prevalent cell type derived from the granulocyte lineage-PMNs. Many of the mechanisms identified for neutrophil induction, maturation and their terminal state are partially shared with those necessary for the CMP-GMP transition. Additionally, specific signaling directs neutrophil differentiation have been identified.

Derived from the CMPs (Sca-1-Lin-Kit+CD34+), the GMPs undergo downstream induction through c-Kit and SCF stimulation. GMPs are characterized by a higher expression of c-Kit in comparison to quiescent HSCs. This increase then declines as the GMPs differentiate towards PMNs, triggering the necessary proliferative program for generating neutrophils[96].

GMPs with neutrophilic commitment depend on the deregulation of the interactions between CXCL12 and CXCR4, as specific CXCR4 receptor activity is characterized by the maintenance of neutrophil retention in the BM niche prior to their terminal maturation and release into circulation. CXCR4 is downregulated also by specific cytokines identified to lead the neutrophilic stimuli: GM-CSF and G-CSF[97].

GM-CSF, which is expressed by a variety of immune and BM stromal cells, acts on GMPs via the GM-CSF receptor (GM-CSFr). The expression of this receptor is controlled by the

transcription program defined by PU.1 and C/EBP. Binding to the GM-CSFr inhibits apoptosis, and promotes proliferation and further downstream maturation[98,99]. Meanwhile, G-CSF is a growth factor that plays a specific role in neutrophil differentiation. The G-CSF receptor (G-CSFr) is expressed at the highest levels in neutrophilic granulocytes undergoing terminal maturation[100]. G-CSF can also be expressed by a wide range of cells, from BM stromal cells to other immune cells. Its production and release, which induce neutrophil maturation, are closely promoted by inflammatory factors that operate systemically and provide signaling indicating systemic immune needs, to further control the frequency of neutrophils in circulation necessary. Two of the most relevant inflammatory factors involved include IL-23 and IL-17, whose dosage can either dictate steady-state or perturbed neutrophil requirements, as well as products released from the gut microbiota that stimulate toll-like receptor signaling, which functions as a mechanism of pathogen-sensing[101,102]. This dictates either basal, steady-state neutrophil production or the need for emergency-induced neutrophilia in response to inflammation. Nevertheless, even though inflammatory GM/G-CSF signaling are among the historically best-described pathways known to directly promote and induce GMPs-neutrophil differentiation, these stem from systemic factors and are not unique to BM. Furthermore, deletion of either of these CSFs produces neutropenia, but not complete neutrophil depletion in the BM. Therefore, specific BM-neutrophilic niche stimuli are still present and primordial to GM/G-CSFs but have not yet been fully identified[100,103].

1.3.4 Granulopoietic-neutrophilic development

As part of myeloid differentiation towards GMPs-PMNs, developmental stages involve gaining the competence to form primary azurophilic granules, both transcriptionally and phenotypically, the latter mostly described in the human context. Following differentiation of the CMPs into myeloblasts, the latter undergo a transition from an early phenotype lacking granules (type I myeloblast) to a next stage with formation of primary granules in the cytoplasm (type II myeloblast). This maturation process continues until the myeloblast increases in size and is filled with primary granules (promyelocyte/progranulocyte). Ultimate maturation of the myelocyte/granulocyte is characterized by the transition in phenotype towards secondary granule production and a decrease in primary granules and cell size smaller than promyelocytes[104,105]. These myelocytes represent the final stage at which cell division occurs, achieving a ratio of 16–

32 myelocytes per myeloblast. These cells then commit to either of the PMNs, which is dominated by neutrophils[104].

As previously mentioned, the signalling required for the CMP-GMP transition depends on IL-3, GM-CSF and IL-6 stimuli. Meanwhile, the GMP-neutrophil transition is primarily marked by G-CSF signalling, which induces the acquisition of adhesive, chemotactic and phagocytic functions[99,100]. Changes in adhesion are mostly characterised by a decreased capacity for cell retention in the BM niche, which is dominated by attachment to vascular surface proteins. Meanwhile, cells gain adhesive-rolling capabilities through surface proteins such as CD11b[104]. Furthermore, the granule formation program matures from primary or secondary azurophilic granules in CMPs and GMPs to secretory granules[105].

1.3.5 Granulopoietic-basophilic and eosinophilic development

In addition to neutrophils, GMPs have the oligopotent capacity to produce the remaining two types of PMNs: basophils and eosinophils.

In mouse, eosinophils derive from the GMPs, meanwhile in humans, the eosinophil progenitor can directly arise from the CMPs[106]. In contrast to GMP-derived neutrophils, eosinophils have low c-Kit expression and high IL-5 receptor (IL-5r) expression. This competence is acquired through a transcriptomic program mediated by GATA-1, PU.1, C/EBPα, C/EBPβ and interferon regulatory factor-8 (IRF8). Further induction of the eosinophil progenitor program depends on IL-3, GM-CSF and IL-5, in the absence of G-CSFR. Hence, eosinophils do not respond to the main neutrophil-inductive signalling. Once terminal differentiation of eosinophils is achieved, IL-5 signalling dominates the inductive stimuli, while the relevance of GM-CSF is relegated to the early eosinophil progenitor[106]. Ultimately, IL-5 prevents apoptosis and promotes release from the BM.

Meanwhile, the origin of basophils is less clear, as basophil progenitors have been identified as developing from both CD34+ HPSCs-CMPs and bipotent progenitors derived from GMPs[107–109]. The transcriptomic program involves the upregulation of GATA-2 and the subsequent transient downregulation of C/EBPα. The reactivation of C/EBPα then directs the final stage of basophil production[110]. The specific inducers of basophil fate are not yet known, unlike for neutrophils with G-CSF and eosinophils with IL-5. Instead, basophils depend mostly on IL-3

and GM-CSF for the proliferative stages, as well as IL-5, nerve growth factor (NGF) and TGFb[107,108]. However, despite IL-3 seemingly being the most relevant factor in basophilic induction, mice deficient in IL-3 do produce basophils in unperturbed conditions[111]. Finally, upon basophil maturation, IL-3 and GM-CSF induce effector functions based on histamine production, resulting in the migratory phenotype of the mature basophil and its release into circulation[111].

1.4 Multiplexed immunofluorescence for 3D imaging of bone marrow

The BM microenvironment contains a great variety of cell types, along with complex ECM components on which stromal cells depend to perform their tissue-specific physiological and inductive niche stimuli functions. These cell populations and their roles have been studied extensively, as the functional composition of BM niches that direct hematopoiesis and myelopoiesis is considered the *holy grail* of the field. However, as previously mentioned, this robust body of research, techniques and results relies on processes that either heavily disrupt the architecture of the BM (in vitro and flow cytometry assays), provide inadequate 2D information (imaging of thin cryo-sections), or analyze niche cells and hematopoietic cells separately (transcriptomics studies).

Imaging bone and BM pose several challenges. Skeletal tissues and their matrix components are notoriously auto fluorescent (AF), which is a physical reaction resulting from the intrinsic composition of ECM such as collagen and crosslinking induced by tissue fixation[112]. This AF decreases resolution and signal-to-noise ratio, impeding the detection and collection of useful data with sufficient thickness to generate 3D spatial data[112]. These challenges limited the characterization of the in situ BM-niche architecture and sometimes led to controversial interpretation among reported findings[59,113,114].

To overcome these challenges and advance the effective and efficient exploration of the spatial composition of complex cell types and ECM components within the ecosystem, my supervisor, Dr. Daniel Coutu, led the design, optimization and implementation of effective pipelines for IF-based multi-colour 3D imaging of thick bone-BM sections. Capable of robust identification of cell types, such as bone and BM stromal cells (e.g. osteoblasts, osteocytes, chondrocytes, endothelial cells, perivascular cells, adipocytes, neuronal innervations, Schwann cells and mesenchymal stromal cells), bone ECM components (e.g. bone, cartilage, vasculature and periosteum) and hematopoietic cells. Achievements were made possible by means of bone

tissue collection, fixation, decalcification, thick sectioning, immunostaining, tissue clearing and confocal microscopy 3D imaging[62,115,116].

Moreover, the robustness of the spatial data collected is another limitation of the deep exploration of in situ data. Image segmentation tools are crucial for processing the extensive data collected per analyzed sample, which can exceed 100 GB (representing >1.5e5 individual images) and result in lengthy processing times. To relieve the strain on these essential computing functions, such as counting, morphology, fluorescence intensity and spatial distances, for each of the millions to billions of cells available in the dataset, our lab also pioneered the development of the open-access software XiT. This tool relies on statistical parameters collected through image segmentation to efficiently reduce data size and processing time, enabling image cytometry analysis of the spatial data by means of fluorescence intensity statistics[117].

1.5 Immunostaining of surface markers, granulocytes-neutrophils

The epitope targeted by the anti-Gr1 (RB6-8C5) antibody (AB) has historically been one of the most applied antibodies in immune cell research. First characterized in 1993 as an antibody for depleting mouse neutrophils, it has since become one of the main myeloid-related epitope-targeting tools for granulocytes with neutrophilic potential, particularly in mouse BM, as it is absent in human neutrophils and its expression is almost absent in circulating neutrophils[118]. It has since been used in immunophenotyping panels to target diverse cell types across GMP-neutrophil early differentiation stages, primarily alongside CD11b, CD11c, and CD16, illustrating the range of cells that exhibit Gr1 binding[119–121].

Anti-Gr1 AB targets the surface protein resulting from the expression of the Ly6G gene with high affinity, and to a lesser extent the surface protein encoded by Ly6C, which is mostly representative of monocytes[118]. Therefore, Gr1 staining is not exclusively associated with neutrophils; it has been demonstrated that BM Gr1+ cells exhibit both neutrophil and monocyte potential, reflecting its relevance for detecting downstream cells originating from myeloid progenitor GMPs.

Moreover, as mentioned above, the Gr1 epitope is reduced or absent in circulating neutrophils and mostly represents BM-resident granulocyte-neutrophilic cells. Further scRNA-seq

experiments confirm the Ly6g gene's transcriptomic expression profile in the early stages of neutrophils in the BM[121].

Other myeloid cell types can be labelled using further highly specific surface markers. These include erythroid-derived lineages, labelled using ABs anti TER119 and Glycophorin A (CD235a); megakaryocytes, using anti-CD36; and monocytes, labelled using anti-CD16, CD11b and CD11c[121–125]. However, many of these ABs were developed for flow cytometry applications and may require further optimization of tissue processing conditions for IF applications.

1.6 Immunostaining of surface markers, niche cells

As previously mentioned, the cell populations in the bone-BM ecosystem that have been identified as active inductive niche cells for myelopoiesis include BM stromal cells and mesenchymal lineage cells, which are mostly represented by MSCs, as well as osteogenic lineage cells, endothelial cells and perivascular cells. These cells are characterized by the expression of the crucial chemoattractant and proliferative inducing factors, CXCL12 and SCF. However, the mechanisms of these factors (mostly considered soluble-secreted elements), have made it difficult to identify these specific elements using IF strategies. Hence, the IF strategy to follow takes advantage of the pipelines and methods described and optimized by our lab[62,115,116].

The osteogenic niche can be identified by means of bone-specific ECM or osteoblastic staining. The ECM protein most representative of the structural portion of the bone, is collagen type I. Meanwhile, the osteoblastic protein alkaline phosphatase (ALP), which is crucial for hydroxyapatite deposition and bone formation, can stain osteoblasts actively participating in osteogenic niche remodeling[62].

Despite not being considered a niche element of hematopoietic-myelopoietic functions, chondrogenic cells are one of the most relevant cell types present in bone units. They cover regions of bone in a relevant anatomical position to act as a putative niche; an example is the growth plate cartilage (GP)[126]. Unlike the articular cartilage (AC), the GP delineates the metaphysis from the epiphysis in bones. It is a proliferative and metabolically active region of differentiation of growth plate chondrocytes (GPCs), which undergo cell division to induce longitudinal bone growth[126]. The GP is characterized by ECM staining of collagen type II, type XI and aggrecan (ACAN)[127].

Among the most relevant cells that make up a myelopoietic niche are endothelial cells (ECs). The vascular network is one of the most abundant non-hematopoietic elements available in the BM ecosystem. In particular, the niche function is identified among sinusoids, LepR+ cells and cells expressing CXCL12[64,76,128]. This niche can be identified by the specific ECM that forms the basal membrane of the vessels in the bone-BM context, such as collagen type III, which is an active ECM component during embryonic skeletal development and osteoblastogenesis in adult mouse, and vitronectin (VTN)[62,129]. Meanwhile, cell surface markers represent a pan-endothelial target that can be used to identify the entirety of the vascular network, such as CD31 (*Pecam-1*), which is an adhesive protein that is known to be involved in the adhesion dynamics of myeloid cells[62,130].

Finally, another vascular niche cell associated with this process is the perivascular portion, including pericytes. These smooth muscle cells, which some of them surround the arteriolar vasculature, are among the most extensively studied components of the hematopoietic inductive niche[52]. They are readily distinguished by their expression of the muscle-associated surface protein SM22 (encoded by *Tagln*), in combination of the hematopoietic stemness marker Sca-1 and CD90 (*Thy1*)[62].

1.6.1 Measuring proliferation in bone marrow using imaging

One option for image-based techniques to identify proliferative cells is to detect the incorporation of nucleoside analogues (e.g. thymidine analogues used in BrdU or EdU-based assays), whereby a modified thymidine nucleoside is incorporated into the de novo synthesized DNA during the S phase. In the case of EdU proliferation assay, these analogues can then be labelled using a copper-catalyzed (click-it) reaction with azide-containing fluorescent dye, providing a robust, non-specific dye for dividing cells[131–133].

1.7 Single-cell RNA sequencing

Protocols and technologies that can identify and collect the entire transcriptome of biological samples, including complete tissues, at single-cell resolution have represented one of the most valuable advances in the study of cell-intrinsic genetic competence associated with specific cellular functions[134,135]. Generally speaking, unlike the genome, which stores all available data on genes and non-coding DNA sequences shared by all cells in an organism, the transcriptome reveals the set of genes that are actively expressed in a given cell type and their associated

functions[134,135]. This reveals the unique competence of the cell of interest in the context of the study. These techniques rely on detecting, amplifying and identifying RNA content to generate libraries[134,135]. Similar to approaches in flow cytometry, this process relies on the isolation of single cells to extract RNA. Consequently, extensive transcriptomic data collection relies on the destruction of innate tissue architecture and lacks complete spatial tissue context.

Several commercially available single-cell RNA sequencing (scRNA-seq) assays and platforms have been developed. These are capable of detecting and generating transcriptomic libraries using different cell isolation and sorting strategies, as well as analyzing cells, mRNA architecture targets, and amplification strategies. Examples include Smart-seq, Smart-seq2, Drop-seq, and 10x Genomics[135–139].

The extensive data collected, ranging from thousands of genes detected at single-cell resolution among thousands of cells collected and sorted, is robust and poses several analytical challenges. To enable the analysis of such extensive libraries, open-source bioinformatics tools have been developed and are readily available for in silico transcriptomics analysis.

1.8 Bioinformatics tools for in silico transcriptomics analysis

The introduction of techniques capable of detecting the transcriptome of large portions of cells in specific tissues has provided the capacity to collect the transcriptomic profile of entire cell series, offering new insights into the expression patterns of genes associated with cell functions, heterogeneity and developmental stages[140,141].

These techniques have naturally been applied to study the mechanisms by which myelopoiesis operates and regulates the differentiation and maturation steps necessary for acquiring required phenotypes[31,142–145]. Furthermore, it is possible to identify transcripts of actively expressed proteins that are involved in ligand-receptor dynamics and have the potential to reveal cell communication[146].

Given the extensive and robust data volumes that the transcriptome represents conformed by thousands of cells, open-source bioinformatics tools R and Python-based have been developed to identify, classify, cluster, represent and analyze the vast transcriptomic data.

1.8.1 Single cell transcriptomics datasets, integration tools

One of the most in-demand tools for analyzing scRNA-seq is the ability to integrate transcriptomic libraries generated by different laboratories[140]. As these transcriptomic analyses are time-consuming and complex, it is difficult for individual groups to capture large numbers of cells and tissues. Moreover, many of these efforts restrict their analyses to specific tissues in an attempt to avoid contamination or biased results in subsequent transcriptomic analyses. Therefore, cell-tissue approaches, especially those concerning the holistic capture of both bone and BM cells, are limited. Most studies have focused on niche cells or tracking cells expressing the known ligands CXCL12 and/or SCF, and the LepR, or on osteogenic-specific or vascular-specific cells[36,74,142]. Meanwhile, other efforts have effectively captured BM cells only, usually by lineage depletion of mature cell identities[143]. Many of these efforts target the aforementioned cell surface proteins. Only the library generated by Baccin et al. aimed to capture a holistic series of BM cells with mature immune types (including granulocytes and neutrophils)[142].

Thanks to available informatics tools such as the Python-based ScANVI-SCVI, it is possible to use machine learning-based strategies to identify, classify and determine transcriptomic states, and produce latent representations of shared transcriptomic states by means of probabilistic modelling. This modelling approach is novel compared to gene expression patterns based on linear models, as it implements a series of full dataset reconstructions to reach robust posterior probabilistic parameters. The aim is to infer, after different reconstruction rounds, the latent space of shared transcriptomic states with great confidence, while also identifying previously unknown heterogeneity among cell types[145,147]. This is particularly relevant considering that HPSCs, GMPs and PMNs do not operate as fully distinct cell identities, but rather as a series of cells in a continuum-like spectrum of highly shared transcriptomic competence among their downstream, more specialized cell identities.

1.8.2 Cell communication inference tool CellChat

For the purpose of cell communication dynamics, the available transcriptome includes genes that are actively expressed and associated with protein units that are known to form receptor complexes with their associated ligands. Hence, tools such as CellChat take advantage of robust databases of ligand-receptor interactions[146,148]. By registering the genes expressed by each cell in

its respective cluster, it is possible to identify which genes encode either the ligands or the receptors and use this information to infer cell communication.

In the case of CellChat, these inferred cell communications are classified under four interaction mechanisms: cell-to-cell contact; secreted signaling; ECM-receptor; and non-protein interactions. Within each context, CellChat classifies cells expressing the ligand as the signaling source of the signaling pathway (outgoing role), and cells expressing genes associated with targeted receptors as the signaling target (incoming role). Moreover, these inferences fall under known pathways, including those with an extensive physiological magnitude. The proportion of gene transcripts detected can provide a probabilistic value for each inferred pathway[146,148].

Finally, these inferred communication crosstalk function as a valuable resource for forming hypotheses to be explored in further research.

1.9 Research rationale

Clearly, there is a need to study the in situ architecture of the BM more thoroughly and to identify the specific niches in which cells operate, self-renew, proliferate and differentiate. This information could help to fill significant gaps in our understanding of the in vivo dynamics of BM-myelopoietic cells. It could also provide new tools for diagnosing pathological hematopoietic-myelopoietic diseases by assessing niche changes. Furthermore, it could offer new therapeutic targets and help us to better understand how ageing affects myelopoiesis and to design novel regenerative medicine approaches to treat hematological disorders.

Bearing this in mind, I took advantage of the tools and imaging pipeline developed in our lab, whose research focuses primarily on skeletal stem cells, and applied them to the study of hematopoiesis. I first noticed that EdU was preferentially incorporated in BM hematopoietic cells in specific areas in mouse femurs. This EdU+ incorporation was primarily found in BM cells located in the distal portion of the mouse femur, within the trabecular bone cavities of both the metaphysis and the epiphysis.

To further characterize these EdU+ BM cells, we asked our collaborators at the University of Toronto led by Dr Tikhonova and MSc student Ximing Li, to replicate the EdU regimen in mice and analyze EdU incorporation in BM cells using flow cytometry. The marker panels including Lin- HSCs and HPSCs, Lin+ myeloid and lymphoid lineage progenitors and mature hematopoietic

cells. As expected, they found that EdU integration was reproducible in BM cells, with the majority of incorporation occurring in cells associated with the myeloid-granulocyte lineage (Lin+Gr1+CD11b+), such as GMPs and granulocytes, with lower incorporation in B-cell progenitors and HSPCs.

Therefore, I set out to map and characterize the BM cells in active proliferation, as well as the spatial, cellular, and molecular composition of their niche.

1.10 Hypothesis

I hypothesize that bone marrow (BM) cells incorporating the proliferation label EdU among femur bone sections, particularly in the trabeculae of the distal epiphysis and metaphysis, are composed of granulocytes and neutrophils undergoing cell division. These cells are arranged in a specific spatial configuration within the bone-BM ecosystem, reflecting their inductive niche. This niche composition is characterized by osteogenic lineage cells (osteoblasts) and vascularity (endothelial and perivascular cells).

Finally, I hypothesize that once I have identified the relevant BM niche composition by means of IF microscopy and 3D imaging analysis, integrated single-cell transcriptomic datasets will reveal potential cell communication pathways between the pertinent niche and GMP-neutrophils of interest, based on their genetic competence with regard to the actively expressed genes of paired ligands and receptors.

1.11 Specific aims

***Aim1**. Identification of proliferative myeloid cells in the BM*

Identify, map and characterize the BM myeloid-granulocyte cells with EdU+ incorporation in mice femurs by means of IF staining of myeloid markers, confocal imaging and cytometry.

***Aim2**. Identification of the niche composition of the proliferative myeloid cells in the BM*

Identify, map and characterize the BM niche composition of the proliferative myeloid-granulocyte cells in mice femurs by means of IF staining of niche markers for osteogenic, chondrocyte, endothelial and peri-vascular cells, confocal imaging and cytometry.

***Aim3.** Inference of cell communication crosstalk between identified BM niche cells and the myeloid cell types of interest*

In silico analysis of cell communication inferred pathways between granulocyte progenitors, neutrophils and the previously identified BM niche cells using publicly available scRNA-seq datasets, integration tool SCVI, and cell communication inference tool CellChat v2.

Chapter 2: Materials and methods

General

Reagents used and described in the present project were used following the specifications stated by the manufacturer's user manuals and guidelines. The chemical solutions were prepared using commercial reagents. Reagents and solutions with pH specific requirements were tested using the accumet® AE150 pH meter (Thermo Fisher Scientific Inc.). Reagents here described were prepared using phosphate-buffered saline (PBS, pH = 7.4) (preparation in Sections 2.4), list of reagents in section 2.11 Appendix.

2.1 Animal care

Ethics

All animal experiments were conducted following the approved animal protocols in compliance of the regulations upheld by the animal care and veterinary service (ACVS) of the University of Ottawa, Faculty of Medicine.

Animals

20 wild type mice C57BL/6 (strain code: #:027) at 8 to 9-week-old age (considered here as juvenile), from which 10 were male and 10 were female, were acquired from Charles River Laboratories©. All animals were received and processed using the University of Ottawa's ACVS at the Roger Guindon Hall (RGN) campus of the Faculty of Medicine.

Injections and drug administration

EdU solid compound (Sigma-Aldrich, catalogue number: 900584), dosage preparation of 12.5mg/kg in PBS vehicle were performed under sterile conditions al BSC2. Dissolved EdU injections were used for the in vivo proliferation assay. Stock concentration per pulse/mouse 2.5mg/ml (stored at -20 °C until required for injection), EdU stock at room temperature administered via intraperitoneal (IP) injection.

EdU injections regime consisted of IP injections performed once during three consecutive days per mouse (3 pulses) of the abovementioned dosage.

2.2 Bone harvest, preparation and processing

Once the EdU injection regime was completed all mice were chased during 48 hours before euthanasia. Mice euthanasia was performed at the designated ACVS necropsy facilities, following the SOPs described and approved for CO_2 inhalation and cervical dislocation at endpoint

Following euthanasia, both femur bones were dissected from each mouse, immediately placed in cold PBS, and cleaned from muscle and excessive connective tissue without compromising the innate structural composition of the femur bone. 40 femurs were collected and immediately transferred to 4% PFA (paraformaldehyde in PBS) for overnight fixation (between 16 to 18 hours maximum) with gentle shaking, at 4ºC. Fixed bones were transferred to 10% EDTA (pH=8) solution for the purpose of decalcification during 14 days (2 weeks), with gentle stirring, EDTA volumes were refreshed every 48 hours, and kept at 4ºC. After decalcification, the bones were stored in cold PBS until needed for embedding.

All the 40 decalcified femurs were placed individually laying down with their anterior portion facing up, on plastic embedding molds. Embedding was performed with agarose prepared at a 4% concentration of low-gelling, high gel strength agarose (Fisher scientific, catalogue number: BP160-500), dissolved in PBS and heated in microwave. The prepared agarose intended for embedding was placed in a water bath to reach 41ºC, then each bone was embedded individually. Each embedded unit was transferred to ice for 1 hour and then placed in 4ºC until further use.

For the purpose of sectioning, the embedded samples were glued to the sample holder of vibratome (Leica Biosystems VT1200 S) and kept in cold conditions in PBS at 4ºC, then sectioned using zirconia ceramic injector-type blades (Cadence Inc.), keeping the thickness at 300µm per section. The collected sections were stored in PBS and kept in 4ºC refrigeration until further use.

Each section containing relevant portions of visible femur bone and BM selected for immunostaining were placed in custom-designed silicone slide spacers (Grace Bio-Labs ©) glued to Superfrost microscopy slides (Fisher), and sitting on nylon mesh (Ted Pella, inc.).

2.3 Immunostaining

Antibodies were resuspended as per manufacturer specifications followed by 1:1 dilution in glycerol (GLY001), to store at -20 °C while preventing freezing and crystallization.

Antibody dilutions remained consistent throughout the project. Antibody washes were prepared using a dilution ratio of 1:50 for primary antibodies, 1:200 of all secondary/tertiary antibodies, and 1:500 for the DAPI nuclear counterstain.

Bone sections were placed in blocking buffer for one hour prior to initial staining. If necessary, streptavidin/biotin blocking was then performed by placing samples in streptavidin solution for one hour followed by fifteen minutes in wash buffer, with the same process repeated for biotin solution.

Sections were then submerged in each iterative AB-solution overnight (O/N) followed by five washes of one hour each in wash buffer.

To summarize, the comprehensive staining progression is as follows:

Blocking buffer (30 min), streptavidin solution (1 hr), wash buffer (15 min), biotin solution (1 hr), wash buffer (15 min), Click-iT™ EdU imaging kit (O/N), wash buffer (5 x 1 hr), primary antibody (O/N), wash buffer (5 x 1 hr), biotin antibody (O/N), wash buffer (5 x 1 hr), secondary (or tertiary) antibody (O/N), wash buffer (5 x 1 hr).

2.4 Optical clearing & Mounting

Samples were submerged in Histodenz (pH = 8.5) and left on active stirring, in the dark O/N. Histodenz was then aspirated and refreshed, followed by mounting. Samples were stored faced down at 4°C in the dark until imaging.

2.5 Confocal Microscopy

Confocal microscopy for 3D Imaging was performed on Leica SP8 Confocal Microscope at ambient conditions.

Microscope lasers: ultraviolet diode (405nm), visible argon (458, 476, 488, 496, and 514nm), and three helium-neon (561, 594, and 633nm) lasers.

Microscope emission detectors: three photomultiplier tube (PMT) and two hybrid (HyD) detector modules using virtual filters.

Fluorescence signal acquisition: sequential scanning, in which fluorophores were separated based on their excitation (Ex) and emission (Em) bandwidths. All regions-of-interest were imaged in their entirety using a 20x multiple immersion lens (NA = 0.75, FWD = 0.680 mm) and Type G (Glycerol) immersion liquid.

Voxel settings: For sections with distal femur epiphysis and metaphysis only were acquired by 8-bit, 1024x1024 resolution, 600 Hz, bidirectional mode with phase correction, 3 sequences, 2.5µm z-spacing, with 10% tile overlap for stitching. For whole femur sections were acquired by 8-bit, 512x512 resolution, 600 Hz, bidirectional mode with phase correction, 3 sequences, zoom factor 2x, 2.5µm z-spacing, Galvo-flow, with 10% tile overlap for stitching.

2.6 Image segmentation and cytometry

Images segmented using Imaris v10.2.0 software, after which statistical data for segmentation was exported. Data collected: Spots function (cells), surface function (surfaces/extended fluorescence patterns), distance (shortest) to spots and to surfaces, fluorescence intensity (mean, median, min, max) and position (x-position, y-position, z-position).

Analysis was performed using the open-access data analysis platform XiT[116].based on fluorescence intensity mean of Gr1-associated signal, and statistical spatial data.

Random dots generated by XiT, 500 RDs in triplicates among the bones with best preserved femur and BM tissue.

2.7 Statistical analysis

All statistical analyses were performed using GraphPad Prism version 10.2.1 (GraphPad Software ©).

Statistical test used: Two-way ANOVA (Ordinary), alpha value: 0.05. P value “ns”, when not significant. P value “*”, “**”, “***”, and “****”, when significant (**** when P value <0.0001).

2.8 Solution & reagent preparation

The following section describes the preparation of in-house solutions required for the methodologies in the present project. The only omissions are common laboratory preparations, which are simple to prepare following manufacturer's instructions and general SOPs and leave little room for error or variation (e.g., NaOH, HCl, TAE solutions). All reagents necessary are listed in section 2.11 Appendix, table 2.1 List of reagents.

4% Paraformaldehyde (PFA)

1. 16% Formaldehyde (w/v) (Thermo Fisher Scientific Inc. catalogue number: 28908), in 10mL deionized water per ampule.
2. The volume in the ampule was dissolved in 30.0mL PBS, final volume: 40mL.
3. Final concentration per 40mL: 4% PFA (w/v) in 40mL volume, 3.33milimolar.
4. Each formulation was prepared and used fresh for each fixation step.
5. Any remaining 4% PFA solution was either stored at 4 °C and used within 24 hours or discarded.

Blocking buffer

1. 10.0mg normal donkey serum powder (Jackson ImmunoResearch Inc., catalogue number: 017-000-121) dissolved in 10.0mL ddH_2O, for a concentration of 0.1% w/v.
2. 0.5mL aliquots of dissolved donkey serum stored in -20 °C until needed.
3. Each aliquot dissolved in 9.5mL permeabilization wash buffer (wash buffer with 0.03% Triton X-100), final volume: 10mL.
4. Each solution was then stored at 4 °C for up to one week for use, after which it was discarded.

10% Ethylenediaminetetraacetic acid (EDTA)

1. 100.0g of EDTA powder (Bio Basic Inc., catalogue number: 6381-92-6) dissolved in ~800 mL ddH_2O with active stirring.
2. NaOH salt added gradually to adjust pH at 8.0 (basic).
3. ddH_2O added to a final volume of 1.0L, 10% EDTA (w/v), 268.64millimolar.
4. Final solution was autoclaved and stored at 4 °C.

Histodenz clearing solution

1. 40.0g of Histodenz powder (Sigma-Aldrich®, catalogue number: D2158) dissolved in 30.0 mL of 1x TBS (pH = 7.5), stirred at room temperature.
2. Final concentration of 88.0% Histodenz w/v in TBS, 1.62molar.
3. Addition of 50.0µL of Tween-20 and 5.0µL of 10% NaN3 stock solution in active stirring until incorporated.
4. 1.0M NaOH solution was added gradually to adjust pH at 8.5.
5. The refractive index expected value must be of 1.46.
6. Once prepared, the solution was stored at room temperature in the absence of light.

Phosphate-buffered saline (PBS, 10x stock)

1. In 800 mL ddH_2O dissolved 80.0g NaCl, 2.0g KCl, 14.4g Na_2HPO_4, and 2.4 g KH_2PO_4.
2. Gradual addition of HCl until pH is adjusted at 7.4.
3. Volumes of ddH2O was added to achieve a final volume of 1.0 L.
4. The final solution was autoclaved and stored at room temperature.
5. Working PBS solutions used at 1x by diluting the 10x stock 1:10 with ddH2O.
6. Diluted working PBS solutions were stored at room temperature.

Tris-buffered saline (TBS)

1. TBS I: 75.71g tris base and 54.79g NaCl in ddH2O for a final volume of 500.0 mL, pH= ~10.4.
2. TBS II: 98.5g tris HCl and 54.79g NaCl in ddH2O for a final volume of 500.0 mL, pH= ~4.4.
3. 12.5x TBS stock was prepared by adding TBS I in volume of TBS II until pH was adjusted to 7.5 (a 1:6 ratio approximately).
4. Stock was then autoclaved and stored at room temperature.

Wash Buffer

1. Prepared in volumes of 100.0mL by mixing 8.0mL of 12.5x TBS (pH = 7.5), 72.0 mL ddH2O, 20.0mL DMSO, and 50.0µL Tween-20.
2. Wash buffer was stored at room temperature.

2.9 Bioinformatics analysis, SCVI integration and DE analysis

ScRNA-seq datasets

- Baccin C, et al. 2020, GEO: GSE122467. Raw counts[142].

C56Bl/6J female mice, 8-12 weeks old (Jackson Laboratory). Single cell RNA-seq commercial assay used: Chromium Single Cell 3' v2 Reagent Kit protocol (10x genomics, Pleasanton, CA).

- Baryawno N, et al. 2019, GEO: GSE128423. Raw counts from steady-state only mice[74].

C57BL/6 male mice, 6-8 weeks old (Jackson Laboratory). Single cell RNA-seq commercial assay used: Chromium Single Cell 3' v2 Reagent Kit protocol (10x genomics, Pleasanton, CA).

- Tikhonova A, et al. 2019, GEO: GSE108892. Raw counts from non-treated mice with chemotherapy drug 5-FU[36].

B6.FVB-Tg(Cdh5-cre)7Mlia/J (VE-Cad–Cre, 12 weeks old, Jackson Laboratory), B6.129-Leprtm2(cre)Rck/J (LEPR–Cre, 12 weeks old, Jackson Laboratory), and B6.Cg-Tg(Col1a1-creERT2)1Crm/J (COL2.3–Cre, 16 weeks old, Jackson Laboratory). Single cell RNA-seq commercial assay used: Chromium Single Cell 3' v2 Reagent Kit protocol (10x genomics, Pleasanton, CA).

- Kucinski S, et al. 2024, GEO: GSE207412. Raw counts from 7w11w and 16w labelled mouse[143].

Hoxb5-CreERT2-Tomato, 8-12 weeks old (mouse line produced by themselves). Single cell RNA-seq commercial assay used: Single Cell 3' v3 Reagent Kit protocol (10x genomics, Pleasanton, CA).

Pre-integration design

Programming language used and version: Python version: 3.12.11, packaged by Anaconda.

Main package used and version: Single-cell variational inference tool (SCVI-tools), version: 1.3.2

Data preprocessing design: Mitochondrial and ribosomal gene metrics for QC were defined, and I decided to remove cells with more than 5% mitochondrial reads, higher

mitochondrial percentages lead to generated clusters with mitochondrial marker genes. Minimum gene count was set to 200, and gene filter was set to minimum of 3 cells to account for the low frequency of HSCs and HSPCs, and raw counts were persevered before any normalization with the key "raw_counts".

Initial cell type scoring and merging

DecoupleR, Bioconductor package, version: 2.1.1. And CellTypist (Teichlab), version: 1.7.1[149,150].

Markers list from the database PanglaoDB based on mouse tissue and cell type.

Tissues selected: 'Brain', 'Immune system', 'Connective tissue', 'Vasculature', 'Blood', 'Bone', 'Skeletal muscle', and 'Smooth muscle'.

Cell types selected from such tissues: 'B cells', 'B cells memory', 'B cells naive', 'Basophils', 'Cholinergic neurons', "Dendritic cells", 'Dopaminergic neurons', "Endothelial cells", 'Eosinophils', 'Erythroblasts', 'Erythroid-like and erythroid precursor cells', 'Gamma delta T cells', 'Glycinergic neurons', 'Hematopoietic stem cells', 'Macrophages', 'Mast cells', 'Megakaryocytes', 'Monocytes', 'Motor neurons', 'Myeloid-derived suppressor cells', 'Natural killer T cells', 'Neuroendocrine cells', 'Neutrophils', 'NK cells', 'Noradrenergic neurons', 'Osteoblasts', 'Osteoclast precursor cells', 'Adipocyte progenitor cells', 'Adipocytes', 'Chondrocytes', 'Fibroblasts', 'Stromal cells', 'Osteoclasts', 'Osteocytes', 'Pericytes', 'Plasma cells', 'Plasmacytoid dendritic cells', 'Platelets', 'Red pulp macrophages', 'Reticulocytes', 'Schwann cells', 'Serotonergic neurons', 'T cells', 'T follicular helper cells', 'T helper cells', 'T memory cells', 'T regulatory cells', 'Myoblasts', 'Myocytes', and 'Vascular smooth muscle cells'.

From each cell type, the marker genes to be considered were set to reach higher score than 0.5.

Merging and integration

Merging of the raw datasets was performed with simultaneous data preprocessing parameters. The resulting combined anndata object consists of 114,085 cells and 21,018 variable genes.

Final integration settings: Hidden nodes 256, dimensionality of latent space 45, and number of hidden layers 2. Based on these settings the model was trained through 150 epochs (complete passes through the entire dataset). The trained model achieved a flat reconstruction loss measurement below 7,200 starting before the 20th Epoch, closely following the validation curve.

Clustering and DE analysis

Leiden method clustering resolution: 1.2.

Leiden clusters ran through DE model analysis function on '1 vs all DE test mode', where each cluster's identified marker genes set is compared against the rest clusters. After performing DE analysis, marker genes were selected based on top 5 scored marker genes.

Subclustering was performed by Leiden resolution: 0.15, 45 iterations. Followed by UMAP reduction, filtering of genes and cells with minimum counts of 3, and final ranking of gene by T-test method.

2.10 Bioinformatics analysis, CellChat communication inference

Programming language used and version: R version 4.5.0.

Main package used and version: CellChat v2, version: 2.2.0

CellChat parameters

CellChat analysis was performed as described in vignettes, unless otherwise specified below.

CellChat database used: CellChatDB.mouse. Subset database: "Cell-Cell Contact", "Secreted Signaling", and "ECM-Receptor".

CellChat smoothdata function was used based on PPI.mouse. Communication probability method: TriMean, raw.use = false.

Communication filter with minimum of 4 cells.

Communication source cells for vascular niche: sources.use = "Pericytes", "ECs", "ECs1", "CD34+SCA1+Ng2- BMECs", "Sinusoidal Ecs1", "Sinusoidal Ecs".

Communication source cells for osteo-chondro niche: sources.use = "BM-MSCs-LepR", "MSCs-Osteo", "Col-Osteoblasts", "BM Fibroblasts", "MSCs Subpop", "MSCs-Chondro".

Communication target cells for granulocytes and neutrophils: targets.use = "Neutro Prog", "Neutro Prog1", "Baso Prog", "Eo/Baso-Prog", "Neutrophils", "Neutrophils1".

2.11 Appendix: Reagents, antibodies and miscellaneous

Reagent	**Manufacturer**	**Catalogue number/ID**
Agarose (Electrophoresis)	Thermo Fisher Scientific Inc	BP-160
Normal donkey serum	Jackson ImmunoResearch Inc.	017-000-121
DMSO 67-68-5	Sigma-Aldrich®	67-68-5
EDTA 6381-92-6	Bio Basic Inc	6381-92-6
EdU	Sigma-Aldrich®	900584
Histodenz™	Sigma-Aldrich®	D2158
16% Formaldehyde Solution (w/v)	Thermo Fisher Scientific Inc.	28908
Click-iT™ EdU Alexa Fluor™ 488 Imaging Kit	Thermo Fisher Scientific Inc.	C10337
Streptavidin/Biotin Blocking Kit	MJS BioLynx Inc.	SP-2002
Triton X-100	BioShop® Canada Inc.	RX777
Tween® 20	BioShop® Canada Inc.	TWN510
DAPI	Thermo Fisher Scientific Inc.	D1306

Table 2.1. List reagents used for the present project.

Antibody	**Manufacturer**	**Host**	**Catalogue number/ID**
Anti-rat biotin	Thermo Fisher Scientific Inc.	Mouse	SA1-25262
Anti-goat AlexaFluor™ 488	Invitrogen	Donkey	A32814
Anti-rabbit AlexaFluor™ 633	Biotium	Donkey	20125
Streptavidin, AlexaFluor™ 555 conjugate	Invitrogen	-	S32355
Anti-mouse Gr1 (Ly6g/Ly6c)	Thermo Fisher Scientific Inc.	Rat	14-5931-82

Anti-mouse TER119	Biolegend®	Rat	116202
Anti-mouse CD11b	Thermo Fisher Scientific Inc.	Rat	14-0112-82
Anti-mouse PDPN (Podoplanin)	R&D/Bio-techne Canada	Goat	AF3244
Anti-mouse ALP (Alkaline phosphatase, tissue non-specific)	Cedarlane/R&D	Goat	AF2910
Anti-mouse THBS4 (Thrombospondin 4)	Abcam	Rabbit	ab263898
Anti-mouse CD31 (PECAM-1)	R&D Biotechne	Goat	AF3628
Anti-mouse SM22 (TAGLN/Transgelin)	Abcam	Rabbit	AB14106
Anti-mouse CD16	Thermo Fisher Scientific Inc.	Rabbit	bs-6028r
Anti-mouse CD235a (Glycophorin A)	BioOrbyt	Rabbit	orb447561
Anti-mouse Aggrecan (Acan)	LSBio	Rabbit	LS-C359243
Anti-mouse Collagen type 2	Thermo Fisher Scientific Inc.	Rabbit	BS-0709R

Table 2.2. List antibodies used for the present project

Item	**Manufacturer**	**Catalogue number/ID**
10 x 32 x 0.75 mm A18 Adhesive silicone isolator	Grace Bio-Labs ©	RD500370
55 mm No. 1.5 Cover Slips	Epredia ©	152455
Endurium® Injector Solid Ceramic 0.010” Blades	Cadence Inc.	EF-INZ10
Nylon screen	Ted Pella, Inc.	41-3110
Superfrost Plus Microscope Slides	Thermo Fisher Scientific Inc.	12-550-15

Table 2.3. List miscellaneous items used for the present project.

Chapter 3: In situ characterization of proliferative myeloid cells in their bone marrow niche

3.1 Introduction

Myeloid-lineage cells derive from Lin-negative HPSCs primed towards myeloid differentiation up to the fully mature cell populations that form the red blood cells, platelets, and the innate immune system such as macrophages, neutrophils, eosinophils, basophils, and dendritic cells. This process is called myelopoiesis and occurs in the BM where it follows intricate steps defined by fast paced events of cell division and differentiation across cell identities including CMPs, MEPs, GMPs.

Myelopoiesis is a complex multistage process that always maintains consistent numbers of mature cells in circulation across tissues. Moreover, these mature cells differ in lifespans and functions, and their numbers vary depending on cases such as diseases, trauma, and infection. Hence, myelopoiesis is regulated and reactive to feedback from cells and molecules in the BM niche and from systemic factors.

Myelopoiesis has been extensively studied using flow cytometry, transplantation assays, and in vitro colony forming assays (CFUs). However, the BM niches where myeloid cells proliferate and differentiate remain elusive, with perhaps the exception of erythrocytes and megakaryocytes. Therefore, little is known about the BM niche cells and molecules that drive other aspects of myelopoiesis, including granulopoiesis.

Our lab recently identified a pattern of proliferative BM cells incorporating EdU that spatially distribute among the bone trabeculae of the epiphysis and metaphysis of the distal mouse femur. Moreover, our colleagues at the University of Toronto led by Dr Tikhonova determined that EdU incorporation occurs mostly among myeloid/granulocyte progenitor cells defined by the phenotype of Gr1 (Lin+Gr1+CD11b+), by means of flow cytometry (erythroid cells were not included in this assay, as they are known as the most proliferative cell type in BM) (Figure 3.2).

Following these findings, my thesis aimed at: 1. Confirming that the discrete patterns of proliferating BM cells observed in the metaphysis and epiphysis were indeed granulocyte progenitors, and 2. Identifying cells and molecules surrounding these proliferating cells to determine the composition of spatially relevant niches for granulocyte progenitors.

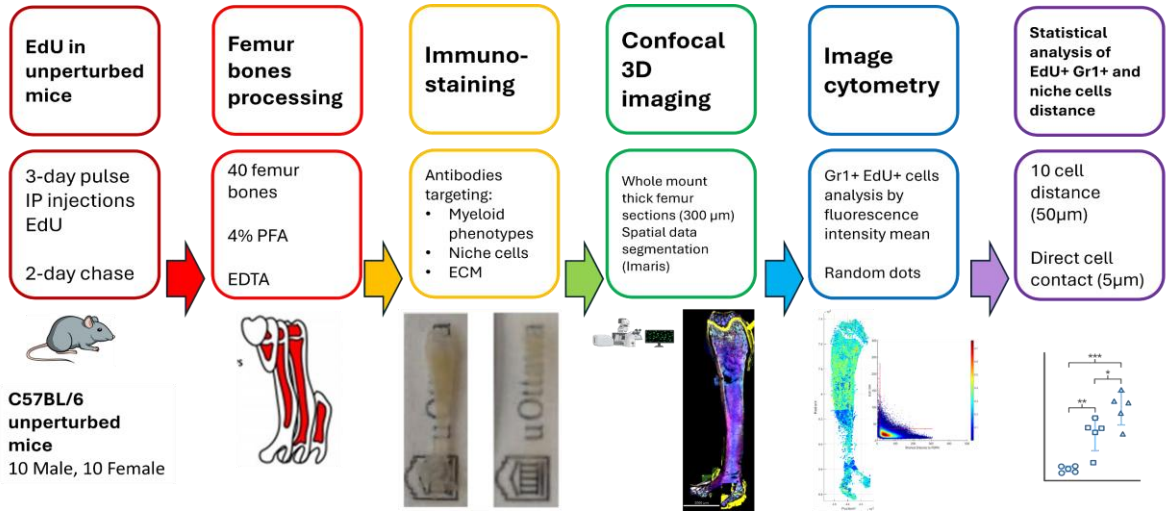

Figure 3.1 **Chapter 3 workflow followed to map the Gr1-myeloid proliferative niches in adult mouse femurs in situ**. Summary on the main steps followed to generate results described in Chapter 3, including details of the mouse model used, the amount of femur units, the femur bone processing (fixation and decalcification), IF staining, 3D imaging, image cytometry and statistical analysis of the distance variables.

3.2 Results

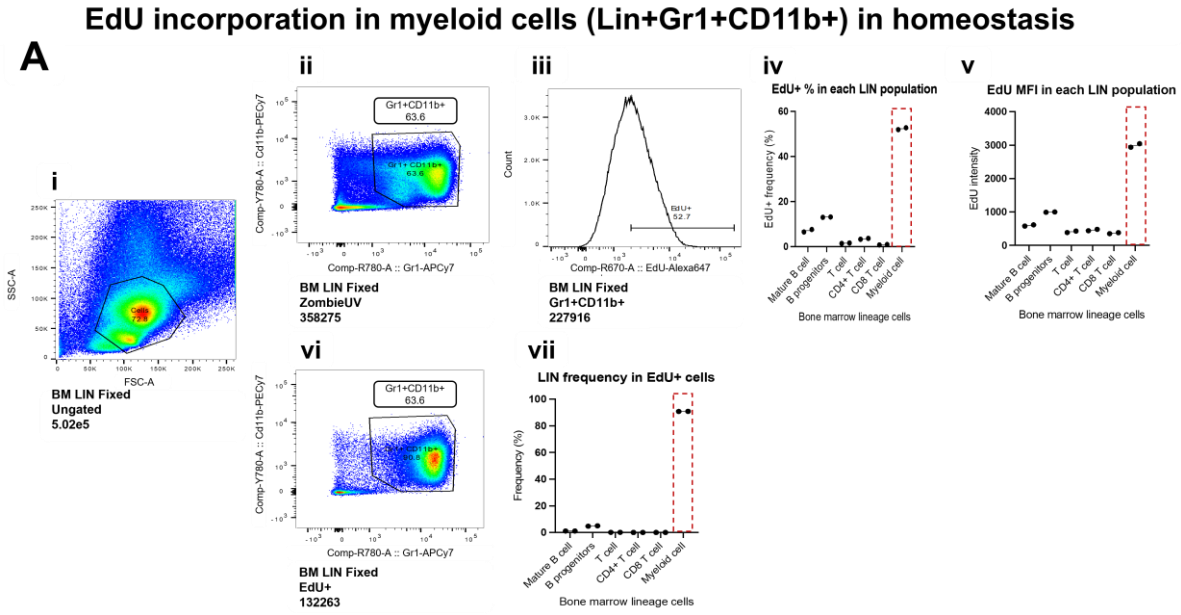

Figure 3.2 **EdU incorporation on hematopoietic panel reveals myeloid lineage cells as the most proliferative cells in the BM in homeostasis.** Flow cytometry performed by collaborators at the University of Toronto, MSc Candidate Li, Ximing led by Dr Tikhonova, Anastasia. EdU regime similar as described in Chapter 2, followed by hematopoietic panel to identify lymphoid (B220+high/int for progenitors or mature B cells, and CD3+. CD4+ and CD8+ for T cells, not shown) and myeloid lineage cells discarding the erythroid lineage. (A) Ungated BM cells (i), gating on specific Lin+ myeloid lineage Gr1+CD11b+ cells (ii), EdU proportion (Alexa 647, x-axis) in Gr1+CD11b+ counts (y-axis) (iii), and the plotted values of EdU frequency (%) and MFI (intensity) in y-axis across lineages included in the present assay in x-axis (iv, and v respectively), second gating strategy identifying EdU+ cells first in Lin+ myeloid lineage Gr1+CD11b+ cells among EdU+ counts (vi), and the plotted values of lineage frequencies (%) in EdU+ cells (vii). Data from X. Li & A. Tikhonova, University of Toronto.

3.2.1 EdU+ cells can be identified and imaged across the BM with great specificity by means of confocal microscopy

To confirm the specificity of EdU incorporation in proliferative cells, I initially looked at areas of the bone known to contain readily identifiable proliferative cells, such as the growth plate (GP) cartilage (Figure 3.3. B-D, GP). The GP can be divided in three distinct zones based on the size, shape and arrangement of chondrocytes: 1. A resting zone (RZ) towards the epiphysis where cells are quiescent, round, small sized and lack specific organization; 2. A proliferative zone (PZ) where cells are flat-shaped and arranged into columns of highly proliferative cells; and 3. A hypertrophic zone (HZ) where cells are larger in comparison to the previous regions and cease proliferation (Figure 3.3. D).

The PZ is composed of growth plate chondrocytes (GPCs) undergoing rapid proliferation and differentiation towards a hypertrophic phenotype[151]. Considering that the mice used were of juvenile age (12 weeks old), these GPCs in the PZ are known to be in active proliferation maintaining the longitudinal growth of the femoral bone. Given the cellular proliferation kinetics described in the GP, I confirmed the specificity of EdU incorporation and detection to proliferative cells (Figure 3.3). Therefore, I proceeded to screen antibodies for their capacity to detect myeloid cells in optically cleared, thick bone sections from postnatal mice.

3.2.2 Screening of antibodies to identify myeloid cells in the BM

In accordance with literature and our collaborators' initial flow cytometry screening (Figure 3.1), different antibodies were tested to attempt to detect different myeloid cell types, and these were as follows: 1) Granulocytes-neutrophils: Gr1 (Ly6G/Ly6C), 2) Monocytes-macrophages: CD11b (ITGAM, CD11b/CD18 Mac-1 heterodimer), 3) Monocytes, polymorphonuclear neutrophils and NK cells: CD16 (FCGR3A and FCGR3B, FC gamma receptor III), 4) Early and late-stage erythroblasts: CD235a (Glycophorin A), 5) Pan-erythroid cells: TER119 (Glycophorin A associated antigen).

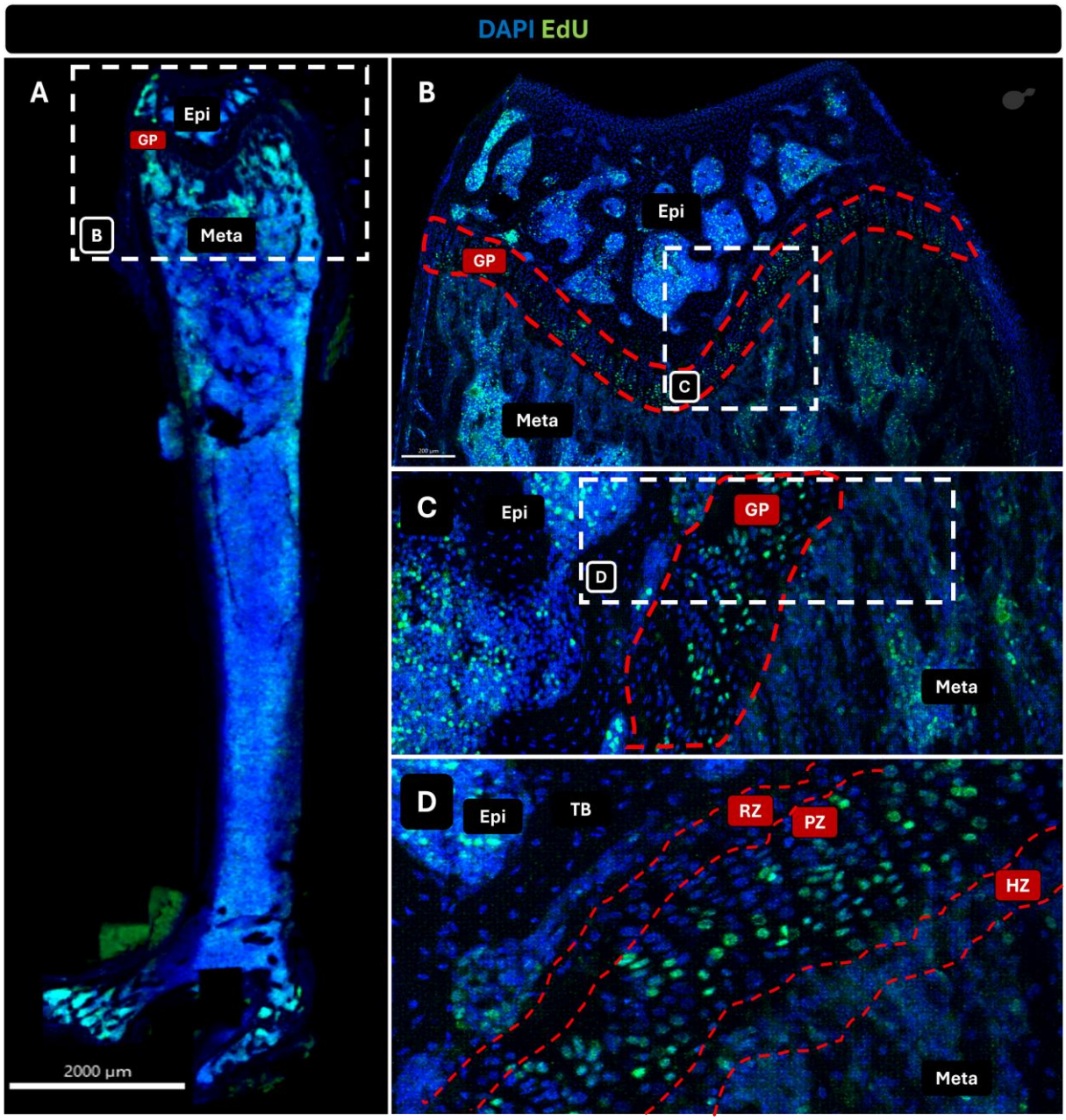

Figure 3.3 **EdU incorporation across the BM, cartilage, and bone.** 12-week-old C57Bl/6 mice were pulsed with EdU via IP injections for three consecutive days and femurs were harvested after 48h. 300µm-thick sections were stained with EdU Click-IT AlexaFluor594 detection kit (green) and nuclei were counterstained with DAPI (blue). (A) Whole femur section of female mouse, dashed region representing the area of interest containing the GP to identify EdU+ cells, full Z-volume snapshot, Scale bar: 2000µm. (B) Closer view of the distal femoral epiphysis and metaphysis shown in (A), red dashed region representing the GP. 35µm optical Z-volume slice shown. (C) Closer view of the GP (white dashed region in B) where columns of EdU+ GPCs are observed in the PZ and pre-hypertrophic zone, 35µm optical Z-volume slice shown. (D) Close up of the GP (white dashed region in C) showing each part of the GP: RZ with DAPI-only cells, PZ with DAPI and EdU+ cells arranged in columns, HZ with mostly enlarged DAPI EdU- cells. EdU+ integrates exclusively in nuclei of cells following cell division and de novo synthetized DNA, hence the specificity and differential fluorescent patterns between DAPI and DAPI EdU+ (green) stained nuclei.

From all antibodies tested, I was only able to optimize the use of Gr1 and TER119 antibodies. Other antibodies did not produce a detectable fluorescence signal when compared to controls or produced non-specific staining patterns (in bone, blood vessels, adipocytes, or other tissues) (not shown).

TER119 antibody produced an expected staining pattern (Figure 3.4. A-ii). Most TER119+ cells were found distributed within the vascular network (vascular network, Figure 3.4. A-i. TER119+ inside vascularity Figure 3.4. B-i). TER119+ with DAPI signal have prominent nuclei, with sizes around 6-10μm (Figure 3.4. B-ii, arrows). Meanwhile, TER119+ without DAPI are small sized around 2-5μm in diameter, sometimes smaller than DAPI stained nuclei, and appear flattened when seen perpendicularly to the Z-axis (Figure 3.4. Bi). Furthermore, these TER119+ cells appear clumped in confined vessels, impeding further segmentation (Figure 3.4. B-i, arrows). As expected, TER119+ cells depict cell morphology characteristics consistent to the series of myeloid cells from the early/late-stage erythroblast to erythrocytes in circulation, where is not possible to identify particular erythroid maturation stages by this signal alone (Figure 3.4).

Gr1 antibody produced a strong fluorescent signal when detected with streptavidin Alexa Fluor 555 amplification (Figure 3.5. A-B). The staining pattern observed was consistent with previous observations from our group (Coutu DL, personal communication) and recent literature also achieving staining of the BM tissue directly in situ[152]. The staining was restricted to the cell membrane of small and mostly round hematopoietic cells with prominent nuclei in the BM (Figure 3.5. C-ii), with clear distinguished signal from background staining (Figure 3.5. C i-ii). Overall, Gr1+ cells present in BM are nucleated small-sized with most of them ranging between 6-8μm in diameter, with prominent round nuclei that occupies most of the cell volume (Figure 3.5. C-ii).

In summary, I was able to optimize antibody staining for two myeloid cell markers on optically cleared, thick femur sections of postnatal mice. While our collaborators did not analyze EdU incorporation in erythroid cell populations by flow cytometry, is it well known that the erythroid lineage represents the majority of proliferative cells in BM[153]. However, since their proliferative and differentiation niche is already well described[154], I decided to pursue the study of Gr1+ granulocyte progenitors in subsequent experiments. The same population shown to be highly proliferative in the BM by our collaborators. Therefore, I proceeded to verify if the EdU+ cells we observed in the distal femur by means of co-staining of Gr1.

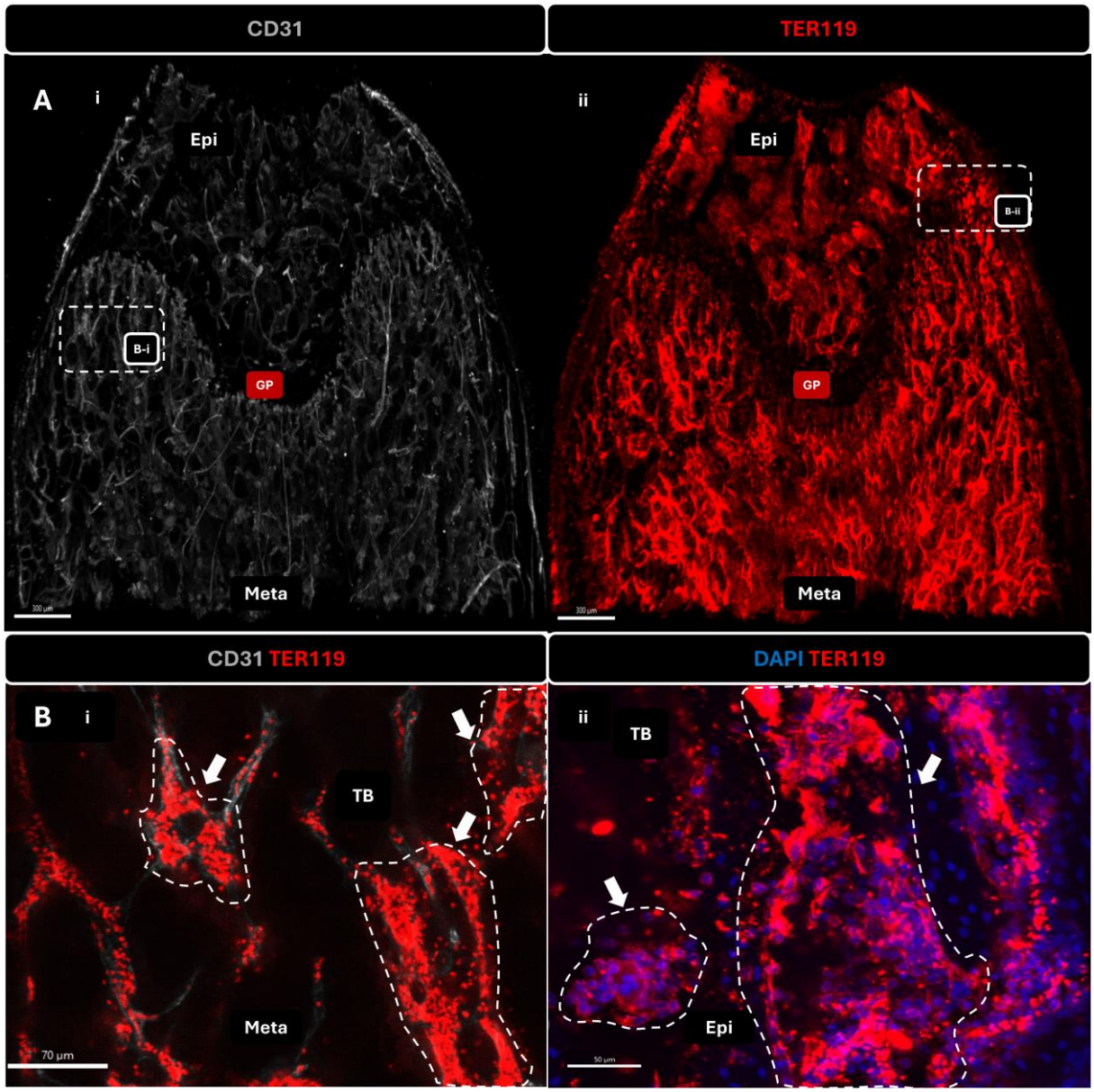

Figure 3.4 **TER119+ cells appear clumped and saturated in enclosed volumes.** 12-week-old C57Bl/6 female mice 300µm-thick femur section, labelling of Ter119+ cells and anti-biotin SA-AlexaFluor 555 amplification (red), CD31 (grey), and nuclei were counterstained with DAPI (blue). (A) Distal portion of femur bone, CD31 vasculature (i) and Ter119+ (ii); TER119+ cells distributed within BM and in the sinusoidal vascular network. Bone regions epiphysis (Epi), metaphysis (Meta) are shown; region of interest (dashed region), full volume snapshot, Scale bar: 300µm. (B) Close view of dashed regions in A), TER119+ small-sized cells inside CD31 vasculature (grey and arrows), cells appear clumped and saturated, not possible to effectively segment (i); TER119+ cells and their DAPI stained nuclei (blue) are small sized between 5-8µm with prominent nuclei, they appear clustered together and surrounded by non-nucleated cells saturating the signal (ii and arrows); 25µm optical Z-volume slice shown, scale bar: 70µm in B-i and 50µm in B-ii.

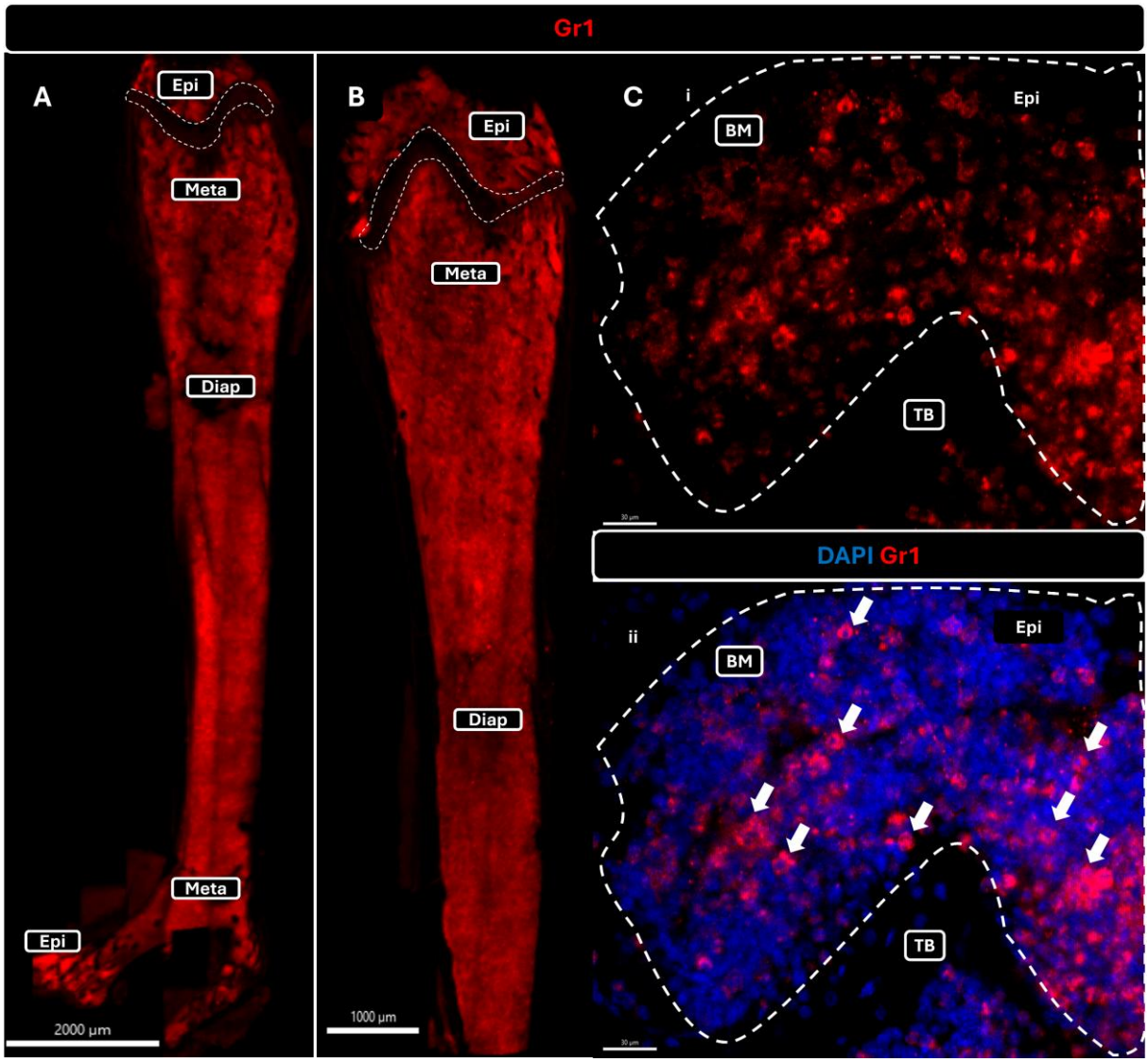

Figure 3.5 **Gr1 cells distributed homogeneously among the BM and stain specificity**. 12-week-old C57Bl/6 mice 300µm-thick femur section, labelling of Gr1+ cells and anti-biotin SA-AlexaFluor 555 amplification (red) and nuclei were counterstained with DAPI (blue). (A) Full femur bone section from female mouse (same female femur bone as in Figure 3.3), Gr1+ cells distributed with high homogeneity across the BM, bone regions epiphysis (Epi), metaphysis (Meta), and diaphysis (Diap); dashed region GP is shown. Full volume snapshot, Scale bar: 2000µm. (B) Half femur bone section from male mouse, Gr1+ cells distributed with high homogeneity across the BM, bone regions Epi, Meta, and Diap; revealing similar homogeneous distribution as seen in female femur in A, dashed region GP is shown. Full volume snapshot, Scale bar: 1000µm. (C) Close view of Gr1+ cells in female mouse femur epiphysis region divided by trabecular bone (TB) matrix, and BM contained inside trabeculae volume, 10µm optical Z-volume shown, Scale bar: 30µm (i); Close view of Gr1+ cells and DAPI as in (C-i), cells with clear prominent nuclei (examples indicated by white arrows), 10µm optical Z-volume shown, Scale bar: 30µm (ii).

3.2.3 Detection of proliferative Gr1+ cells in their bone marrow microenvironment

Our collaborators repeated the EdU incorporation regimen and showed, using flow cytometry, that Gr1+ granulocyte progenitors (Lin+Gr1+EdU+) were highly proliferative in the BM of juvenile mice. Following these results, I observed a spatially and anatomically enriched localized incorporation of EdU in BM cells located near trabecular bone (TB) in the distal metaphysis and epiphysis of 12wo mouse femurs.

After having optimized the staining protocol allowing me to detect proliferating cells incorporating EdU (Figure 3.3) and optimized the staining for Gr1 in these postnatal mice (Figure 3.5), I proceeded to optimize and confirm the co-staining for detection of EdU+ proliferative Gr1+ myeloid cells (Figure 3.6. A).

EdU was found to be incorporated by hematopoietic cells throughout the BM but showed a stronger signal near TB in distal metaphysis and epiphysis, and near cortical bone (CB) in the diaphysis (Figure 3.6. A-iii). On the other hand, Gr1+ cells were found mostly homogeneously distributed among the entire BM without a clear spatial organization (Figure 3.6. A-ii). In both cases (EdU and Gr1 staining), the fluorescent signal was well above the background fluorescence observed in artifacts among controls (Figure 3.6. B and C). Finally, the signals of both EdU+ and Gr1+ fluorescence provide a pattern useful to identify initial spatial distribution of the proliferative granulocytes of interest (Figure 3.6. A-i, dashed regions). Nonetheless, this initial pattern identified by optical means requires further quantitative-cytometry validation explored in in section 3.2.6.

Having established co-staining for Gr1+ and EdU+ cells useful for further co-localization, I next focused on exploring the spatial relationship between these cells and their microenvironment to identify the composition of their local niche. To do so, I screened antibodies and optimized immunostainings for various niche cell populations present in bone/BM that have been proposed to play a role on myelopoiesis/granulopoiesis, with a focus on cell types known to be abundant near trabecular or cortical bone (osteoblasts, chondrocytes, endothelial cells, and pericytes).

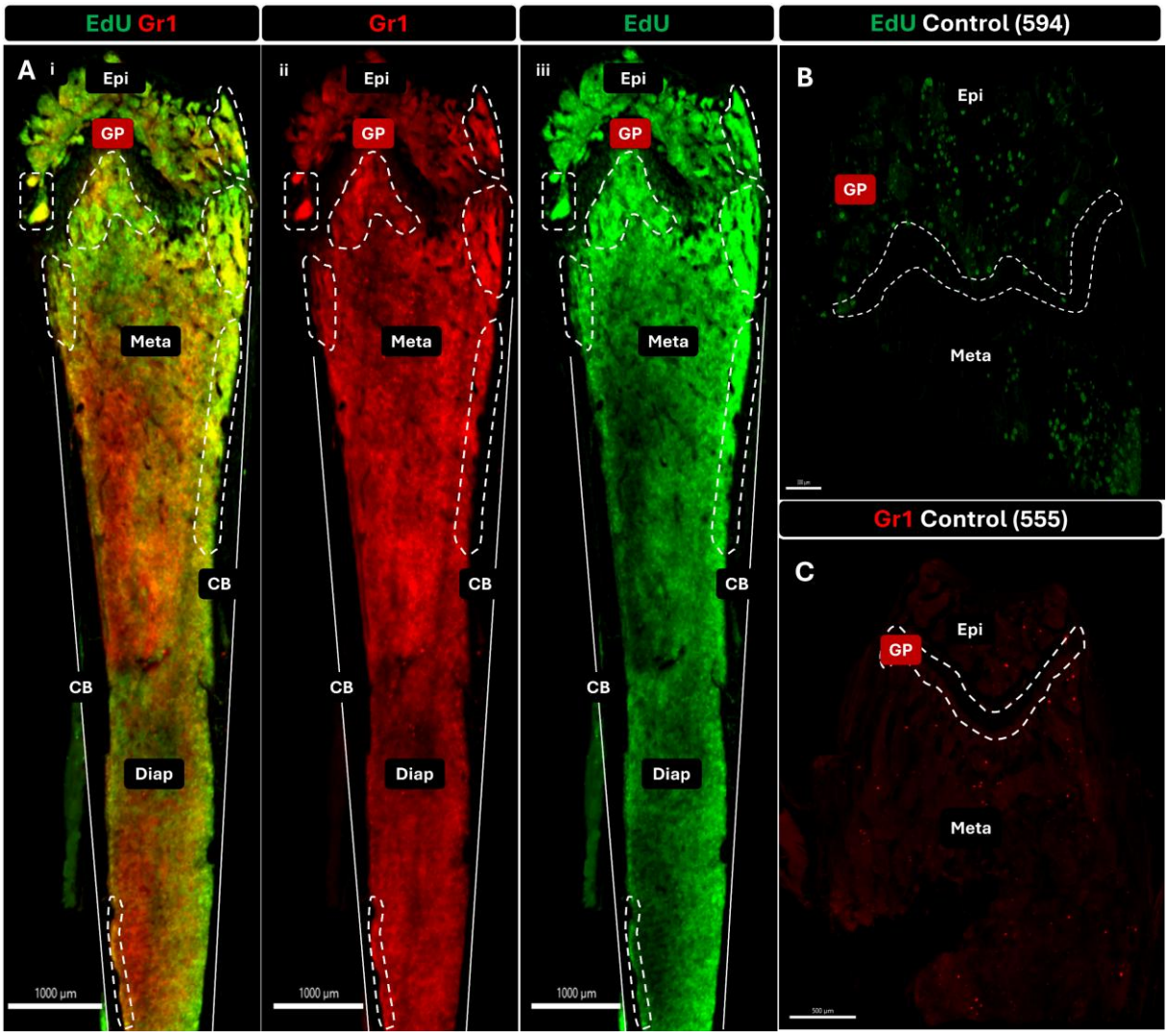

Figure 3.6 **Gr1+ EdU+ cells organized close to cortical bone and GP**. 12-week-old C57Bl/6 male mice 300µm-thick femur section (same male femur bone as in Figure 3.5. B), labelling of Gr1+ cells with anti-biotin SA-AlexaFluor 555 amplification (red) and EdU incorporation with AlexaFluor 594 (green). (A) Femur bone section, merged signals, Gr1+ cells and EdU+ cells distributed across the BM, bone regions epiphysis (Epi), metaphysis (Meta), diaphysis (Diap), and cortical bone CB; dashed region of BM where Gr1+EdU+ cells can be found are shown (i). Gr1+ stains the membrane of cells mostly homogeneously distributed across the BM, bone regions: Epi, Meta, Diap, and CB; dashed region of BM where Gr1+EdU+ cells can be found are shown in A-i) (ii); EdU+ cells (stained nuclei) distributed across the BM with clear higher presence close to CB and especially among the trabeculae of the Epi Meta, bone regions Epi, Meta, Diap, and CB; dashed region of BM where Gr1+EdU+ cells can be found are shown in A-i) (iii). Full volume snapshot, Scale bar: 1000µm. (B) Distal Epi and Meta of control sample without AlexaFluor 594, dashed region: GP, full volume snapshot, Scale bar: 500µm. (C) Distal Epi and Meta of control sample, without anti-Gr1 primary antibody treated with anti-biotin SA-AlexaFluor 555 amplification, dashed region: GP, full volume snapshot, Scale bar: 500µm.

3.2.4 Identification of osteochondral cells in postnatal bone/marrow

To stain, identify, image and analyze the bone and cartilage-associated tissues and cells, I selected three markers aimed to stain osteo-lineage derived cells. After screening several antibodies for their capacity to label osteoblasts and chondrocytes in postnatal bones, as well as

their compatibility for multiplexing with EdU and Gr1 staining. The three identified markers here selected and identified to be effectively stained with the present antibody strategy were: 1) alkaline phosphatase (ALP) antibody was found to label osteoblasts lining TB and CB matrix, 2) Podoplanin (PDPN) antibody to labeled osteoblasts in their final stage of their osteoblast-osteocyte transition most of them lining the bone surfaces across the entire femur, and a few of them embedded within the bone matrix; and 3) thrombospondin 4 (THBS4) antibody showed strong labeling of chondrocytes in the GP cartilage and articular cartilage (AC), as well as periosteal cells near the GP (Figure 3.7).

ALP stained the surfaces of bone structures across the entire femur. It provides a detailed fluorescent pattern that allows to appreciate the intricate bone structures that define the trabeculae at the epiphysis and metaphysis, as well as the surface of the endosteal and periosteal surfaces of CB (Figure 3.7. A). Furthermore, it did not stain the inner volume of the bone matrix, suggesting expression in bone lining osteoblasts (Supplemental Figure 3.1. Ai-ii). ALP was also observed in the HZ of the GP in a less intense fluorescent pattern.

PDPN was found to specifically stain the membrane of large cells (10-15μm radius), most of them located on the bone surfaces facing towards the volume where BM is found in both TB and CB. In a lesser extent, some PDPN+ cells are found embedded in the bone matrix of both TB and CB (Figure 3.7. B). This suggests that PDPN is a reliable marker of late-stage osteoblasts and some matrix-embedded osteocytes with their particular stellate-like morphology as literature suggests. Like ALP stain, PDPN is also found in the HZ of the GP with a less intense fluorescence (Supplemental Figure 3.1. Bi-ii).

As already mentioned, THBS4 antibody showed expression in all cartilage structures (GP and AC) but also in periosteal cells located near the GP (Figure 3.7. C). It stained the entire thickness of the GP, which is the relevant region here explored as putative chondrogenic niche of Gr1+EdU+ cells (Supplemental Figure 3.2).

All of these antibodies provided a fluorescence signal well above and specific of that from controls (Figure 3.7. D-E).

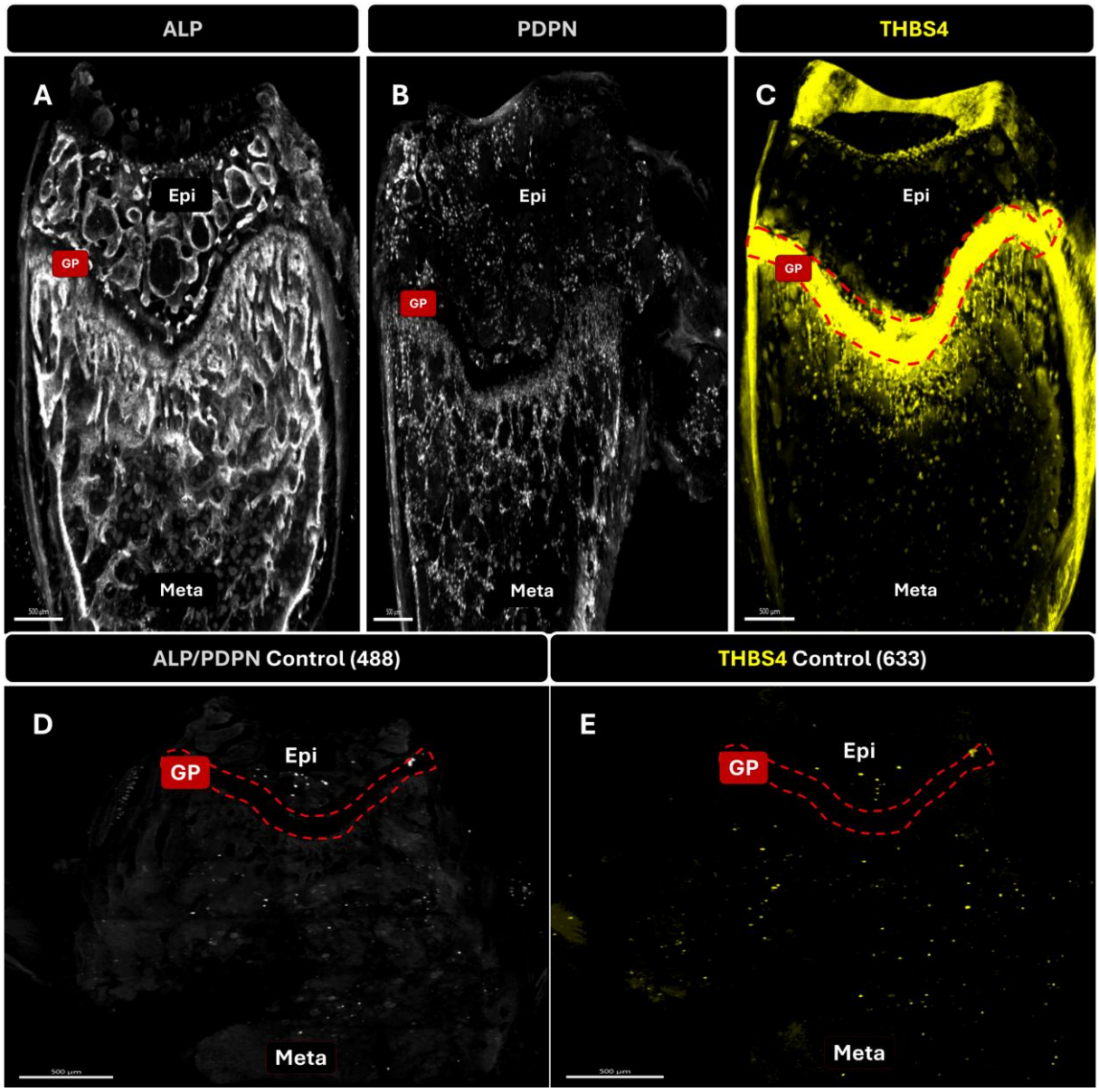

Figure 3.7 **ALP, PDPN and THBS4 identifies osteo-chondral tissues**. Immunostaining of ALP (AlexaFluor 488, white), PDPN (AlexaFluor 488, white), and THBS4 (AlexaFluor 633, yellow), reveal bone surfaces, osteoblasts-osteocytes, and chondrocytes, respectively. 12-week-old C57Bl/6 mice 300µm-thick femur section. (A) Distal epiphysis (Epi) and metaphysis (Meta) of female mouse femur, showing ALP expression at the surfaces of bone structures defining the intricated trabeculae spatial pattern, and the endosteal surface of CB, full volume snapshot, Scale bar: 500µm. (B) Distal Epi and Meta of male mouse femur, with specific PDPN staining of the osteoblasts-osteocytes across the bone structures defining the intricated trabeculae spatial pattern, full volume snapshot, Scale bar: 500µm. (C) Same region shown in (A), with THBS4 staining of chondrocytes within the GP (dashed region) as well as in articular cartilage and periosteal cells, full volume snapshot, Scale bar: 500µm. (D) Distal Epi and Meta of control sample, without anti-ALP or anti-PDPN primary antibodies treated with secondary anti-goat AlexaFluor 488, dashed region: GP, full volume snapshot, Scale bar: 500µm. (E) Distal Epi and Meta of control sample, without anti-THBS4 primary antibody treated with secondary anti-rabbit AlexaFluor 633, dashed region: GP, full volume snapshot, Scale bar: 500µm.

3.2.5 Identification of vascular and perivascular cells in the postnatal BM

To identify vascular and perivascular cells in the postnatal BM, I chose two of the best-known antibodies for their capacity to detect vascular cell types and the possibility to multiplex in conjunction with Gr1 and EdU staining. These two antibodies were: 1) one targeting the "pan-endothelial" marker CD31 (Pecam-1), and 2) on targeting the smooth muscle cell marker SM22 (Transgelin, *Tagln*).

CD31 successfully stains the entire, extensive and intricate network of blood vessels that fill most of the BM volume. The stained vessels can differ from their caliber size drastically, from the thin arterioles and capillaries to the larger venous sinusoids (Figure 3.8. A-i). Notably, no vascularity can be found across the GP, similar to the disposition of Gr1 cells.

In contrast, SM22 stains with great specificity the pericytes surrounding the large arteries stained by CD31. The pericytes are clearly arranged in a ring-shaped morphology of consecutive smooth muscle cells covering the entire CD31+ surface of arteries. These pericytes start showing a scattered pattern between each other once the arteriole extends beyond the CB into the BM volume, until they become completely absent (Figure 3.8. A-ii), with a few exceptions seen in the distal epiphysis (Supplemental Figure 3.3. Red arrows). Finally, these pericytes present the characteristic flattened and elongated nuclei (Supplemental Figure 3.3. Red arrows).

When merged, it is possible to identify and differentiate the arteriolar and the sinusoidal-capillary vasculature, where arteries with SM22+ cells locate mostly embedded inside the matrix of CB at the metaphysis and part of diaphysis, and the remaining CD31+ extents all over the Bone/BM except for the GP (Figure 3.8.A-iii, and Supplemental Figure 3.3).

Both antibodies provided a fluorescence signal well above and specific of that from the controls (Figure 3.8. B-C).

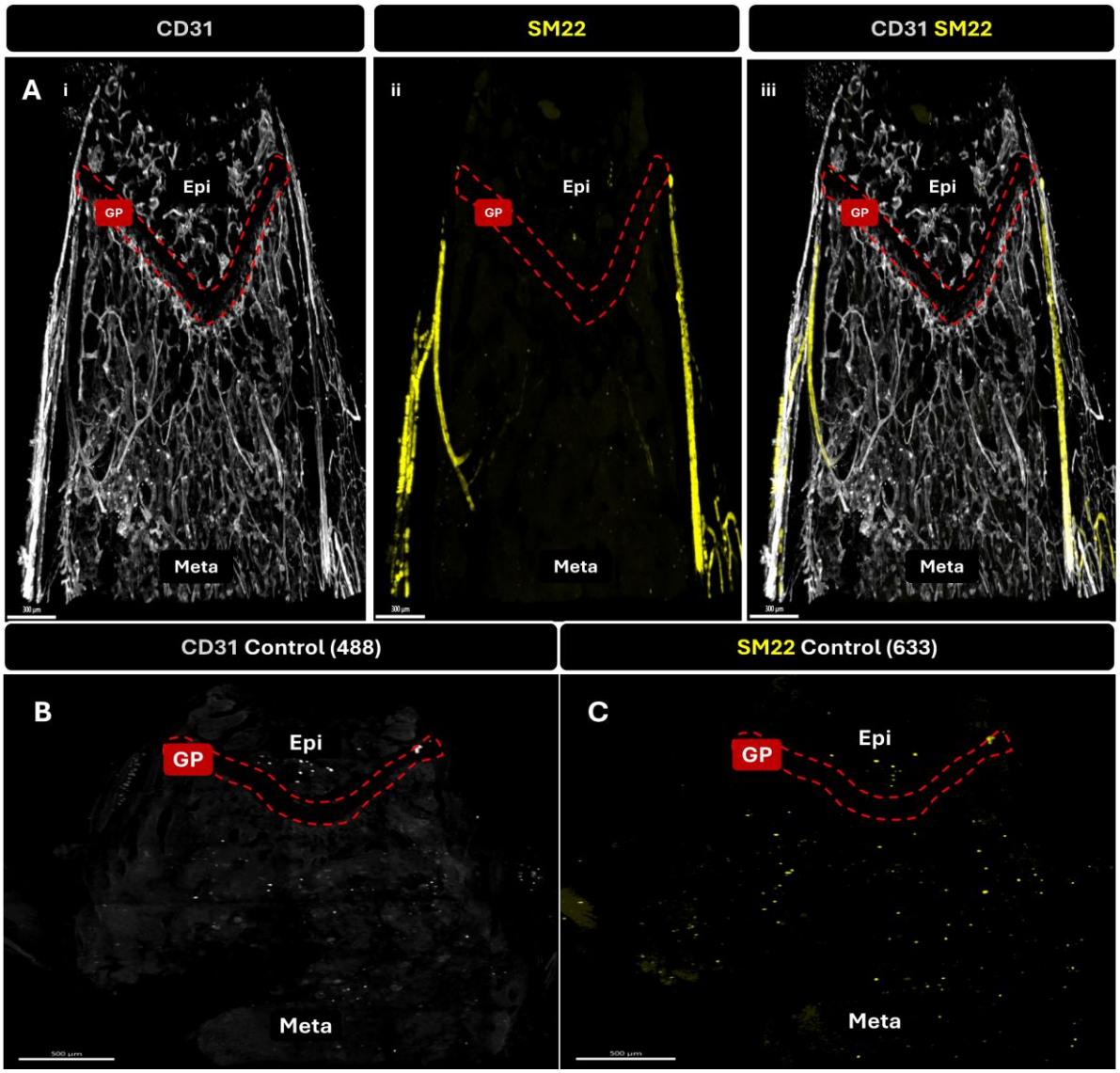

Figure 3.8 **CD31 and SM22 identify vascular and perivascular cells.** Immunostaining of vascularity with CD31 and AlexaFluor 488 (white), and pericytes on arteries/arterioles with SM22 and AlexaFluor 633 (yellow) cells, reveal the entire network of vascularity across the BM and bone. 12-week-old C57Bl/6 female mice 300µm-thick femur section. (A) Distal epiphysis (Epi) and metaphysis (Meta) of femur, with highly specific extensive CD31+ marker fluorescent pattern of the entire vascular network, from different caliber sized vessels across the BM and the bone, with clear absence inside the GP. Full volume snapshot, Scale bar: 300µm (i); highly specific SM22+ marker fluorescent pattern of the pericytes cells around the thickest vessels mostly restricted to the CB of the distal Meta towards the diaphysis, full volume snapshot, Scale bar: 300µm (ii); merged CD31+ and SM22+ florescence, showcasing the specificity of the stain to identify differentially the arteriole vascularity depicted by the conjunction of CD31 and SM22, full volume snapshot, Scale bar: 300µm (iii). (B) Distal Epi and Metta of control sample, without primary anti-CD31 treated with secondary AB (anti-goat AlexaFluor 488), dashed region: GP, full volume snapshot, Scale bar: 500µm. (C) Distal Epi and Meta of control sample, without primary anti-SM22 treated with secondary AB (anti-rabbit AlexaFluor 633), dashed region: GP, full volume snapshot, Scale bar: 500µm.

3.2.6 Spatial and anatomical relationship between EdU+Gr1+ cells and their BM niche

Having established an IF staining panel and protocol for optimal multiplexing to identify and locate proliferative Gr1+ cells and niche cells within their microenvironment, I proceeded to compute and quantify the spatial and anatomical relationships between these cell types. This would allow me to identify which niche cells are spatially-locally enriched and may be involved in inducing proliferation of Gr1+cells. To achieve this, femurs were stained for EdU and Gr1, as well as the niche cell markers described in section 3.2.4 and 3.2.5. Following confocal imaging, the Gr1+ cells were segmented using Imaris, their EdU incorporation was quantified and their 3D spatial relationships with the niche cells were computed and compared with random dots (RDs) generated with XiT, with the RDs representing a random distribution of cells within the BM. Finally, these image cytometry results and analysis were performed based on the EdU-FMO, which determined the threshold of the mean fluorescent intensity (MFI) set at 35-MFI, generated by AF and artifacts detected in the EdU-fluorescent associated channel in control samples, hence, the results here reached are of EdU-MFI above the FMO threshold.

To examine the spatial relationship between proliferating Gr1+ cells and bone cells, I first co-stained femurs with EdU, Gr1 and ALP (Figure 3.9. A-i). As previously mentioned, segmented Gr1+ cells showed a nearly homogeneous distribution in the BM of the distal epi-metaphysis (Figure 3.8. A-ii, left). However, when in conjunction, the distribution of Gr1+EdU+ cells is found to be enriched in hotspots across the BM located in trabeculae cavities (Figure 3.9. A-ii, right). Quantification demonstrated that the majority of Gr1+EdU+ cells were located within 5-cell diameters (50μm) of ALP+ cells (Figure 3.9. A-iii). Indeed, 81.13% (+/- 3.62 SD) of Gr1+EdU+ cells were located near ALP+ osteoblasts, as opposed to 18.27% (+/- 3.62 SD) located further than 5-cell diameters from osteoblasts (Figure 3.9. A-iv). This spatial tendency was significantly different compared to RDs, that showed almost equal distribution close (<50μm) and far (>50μm) from osteoblasts. Overall, this suggests that proliferating Gr1+ cells locate preferentially close to ALP+ osteoblasts, in a non-random spatial distribution pattern.

In the femoral diaphysis TB is absent, ALP+ osteoblasts are observed only restricted to the endosteal surface of CB (Figure 3.9. B-i). Here again, Gr1+ cells appear homogeneously distributed throughout the BM cavity (Figure 3.9. B-ii, left), and their incorporation of EdU appears higher near cortical bone surfaces (Figure 3.9. B-ii, right). However, this enrichment near

bone is not as pronounced (Figure 3.9. B-iii) and varies between samples analyzed. Moreover, this spatial distribution was not different when compared to RDs (Figure 3.9. B-iv).

To account for the distribution and quantification of Gr1+EdU+ cells that were in direct contact with ALP+ osteoblast to identify the most proximal spatial niche arrangement in the distal epi-metaphysis, I reduced the distance value to 5μm (Figure 3.9. C). Although a significant proportion of Gr1+EdU+ were found in direct contact with ALP+ osteoblasts (24.25%, with +/- 6.245 SD), the majority were found further away (75.75%, with +/- 6.245 SD). Moreover, this distribution was not significantly different from RDs spatial distribution. This suggests that a potential crosstalk between osteoblasts and Gr1+ cells promoting their proliferation is more likely through soluble factors rather than direct cell-cell contact.

To confirm the preferential enrichment of Gr1+EdU+ cells near osteoblast-lineage cells, I performed the same analysis, this time using PDPN to identify bone cells (Figure 3.9. D-i). Once again, proliferating Gr1+ cells were found enriched near PDPN+ cells (Figure 3.9. D-ii). Furthermore, the plotted replicate values revealed a higher proportion of 91.14% (+/- 7.779 SD) of Gr1+EdU+ cells closer than 50μm, a tendency significantly different than a random distribution (Figure 3.9. D-iii).

To further confirm the preferential enrichment of proliferating Gr1+ cells near bone-related cells, I then quantified their spatial relationship with THBS4+ chondrocytes (Figure 3.9. E-i). As expected, the majority of Gr1+EdU+ cells (50.33%, +/- 18.09 SD) localized further than 5-cell diameters (>50μm) from chondrocytes (Figure 3.9. E-ii), a spatial distribution pattern that was not significantly different from RDs (Figure 3.9. E-iii). Meanwhile, there are very few Gr1+EdU+ cells in direct contact with THBS4+ chondrocytes (3.9%, +/- 2.285 SD) (Figure 3.9. E-iv).

Finally, to analyze spatial relationship between proliferating Gr1+ cells and vascular/perivascular cells, I co-stained EdU, Gr1, CD31, SM22, and DAPI (Figure 3.10. A). As in previous results, Gr1+ cells uniformly distributed across the BM volume in the distal epi-/metaphysis (Figure 3.10. B, left), with Gr1+EdU+ consistently located in hotspots among TB (Figure 3.10. B, right). Here, Gr1+EdU+ cells were found enriched close to CD31+ blood vessels (Figure 3.10. C), which is coherent with the abundance of blood vessels in BM. However, this spatial relationship was significantly different from that of RDs (Figure 3.10. D), with nearly 100% of Gr1+EdU+ cells localizing closer than 5-cell diameters from blood vessels (98.94%, +/- 0.97

SD, compared to 40.75%, +/- 3.21 SD for random dots). Moreover, 63.52% (+/- 10.52 SD) of the Gr1+EdU+ cells were found in direct contact with CD31+ blood vessels (Figure 3.10. E), as opposed to the 7.26% (+/- 2.81 SD) for randomly distributed dots. In contrast, when analyzed the spatial relationship between Gr1+EdU+ cells and SM22+ perivascular cells, I found that Gr1+EdU+ cells did not show a preferential enrichment close to SM22+ pericytes (Figure 3.10. F). This was not surprising given to low abundance of SM22+ pericytes in BM. However, when I compared this spatial distribution to RDs, I found that Gr1+EdU+ cells distribute preferentially closer to SM22+ pericytes than a random distribution could account for (Figure 3.10. G). The number of Gr1+EdU+ cells in direct contact with SM22+ pericytes was on the other hand not different from RDs (Figure 3.10. H).

Taken together, these results suggest that proliferation of Gr1+ cells may be promoted by osteoblasts-like cells through soluble factors, by endothelial cells through soluble factors and direct cell-cell contact, and by pericytes through soluble factors. To identify molecular pathways and crosstalk between Gr1+ granulocyte progenitors and their niche that could provide further clues of this increase in proliferation through cell communication mechanisms, I decided to interrogate gene expression in these target cell types using bioinformatics and single cell RNAseq databases available from the literature.

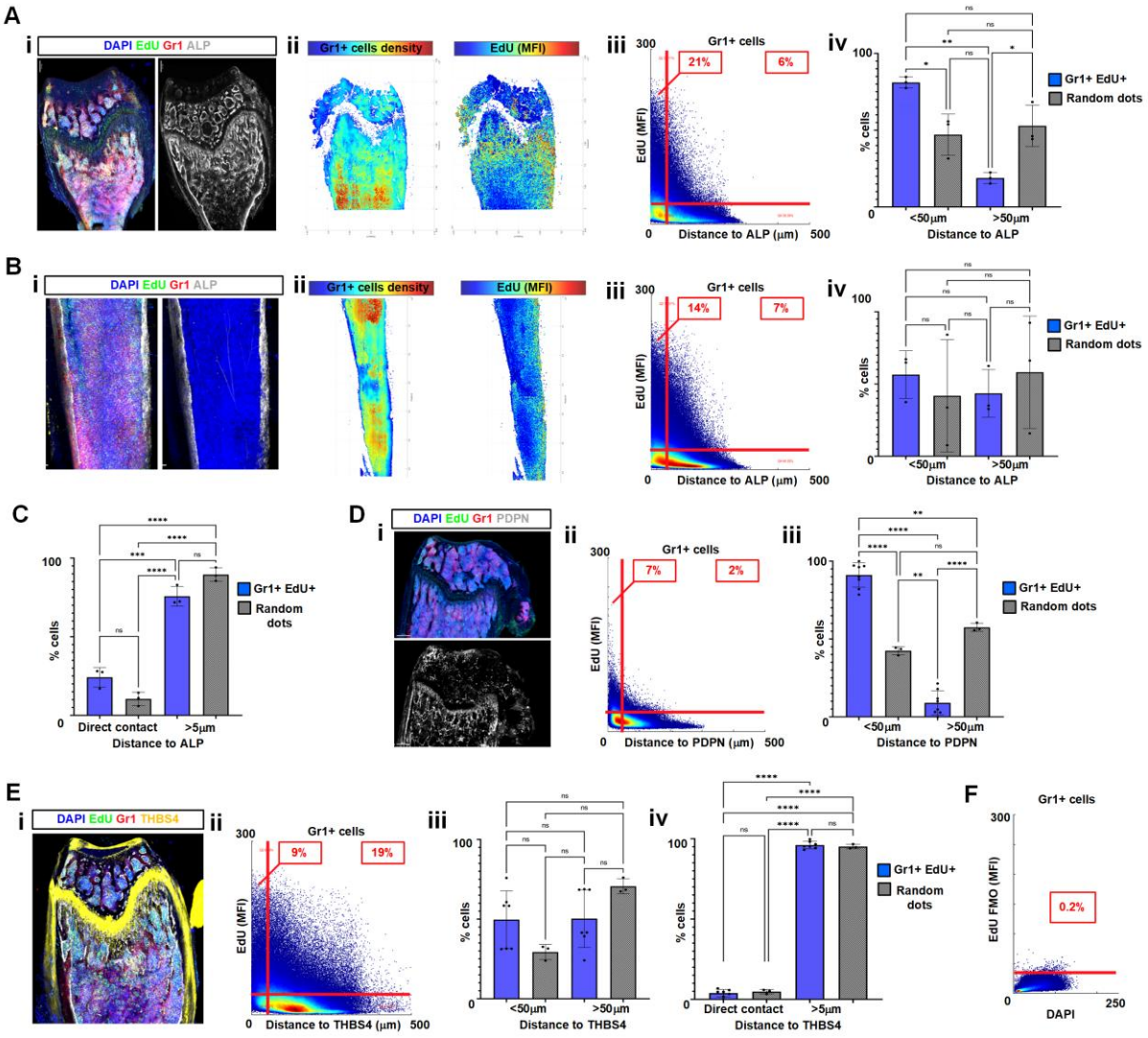

Figure 3.9 **Spatial and anatomical relationship between Gr1+EdU+ cells and the osteochondral niche**. Data collected from 12-week-old C57Bl/6 mice of both male and female sex, based on 300µm-thick femur sections obtained after daily pulse of EdU (3 days) though IP injection, and sample collection after 48 hours. Statistical analysis done based on replicate (triplicates at minimum) data collected. Imaging datasets were spatially split to analyze the distal epi-/metaphysis and diaphysis separately. (A) Femur were stained with Click-IT EdU detection kit (green), Gr1 antibody (red), ALP antibody (grey), and nuclei counterstained with DAPI (blue) (i). In the distal epi-/metaphysis, Gr1+ cells were segmented (ii, left) and their expression of EdU quantified (ii, right). The shortest distance between Gr1+EdU+ cells and ALP+ osteoblasts was computed (iii) and compared to randomly distributed dots (iv). (B) Same analysis as in (A) but performed on the diaphysis. (C) Analysis of direct cell-cell contact between Gr1+EdU+ cells and ALP+ osteoblasts in the distal epi-/metaphysis. (D) Same analysis as in (A-B) but with PDPN (grey) as an osteo-lineage cell marker. Only distal epi-/metaphysis shown. (E) Same analysis as in (A-B-C) but with THBS4 (yellow) as a chondrocyte marker. Only distal epi-/metaphysis shown. (F) FMO control for EdU staining showing the gating threshold used in all analyses. Bar graphs show mean +/- SD of all replicates overlayed with individual data points (blue); with random dots analyses performed in triplicate (grey).

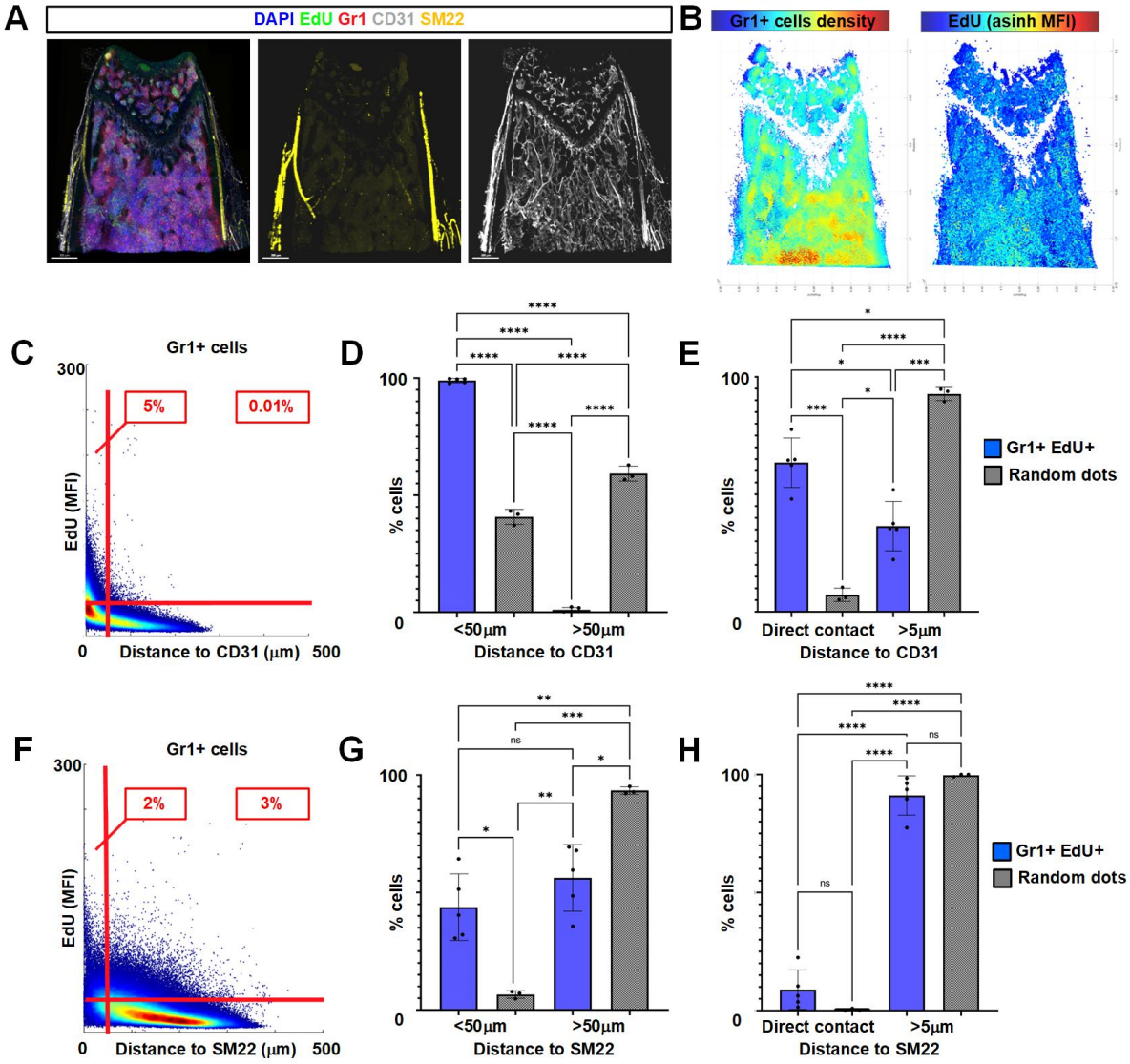

Figure 3.10 **Spatial and anatomical relationship between Gr1+EdU+ cells and the vascular/perivascular niche**. Data collected from 12-week-old C57Bl/6 mice of both male and female sex, based on 300µm-thick femur sections obtained after daily pulse of EdU (3 days) though IP injection, and sample collection after 48 hours. Imaging datasets were spatially split and only the distal epi-/metaphysis is shown. (A) Femur were stained with Click-IT EdU detection kit (green), Gr1 antibody (red), CD31 antibody (grey), SM22 antibody (yellow), and nuclei counterstained with DAPI (blue). (B) Gr1+ cells were segmented (left) and their expression of EdU quantified (right). (C) The shortest distance between Gr1+EdU+ cells and CD31+ endothelial cells was computed. (D) The spatial distribution of Gr1+EdU+ cells around CD31+ blood vessels was compared to randomly distributed dots. (E) Direct contact between Gr1+EdU+ cells and CD31+ blood vessels was compared to randomly distributed dots. (F) The shortest distance between Gr1+EdU+ cells and SM22+ pericytes was computed. (G) The spatial distribution of Gr1+EdU+ cells around SM22+ pericytes was compared to randomly distributed dots. (H) Direct contact between Gr1+EdU+ cells and SM22+ pericytes was compared to randomly distributed dots. Bar graphs show mean +/- SD of all replicates overlayed with individual data points (blue); with random dots analyses performed in triplicate (grey).

3.3 Supplemental data

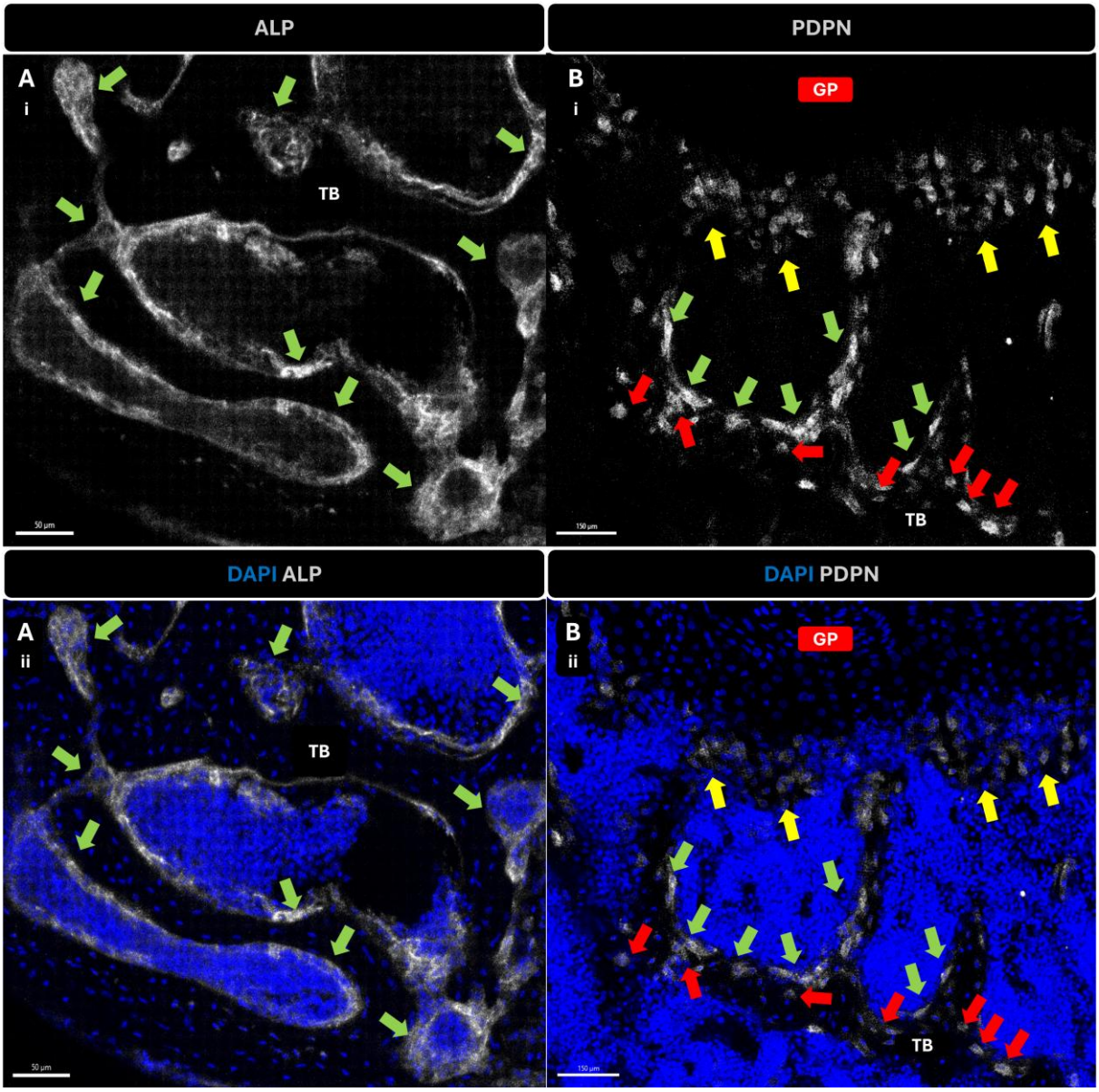

Supplemental Figure 3.1

Detailed staining of ALP+ and PDPN+ osteogenic niche cells. Immunostaining of ALP (AlexaFluor 488, white) and PDPN (AlexaFluor 488, white), revealing distinct patterns of staining of osteoblasts and osteoblasts-osteocytes, respectively. 12-week-old C57Bl/6 mice, 35µm optical Z-volume slice shown. (A) Distal epiphysis of female mouse femur, showing ALP expression at the surfaces of bone structures defining the bone forming-remodelling osteoblasts (green arrows) across the trabeculae (TB) spatial pattern (i), and the specificity of the ALP staining restricted to only cells facing towards the TB cavities in contact with the BM cells (not embedded in bone matrix) as revealed by counterstain DAPI (ii). Scale bar: 50µm. (B) Distal metaphysis of male mouse femur, with specific PDPN staining of the osteoblasts-osteocytes across the TB, PDPN+ cells can be found deriving from the GP (yellow arrows), lining the TB surfaces facing towards the TB cavities in contact with the BM cells (green arrows) and osteocytes embedded inside the TB matrix (red arrows) pattern (i), and extra detail of the BM, bone and GP cells with counterstain DAPI (ii). Scale bar: 150µm.

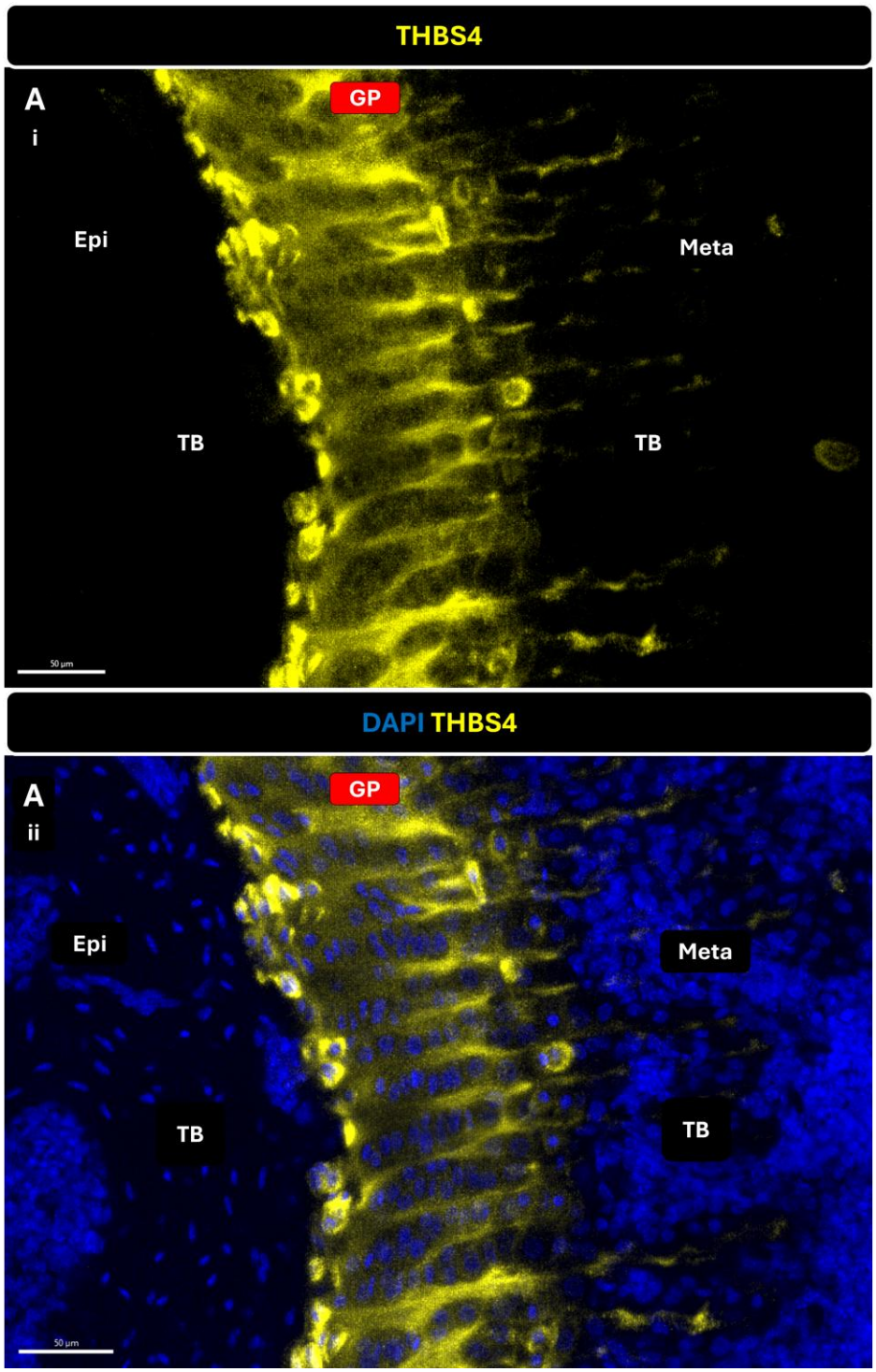

Supplemental Figure 3.2

Detailed staining of THBS4+ chondrogenic niche cells. Immunostaining of THBS4 (AlexaFluor 633, yellow) defining the chondrocytes across the growth plate (GP). 12-week-old C57Bl/6 mice, 35µm optical Z-volume slice shown. (A) Distal epiphysis (Epi), GP and metaphysis (Meta) of female mouse femur, showing THBS4 expression as an ECM component surrounding the columns of growth plate chondrocytes (GPCs) throughout the entire thickness of the GP, and its restricted extension towards the TB of the metaphysis where THBS4 fades (i), and the specificity of the THBS4 staining restricted to only GPCs as revealed by counterstain DAPI (ii). Scale bar: 50µm.

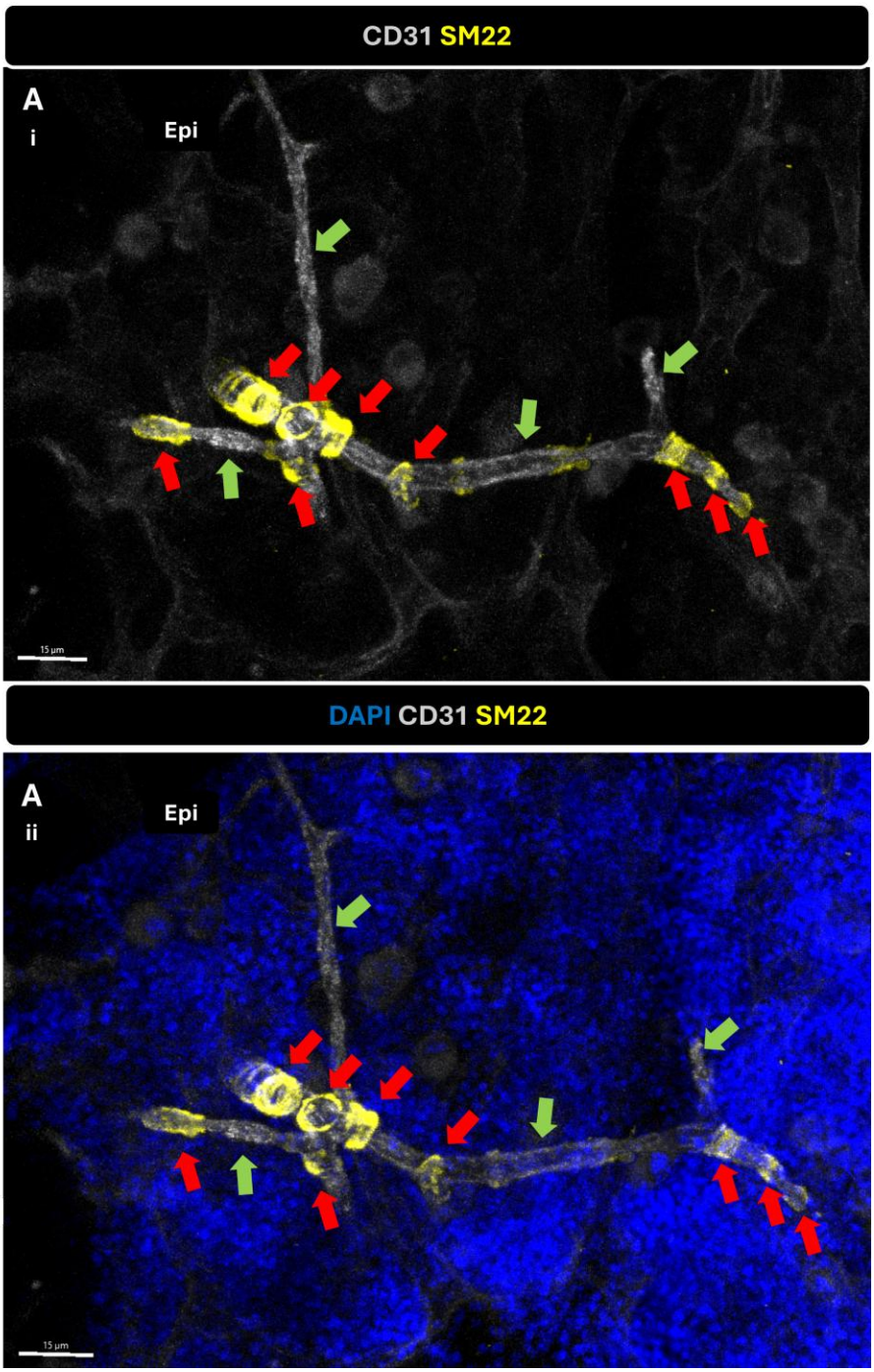

Supplemental Figure 3.3

Detailed staining of CD31+ and SM22+ vascular and perivascular niche cells. Immunostaining of CD31+ (AlexaFluor 488, white) and SM22+ (AlexaFluor 633, yellow), cells staining the endothelial cells (ECs) of the entire BM vascularity and the BM pericytes, respectively. 12-week-old C57Bl/6 mice, 35µm optical Z-volume slice shown. (A) Distal epiphysis (Epi) of female mouse femur, showing CD31+ expression of the BM vascularity by staining all of the ECs, revealing the diverse BM vascular network such as thin vessels (CD31+ ECs, green arrows) and thicker arterioles (CD31+ ECs and SM22+ pericytes, red arrows) across the BM volume in one of the few instances where arterioles could be found across the of BM of the Epi, spatial pattern (i), and the specificity of the CD31+ and SM22+ staining restricted to the BM vascular network across the BM volume as revealed by counterstain DAPI (ii). Scale bar: 15µm.

Chapter 4: Molecular communication networks between myeloid progenitors and their niche at single-cell transcriptomics resolution

4.1 Introduction

Transcriptomic-based assays that can sequence the entire transcriptome at a single-cell resolution are powerful tools for identifying specific cell subpopulations and the set of differentially expressed genes that define their cellular identity.

Briefly, each cell identity is determined by the combination of actively transcribed genes which provide the cells with competence to perform unique tasks under the context of their residing tissue. Therefore, identifying the transcriptome at single-cell resolution enables the effective differential analysis of active genes and cell functions related to the tissue of interest and has the potential to reveal previously unknown functional cellular heterogeneity with key features.

For BM and niche cells, one of the most relevant public datasets was generated by Baccin, et al, with the purpose of exploring further the cellular source of two well-known key cytokines that mediate HSCs functions, CXCL12 and Stem Cell Factor (SCF, or KitL)[142]. Other datasets have been generated with the sole focus to identify the cell composition of the BM stroma and better describe its taxonomy (Baryawno, et al. and Tikhonova, et al)[36,74]. They followed the expression of key markers expressed by non-hematopoietic mesenchymal cells critical to the BM niche maintenance, such as CXCL12, SCF, LepR and NG2[74]. Finally, to overcome the limitations of the low frequency of HSCs and HPSCs with relevant myeloid potential, the dataset generated by Kucinski, et al. became useful, as they focused on sequencing HSCs and HSPCs at different time points following labeling of HSCs using the Hoxb5-CreERT2-Tomato mice line, to explore kinetics of differentiation from HSCs to HSPCs towards more differentiated stages[143].

In this chapter, I used the python-based probabilistic model for single-cell transcriptomic data SCVI-tools, to merge and integrate these datasets, then identify and annotate relevant cell types representing hematopoietic, myeloid and niche cells. Finally, with this integrated dataset, I explored the inference of cell communication networks using the R-based tool CellChat v2, with particular focus on Gr1+ myeloid cells, granulocyte progenitors and niche cells. (Figure 4.1). My analysis focused on the molecular crosstalk between the relevant niche cell types identified in

Chapter 3 and the myeloid progenitors, to explain why the latter cells proliferate preferentially in spatial proximity to the former.

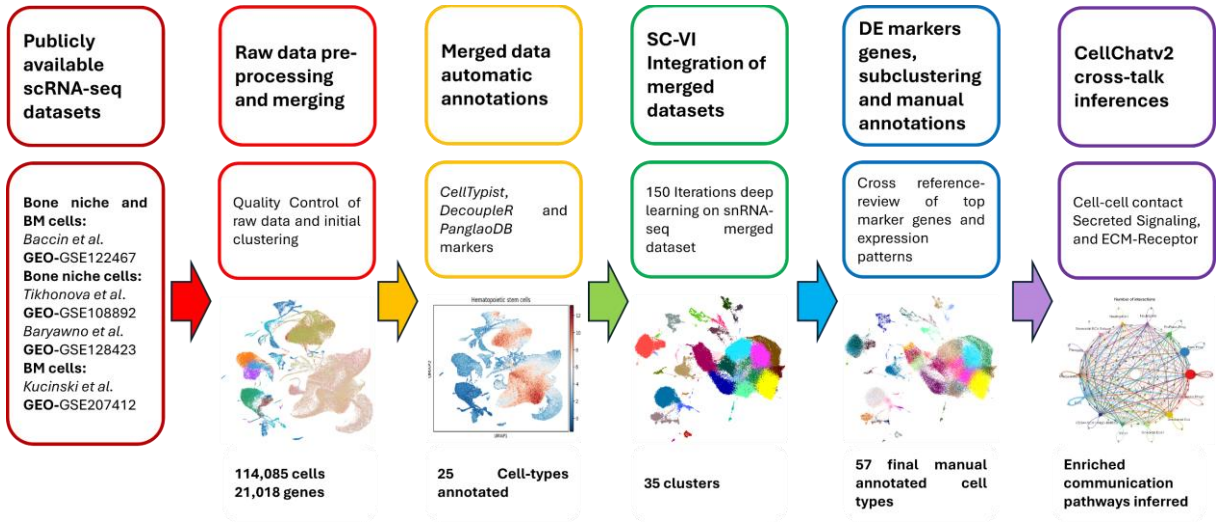

Figure 4.1 **Chapter 4 workflow followed to analyze and infer cell communication networks based on scRNA-seq data.** Summary on the main steps followed to generate results described in Chapter 4, process including single cell transcriptomics dataset selection, merging, annotations, integration, and cell communication pathways inference. Further details can be found in Chapter 2.

4.2 Results

4.2.1 Pre-integration modelling identifies shared biological features among datasets

The datasets were initially merged based solely on their raw data, then preprocessed according to quality control measurements to avoid interference with gene analysis induced by mitochondrial genes. The resulting merged scRNA-seq object contained a total of 114,085 cells and 21,018 genes. The merged object was then processed as indicated in the vignettes to identify relevant clusters and neighbours, as well as a spatial projection, without any biological or functional context coming from their previous annotations (Figure 4.2).

The resulting UMAP projection coloured by data source shows distinctive neighbourhood patterns, with the data from Kucinski, S. et al. (tagged as GottDatRaw0-7) remaining close to each other, consistent with their efforts to capture HSCs and HPSCs. Conversely, the data from Baccin et al. (tagged as SimDatRaw), which includes the greatest variety of bone and BM cells, is distributed amongst distinctive neighbourhoods dominated by the Baryawno et al. (tagged as BarDatRaw) and Tikhonova et al. (tagged as TikDatRaw0-6) datasets. This pattern is consistent

with the efforts of Baccin et al. to capture both niche and haematopoietic cells. Finally, The Baryawno N et al. and Tikhonova A et al. datasets, consisting mostly of bone and bone marrow niche cells, share most of the neighbourhoods, with the clear distinction of TikDataRaw2 and TikDataRaw6. The latter two data series were included because they contain counts of Lineage (Lin)-SCA-1+CD117+ (LSK) cells from untreated mice (GSM3330197_LSK-CTRL.counts.txt and GSM3330198_LSK-KO.counts.txt). Based on the absence of 5-FU stressor stimuli, these were deemed a useful source of data on HSCs.

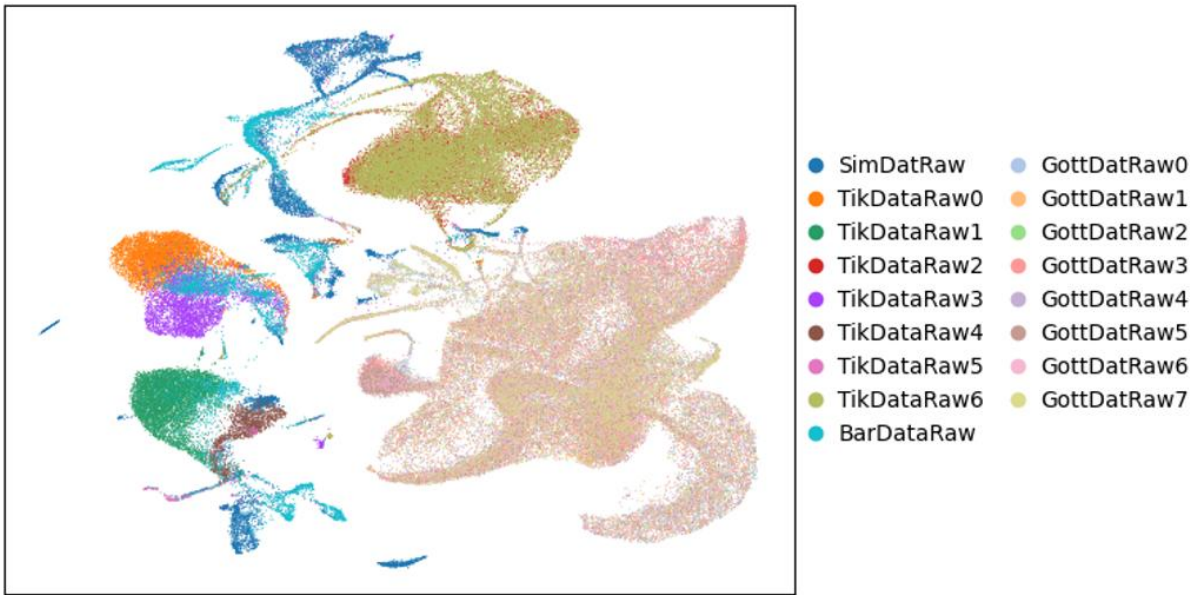

Figure 4.2 **UMAP projection of initial cluster and neighborhood architecture of merged dataset**. Resulting UMAP projection of merged anndata object, 114,085 cells, coloured based on data source. Baccin, et al. data set: SimDatRaw, Tikhonova A, et al. datasets: TikDataRaw0-6, Baryawno N, et al. data set: BarDataRaw, and Kucinski S, et al. datasets: GottDatRaw0-7. All datasets generated with commercial assay Chromium Single Cell (10x genomics).

The patterns shown in Figure 4.2 suggest that there are no significant batch effects introducing biased clustering, and that shared biological features are recognised among datasets.

4.2.2 Automatic cell type annotations in merged object

Having decided to work with the available raw data without cell type context and having achieved the initial UMAP projection, which followed the expected patterns of shared biological features, it was necessary to identify the initial cell type annotations (Figure 4.2). In order to gain an understanding of the prospective cell types I am dealing with, their neighbourhood architecture,

and how these neighbourhoods would be affected by integration, I opted to use automatic cell type scoring tools. This would provide a pre-integration reference point for downstream comparison.

The initial cell type annotation tools, DecoupleR and CellTypist, used the publicly available PanglaoDB database. The cell types selected from this database are listed below: 'B cells', 'Basophils', "Dendritic cells", "Endothelial cells", 'Eosinophils', 'Hematopoietic stem cells', 'Macrophages', 'Mast cells', 'Monocytes', 'Neutrophils', 'NK cells', 'Osteoblasts', 'Adipocytes', 'Chondrocytes', 'Fibroblasts', 'Osteoclasts', 'Pericytes', 'Plasma cells', 'Plasmacytoid dendritic cells', 'Platelets', 'Red pulp macrophages', 'Schwann cells', 'T cells', 'Gamma delta T cells', and 'Myoblasts' (to identify potential sources of contamination).

From these automatically identified cell types (Figure 4.3), those relevant to the myeloid-lineage identities with granulocyte-derived characteristics are basophils, eosinophils, and neutrophils. These three myeloid populations can be found in precise and discrete locations among the merged dataset, except for the neutrophil label, which spans three major neighborhoods, in part due to the poor specificity of gene markers for this population in PanglaoDB. Another relevant myeloid cell type identified with high specificity is the monocyte-macrophage identity. Finally, PanglaoDB failed to provide specific markers distinguishing the heterogeneous HSCs-HSPCs population. Therefore, most of these cell types are likely embedded under the category “Hematopoietic stem cells” (HSCs), spanning across the GottDataRaw and LSK cells from TikDataRaw2-6 (Figure 4.2).

As expected, niche cells are distributed distinctly among neighbourhoods at the opposite end of the UMAP projection, which is consistent with the source datasets that aimed to collect mostly bone marrow stromal populations (Figure 4.4). The labelled niche cell types include osteoblasts, chondrocytes, pericytes, fibroblasts, Schwann cells, adipocytes and endothelial cells. These annotated cells have clear neighbourhood locations, except for endothelial cells and adipocytes, which show significant overlap. Finally, the fibroblast label, which in the database is a broad term associated with the highest number of markers (179), shows partial overlap with the osteo-lineage population. This suggests that fibroblast-like cells are poorly defined and understood in terms of their tissue-specific biological functions and marker expression in the context of bone.

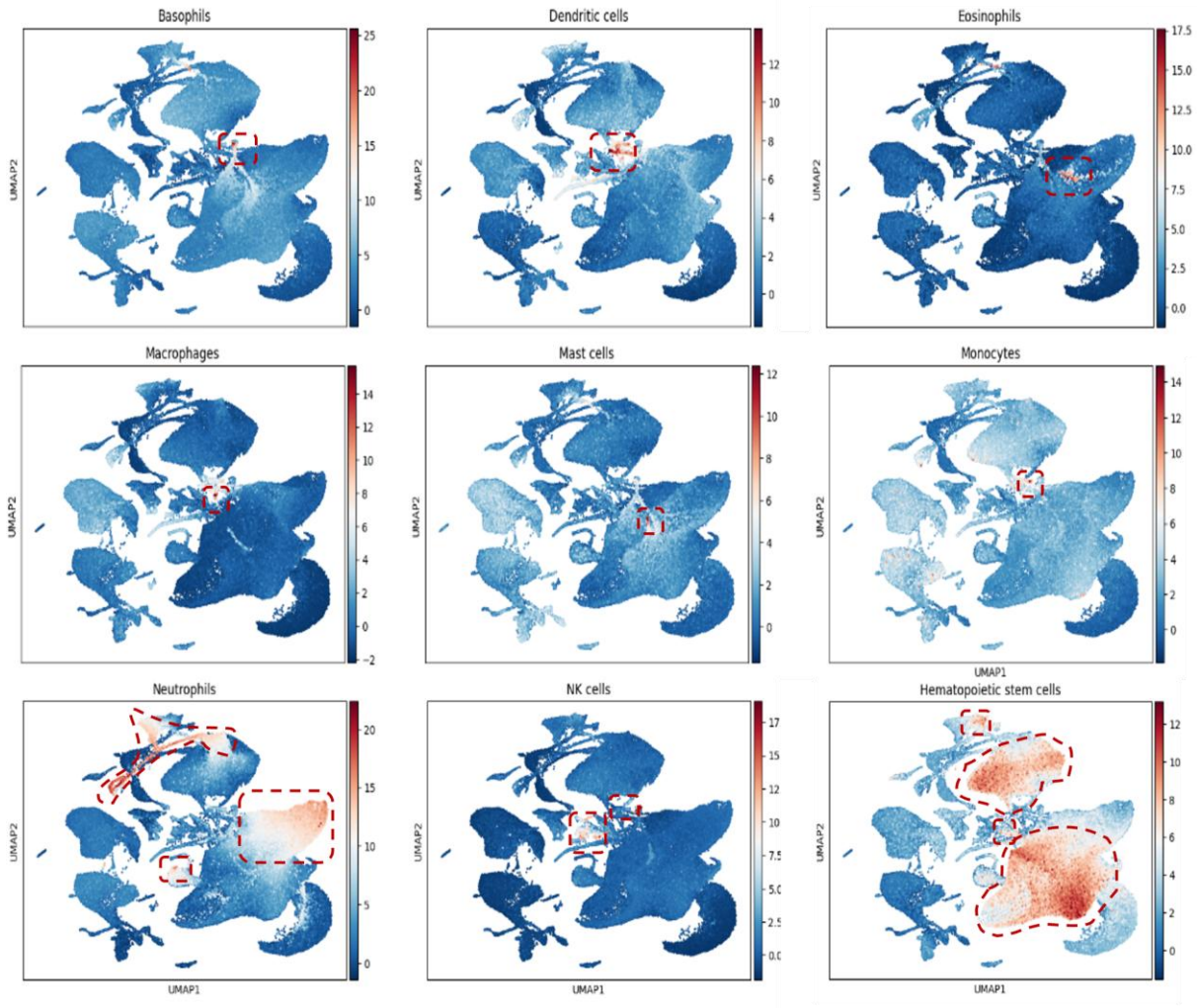

Figure 4.3 **Automatic cell type annotations on pre-integrated dataset identifies mature myeloid identities and HSCs**. Myeloid cells and HSCs identified by DecoupleR and CellTypist in pre-integrated dataset. Resulting UMAP projection of pre-integrated dataset (Figure 4.2), coloured by identified relevant myeloid-lineage cells (mature myeloid cells) and HSCs, identified by the automatic cell type annotation tools. Precise location of annotated cells inside red-dashed regions.

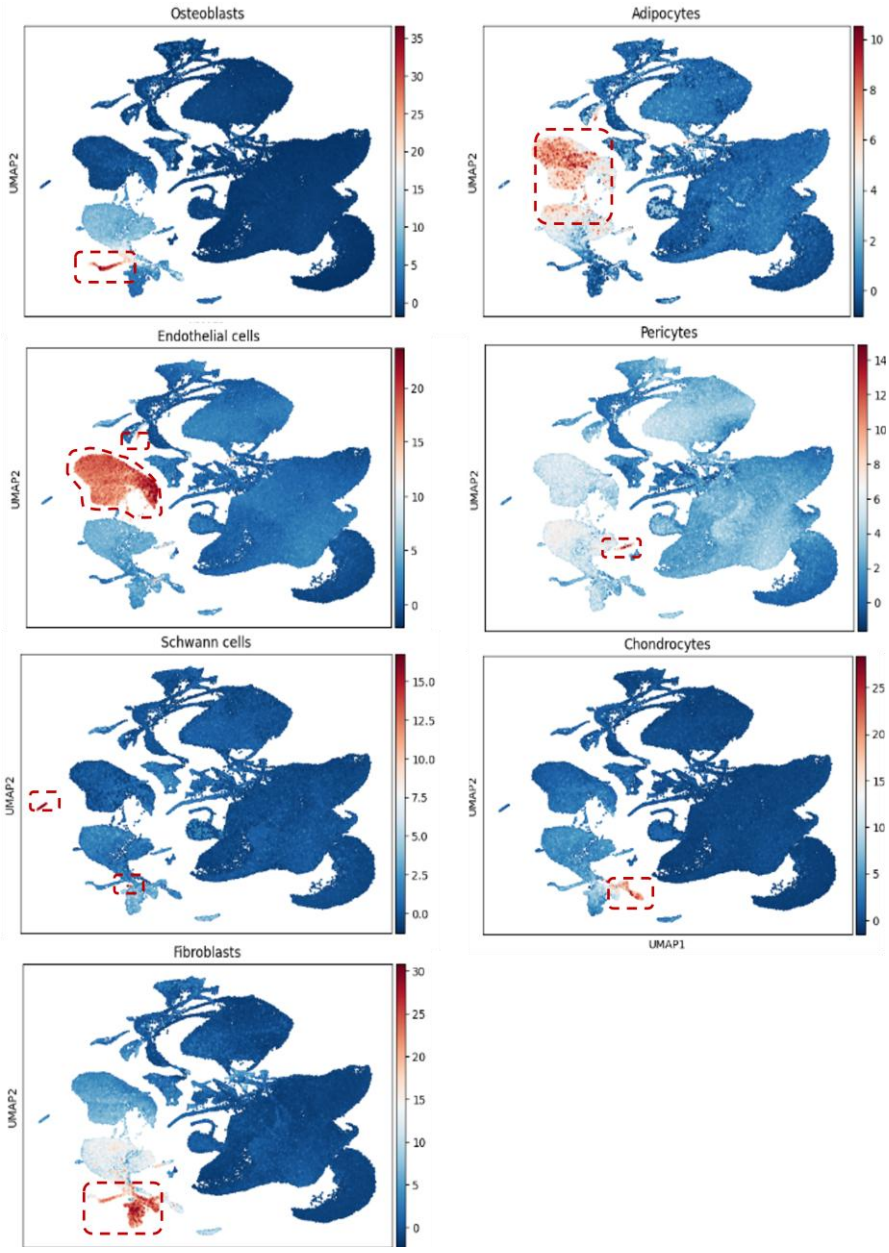

Figure 4.4 **Automatic cell type annotations on pre-integrated dataset identifies major BM niche cell types.** Niche cells identified by DecoupleR and CellTypist in pre-integrated dataset. Resulting UMAP projection of pre-integrated dataset (Figure 4.2), coloured by identified relevant niche cells identified by the automatic cell type annotation tools. Precise location of annotated cells inside red-dashed regions.

4.2.3 Integration of datasets provides an improved cohesive clustering of cell populations

Following the evaluation of the initial cell type annotation described in 4.2.2, SCVI model training was performed. In summary, SCVI is a probabilistic-modelling tool that uses the gene expression data of each cell to generate a latent representation of the biological signal, representing transcriptomic states. By means of its probabilistic features, it integrates data based on the

inference achieved by robust latent representation reconstruction rounds (150 rounds in the case of the present project) of the entire scRNA-seq dataset. This provides a hierarchical Bayesian integration score for the relevant transcriptomic states and integrates all datasets from different sources. Ultimately, this generates a model in which each transcriptome is organized by shared states with a reliable posterior probability value.

The latent representation generated by the trained model was then clustered using the standard workflow with PCA, neighbors and UMAP reduction for visualization. When the UMAP of the integrated trained model is plotted based on the data source, neighbours and cells with improved embedded patterns are evident, particularly in the GottDatRaw series, which shares a neighborhood with LSK cells registered in TikDataRaw2 and TikDataRaw6 (Figure 4.5). Meanwhile, data series with niche cells are differentially organized into better-defined, more cohesive neighborhoods.

4.2.4 Integrated dataset maintains cohesion of initial automatically annotated cell labels

After reviewing the latent representation based on the source of the data, I decided to explore how the automatic annotations done in 4.2.2 remained organized based on this UMAP projection.

The organization of labelled cells in this new projection remained highly consistent, which is most noticeable with mature immune cell types such as basophils, monocytes, macrophages, and plasma cells (Figure 4.6). Neutrophils are localized into two major hotspots, one clear dominated only by neutrophil-labelled cells, and the second one embedded in the major neighborhood dominated by HSCs (Figure 4.6. Neutrophils). In addition, the new distribution of HSC-labelled cells is now more consistent within one major neighborhood, followed by a divergence into three branches (Figure 4.6. Hematopoietic Stem Cells).

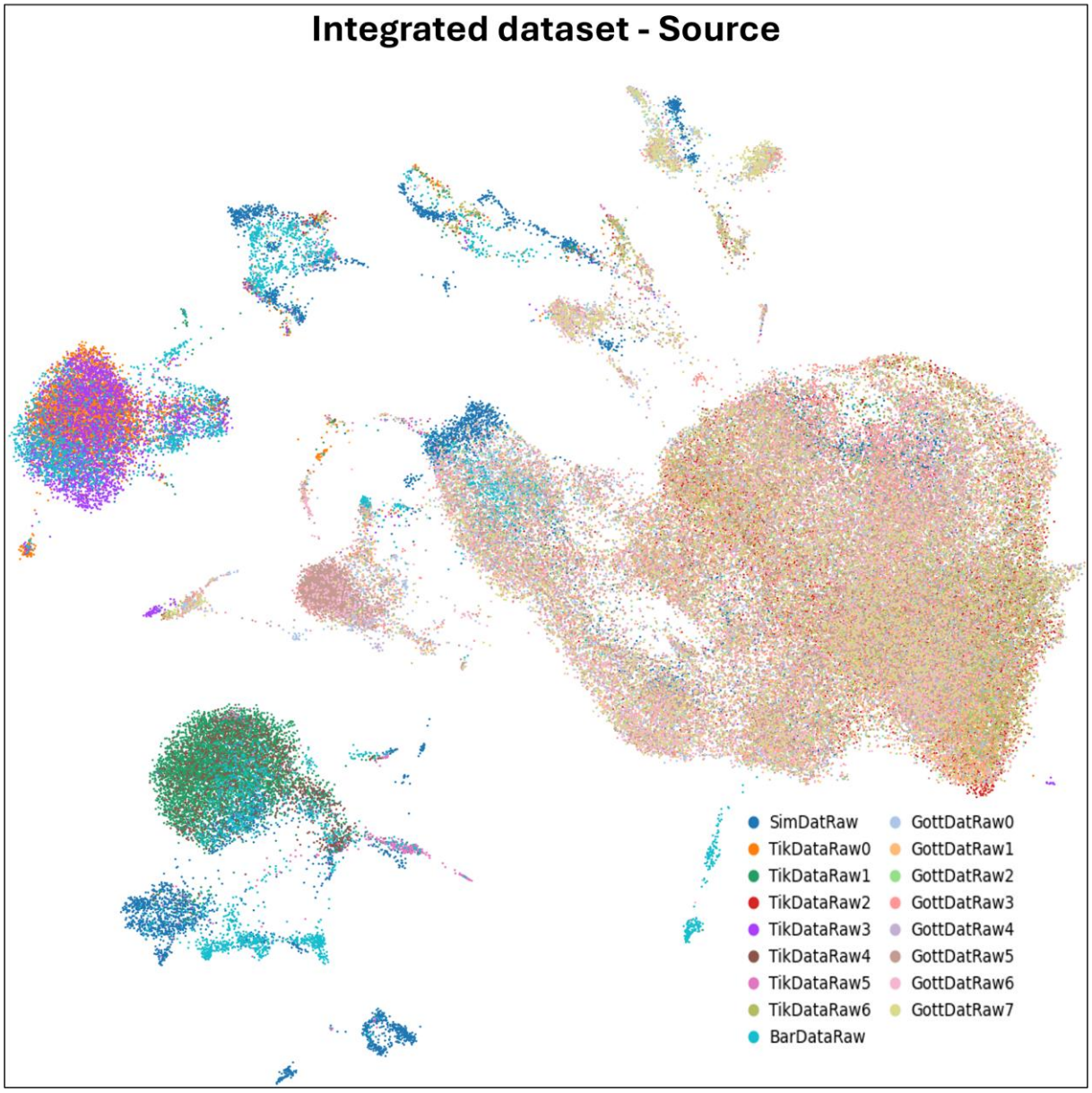

Figure 4.5 **UMAP projection of cluster and neighborhood architecture of fully integrated dataset.** Integrated dataset provides a better consistent and cohesive organization of cell neighborhoods, resulting UMAP projection of integrated dataset, after 150 training iterations, merged neighborhoods with distinctive locations and cohesive patterns according to expected cell populations contained in each source dataset.

In the case of niche cells labels, Endothelial cells remained highly well organized in a single discrete and more condensed neighborhood compared to the previous projection (Figure 4.7 Endothelial Cells). Osteoblasts and chondrocytes also conserved their well-organized arrangements in smaller discrete neighborhoods, with a portion of the fibroblasts labelled cells still organizing close to the osteoblast neighborhood (Figure 4.7. Osteoblasts, Chondrocytes and Fibroblasts). Nonetheless, adipocytes are still overlapping the region of endothelial cells. Finally,

regarding the minor neighborhoods at the bottom, the initial labelling reveals that the most relevant cell type identified are Schwann cells (Figure 4.7. Schwann cells).

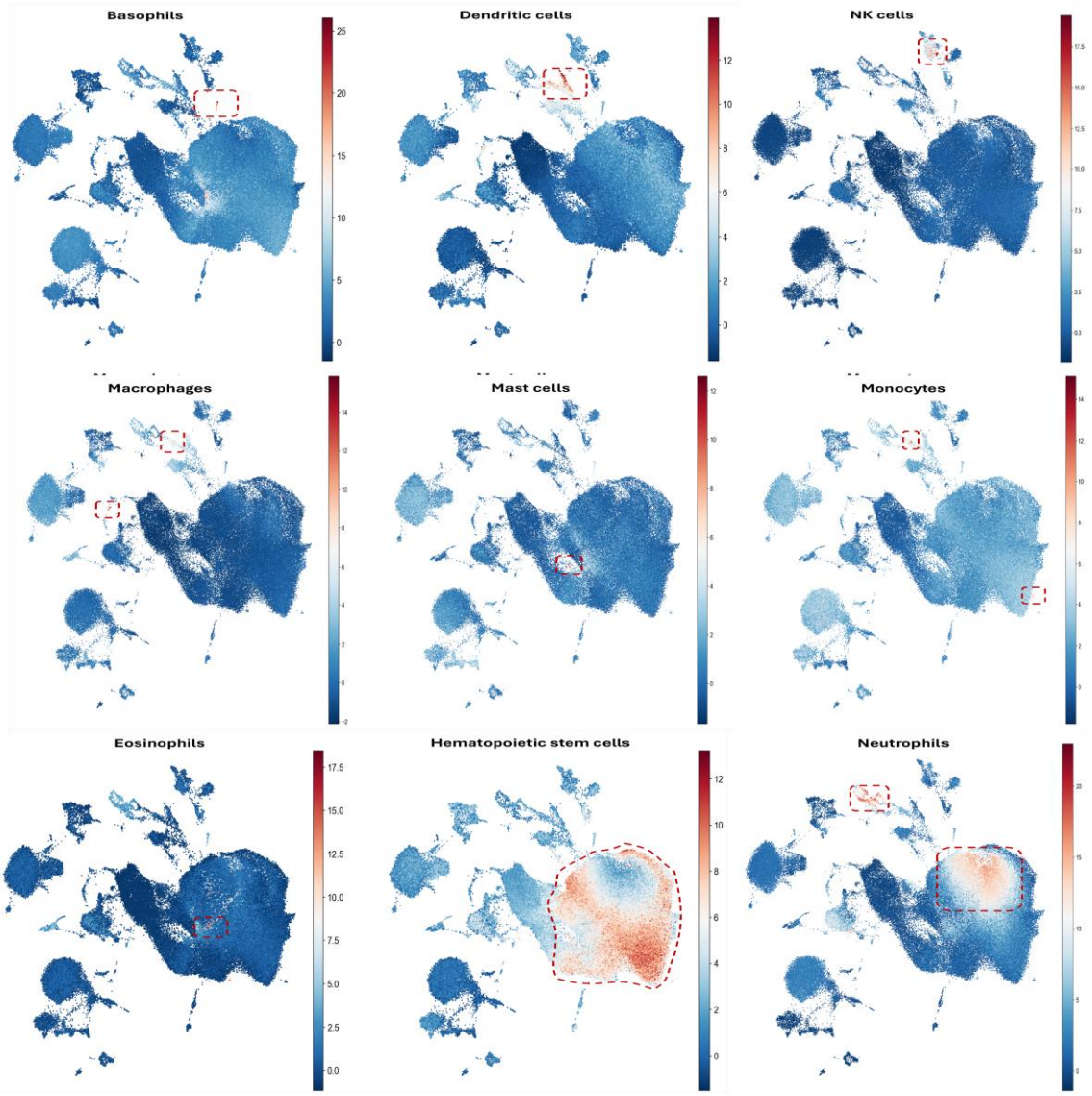

Figure 4.6 **Automatic cell type annotations on integrated dataset displays a more cohesive architecture among mature myeloid identities and HSCs.** Myeloid cells and HSCs identified by DecoupleR and CellTypist in integrated dataset (Figure 4.5). Resulting UMAP projection of SCVI-integrated dataset, coloured by relevant myeloid-lineage cells (mature myeloid cells) and HSCs, identified by the automatic cell type annotation tools in 4.2.2. Precise location of corresponding annotated cells inside red-dashed regions.

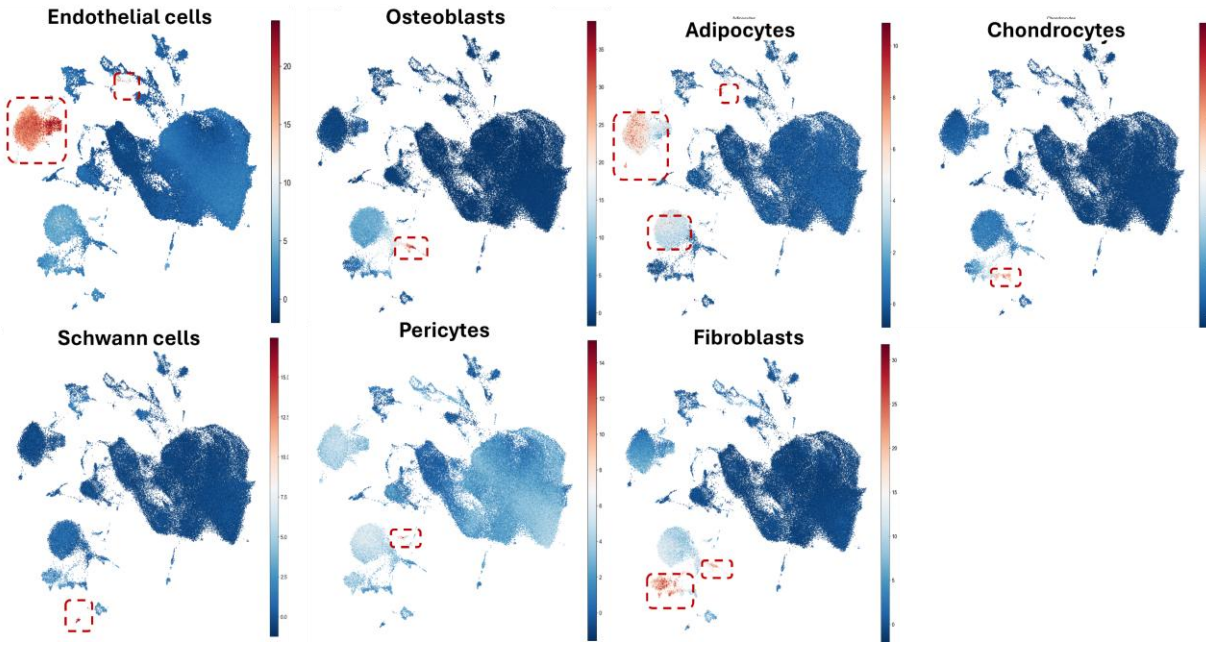

Figure 4.7 **Automatic cell type annotations on integrated dataset maintains a consistent architecture among BM niche cell identities.** Niche cells identified by DecoupleR and CellTypist in integrated dataset (Figure 4.5). Resulting UMAP projection of SCVI-integrated dataset, coloured by relevant niche cells of bone, cartilage, vascular, adipose and peripheric nervous system tissues, identified by the automatic cell type annotation tools in 4.2.2. Precise location of corresponding annotated cells inside red-dashed regions.

4.2.5 Limitations of automatic cell type annotation tools and database-reference

Since the projection of the integrated dataset showed consistent organization and patterns of cell labelling, Leiden-based clusters were generated. The final architecture of the integrated dataset comprised 35 distinct clusters. This cluster composition was then used to run a model analysis function in "1 vs all differential expression (DE) test mode", comparing each cluster's identified set of marker genes against the remaining 34 clusters. After performing the DE analysis, the marker genes were selected based on the top five scored genes per cluster. Notably, the initial ULM-score-based automatic annotation identified only 25 cell types, which was insufficient to accurately describe the 35 observed clusters. Given that the PCA, neighbourhood analysis and UMAP reduction settings used here were deemed to perform best, it was necessary to account for the remaining 10 clusters without a clear annotation.

Taking this into account, I decided to re-examine and re-run the ULM scores to identify the top three cell type predictions based on the PanglaoDB sets of marker genes for all 35 Leiden-based clusters. The aim was to review the performance of the predictions and gain insight into the cell types representing all 35 Leiden clusters, especially with regard to HSCs or HSPCs, which are

expected to have a transcriptome state that closely resembles those of their downstream myeloid or lymphoid lineages. Finally, I also reviewed the inference consistency and specificity in identifying endothelial cells, fibroblasts and adipocytes, which share features with other mesenchymal or endothelial niche cells (Table 4.1).

Scored cell types by automatic annotation tools reveals lack of precision to account for heterogeneity.			
Leiden cluster	**Top 3 ULM-score cell types**	**Leiden cluster**	**Top 3 ULM-score cell types**
0	‘HSCs’, 'Basophils', 'Monocytes'	**18**	'T cells', 'NK cells', 'Gamma delta T cells'
1	'Neutrophils’, HSCs’, 'Dendritic cells'	**19**	'T cells', 'Macrophages', 'Eosinophils'
2	'Neutrophils', 'Dendritic cells', 'Gamma delta T cells'	**20**	'Fibroblasts', 'Osteoblasts', 'Osteoclasts'
3	'Endothelial cells', 'Adipocytes', 'Macrophages'	**21**	'T cells', 'NK cells', 'Gamma delta T cells'
4	‘HSCs’, 'Basophils', 'Gamma delta T cells'	**22**	'Dendritic cells', 'Macrophages', 'B cells'
5	'Osteoblasts', 'Fibroblasts', 'Adipocytes'	**23**	'Gamma delta T cells', 'Platelets', 'NK cells'
6	No prediction	**24**	'Myoblasts', 'Fibroblasts', 'Schwann cells'
7	'HSCs', 'Basophils', 'Platelets'	**25**	'Macrophages', 'B cells', 'Plasma cells'
8	'HSCs', 'Platelets', 'Basophils'	**26**	'Platelets', 'Plasma cells', 'Osteoclasts'
9	'HSCs', 'Gamma delta T cells', 'Mast cells'	**27**	'Adipocytes', 'Endothelial cells', 'Pericytes'
10	'Platelets', 'HSCs', 'Gamma delta T cells'	**28**	'Macrophages', 'Red pulp macrophages', 'Dendritic cells'
11	'Myoblasts', 'Red pulp macrophages', 'Neutrophils'	**29**	‘Schwann cells', 'Neurons', 'T cells'
12	'Platelets', 'HSCs', 'Basophils'	**30**	'Fibroblasts', 'Pericytes', 'Chondrocytes'
13	Basophils', 'Mast cells', 'Eosinophils'	**31**	'Myoblasts', 'Red pulp macrophages', 'Osteoblasts'
14	'Fibroblasts', 'Chondrocytes', 'Schwann cells'	32	'Monocytes', 'Basophils', 'Pericytes'
15	'Dendritic cells', 'B cells', 'Plasmacytoid dendritic cells'	33	'Neutrophils', 'Gamma delta T cells', 'Eosinophils'
16	'B cells', 'Schwann cells', 'Plasma cells'	34	'Pericytes', 'Basophils', 'Monocytes'
17	'Plasmacytoid dendritic cells', 'Dendritic cells', 'B cells'		

Table 4.1 Leiden clusters and their corresponding top 3 predicted cell identity by ULM-based scoring with DecoupleR and CellTypist, according to PanglaoDB marker database.

The top three cell types, as scored by the automatic tools employed in 4.2.2, revealed inconsistencies in cell identity. Therefore, annotations were only placed temporarily in the context of the predictions provided in Table 4.1. These temporary annotations can be seen in the UMAP projection shown in Figure 4.8.

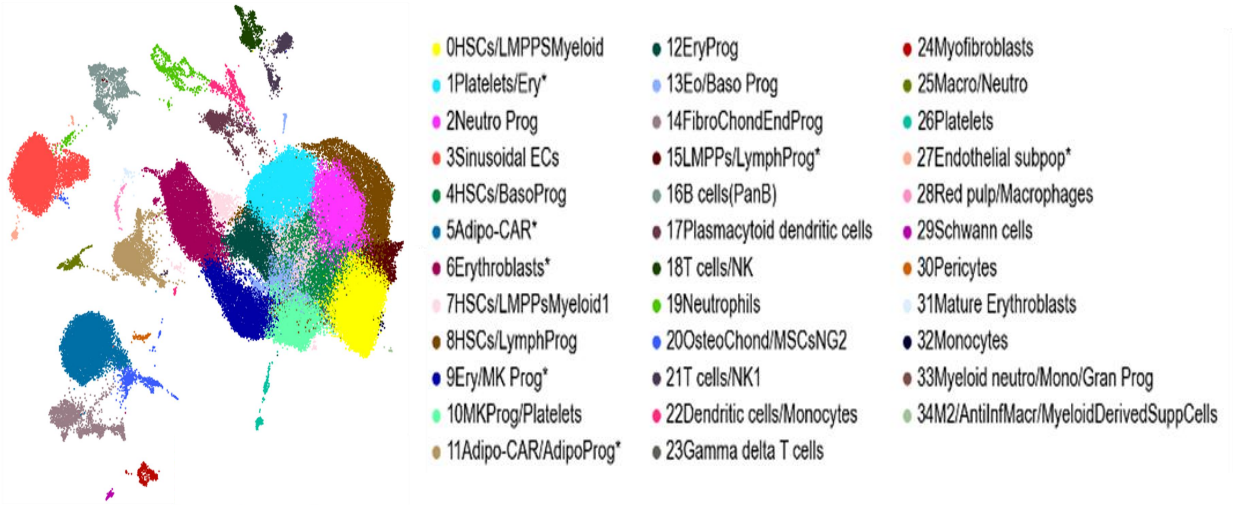

Figure 4.8 **UMAP projection and temporary labels based on automatic cell type annotations scores**. UMAP projection of the integrated dataset coloured by Leiden clusters and their corresponding temporary annotations based on the automatic cell type score tools, revealing lack of precision to account for heterogeneity.

4.2.6 Sub clustering improves resolution of cellular heterogeneity

To achieve a curated manual cell type annotation all marker genes identified were analyzed and reviewed further based on published references and the expression patterns found across the Single Cell exploration tools available for each of the scRNA-seq datasets used in the present project.

This review revealed that some clusters representing putative cell populations of niche and relevant myeloid identities were not precise enough, potentially underrepresenting relevant heterogeneity, and thus requiring sub-clustering and further manual annotation.

Niche clusters representing mesenchymal lineage-derived cells, such as adipocyte lineage, osteocyte lineage and chondrocyte lineage, were initially labelled '5Adipo-Car*',

‘20OsteoChondro/MSCsNG2’ and ‘14FibroChonEndProg’, were found to be clustered in a neighbouring fashion, suggesting a closely shared transcriptomic blueprint. These clusters were therefore isolated and sub-clustered to refine my cell type annotations (Figure. 4.9-A).

Eight new clusters were identified from the original three niche clusters, each with a significantly well-defined expression signature. The most relevant gene signatures were found in cluster 5, which expresses osteoblast-related genes *Col1a1* and *Col1a2*, as well as *Sparc* (also known as osteonectin); cluster 6, which expresses chondrocyte- and SSC-related genes *Mia* and *3110079o15rik* (also known as secondary ossification center associated regulator of chondrocyte maturation, SNORC), as well as the transcription factor *Sox9*; cluster 7, which expresses vascular-related genes *Egfl7* (epidermal growth factor-like protein 7), *Cdh5* (cadherin 5, also known as *VE-cadherin*), and *Mmrn2* (multimerin-2); and cluster 0, which expresses the highest level of *Cxcl12* (Figure. 4.9-B).

In the case of cluster 3 Sinusoidal ECs, sub-clustering revealed further vascular heterogeneity in four new clusters. One of the top genes that define new cluster 2, which remains constant in clusters 1 and 0, is *Ly6a* (lymphocyte antigen 6 family member A). In mice, *Ly6a* encodes the membrane protein Sca-1 and has recently been described as a consistent phenotype in ECs of the arterial vasculature. This is followed by CD34, a gene with a strong presence among ECs, and *Ly6c1* (lymphocyte antigen 6 family member C1), which. in combination with *Ly6a* indicates either type S vasculature or an arterial vasculature signature. Cluster 1 is defined by the expression of *Hspa1a* and *Egr1*, as well as the highest mean expression of *Vcam1*. Cluster 0 is defined by the genes *Rps12* and *Tpt1*, and cluster 3 is defined by the most highly ranked gene, *Cebpb* (Figure. 4.9-C).

The remaining cluster representing a putative endothelial niche population according to automatic labelling scores, cluster 27Endothelial subpop*, was also able to provide an improved resolution. This is the smallest cluster across the niche cell types, with only 179 cells. New cluster 0 is defined by the differential expression of the *Fabp4* (fatty acid binding protein 4) gene, which is involved in fatty acid metabolism and has been mainly expressed in endothelial cells (ECs) under homeostatic conditions. This is followed by *Fam167b* (family with sequence similarity 167, member B), which has been described in ECs of the aortic vasculature, and *Tfpi* (tissue factor pathway inhibitor), which has antithrombotic functions in ECs. Meanwhile, new cluster 1 is

characterised by *Cxcl12* gene expression and the highest mean expression of the *H2-D1* (histocompatibility 2, D region locus 1), and *Bgn* (biglycan) genes, the latter recently been described of great importance in bone vasculature[155] (Figure. 4.9-D).

4.2.7 Sub-clustering of putative myeloid cells only improved resolution in putative megakaryocyte-erythroid lineage cells

The next step was to perform sub-setting and sub-clustering in putative HSCs and myeloid-related clusters. However, only a few of these provided improved heterogeneity resolution with ranked genes that were mostly restricted to the expected functions of the original cluster and not shared across the other clusters initially annotated.

The sub-clustering results only involved cell types related to erythroid and megakaryocyte identities, such as the clusters initially annotated as 1PlateletsEry, 6Erythroblasts*, 9Ery/MKProg* and 10MKProg/Platelets (see Supplemental Figure 4.1). This new cluster architecture was applied to the final annotations, which are described below.

4.2.8 Final cell-type manual annotation and differential gene expression re-examination

Following the improved resolution of new clusters identified in sections 4.2.6 and 4.2.7, which had relevant transcriptomic signatures that could be corroborated in the reviewed literature and identified among the original scRNA-seq datasets, new cell-type annotations were necessary to improve the representation of the heterogeneity revealed.

Unfortunately, the available bioinformatics tools for cell-type annotation depend on previously generated and validated scRNA-seq datasets, which usually cover either immune cells or BM stromal cells. Very few datasets include both BM and bone-niche cell populations together. Furthermore, most databases do not provide a repertoire of cell annotations with extensive myeloid lineage identities characterized. Therefore, to avoid misrepresenting the newly found heterogeneity, manual verification and annotation were performed for each of the 57 clusters. This achieved a final integrated dataset architecture (Figure 4.10), which is useful for identifying both the niche and granulocyte-neutrophil cells of interest explored in Chapter 3 (Figures 4.10A–D).

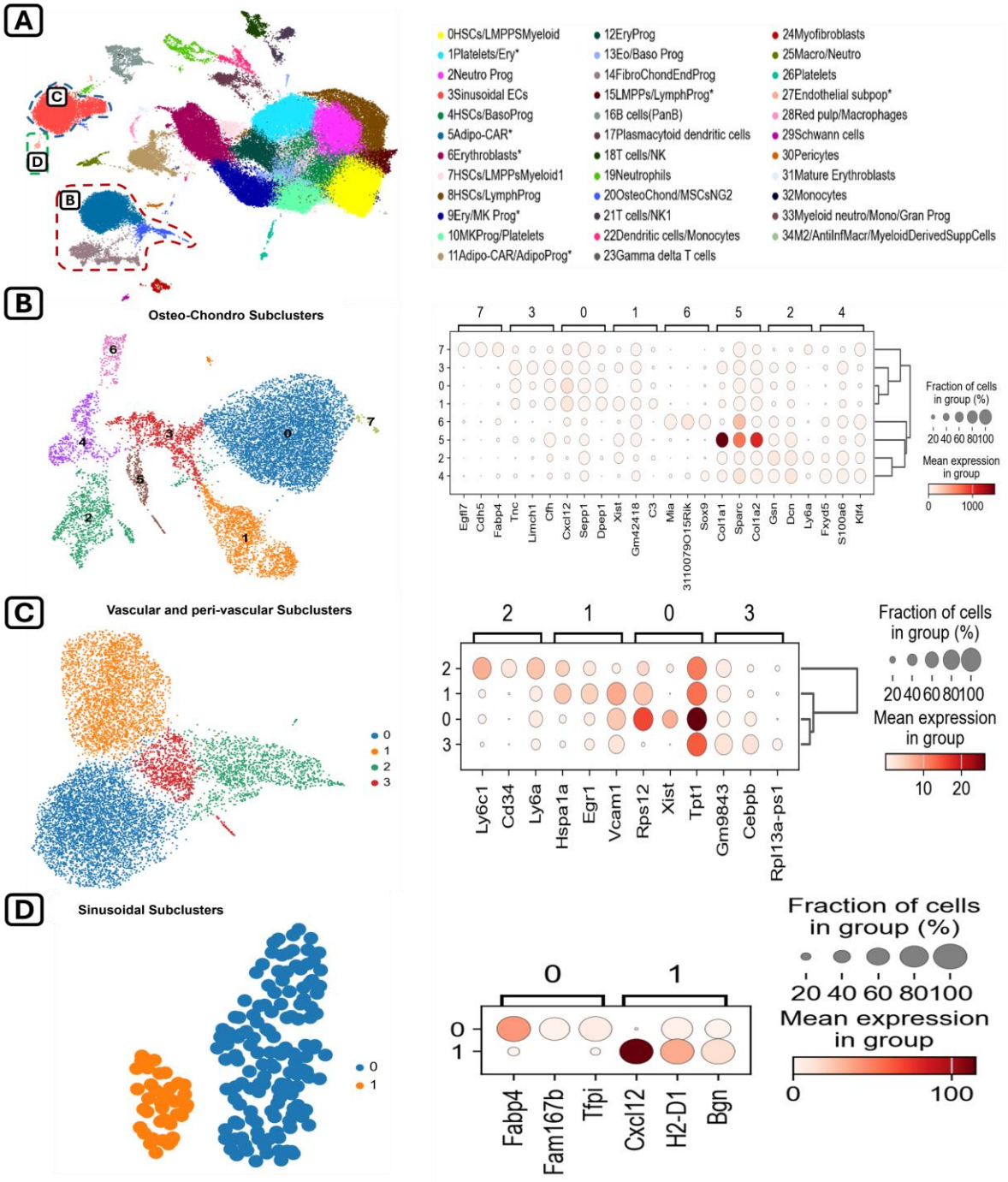

Figure 4.9 **Sub clustering of putative niche cells populations identified underrepresented heterogeneity**. (A) UMAP projection and temporary labels based on automatic cell type annotations scores (Figure 7), niche clusters used for sub-clustering inside dashed regions, osteo-chondro clusters inside red dash box, main endothelial cell cluster inside blue dash box, endothelial cells subpopulation inside green dash box. (B) UMAP of newly identified 8 clusters from the clusters annotated in A as '5Adipo-Car*', 20OsteoChondro/MSCsNG2' and '14FibroChonEndProg'; followed by top genes identified per cluster by DE analysis, heatmap coloring format based on mean expression of gene per cluster. (C) UMAP of newly identified 4 clusters from the cluster annotated in A as '3Sinusoidal ECs', followed by top genes identified per new cluster by DE analysis, heatmap coloring format based on mean expression of gene per cluster. (D) Newly identified 2 clusters from the cluster annotated in A as '27Endothelial subpop*', followed by top genes identified per new cluster by DE analysis, heatmap coloring format based on mean expression of gene per cluster.

To confirm the consistency of the final manual cluster annotations used to identify the cell types accounting for the revealed heterogeneity, the Differential Expression function was performed again as described above in 4.2.5, this time analyzing each cluster against the rest of the 56 clusters.

The marker genes identified in this step can be found in Supplemental Table 4.1.

4.2.9 Molecular crosstalk between granulocyte progenitors and their niche

The main objective of this chapter is to determine, at the molecular level, why Gr1+ granulocyte progenitors proliferate almost exclusively in specific BM niches rich in osteoblasts, blood vessels, and pericytes, as observed in Chapter 3. To achieve this, I employed CellChat, an algorithm designed to identify and categorize signaling interactions/crosstalk between selected cell types based on scRNA-seq data. The signaling patterns is then categorized as outgoing (signal sender) or incoming (signal receiver) depending on the ligand-receptor gene pairs expressed by the cells of interest.

For this analysis, I selected the following clusters from my integrated and annotated dataset, representing Gr1+ cells: Neutrophils. The granulocyte progenitors: Neutro Prog, Neutro Prog1, Baso Prog, and Eo/Baso-Prog. Finally, I decided to include the secondary neutrophil cluster called Neutrophils1, despite having low to no Ly6g-Gr1 expression in case of having relevant interactions.

For the osteo-lineage niche cells, I selected the following clusters: BM-MSCs-LepR, MSCs-Osteo, Col-Osteoblasts, BM Fibroblasts, MSCs-Chondro, and MSC-Subpopulation. For the vascular niche cells, the following clusters were used: ECs, ECs1, Sinusoidal ECs, Sinusoidal ECs1, Sinusoidal ECs Subpop, Pericytes, MSCs, and CD34+SCA1+Ng2-BMECs. Since my data in Chapter 3 suggested that interactions between Gr1+ cells and their niche involved different mechanisms, I used CellChat to infer communication pathways through: 1) direct cell-cell contact signaling, 2) secreted signaling, 3) and ECM-receptor signaling.

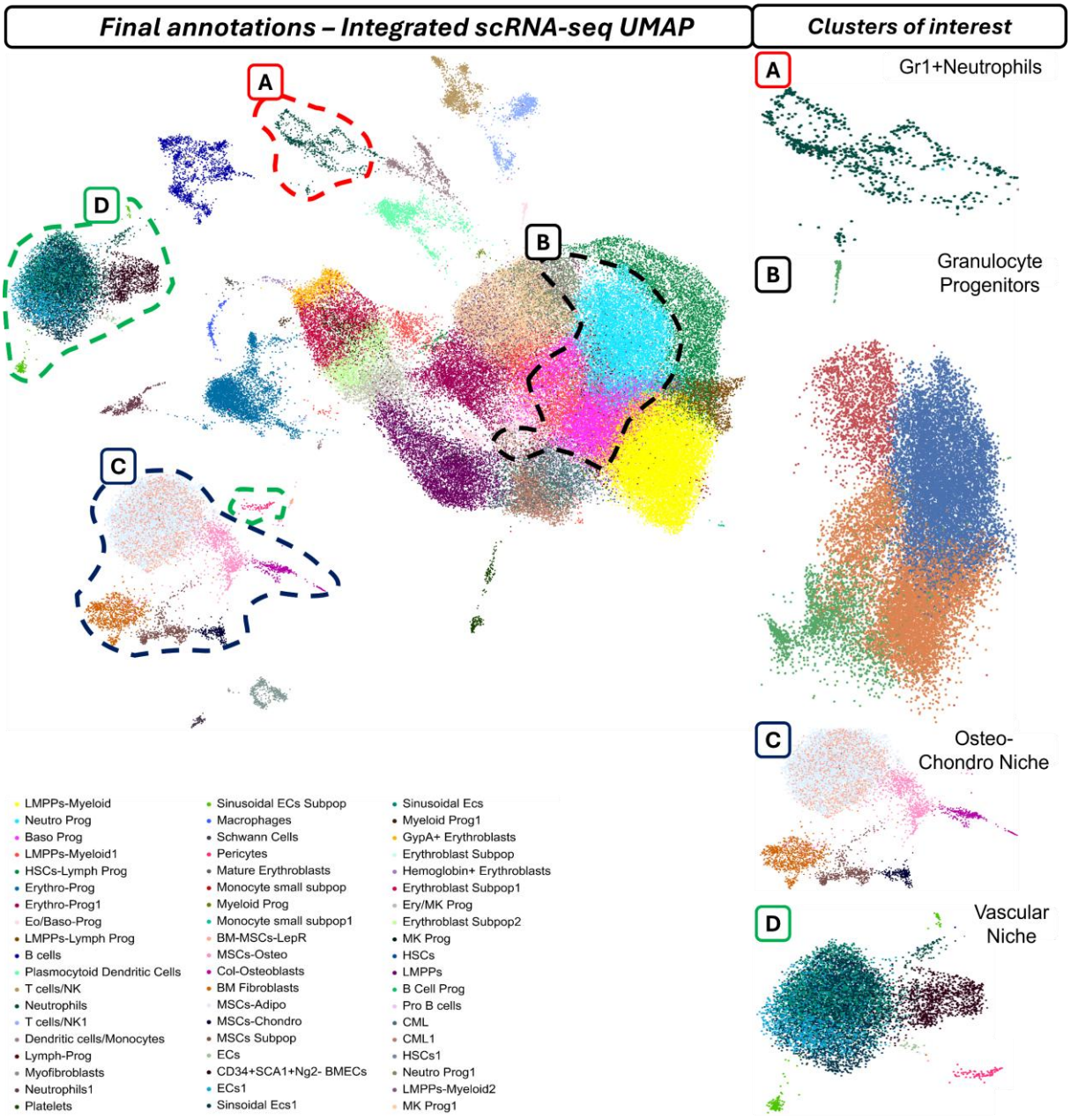

Figure 4.10 **UMAP projection and final manually annotated labels based on sub clustering results and cross reference of marker genes.** UMAP projection of integrated dataset achieved in section 4.2.3 with final manual annotations. (A) Neutrophils cluster representing the Ly6g/Gr1+ cell population of interest explored in Chapter 2. (B) clusters Neutro Prog, Neutro Prog1, Baso Prog, and Eo/Baso-Prog; representing the relevant granulocyte-progenitor cells identified as direct progenitors of the Ly6g/Gr1+ neutrophils in A). (C) Niche cells identified to represent the osteo and chondro-derived cells and their closely related MSCs clusters. Clusters: BM-MSCs-LepR, MSCs-Osteo, Col-Osteoblasts, BM Fibroblasts, MSCs-Chondro, and MSC-Subpopulation. (D) Niche cells identified to represent the vascular cells. Clusters: ECs, ECs1, Sinusoidal ECs, Sinusoidal ECs1, Sinusoidal ECs Subpop, Pericytes, MSCs, and CD34+SCA1+Ng2- BMECs.

4.2.9.1 Molecular crosstalk between granulocyte progenitors and osteo-chondro niche – cell to cell contact

I selected only those pathways that showcase a communication pattern with specific roles, in which niche cells act as signal senders, targeting our cells of interest (granulocyte-neutrophils) acting as signal receivers. This concentrates the analysis on the pathways in which niche cells may directly act as the inductive niche of our cells of interest.

Some of the selected pathways involve opposite mechanisms of immune function, such as neutrophil activation and its direct inhibitory stimuli. One example of this is ICAM and SIRP, where niche cells interact with both neutrophils and granulocyte progenitors. However, it is unclear if they have a direct function as granulopoiesis-inducing factors. Pathways that specifically target cells with the strongest Ly6g-Gr1 expression (Neutrophils) can also be determined, as with the *Thy1* pathway originating from BM fibroblasts. Similarly, the ADGRG pathway, which is involved in inflammation, also originates from niche cells and targets granulocyte-associated progenitor cells. Finally, collagen-expressing osteoblasts have a direct communication mechanism that targets progenitors only by means of CD276 (Figure. 4.11. A-B).

4.2.9.2 Molecular crosstalk between granulocyte progenitors and osteo-chondro niche – secreted signaling

In the context of pathways involving secreted factors, this communication mechanism had the greatest number of identified inferences based on L-R gene pairs and the most pronounced contrast in signaling roles.

The outgoing role is clearly dominated by niche cells, particularly in the Midkine (*Mk*), Osteopontin (*Spp1*), Pleiotrophin (PTN) and Insulin-like growth factor (IGF)/Insulin-like growth factor binding protein (IGFBP) pathway (Figure. 4.12. A). In this communication context we can identify some of the most relevant pathways involving the chemoattractant family CXCL and KIT (including KitL/SCF) pathways. Interestingly, despite the direct removal of cells annotated as MSCs-Adipo, adiponectin remains a relevant factor when exploring MSCs with LepR expression, stochastically targeting the remaining cell types. Further stochastic-targeting effects are also appreciated in the MK pathway and the osteogenesis-associated IGF/IGFBP pathways. Finally, in tune to relevant pathways associated with osteogenesis, the SPP1 pathway expressed by MSCs-

LepR cells, MSCs-Osteoblasts and Osteoblasts expressing collagen have a broad inferred impact across all granulocyte-associated cells (Figure. 4.12. B).

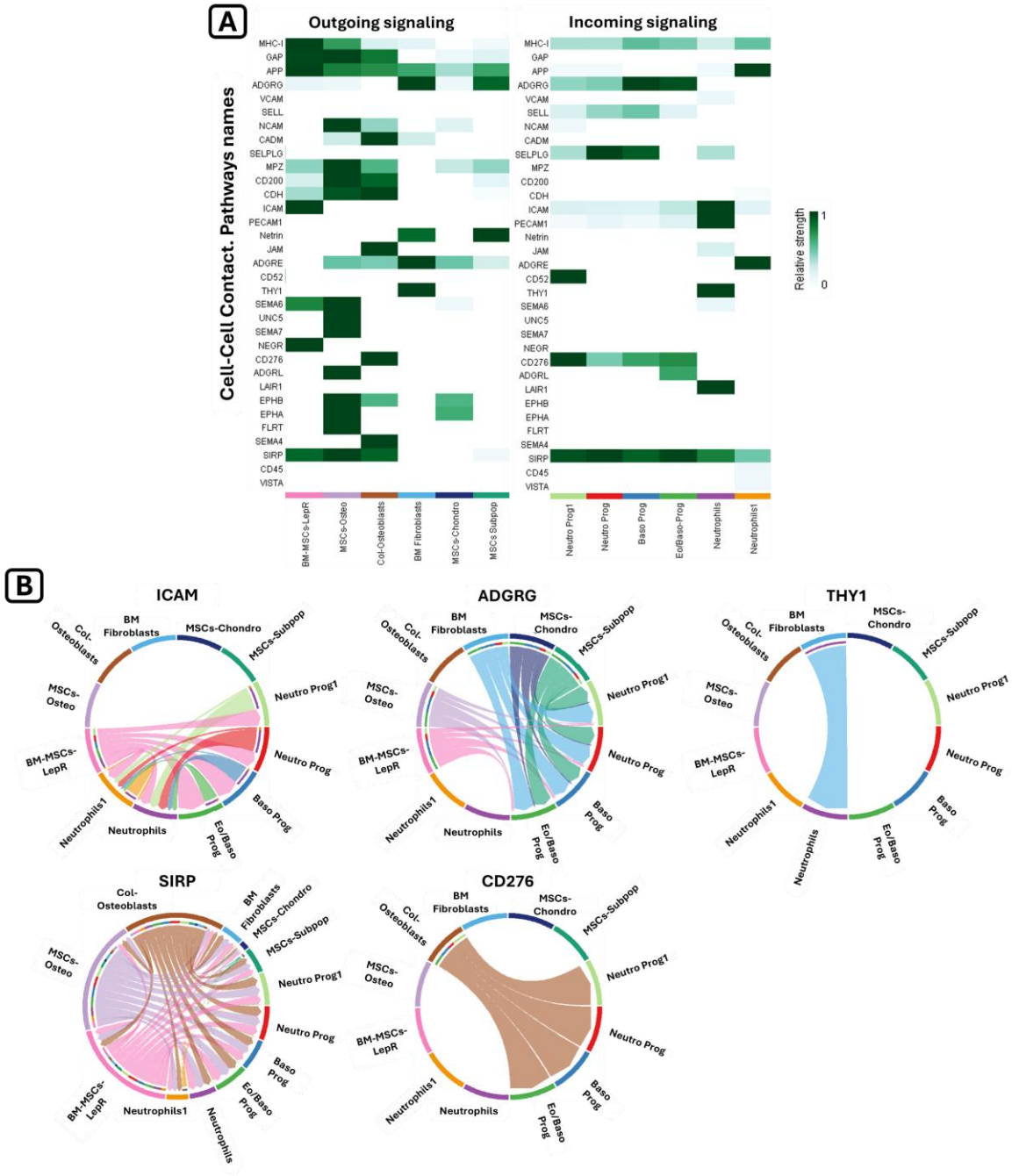

Figure 4.11 **Cell-cell contact communication pathways inferred between osteo-chondro niche cells and the granulocyte-neutrophil cell types**. (A) Cell communication pathways inferred by CellChat under the context of direct cell-cell contact plotted based on pathway strength inference (green heatmap coloured format), cell types selected (X-axis) and the name of the pathways (Y-axis). Outgoing pattern (signal sender) niche cells (left), and incoming pattern (signal receiver) granulocyte-neutrophils (right) signaling roles. (B) Chord plots of the selected pathways with signaling patterns with niche cells as senders and granulocyte-neutrophil cell types as receivers, the direction of the signaling (coloured arrow) depicting what cell type produces the signal and the receptive cell type (direction of the arrow).

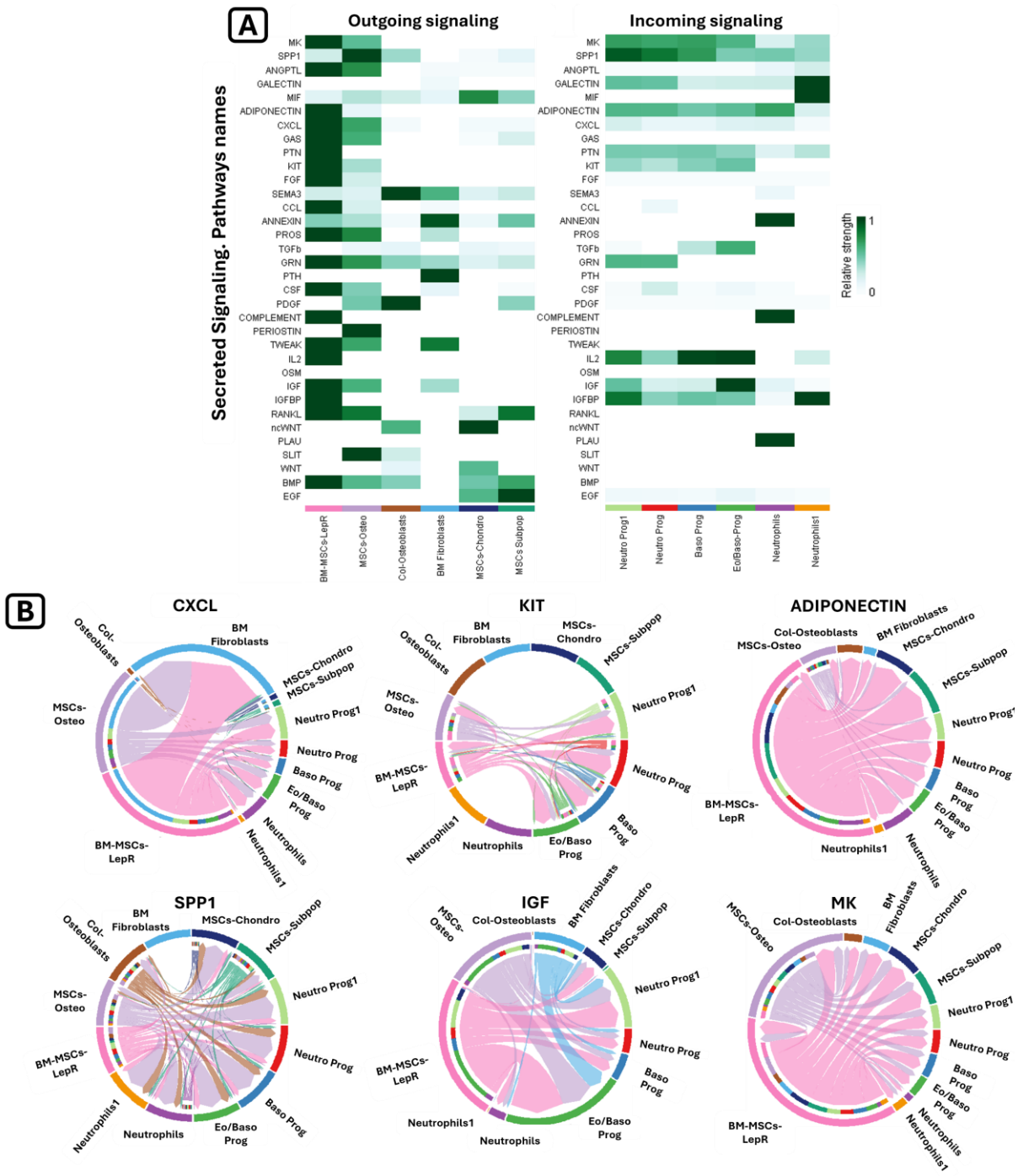

Figure 4.12 **Secreted signaling communication pathways inferred between osteo-chondro niche cells and the granulocyte-neutrophil cell types**. (A) Cell communication pathways inferred by CellChat under the context of secreted signaling plotted based on pathway strength inference (green heatmap coloured format), cell types selected (X-axis) and the name of the pathways (Y-axis). Outgoing pattern (signal sender) niche cells (left), and incoming pattern (signal receiver) granulocyte-neutrophils (right) signaling roles. (B) Chord plots of the selected pathways with signaling patterns with niche cells as senders and granulocyte-neutrophil cell types as receivers, the direction of the signaling (coloured arrow) depicting what cell type produces the signal and the receptive cell type (direction of the arrow).

4.2.9.3 Molecular crosstalk between granulocyte progenitors and osteo-chondro niche – ECM receptor

Finally, in the case of the ECM-receptor communication pathways, the fewest pathways were revealed, but at the same time, some of the most widespread effects upon our granulocytes and neutrophils of interest were observed.

As expected, these osteo-chondro niche cells are responsible for ECM production in outgoing signaling roles (Figure. 13 A). The most well-known ECM elements identified include collagen and laminin, the two main components of the bone matrix, which have drastically different effects on granulocytes; the latter is the most active signal. Furthermore, fibronectin-1 (*Fn1*) is essential for ECM assembly and migration and interacts mostly stochastically with all granulocytes. However, quite surprisingly, the THBS pathway, which originates mostly among the MSC-Chondro and MSC-Subpop cells, has the greatest stochastic incoming effect on all Gr1+ and granulocyte-lineage cells (greater than collagen). This is in stark contrast to the spatial relationship between THBS4 and Gr1+EdU+ cells reported in Chapter 3 (Figure. 4.13 B).

4.2.9.4 Molecular crosstalk between granulocyte progenitors and vascular niche – Cell to cell contact

Crosstalk pathways identified in the context of cell-to-cell contact between the vascular niche and our cells of interest are highly conserved and similar to those identified for osteochondral niche cells. This is evident in the case of MHC-1, *Gap*, *App* and *Pecam-1* (Figure. 14 A). Among these conserved pathways, ICAM, ADGRG and SIRP remain active, targeting most granulocytes and neutrophils. Meanwhile, the THY1 pathway, while also conserved, now only originates from pericytes and targets Gr1+ neutrophils. Of the pathways found only in this vascular niche context, SELE stems mostly from the two sinusoid clusters and the main EC cluster, impacting the granulocyte clusters. Finally, the well-known murine endothelial progenitor surface marker CD34 appears in an unexpected pattern, as it directly targets ECs and both sinusoidal ECs clusters coming from granulocyte progenitors. This suggests that some of the niche-granulocyte crosstalk mechanisms may also involve granulocyte progenitors influencing a variety of endothelial cells (Figure. 4.14 B).

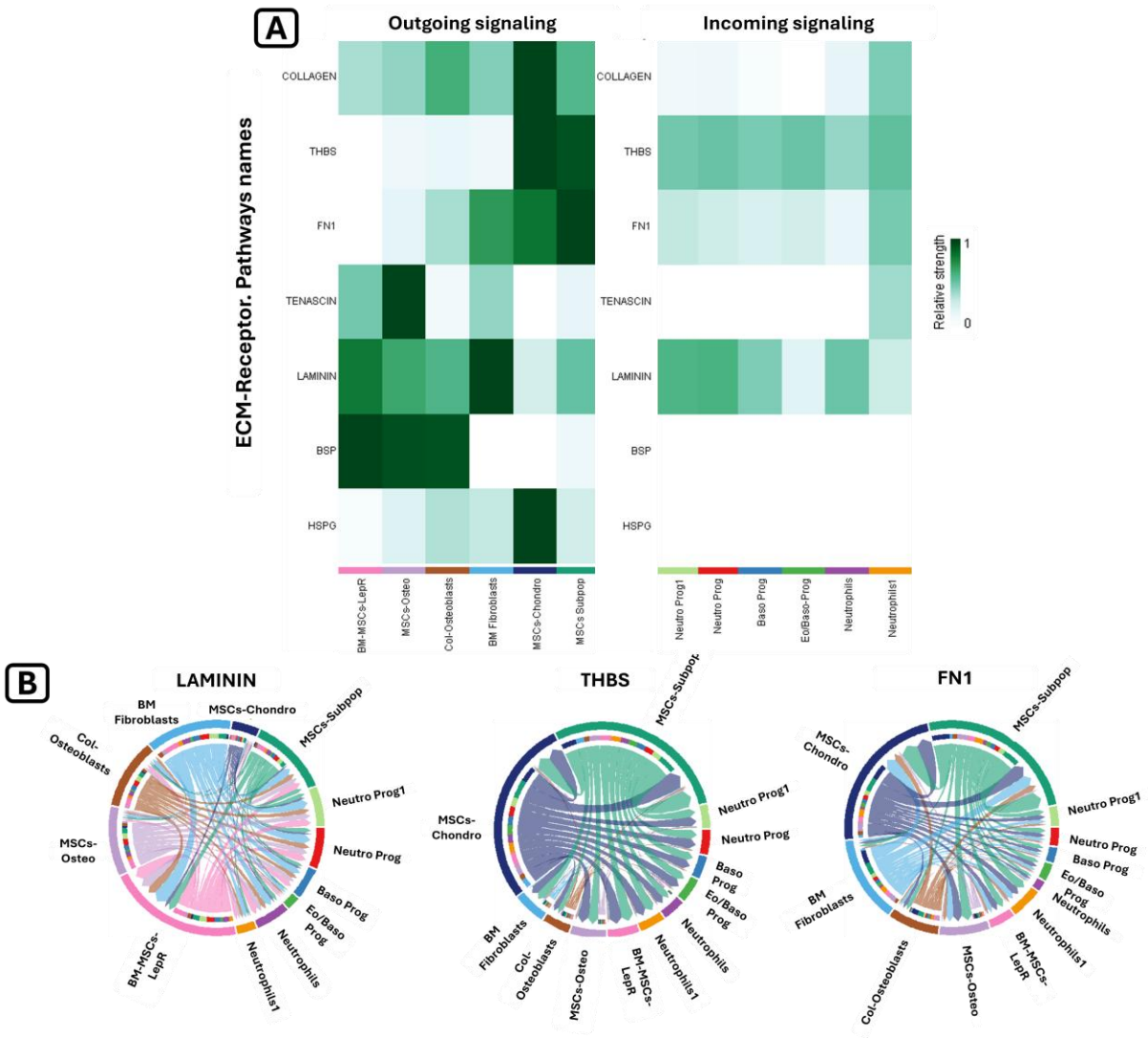

Figure 4.13 **ECM-Receptor communication pathways inferred between osteo-chondro niche cells and the granulocyte-neutrophil cell types**. (A) Cell communication pathways inferred by CellChat under the context of ECM-Receptor plotted based on pathway strength inference (green heatmap coloured format), cell types selected (X-axis) and the name of the pathways (Y-axis). Outgoing pattern (signal sender) niche cells (left), and incoming pattern (signal receiver) granulocyte-neutrophils (right) signaling roles. (B) Chord plots of the selected pathways with signaling patterns with niche cells as senders and granulocyte-neutrophil cell types as receivers, the direction of the signaling (coloured arrow) depicting what cell type produces the signal and the receptive cell type (direction of the arrow).

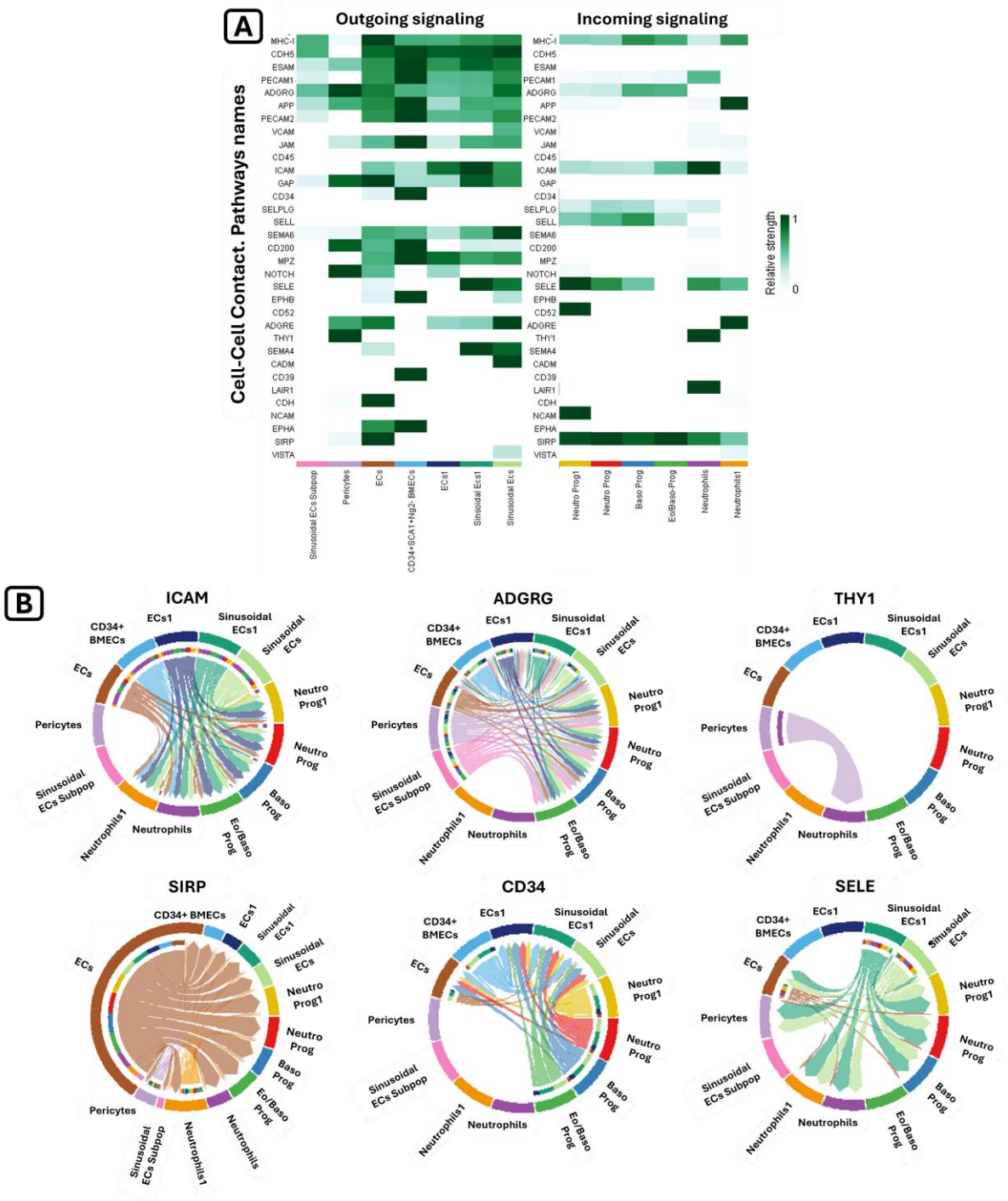

Figure 4.14 **Cell-cell contact communication pathways inferred between vascular niche cells and the granulocyte-neutrophil cell types**. (A) Cell communication pathways inferred by CellChat under the context of cell-cell contact plotted based on pathway strength inference (green heatmap coloured format), cell types selected (X-axis) and the name of the pathways (Y-axis). Outgoing pattern (signal sender) niche cells (left), and incoming pattern (signal receiver) granulocyte-neutrophils (right) signaling roles. (B) Chord plots of the selected pathways with signaling patterns with niche cells as senders and granulocyte-neutrophil cell types as receivers, the direction of the signaling (coloured arrow) depicting what cell type produces the signal and the receptive cell type (direction of the arrow).

4.2.9.5 Molecular crosstalk between granulocyte progenitors and the vascular niche – Secreted signaling

Similarly, conserved pathways emerged among the secreted signaling of vascular niche cells, such as GRN, galectin, IL2 and IGF/IGFBP (Figure. 4.15. A). Some of the most important expected conserved crosstalk includes pathways defined by factors such as CXCL, KIT and adiponectin, while lesser-explored conserved pathways include MK. However, SPP1 was found to originate from ECs and pericytes once again, despite being mostly known for its role in osteogenesis. These two niche cells also interact through the IGF pathway, which targets the entire series of myeloid cells with great specificity. The only instance in which a pathway targets only neutrophil cells is the macrophage migration inhibitory factor (MIF). Finally, other interesting pathways with known functions in proliferation include urokinase plasminogen activator (PLAU) and epidermal growth factor (EGF) (Figure 4.15. B).

4.2.9.6 Molecular crosstalk between granulocyte progenitors and the vascular niche – ECM receptor

Finally, the ECM-receptor pathways inferred for the vascular niche are consistent with those of the osteo-chondro niche, including collagen and laminin pathways. This is as expected, given that these ECM components have a wide variety of subtypes and many of them are part of the basal lamina of the vasculature (Figure. 4.16. A). The most relevant unique pathway in this context is that of vitronectin (VTN), which is mostly described in terms of brain pericytes, capillaries or microvasculature. However, this does not align with our findings in Chapter 3, where pericytes are only present in large-caliber vasculature embedded in the bone matrix. Nevertheless, the most unexpected pattern inferred is that of thrombospondin (THBS), which remains present but originates only from Gr1+ neutrophils and impacts all the other cells holistically. This may suggest a potential marker for BM neutrophils with a Gr1+ phenotype (Figure. 4.16. B).

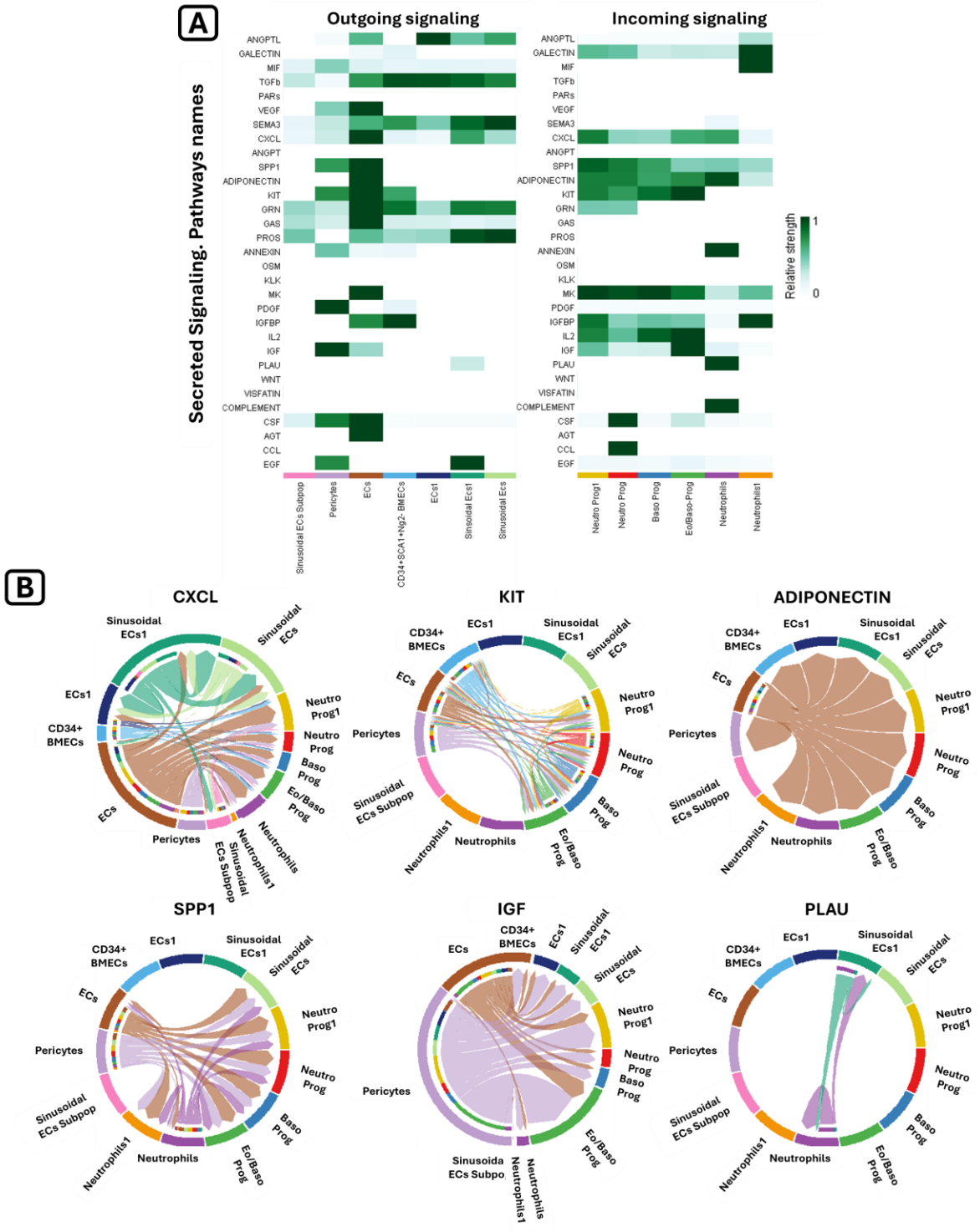

Figure 4.15 **Secreted signaling communication pathways inferred between vascular niche cells and the granulocyte-neutrophil cell types**. (A) Cell communication pathways inferred by CellChat under the context of secreted signaling plotted based on pathway strength inference (green heatmap coloured format), cell types selected (X-axis) and the name of the pathways (Y-axis). Outgoing pattern (signal sender) niche cells (left), and incoming pattern (signal receiver) granulocyte-neutrophils (right) signaling roles. (B) Chord plots of the selected pathways with signaling patterns with niche cells as senders and granulocyte-neutrophil cell types as receivers, the direction of the signaling (coloured arrow) depicting what cell type produces the signal and the receptive cell type (direction of the arrow).

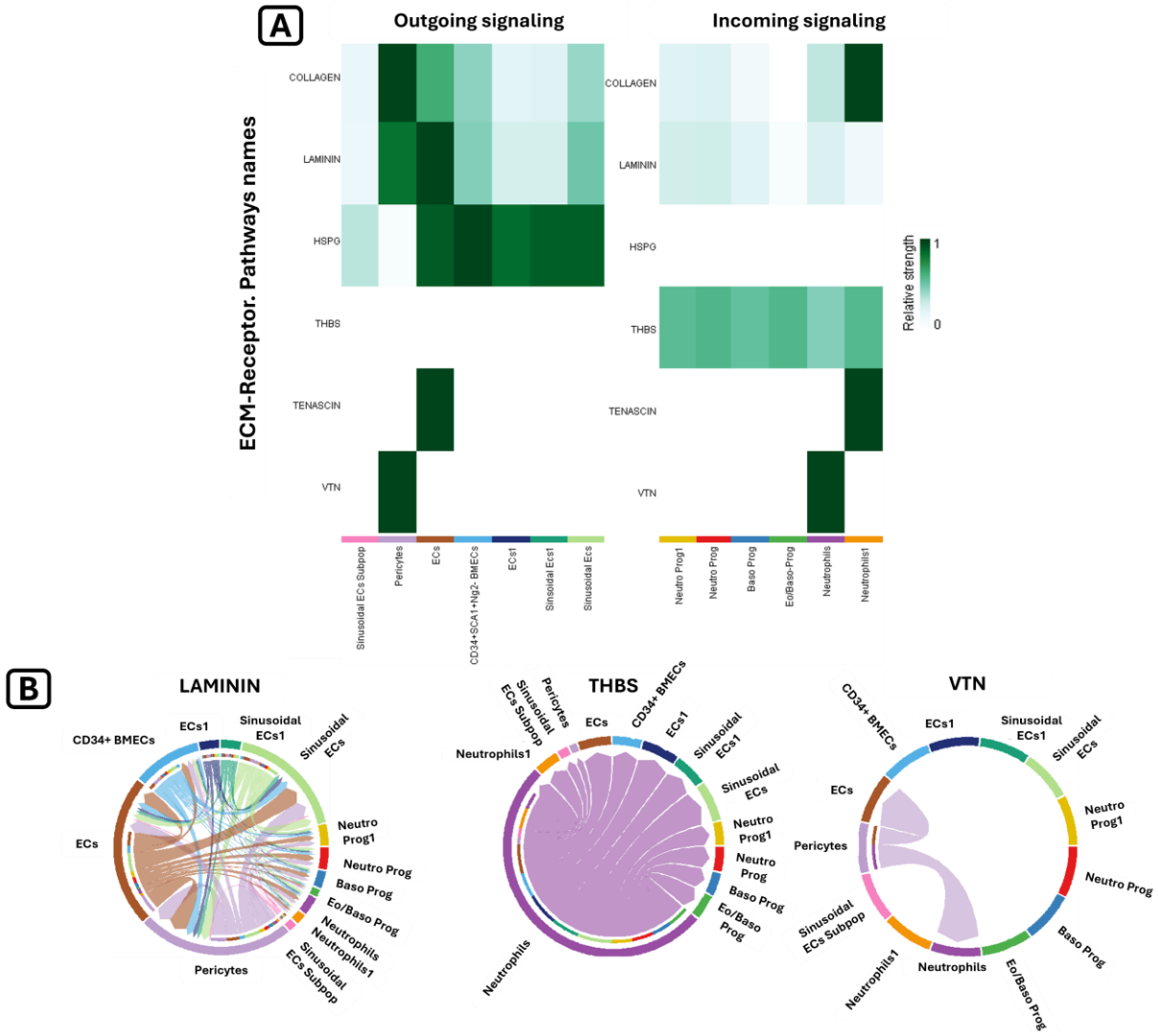

Figure 4.16 **ECM-Receptor communication pathways inferred between vascular niche cells and the granulocyte-neutrophil cell types**. (A) Cell communication pathways inferred by CellChat under the context of ECM-Receptor plotted based on pathway strength inference (green heatmap coloured format), cell types selected (X-axis) and the name of the pathways (Y-axis). Outgoing pattern (signal sender) niche cells (left), and incoming pattern (signal receiver) granulocyte-neutrophils (right) signaling roles. (B) Chord plots of the selected pathways with signaling patterns with niche cells as senders and granulocyte-neutrophil cell types as receivers, the direction of the signaling (coloured arrow) depicting what cell type produces the signal and the receptive cell type (direction of the arrow).

4.3 Supplemental information

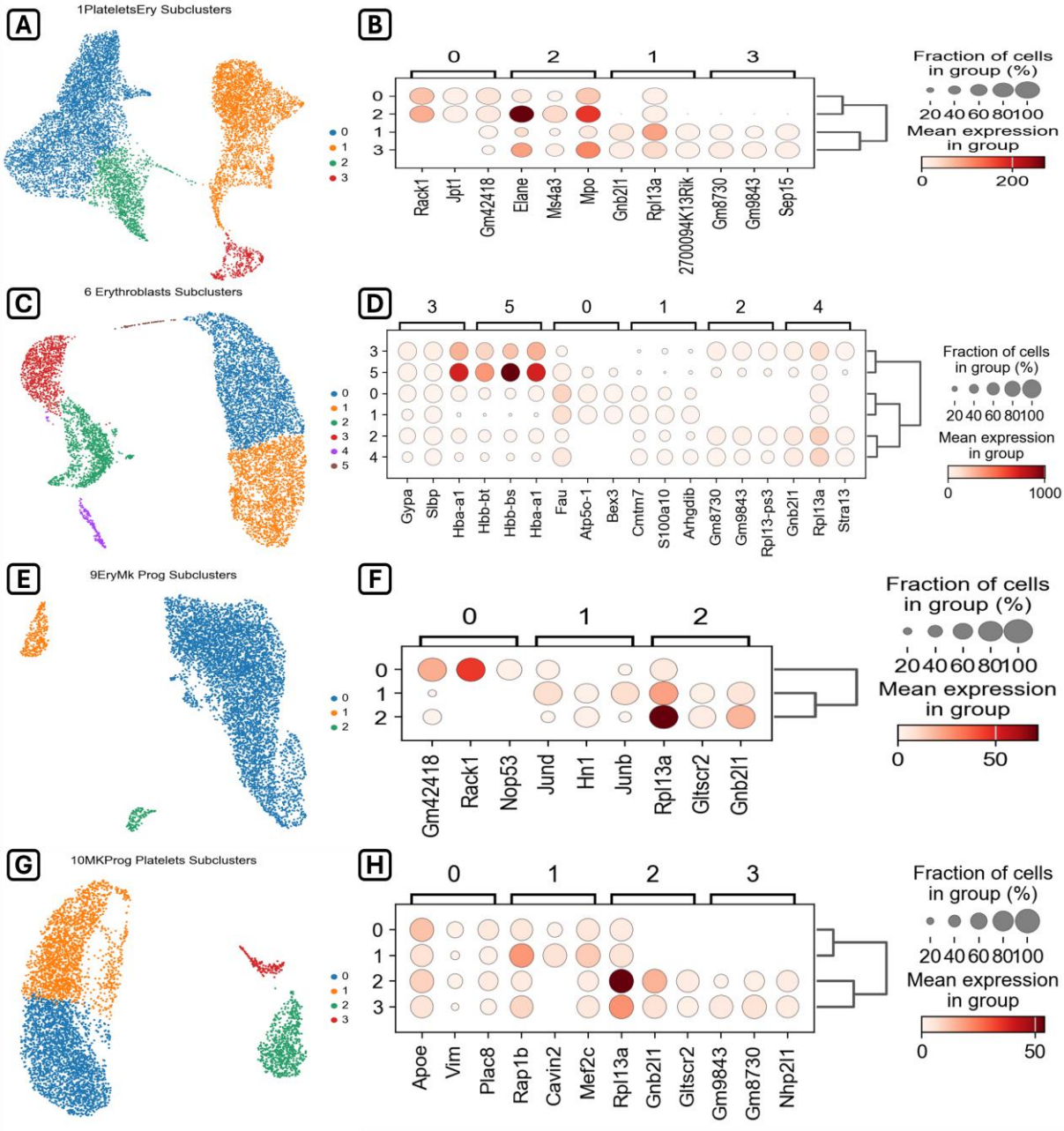

Supplemental Figure 4.1

Sub clustering of putative megakaryocyte-erythroid cell populations reveal relevant heterogeneity. (A) Newly identified 4 clusters from the cluster annotated in 4.2.7 as '1PlateletsEry'. (B) Top genes identified per cluster by DE analysis, heatmap coloring format based on mean expression of gene per cluster in A. (C) Newly identified 6 clusters from the cluster annotated in 4.2.7 as '6Erythroblasts*'. (D) Top genes identified per new cluster by DE analysis, heatmap coloring format based on mean expression of gene per cluster in C. (E) Newly identified 3 clusters from the cluster annotated in 4.2.7 as '9Ery/MK Prog*'. (F) Top genes identified per new cluster by DE analysis, heatmap coloring format based on mean expression of gene per cluster in E. (G) Newly identified 4 clusters from the cluster annotated in 4.2.7 as '10MKProg/Platelets'. (H) Top genes identified per new cluster by DE analysis, heatmap coloring format based on mean expression of gene per cluster in G.

Differential Gene Expression analysis per cluster	
Final cluster annotation	**Top5 scored marker genes**
LMPPs-Myeloid	'Hlf', 'Gcnt2', 'Gm19590', 'Ifitm1', 'Ltb'
Neutro Prog	'Mpo', 'Prtn3', 'Ctsg', 'Plac8', 'Pgam1'
Baso Prog	'Lig1', 'Dctpp1', 'Hells', 'Stmn1', 'Dtl'
LMPPs-Myeloid1	'Ifitm1', 'Hist1h2ap', 'Stmn1', 'Prtn3', 'Msi2'
MSCs-Adipo	'C2', 'Serpina3c', 'Slc26a7', 'Wdr86', 'Gpr88'
HSCs-Lymph Prog	'Hist1h2bc', 'Ccnb2', 'Hp1bp3', 'Cenpe', 'H2afv'
LMPPs	'Gm15915', 'Vamp5', 'Clec4d', 'Optn', 'Car1'
MK Prog1	'Pabpc1', 'Plscr1', 'Cirh1a', 'Rad23b', 'Eif4a1'
Sinusoidal ECs	'Ralgapa2', 'Amotl1', 'Ccdc85b', 'Zeb1', 'Map4k5'
Erythro-Prog	'AY036118', 'Gm42418', 'Car1', 'AC160336.1', 'Rps26'
Erythro-Prog1	'Mki67', 'Top2a', 'H2afx', 'Prc1', 'Ckap2l'
LMPPs-Myeloid2	'2700094K13Rik', 'Casc5', 'Cks1b', 'Hn1', 'Sgol1'
Sinusoidal ECs1	'Thrsp', 'Lgmn', 'Lrg1', 'Fcgr2b', 'Clca3a1'
CML1	'Nrgn', 'Pf4', 'Cavin2', 'Pbx1', 'Rap1b'
Erythroblast Subpop1	'Stard10', 'C1qtnf12', 'Tmem14c', 'Cldn13', 'Prdx2'
CML	'Nrgn', 'Pbx1', 'Itga2b', 'Fermt3', 'Zfpm1'
Eo/Baso-Prog	'Ms4a2', 'Cpa3', 'Csrp3', 'Fcer1a', 'Lmo4'
Erythroblast Subpop2	'Tmsb4x', 'Car1', 'Prelid2', 'Hspd1', 'Hspe1'
BM-MSCs-LepR	'C3', 'Aldh1a2', 'Ccl19', 'Eef1a1', 'Rnaset2b'
Neutro Prog1	'Elane', 'Ms4a3', 'Prtn3', 'Ctsg', 'Alas1'
LMPPs-Lymph Prog	'Dntt', 'Il12a', 'Arpp21', 'Xrcc6', 'Flt3'
B cells	'Vpreb3', 'Cd79a', 'Chchd10', 'Igll1', 'Blnk'
Myeloid Prog1	'Fam132a', 'E2f4', '5730508B09Rik', 'Cox17', 'Setd8'
Ery/MK Prog	'Car1', 'Gm15915', 'Hdgf', 'Gml2', 'Ermap'
CD34+SCA1+Ng2- BMECs	'Slc9a3r2', 'Tm4sf1', 'Ly6c1', 'Mapk3', 'Pecam1'
Plasmacytoid Dendritic Cells	'Siglech', 'Cox6a2', 'Mpeg1', 'Bst2', 'Irf8'
T cells/NK	'Ms4a4b', 'Cd3g', 'Cd3d', 'Skap1', 'Gimap3'
BM Fibroblasts	'Gsn', 'Mfap5', 'Pi16', 'Igfbp6', 'Tmem100'
MSCs-Osteo	'Alpl', 'Wif1', 'Mmp13', 'Fap', 'Kcnk2'
GypA+ Erythroblasts	'Ctse', 'Arf5', 'Gypa', 'Hbb-bs', 'Carhsp1'
ECs1	'Pim3', 'Sepp1', 'Mgat4b', 'Marcksl1', 'Kcnj8'
Neutrophils	'S100a8', 'S100a9', 'Lcn2', 'Camp', 'Ngp'
T cells/NK1	'Gata3', 'Il7r', 'Bcl11b', 'Rora', 'Id2'
Pro B cells	'Gp9', 'Pbx1', 'Khk', 'Unc119', 'Gp1bb'

Dendritic cells/Monocytes	'Aif1', 'Lgals3', 'Mpeg1', 'Pld4', 'Ccr2'
Lymph-Prog	'Malat1', 'Luc7l2', 'Atp5e', 'Rbm39', 'Prrc2c'
MSCs Subpop	'Cilp', 'Fmod', 'Cilp2', 'Ndufa4l2', 'Chad'
Myofibroblasts	'Pdlim4', 'Chodl', 'Des', 'Fxyd6', 'Meg3'
Neutrophils1	'Jchain', 'C1qc', 'Gzma', 'C1qb', 'Retnlg'
HSCs1	'Lsm5', 'Calm2', 'Sub1', 'Tacc3', 'Slc25a5'
Col-Osteoblasts	'Cpz', 'Col1a2', 'Ifitm5', 'Col22a1', 'Bglap2'
MK Prog	'Pabpc1', 'Plscr1', 'Cirh1a', 'Rad23b', 'Eif4a1'
MSCs-Chondro	'Papss2', 'Mia', 'Acan', 'Col2a1', '3110079O15Rik'
Platelets	'Ppbp', 'Gnaz', 'Gpx4', 'Ywhah', 'Rbpms2'
Sinusoidal ECs Subpop	'S100a13', 'Cyb5a', 'Myl12a', 'Txndc17', 'Rab13'
Erythroblast Subpop	'Fam132a', 'Bex4', 'Gnb2l1', 'Klf1', 'Rpl36al'
Macrophages	'C1qa', 'Hmox1', 'Aif1', 'Cd163', 'Cd5l'
B Cell Prog	'Ldha', 'Pfn1', 'Ywhah', 'Vps37b', 'Nt5c3'
HSCs	'Gm15915', 'Csrp3', 'Tspo2', 'Gnb2l1', 'Khk'
Schwann Cells	'Sirt2', 'Slain1', 'Slc48a1', 'Kctd13', 'Serpind1'
Pericytes	'Olfr558', 'Rgs5', 'Higd1b', 'Tagln', 'Aoc3'
Mature Erythroblasts	'Hba-a2', 'Hba-a1', 'C1qc', 'Hbb-bs', 'Hbb-bt'
Monocyte small subpop	'Isg15', 'Irf7', 'Trim30a', 'Zbp1', 'Xaf1'
ECs	'Col4a2', 'Col4a1', 'Id1', 'Gpihbp1', 'Smad1'
Hemoglobin+ Erythroblasts	'Sox6', 'Slc25a37', 'Trak2', 'Hemgn', 'Spta1'
Myeloid Prog	'Elane', 'Ms4a3', 'Alas1', 'Prtn3', 'Cebpe'
Monocyte small subpop1	'Pde10a', 'Neurl3', 'Gabarapl1', 'Nr4a2', 'Map9'

Supplemental Table 4.1 Final DE gene expression analysis performed on the final manually annotated 57 clusters.

Chapter 5: Discussion, limitations, future directions and conclusion

Historically, studies of the BM have led to crucial discoveries that have advanced our understanding of stem cells, "ecological" stem cell niches, and have led to groundbreaking therapies that exploit the capacity for complete repopulation of the blood and immune system through stem cell transplantation, such as the case in leukaemia treatments. However, a significant knowledge gap still exists, particularly regarding how hematopoietic progenitors interact with their niche in situ to maintain blood and immune homeostasis, in both steady and perturbed conditions.

In situ myelopoiesis studies are scarce, particularly those involving imaging approaches to study the myelopoietic BM microenvironment. This results in a lack of a well-characterised panel of markers for niche cells, knowledge of the cell composition of the myeloid-inductive niche, understanding of the mechanisms by which ligands act, and insights into the impact of pathologies on this ecosystem. Moreover, these knowledge gaps also make it difficult to interpret and extrapolate experiments involving the deletion/deficiency of well-known regulators of hematopoiesis. While current techniques and the rich data generated by scRNA-seq datasets show great potential, better and more detailed annotations representing functional cellular heterogeneity are needed. Therefore, it is imperative to characterize the BM niche using imaging techniques to help with the interpretation of transcriptomic data. Combining both approaches to account for their technical limitation is necessary for a better understanding of myelopoiesis at the cellular and molecular levels. This knowledge could then be used in future functional studies, e.g. conditional knock-out (cKO) of specific genes in specific cell types rather than the current approach of cKO specific genes in poorly defined, broad niche cell populations.

Hematopoietic lineages can be broadly separated into two distinct branches: the lymphoid and myeloid lineages. The myeloid lineage includes the innate immune system, which is the focus of this study. While much research has been conducted into early haematopoiesis mechanisms, the precise manner in which the BM niche orchestrates the myelopoietic and granulocytic-neutrophil differentiation and maturation in situ remains less understood. To this end, I sought to take advantage of our lab's quantitative multiplex immunofluorescence workflow for staining thick, postnatal femur sections and analyze the spatial relationship and interactions between BM niche cells and Gr1+ granulocyte progenitors.

As imaging approaches are time consuming and limited by the availability of relevant antibodies, I also used publicly available single-cell transcriptomic datasets collected by different laboratories to reveal the composition of BM cells of interest. Then, using tools for integrating transcriptomic data and inferring cell-cell communication pathways, I identified relevant cell types, including granulocytic progenitor cells, neutrophils, the osteochondral niche and the vascular niche. Finally, based on their transcriptional competence, I identified the molecular pathways through which the BM niche cells may orchestrate the proliferation and maturation of granulocyte progenitors in situ.

In doing so, I have contributed to our growing understanding of how complex biological mechanisms such as granulopoiesis, are controlled in vivo. I optimized a staining protocol and used it to map the precise anatomical locations where myeloid-progenitor cells proliferate in the BM. I also quantified their spatial relationships with several putative niche components, demonstrating that both osteoblasts and endothelial cells cooperate to form the myeloid niche. Finally, I achieved an integrated dataset of transcriptomic profiles with a robust representation of LSK cells, HPSCs, mature hematopoietic cells, and BM niche cells (over 10e5 cells) and improved its annotation, which is a valuable resource for further efforts to identify BM-niche mechanisms in post-natal mice.

5.1 BM myeloid cells preferentially proliferate in specific BM niches

While studying skeletal stem cells in the femurs of mice using EdU incorporation, I observed an unexpected pattern of labelled proliferative cells in the BM of our lab's samples. Pockets of BM cells close to the cortical and trabecular bone in the distal epiphysis and metaphysis exhibited a stronger EdU signal in a privileged, discrete and distinguishable pattern. Based on this, I asked our collaborators at the University of Toronto to replicate the EdU regime and identify the lineage of the EdU+ cells by means of flow cytometry. They determined that the clear majority of cells incorporating EdU displayed the Lin+GR1+CD11b+ phenotype. This indicates that these cells are part of the granulocyte-neutrophil lineage (erythroid progenitors, well known to proliferate rapidly in BM, were not quantified in this assay). The spatial pattern of proliferation and the phenotype of most EdU+ cells suggested a previously unknown in situ niche that promotes myeloid-granulopoiesis in adult mice.

The dividing cells in situ were identified by incorporation of the thymidine analogue EdU (Click-iT™, Invitrogen), after optimizing the pipeline described by our former laboratory colleague, Dr Stephanie Farhat[156]. According to the references consulted at the time of writing this document, this thymidine analogue has only been used once beyond the efforts of our lab to identify proliferating cells in bone sections by fluorescence microscopy[157]. In most published protocols and studies where thymidine analogues (e.g. BrdU and EdU) have been used, this has been in the context of flow cytometry-based techniques, such as FACS, or in vitro assays collecting proliferating BM and BM stromal cells[158–164]. These studies have been crucial in identifying proliferation rates of hematopoietic cells in different tissues[158], and the of long-lived and short-lived HSCs via EdU retention[161]. Specifically, with regard to myeloid and granulocyte lineages, the effects of CSFs, (such as G-CSF) on granulopoiesis by means of tracking of these analogues on circulating PMNs[162,163], and the differential proliferative dynamics of neutrophils and macrophages[164].

There are also limited alternatives to thymidine analogues for identifying BM HSCs or proliferative HPSCs for imaging-based purposes. One of these alternatives is the tetracycline (Tet)-inducible histone H2B-GFP reporter system[165,166]. This system is useful for the in vivo expression of the fluorescent reporter and for identifying low- and non-cycling HSCs, which can be examined using fluorescence microscopy in relation to their niche[165–168]. Meanwhile, for the purpose of staining pre-neutrophils, the FUCCI (fluorescent ubiquitin-based cell cycle indicator) detection system and S100A9 staining have been used to mark myeloid progenitors in a 250 μm thick femur section, allowing the study of their spatial association with CAR cells[169].

Based on these references and the results in Figure 3.6, administering EdU as described in Chapter 2 is a reliable commercial method for identifying proliferating cells in BM using imaging, through copper reduction reactions with a specific fluorophore. This method can reach tissues with different levels of vascularisation, such as highly vascularised BM and regions with low to no vascularisation, such as the GP of the femur. Furthermore, the click chemistry reaction alleviates the need to detect EdU using antibody staining, facilitating multiplexing, improving signal-to-noise, and avoiding harsh staining conditions to permeabilize nuclei.

Hence, having contrasted the reviewed literature on the expression pattern of Gr1 cells in the BM with my in situ and in silico results, I can confirm that Gr1+EdU+ cells in the BM represent

GMP-derived early to late neutrophil progenitor cells undergoing cell division, as confirmed by EdU incorporation and *Mki67* gene expression.

5.2 Cell markers for in situ staining of osteo-lineage niche cells

Research on osteo-lineage cells and their roles as BM niches are usually performed by immunostaining of ECMs specific of the bone matrix, these include collagen type I (encoded by gene *Col1a1*), osteocalcin (OC, also known as BGLAP) and osteopontin (OPN, encoded by the *Spp1* gene)[62]. Some of these components are associated with different stages of the osteoblastic maturation[62,170]. However, these ECM components extend throughout the entire bone matrix and are not useful for locating specific osteoblast-osteocyte cells to compute spatial information relating to niche functions[62]. Meanwhile, cell membrane markers for IF targeting osteoblasts-osteocytes are limited.

To identify osteoblasts, osteogenic reporter systems in mice have been used, such as Osx-CreERT, 2.3Col-GFP, and OC1.7-GFP[171–173]. However, importing and maintaining mouse colonies is costly and not implementable for every lab. Furthermore, Kucinski et al. have demonstrated that activating the Cre recombinase by means of tamoxifen administration disrupts the steady-state hematopoietic dynamics[143]. Therefore, identifying further cell markers that can be used to label and effectively image osteoblasts and osteocytes in IF protocols is of particular importance.

To this end, the ALP protein, which is expressed and found in the membranes of osteoblasts undergoing maturation and acquiring the phenotypic competence necessary for bone formation/remodeling, can be used in IF protocols (Figure. 3.7. A. Supplemental Figure 3.1. Ai-ii)[62,174]. Physiologically, ALP catalyzes the hydrolysis of the mineralization inhibitor inorganic pyrophosphate and ATP, resulting in the production of the inorganic phosphate necessary for controlling and enabling the formation of hydroxyapatite crystals[174,175].

Moreover, during the screening for ABs targeting osteo-lineage cells with greater specificity than the ALP staining pattern, podoplanin (PDPN) showed specific expression on the cell membrane of osteoblasts and osteocytes (Figure 3.7. B and Supplemental Figure 3.1. Bi-ii). PDPN is a mucin-type transmembrane protein that has mostly been studied in the context of development, cancer research and lymphoid organs[176]. Regarding its relationship with myeloid

functions, it is known that PDPN acts as a ligand for the Clec-2 activation factor in platelets and dendritic cells (DCs)[177,178]. In humans, PDPN is expressed in chondrocytes of fetal cartilage, as part of the cells that define the primary ossification centre[179]; while in adult bones, it is part of the phenotype of self-renewing SSCs (PDPN+CD146−CD73+CD164+)[180]. Meanwhile, PDPN expression in mouse osteo-lineage cells defines the transition of the late osteoblast-osteocyte, as it marks the acquisition for the dendritic phenotype necessary for bone matrix embedding[181].

Based on the in situ results presented in Figure 3.7-B, I confirmed for the first time that PDPN is a reliable cell marker for IF staining of osteoblasts and osteocytes in the bones of adult mice. These cells have a diameter of 12–15µm and are found either lining the surfaces or embedded inside the bone matrix in both the TB and the CB, which are active in bone formation. Meanwhile, ALP stains maturing osteoblasts that are limited to the lining of bone surfaces. Together, PDPN+ and ALP+ cells identify the osteo-lineage cells at different maturation stages across whole-mount bone sections and are especially abundant in the distal epiphysis and metaphysis of the mouse femur.

5.3 In situ identification of GP cartilage

The GP is characterized by distinct populations of resting, proliferating, and hypertrophic chondrocytes (together referred to as GPCs)[126,182]. These GPCs are usually identified by expression of specific TFs such as *Sox9*; or by their ECM rich in collagen type II (*Col2a1*) or aggrecan (*Acan*), using in situ hybridization and inducible transgenic reporters[156,183,184]. However, due to the aforementioned limitations, the confounding effects of tamoxifen, and the fact that few cartilage-specific antibodies are available, I decided to screen ABs for ECM markers such as *Col2a1* and ACAN. Unfortunately, this approach did not produce a reliable fluorescent signal (not shown), maybe due to the shelf life of the available stock as similar IF staining protocols were followed, unlike the staining achieved with the THBS4 marker.

The thrombospondin (THBS) family comprises five members. THBS4 is the least studied member in the context of bone-cartilage, and the literature on it has produced contradictory results. Deletion of the THBS4 gene in a mouse model produced a phenotype of reduced AC tissue thickness, without changes in the GP, suggesting that THBS4 is not required for GPCs[185]. However, in a more recent study investigating GPCs as a source of SSCs, THBS4 was stained and identified as being expressed in GPCs by means of IF on thin cryosections[186].

As demonstrated by my results in Figure 3.7-C and Supplemental Figure 3.2, I confirmed that THBS4 is present across the entire GP in thick mouse femur sections, but not restricted to it, as it is also present in periosteum and AC. Therefore, since the periosteum and the AC are neither in contact with nor at a relevant niche distance from the BM, THBS4 can be used to quantify the spatial interactions between Gr1+EdU+ cells and the GP cartilage matrix.

5.4 In situ staining of vascular endothelial niche cells

The BM harbours a complex network of vascular and perivascular cells. Arteries carrying oxygenated blood and nutrients branch into arterioles that are covered with pericytes identified by markers such as SM22, Sca1 and CD90[52,62,187,188]. These arterioles mostly feed cortical and trabecular bone. These arterioles then empty into venous and fenestrated sinusoids, which comprise most of the BM vasculature and through which hematopoietic cells migrate in and out of the BM[76,189]. Endothelial cells (ECs) in the BM are heterogeneous; some express CD105, VCAM1, CD34, EMCN, SCA-1, NESTIN, VWF and selectins (E- and P-selectins) to varying degrees[28,52,190–194]. However, all BM-ECs express CD31/PECAM-1[62,130]. Hence, to study the spatial distribution of Gr1+EdU+ cells around blood vessels, I used the pan-endothelial marker CD31 and the pericyte marker SM22 described by my supervisor in detail to identify the ECs and arteries/arterioles present in the BM ecosystem, respectively[62].

As expected, based on the literature, the results presented in Figure 3.8-A and Supplemental Figure 3.3 confirmed the pan-endothelial expression of CD31 and the expression of SM22 across peri-vascular cells. These antibodies were also compatible with Gr1 and EdU staining without the need for further optimization.

5.5 Anatomical distribution of Gr1+EdU+ cells within the BM

For myeloid-granulocyte inductive niche functions, most of the proposed niches follow similar mechanisms to those determined for the HSC niches, particularly the niche effects induced by factors such as KitL (SCF) and CXCL12. Preventing apoptosis, inducing cell cycle, regulating adhesion-migration and chemoattractant dynamics. However, the proper function of the myeloid-granulocyte-specific mechanisms are highly context-dependen[70,128].

Studies on ageing have revealed interesting correlations between hematopoiesis and the niches. Firstly, during ageing, skeletal osteoprogenitors become biased towards adipogenesis and

lose their bone/osteogenic potential[195–199]. Secondly, most of the hematopoietic BM (red marrow) in the diaphysis of long bones is replaced by adipocytes (yellow marrow)[195,199–202]. Red marrow becomes restricted to the TB-rich epi-metaphysis[195,200,201]. Concomitantly, hematopoiesis also becomes lineage biased towards myeloid lineages in both human and mice[69,203,204]. It is therefore possible that this age-related hematopoietic lineage bias is caused by the loss of BM-lymphoid niche in the diaphysis, while the myeloid niche is preserved in the metaphysis[69,89,90,92,95,205,206].

My observations that myelopoiesis mainly occurs in metaphysis and close to CB of the diaphysis (see figure 3.9-Aii and Bii; and Figure 3.10-B) support this niche-hypothesis, although cell-intrinsic factors within HSCs/HSPCs (e.g. epigenetic changes) could also be involved[203–205]. I cannot rule out the possibility that epigenetic changes within HSCs/HSPCs are causing changes in the BM niche either. However, this would not explain why myelopoiesis is restricted to the metaphysis and epiphysis in younger animals.

In this context, as described by the reviewed literature, the findings here largely align with the key concepts of the spatial relevance of osteogenic niches as key regulators of myelopoiesis across the TB-rich regions. The molecular interactions between osteoblasts and Gr1+ cells are likely through soluble factors, since direct contact between these cell types does not appear predominant (see Figure 3.9-C). On the other hand, ECs and Gr1+ cells are likely to interact by means of direct cell-contact, since most Gr1+EdU+ cells were found in immediate proximity with CD31 (Figure 3.10-D and E). Of note, close contact between these cells does not rule out soluble factors as potential regulators of Gr1+ cells proliferation.

5.6 Non-random distribution of Gr1+EdU+ cells in the osteoblastic niche

To quantify the spatial distribution of Gr1+EdU+ cells relative to osteochondral cells, I stained femurs for Gr1, EdU, DAPI, and the osteochondral niche markers ALP or PDPN (for osteoblasts), or THBS4 (chondrocytes). I then added a random distribution of spheres (random dots) of a diameter similar to that of Gr1+ cells, within my imaging datasets. After segmenting both Gr1+ cells and niche components, I then computed the distance variables between Gr1+EdU+ cells and RDs with the niche elements. I next split my dataset spatially to analyze the diaphysis separately from the meta/epiphysis by means of fluorescence intensity values. Finally, the distance between Gr1+EdU+ cells was statistically compared to the RDs.

My data demonstrates that in the distal femur (metaphysis and epiphysis), RDs distribute almost equally close (<50µm) and far (>50µm) from ALP+ cells, whereas Gr1+EdU+ cells are non-randomly enriched closer to osteoblasts, with 81.13% (Figure 3.9-Aiv) being localized <50µm from ALP. In the diaphysis, the percentage of Gr1+EdU+ cells localizing close to ALP remained superior, compared to the distal femur, but this was not different than RDs. Similarly, the percentage of Gr1+EdU+ cells in direct contact with ALP (<5µm) was increased in the diaphysis but was not significantly different from RDs. I confirmed these findings using the PDPN marker for osteoblasts and obtained very similar results (Figure 3.9-Diii). Not surprisingly, Gr1+EdU+ cells were not found enriched close to THBS4+ chondrocytes, with no direct contact observed, and this spatial distribution was similar to that of RDs (Figure 3.9-Eiii-iv).

Efforts reported in the literature, based on data generated by similar approaches to the in situ exploration of the HSCs niche and statistical comparisons with RDs have shown that although HSCs localized near sinusoids, this spatial distribution was not different from RDs. The low frequency of HSCs and abundance of sinusoids was proposed to explain this random distribution. Gr1+EdU+ cells appear to distribute non-randomly close to the osteogenic niche but not necessarily at direct contact[63,114].

5.7 Non-random distribution of Gr1+EdU+ in the vascular niche

To quantify the spatial distribution of Gr1+EdU+ cells relative to vascular and perivascular cells, I performed the same workflow as just described for the osteoblastic niche. However, I used the pan-endothelial marker CD31 (PECAM-1) to detect ECs, and SM22 as a marker of arterial pericytes. Generation of RDs, segmentation of (peri-)vascular and Gr1+ cells, minimal distances computation, and statistical analyses were performed as above.

My data shows that nearly all Gr1+EdU+ cells (98.94%) are located close (<50µm) to CD31+ vasculature, a spatial distribution significantly different from a random distribution (Figure 3.10-D). Contrary to the osteoblastic niche, I also observed that a majority of Gr1+EdU+ cells were found in direct contact with vasculature (63.52% direct contact to CD31 vs 24.25% direct contact to ALP), a distribution that was also different from RDs (Figure 3.10-E). On the other hand, Gr1+EdU+ cells distributed almost equally, close and far, from SM22+ pericytes (Figure 3.10-G). Unexpectedly, this distribution does not appear random, as nearly all RDs are located far from pericytes (Figure 3.10-G gray bars, RDs). In addition, little evidence of direct contact

between Gr1+EdU+ cells and SM22+ pericytes was observed (Figure 3.10-H). It is worth noting that, *Pecam-1*, the epitope for the anti-CD31 AB here used, while it was overwhelmingly representative of the ECs and vasculature in the BM as seen in Figure 3.8, I cannot discard the possibility of also had stained a subpopulation of CD31+ HSCs/HPSCs, as it has been reported in literature that this surface marker is also present in detectable proportions of LSK (Lin-Sca1+cKit+CD31+) cells, and preserved in both embryonic, adult and aged (2y.o.) mice[207]. This CD31+ LSK according to literature to have a strong potential towards myeloid-erythroid lineages worth exploring in future research[207].

Taken together, my data suggests that vascular and perivascular cells may be a relevant niche inducing myelopoiesis. CD31+ endothelial cells may interact with Gr1+ cells through direct contact and soluble factors, whereas pericytes appear to interact with them using only soluble factors to account for their distance. Finally, considering the sharp contrast between Gr1+EdU+ cells and RDs regarding their distance to CD31+ cells, this spatial distribution is not dominated by the abundance of the vascular niche itself.

5.8 The single-transcriptomic dataset integration method was effective in identifying HPSCs-granulocytes and niche cells.

Exploring cell markers to identify cell populations in thick femur samples, providing robust 3D spatial data and enabling image cytometry analysis based on fluorescence intensity and statistics is a reliable and crucial tool for analyzing the BM niche and myeloid proliferation in situ. However, this approach has clear limitations stemming from the limited availability of ABs, the need for optimization to achieve appropriate immunostaining, the long times required for staining and imaging, and the number of channels that can be used in multiplex IF approaches, which are usually limited to around 5–7 markers. Consequently, the number of markers and cell types that can be targeted per sample is limited. Nevertheless, to account for these limitations, I also took advantage of publicly available single-cell transcriptomics libraries and analysis tools.

The introduction of scRNA-seq techniques to capture the transcriptome of entire cell components and the development of tools to analyze these data are crucial for identifying previously unknown functional heterogeneity and inferring molecular interactions between different cell types and within complex tissues[75,120,194,208]. Open-source Python- and R-based tools such as SCVI, SCANVI and CellChat are imperative for this purpose[145–148]. However, the study

of the BM has its own limitations, as the vast majority of available datasets rely on approaches targeting either HSCs, HSPCs, mature hematopoietic cells, or niche cells separately. Only the library generated by Baccin et al. aimed to capture both BM and BM niche cells together[142]. Hence, most datasets cannot be used individually if one aims to explore the niche-myelopoiesis interactions at single-cell resolution. For this purpose, the first step was to integrate the datasets here selected[36,74,142,143].

I took advantage of the machine-learning, Python-based tool SCVI as a transcriptomic library integration tool given its robust, probability-based approach, which is useful for identifying biological variations and shared transcriptomic profiles[145,147]. This is different from genome alignment integration methods such as Seurat[209]. My integrated dataset here achieved is the most extensive in terms of cell counts and cell types (LSK cells, HPSCs, mature immune cells and niche cells) of any reported in the literature, comprising more than 110 thousand of cells, 37 GB and a trained model based on 150 iterations of Bayesian variational inference on shared transcriptomic states[145,147,210].

For data integration, the published datasets display significant variability in cell type annotations, reflecting the distinct approaches adopted by each laboratory while exploring the BM-niche ecosystem. This leads to poor consistency in the definition of cell types across datasets, with the greatest impact being seen in mature blood cells and niche cells.

Given the advantageous features of SCVI and the inconsistency of cell annotations, I opted to work with the raw data, which lacked any annotations that could have biased the integration and cell type clustering. The annotations achieved here are therefore the result of a differential gene expression (DE) analysis, identification of marker genes, and cross-referencing of expression patterns among the individual datasets, as well as cross-referencing of each marker gene with the available literature. This was done to achieve the most comprehensive cell annotations possible within the time available for each of the 57 clusters detected, as described in section 4.2.8, Figure 4.10.

Considering the wide range of BM and BM niche cells identified among the 57 clusters, I will focus on those relevant to the osteogenic niche, GPCs, ECs, perivascular/pericytes and granulocyte progenitors-neutrophils.

5.8.1 Marker genes identified reveal 4 granulocyte progenitors populations

The integrated dataset enabled clusters to be identified with gene expression patterns and DE marker genes associated with granulocyte-neutrophil cells. In most cases, these genes could be corroborated with the available literature and the transcriptomic exploration tools, to the best of my ability. However, several of the genes identified as markers behave in a continuum-like manner and are not restricted to a single unique cluster, given the transcriptomic similarities of their shared GMP-derived nature. The relevant clusters annotated are: Neutro Prog, Neutro Prog1, Baso Prog, and Eo/Baso-Prog (Figure. 4.10-B). Their marker genes can be seen in Supplemental Table 4.1.

5.8.1.1 Neutro Prog cluster marks the acquisition of the granule-neutrophil phenotype

This cluster was reviewed and annotated as a population of granulocyte HPSCs that are committed towards neutrophils. The identified marker genes reveal the acquisition of the transcriptomic competence to express key azurophilic granule enzymes. Meanwhile, fate regulatory genes prevent further differentiation downstream and maintain a progenitor identity, seen in Table 4.1-Neutro Prog.

The most representative gene in this cluster is *Mpo* (Myeloperoxidase), which encodes an azurophilic granule enzyme found in both humans and mice. *Mpo* is a highly expressed protein in neutrophils, representing close to 5% of their dry weight[211–213]. The next marker gene identified, *Prtn3*, also functions as a negative differentiation gene in the development of functional neutrophils in mice by antagonizing G-CSF-induced *Stat3* in LSK cells through PRTN3-dependent ubiquitin-mediated degradation of STAT3[214–216]. Furthermore, despite being mostly described in the context of humans, the last genes are considered to be relevant serine proteases, such as the *Ctsg* gene (cathepsin G), which is part of inflammatory granules[217]; *Plac8* (also known as onzin) is crucial for neutrophil function, as its knockout impairs neutrophil phagocytosis and accelerates apoptosis[218]; and the *Pgam1* gene has been identified and validated as being involved in neutrophil activation networks[219].

Hence, this cluster represents the major neutrophil progenitor cells marking the granule formation competence acquisition while also expressing the specific differentiation-maturation antagonist gene of downstream neutrophils.

5.8.1.2 Neutro Prog1 cluster represents a subpopulation of PMNs and neutrophils-progenitors

Interestingly, the integrated model, clustering strategy and DE genes reveal a second transcriptomic profile closely related to that of 'Neutro Prog' (Supplemental Table 4.1-Neutro Prog1), where the genes *Prtn3* and *Ctsg* were also identified. However, there is a clear gene pattern in that the gene *Elane* is differentially expressed. *Elane* is another gene with one of the best-known functions in human neutrophil differentiation. *Elane* mutations in humans cause neutropenia, an effect that is highly disputed in mouse models[220,221]. Meanwhile the *Ms4a3* gene is a clear marker of GMPs that trace downstream to neutrophils, basophils, eosinophils, $LY6C^{HI}$ monocytes and $LY6C^{LO}$ monocytes[222]. The *Alas1* gene is crucial for heme synthesis as it encodes ALA synthase, which is involved in pathways responsible for forming 5-aminolevulinic acid (5-ALA)[223]. Deficient expression and function of the *Alas1* gene have been revealed to affect innate immune system functions related to neutrophils[223,224].

This suggest that this population may represent an intermediate stage between the GMPs and the myeloblast-myelocyte with the transcriptomic competence for PMNs-neutrophil commitment, while competence for the myeloid-erythroid lineage to synthetize the heme protein share distinct functions within PMNs.

5.8.1.3 Eosinophils and Basophils Prog cluster has multipotent characteristics

This cluster comprises a smaller cell population (see Figure 4.10-B green cluster) and depicts a precise transcriptomic profile of the differentiation of granulocytes to early basophils, as indicated by the marker genes *Csrp3* and *Lmo4* (Supplemental Table 4.1-Eo/Baso-Prog)[142,144,225]. The differentiation of late basophils, as indicated by the *Ms4a2* gene, which encodes the high-affinity IgE receptor, and *Cpa3* (carboxypeptidase, which is involved in protein degradation) is expressed in HPSCs, mouse basophils, and its promoter can be used to target PMNs[107,226,227]. Furthermore, the *Fcer1a* gene encodes the FcεRI receptor, marker of multipotent Basophil/Mast cell/eosinophil shared progenitor in human[208,226,228,229]. Despite their association to mast cells, these cells fully mature extramedullary, so is not expected to find them in the BM and lack the key marker genes *Lilrb4a* and *Lilr4b*[225].

Despite the unclear progenitor-lineage continuum of basophils and eosinophils in mice, these gene expression patterns suggest that the genes showcased here reflect oligopotent potential

without definitive lineage commitment markers for basophils, eosinophils or mast cells. Therefore, the annotation considers this oligopotent aspect, treating it as a putative progenitor of basophils and eosinophils.

5.8.1.4 The Basophils Prog cluster has unclear transcriptomic profile but consistent with reported markers

In the case of this last cluster, located between the abovementioned eosinophil and basophil progenitors (see Figure 4.10-B orange cluster), the identified marker genes did not provide a useful transcriptomic profile for determining a particular granulocyte phenotype. This is because *Lig1* (DNA ligase 1), *Dctpp1* (dCTP pyrophosphatase 1), *Hells* (lymphoid-specific helicase), *Stmn1* (stathmin 1) and *Dtl* (denticleless E3 ubiquitin protein ligase) are mostly associated with DNA dynamics, replication, proliferation and repair, and, in the case of *Stmn1*, microtubule dynamics (Supplemental Table 4.1-Baso Prog). For this reason, it was necessary to input and explore the expression patterns of the reported GMPs marker genes in the literature. This allowed me to identify genes related to reported eosinophil and basophil identities with expression gradients extending towards the present cluster. Examples include *Apoe*, *Casp3* and the basophil surface marker *Itga2*, which is expressed at lower levels. Furthermore, key marker genes combinations identified in studies by means of scRNA-seq, as being relevant to basophil differentiation, such as *Gata2*, *Stat5b*, *Spi1*, *Cebpa*, *Ly6a* (Sca-1) and *Cd34*, show a consistent transition expression pattern, suggesting that this cluster comprises committed basophil-only unipotent progenitors. Especially considering that this cluster do not exhibit strong expressions of the Integrin B7 and *Fcer1a* genes, which are identified in oligo/bipotent progenitors (not shown)[144,225].

5.8.2 Marker genes identified for niche cells

There are many ongoing efforts to unravel the heterogeneity among niche cells, as it is necessary to identify the effector cells within the osteo-lineage and the ECs that orchestrate inductive effects towards myelopoiesis[4,75,194]. These cells are known to express key chemoattractant and molecules with hematopoietic-myelopoietic induction functions. However, these mesenchymal lineage cells, which include osteo-lineages, chondrocytes, pericytes, stromal cells or adipocytes have highly similar transcriptomic profiles and cell identities.

For this reason, an initial assessment of the integrated dataset comprising only three major osteochondral cell types and two major ECs did not reflect the expected heterogeneity (see Figure 4.9: red dashed region for osteochondral cells and blue and green dashed regions for ECs). Hence, the further efforts in unraveling relevant heterogeneity by means of subclustering resulted in a more diverse and useful identification of niche cells.

5.8.2.1 MSCs, osteogenic and chondrogenic niche cells have clear transcriptomic profiles

Subclustering and DE analysis of newly identified osteochondral cell clusters, as showcased by marker genes, enabled the identification of eight different clusters (see Figure 4.9-B). Marker genes were used to identify cell types associated with osteo-lineages, chondrocytes, mesenchymal stromal cells and adipocytes. The latter were deemed not useful as the mice analyzed in Chapter 3 were 12 weeks old and adipocytes are not expected to form an important component of the BM niche at that post-natal stage.

The largest cluster identified was annotated as 'BM-MSCs-LepR', which, in addition to having a consistent transcriptomic profile based on the marker genes *C3*, *Aldh1a2*, *Ccl19* and *Eef1a1*, is the most representative of *Lepr* gene expression among niche cells. Lepr+ cells are part of the most relevant and widely studied BM niche cells[48,51,64,128]. Initially considered a population of MSCs committed to adipogenesis, single-cell transcriptomics analysis has revealed that these cells are highly heterogeneous, with Lepr+ gene expression remaining active at different levels among stromal, endothelial and osteogenic-derived cells[48,51,64,128]. Hence, *Lepr* is now considered a general mesenchymal stromal marker and is used in this document to annotate the most representative MSCs cluster[75]. Moreover, the marker gene *Aldh1a2* reinforces stemness functions and is characteristic of retinoid metabolism during embryonic development, KO of this gene leads to embryonic lethality [230,231]. Meanwhile, the gene *Ccl19* stimulates the migration of BM-MSCs and promotes their osteoblastic differentiation[232]. Therefore, this particular LepR+ mesenchymal population represents more osteogenic-aligned stromal population, reflected by its clustering position among the osteochondral lineage cells (see Figure 4.10-C)[232].

The ‘MSCs-Osteo’ cluster is distinguished by the same surface marker used in Chapter 3: ALP. Its encoding gene, *Alpl*, is identified as the top marker gene. Considering the aforementioned functions of ALP in maturing osteoblasts acquiring the competence to participate in bone formation and remodeling, this cluster represents cells that are differentiating from MSCs into

osteoblasts, which have not yet achieved full maturation, which is marked by the expression of collagen type I[62,174]. Furthermore, the second top marker gene, *Wif1* (Wnt Inhibitory Factor 1), is known to be expressed in osteoblasts and is related to the BM environment in preserving the quiescent pool of HSCs by antagonizing both canonical and non-canonical Wnt signaling[233]. This means that these cells may not yet be embedded in the bone matrix (osteocytes) and have the transcriptional competence to interact with the BM[233]. Next, the *Mmp13* gene plays a role in collagen type I recycling, degradation and reabsorption[234]. This metalloprotease helps to maintain bone mass and promote osteoblast differentiation[234,235]. Finally, *Kcnk2* gene has been identified in other scRNA-seq studies as a marker of the transition between osteoblasts and osteocytes[236].

The cluster 'Col-Osteoblasts' was annotated based on the expression of one of the most important collagen genes, *Col1a2*, which encodes collagen type I, alpha chain 2. This indicates that this particular osteo-lineage cluster represents a more mature osteoblast-osteocyte population that is actively involved in maintaining the bone matrix[62,237]. Moreover, the top marker gene, *Cpz* (carboxypeptidase Z), is an ECM component that harbors a cysteine-rich domain and triggers the activation of Wnt/β-catenin in bone matrix remodeling functions[238]. The *Iftm5* gene (interferon-induced transmembrane protein 5) is also implicated in the activation of the Sox9-mediated differentiation program that induces osteoblastic lineage cells; mutations in this gene produce osteogenesis imperfecta type V[239]. Interestingly, this cluster also exhibits the expression of collagen type XXII, a particular ECM component of the TB[240]. *Col22a1*-deficient mouse models develop trabecular osteopenia, while osteogenesis in CB remains unaffected[240]. Hence, these collagen-expressing osteoblasts also represent the particular osteo-lineage cells of interest in the TB, which are explored in Chapter 3[240]. Finally, the marker gene *Bglap2*, which encodes osteocalcin (OC), is one of the most widely studied bone formation genes, regulated by the osteoblastic transcriptomic program, and marks mature osteoblasts [62,237].

The ‘MSCs-Chondro’ cluster is characterized by the marker genes *Acan* and *Col2a1*, which encode for the two most important ECM markers historically used to distinguish chondrocytes in skeletal bone[183,241,242]. Since the AC is usually discarded during sample processing to generate these scRNA-seq libraries, these chondrocytes specifically represent GPCs. Furthermore, the *Mia* (melanoma inhibitory activity) gene is a chondrogenic chemotactic factor that induces chondrogenesis from MSCs and prevents osteoblastic lineage differentiation by inhibiting

BMP2[243]. Finally, the *Papss2* gene (3'-phosphoadenosine-5'-phosphosulfate synthetase 2) plays a role in embryonic skeletogenesis and, in adult mice, induces ALP activity in osteoblast differentiation[244,245]. This reinforces the idea that GPCs adopt an osteoblast-like phenotype during hypertrophy and are capable of terminal transdifferentiation into osteoblasts[245].

In the case of the 'BM-fibroblasts' cluster, this annotation refers to BM stromal cells of the mesenchymal lineage that are present in the BM ecosystem and display fibroblast-like morphology and osteoblastic potential in both humans and mice[246,247]. The marker genes identified, including *Gsn*, have been found to be part of the set of genes that are upregulated upon osteoblastic differentiation treatment of fibroblasts[247]. However, the specific function of *Gsn* is yet unclear, Zhong et al. have categorized BM cells with *Gsn* as a marker gene as early mesenchymal progenitors[248–250]. Following a similar assessment by Zhong et al., *Mfap5* (microfibrillar-associated protein 5) was identified as a marker of early mesenchymal progenitors[250]. Considering that *Mfap5* regulates osteogenesis via the Wnt/β-catenin and AMPK signaling pathways, this reinforces fibroblastic-osteogenic potential while being implicated in the suppression of adipogenic differentiation[251]. The *Pi16* gene has been identified as part of a 'universal' fibroblast genotype found in adult mice, and in particular, it is found in cells preferentially adjacent to developing bone in embryonic mouse stages, proposing that hematopoietic niche CAR-cells originate developmentally from embryonic-universal fibroblasts present in the developing periosteum[252]. Meanwhile, *Igfbp6* (insulin-like growth factor binding protein 6) is distinctly expressed among fibroblasts and, in the context of bone and bone marrow, is associated with the osteoblastic secretome in the activity of bone repair mechanisms[253,254].

Finally, the smallest cluster, annotated as 'MSC-Subpop', represents a transition stage of MSCs-BM fibroblasts, which are mostly associated with the differentiation potential of chondrocytes induced by *Cilp* expression, as identified by Baryawno et al[74]. This marker gene represents a transition continuum; exposure to TGFb1 in BM stromal cells induces the upregulation of *Cilp* and *Prg4* (lubricin) in mice, and *Cilp2* along with the HCs marker genes *Col9a3* and *Col10a1*, in human MSCs under chondrogenic differentiation media[74,255,256]. This reinforces the commitment towards chondrocytes. Nonetheless, the *Fmod* (fibromodulin) gene also refers to the ECM environment aimed at maintaining the stemness of primary MSCs in both

mice and humans[257–259]. Hence, its final annotation reflects this stemness nature more accurately, although further exploration of marker genes is required to annotate this cluster more accurately.

5.8.2.2 Vascular niche clusters annotations rely on a few marker genes and expression pattern of CXCL12 and Stab2

Regarding the vascular niches, my subclustering efforts enabled the identification of significant vascular heterogeneity. Starting with cluster CD34+SCA1+Ng2- BMECs, as seen in Figure 4.9-C, this cluster is distinguished by the expression of *Ly6c1* and *Pecam1* (CD31). The latter is the pan-endothelial marker used in Chapter 3. *Ly6c1* has recently been identified by single-cell transcriptomics analysis as a BM-MSC cell marker with endothelial potential[260]. Hence, its association with *Pecam1* suggests that these cells are aligned with the endothelial transcriptome[130,260]. Meanwhile, *Ly6a* (Sca-1), reinforces the stemness functions of these cells, as resident Sca-1+ progenitors are involved in vascular remodeling coordinated by means of ERG-*Cdh5* with multipotent characteristics, as confirmed by Baryawno et al[74,260–262]. Finally, this cluster contains the highest expression of CD34 across non-hematopoietic cells in my integrated dataset. In the context of BM vasculature, this represents mesenchymal potential to direct angiogenesis and the subsequent acquisition of the CD31 phenotype, while its immunostaining confirms specificity among bone arteries and capillaries[62,263].

Next, the sinusoids are the most representative vascular phenotype in the BM, characterized by its fenestrated architecture. It is one of the most studied vascular niche components. Usually distinguished in literature by expression of *Stab2* (Stabilin2), which has been characterized in different tissues including the liver and BM of adult mice and here used as core marker gene to track sinusoids[36,53,264]. Three major endothelial populations could be identified among clusters expressing *Stab2*: ECs1, Sinusoidal ECs and Sinusoidal ECs1 (Figure 4.10-D). However, these sub-setted clusters lack a strong gene marker profile; only one or two genes in each were useful for identifying further vascular functions.

For ECs1, the marker gene *Sepp1* has been identified as part of the heterogeneity that distinguishes sinusoids in humans, while in mice, it is overexpressed in bone marrow BM-ECs compared to metaphyseal ECs[265–267]. Furthermore, the *Kcnj8* gene has been profiled as part of the transcriptomic profile of sinusoidal ECs in mouse BM[42]. Nonetheless, the lack of robustness between the remaining marker genes made me select a broader annotation rather than a specific

sinusoidal-ECs label, to reflect this lack of reliable marker gene profile. For the cluster Sinusoidal ECs, beyond the expression pattern of *Stab2*, the marker gene *Zeb1* (Zinc-finger E-box-binding homeobox 1) is crucial for Type H vasculature formation and their functions involved in bone formation[268]. Finally, I decided to keep the cluster Sinusoidal ECs1, despite it being one of the smallest, it is the population among *Stab2*+ cells that also expresses CXCL12, despite a lack of relevant marker gene expression. Therefore, these rare sinusoidal ECs may play a significant role in the BM niche functions towards myelopoiesis-granulopoiesis[53].

In contrast to ECs1 cells, the cluster ECs show clear marker genes associated with Collagen type IV (*Col4a1*), a component of the basement membrane ECM of all vasculature [62]. Furthermore, the *Id1* gene has gained popularity due to its role in promoting angiogenesis in both sinusoids and Type H vessels, while maintaining a haematopoietic-inductive niche in the BM[269–271]. Finally, the *Smad1* marker gene is crucial for promoting Type H angiogenesis and osteogenesis, by means of BMP-associated signaling promotes CXCL12 expression in the BM niche, which is of particular relevance given the cluster transcriptome and potential crosstalk with cluster Sinusoidal ECs1 expression of CXCL12[272,273].

Finally, the pericytes are clearly identified by the *Tagln* marker gene, which encodes the SM22 marker used to stain pericytes effectively in Chapter 3, and is supported by the literature[62].

5.9 Molecular interactions between granulocyte progenitors and Gr1+ cells with their niches – an in silico analysis

Having identified cell clusters and robustly annotated niche cell types and granulocyte progenitors (described in sections 5.8.1 and 5.8.2), I proceeded to the final stage of the present thesis project.

Due to the limitations of imaging-based approaches when exploring the in situ spatial architecture of the myeloid-granulocyte-neutrophil inductive niche, I employed the cell communication inference tool CellChat v2. This tool uses the transcriptomic data of each cell type as input to detect the active expression of genes associated with ligands and receptors. Then, based on ligand-receptor (L-R) dynamics databases, it provides as output the probability-based inference of the potential communication pathways taking place between cell types[146].

Therefore, CellChat interprets the transcriptome as the cells' competence to participate in different communication pathways, which are defined by cell-cell contact, secreted signaling and ECM-receptor interactions. It then classifies cells with ligand-associated expressed genes as the signaling source (outgoing role) and cells with receptor-associated expressed genes as the signaling target (incoming role)[146]. The context that defines if the ligand operates under each condition (soluble, membrane bound-contact, and ECM) depends on the database used for the analysis, which collects the details of each ligand and receptor reported to infers their mechanism of action. The database used in the present project was the mouse_CellChatDB, as specified in CellChat's vignettes[148], however, it is possible to curate and use specific databases with collected information regarding the tissue of interest, an option worth exploring in future in silico analysis.

This provides further biological targets to investigate in future research in a hypothesis-forming fashion.

5.9.1 Molecular interactions between granulocyte progenitors and Gr1+ cells with the osteoblastic niche – cell-cell contact

Among the identified cell-cell contact pathways, one of the most widespread involved is the intercellular adhesion molecule 1 (ICAM-1). This pathway has an overall effect on all granulocytes, with varying inferred strength and a higher impact on the Gr1+ neutrophil cluster. Interestingly, the only niche cell cluster acting as the pathway's source is LepR+ MSCs (Figure 4.11-B ICAM). Hence, of the granulocytes of interest, the Gr1+ neutrophils are the most competent in terms of binding to LepR+MSCs through ICAM-1 and ITGAL, ITGAM, ITGB and SPN receptors (Supplemental Table 5.2). According to the literature, this pathway is involved in tissue damage dynamics leading to inflammatory responses[274]. ICAM-1 deficiency induced by *Icam-1* cKO in both osteoblastic, ECs and MSCs across BM niches disrupts the quiescence of HSCs, and induces myelopoiesis, possibly by means of disruption of adhesion dynamics[275]. Notably, *Icam-1* deficiency not only disrupts the lymphopoietic potential, but also biases the myeloid differentiation towards GMPs, reducing MEPs[275]. Taking the literature and my findings together, it is possible to conclude that the ICAM pathway acts on granulocyte progenitors by means of controlling the myeloid potential between MEPs and GMPs by adhesion to the osteoblastic niche, rather than a direct granulocytopoiesis inductive stimulus.

Thy1 (CD90) ligand is expressed only by the BM-Fibroblasts and targets specifically the Gr1+ neutrophils cluster (Figure 4.11-B Thy1). *Thy1* expression can be found across BM stromal cells, which are mostly described as mesenchymal-derived cells with osteogenesis potential[276]. *Thy1* constitutive KO leads to reduced bone mass and increased adipocyte differentiation potential[276]. However, based on IF imaging it is expressed in, or around bone arterioles[62]. Hence, it is unclear if the BM-fibroblasts cluster represents a subtype of BM pericytes around small arterioles instead of BM-stromal fibroblasts, in which case, the effects of *Thy1* KO on osteogenesis would be indirect. Considering that the receptors inferred to act upon *Thy1* include integrins (ITGAM and ITGB2) in addition to ADGRE, this mostly suggests a cellular adhesion mechanism (Supplemental table 5.2). However, the involvement of the ADGRE (CD97) receptor as a target may suggest a regulatory function in granulocytosis described below[277].

In close relationship to the ADGRE-associated receptor, the ADGRG is a member of the adhesion G protein-coupled receptors. *ADGRE1* and *ADGRG1* are the only two ADG-receptors identified to be expressed among GR1+ neutrophils and granulocyte progenitors respectively (Figure 4.11-B ADGRG). According to the L-R genes involved (Supplemental table 5.2), ADGRG receptors are inferred to bind with collagen type III. Despite not being a major component of bone structure or crucial for bone formation, *Col3a1* has been demonstrated to play a significant role in bone, including trabecular bone development and bone remodeling, as its deletion affects ALP and fracture healing (callus formation and mineralization)[129,278]. Furthermore, TGM2 is another ligand predicted to act upon ADGRG1, which may suggest a role in regulating osteoclastogenesis[279]. Hence, these ADGRE and ADGRG pathways point to a negative regulator of myelopoietic-granulopoietic induction.

Another inferred pathway identified in the osteogenic niche involves the expression of CD276 ligand (*B7-H3*) by the Col-Osteoblast cluster and interaction upon all granulocyte-progenitors through the *Treml2* receptor gene (Figure 4.11-B CD276 and Supplemental table 5.2). *Treml2* is known to be expressed among granulocytes and neutrophils, the latter upregulating *Treml2* amidst inflammation signaling[280], suggesting an inflammation response described under the context of emergency granulopoiesis. However, conflicting results regarding the inferred ligand *B7-H3* and *Treml2* have also been found in the literature, making it difficult to conclude a clear role in granulopoiesis[281].

Finally, as shown in Figure 4.11-B SIRP, the SIRP pathway reinforces the effects of cell-to-cell communication on granulocytes. Here, SIRPB1A, SIRPB1B and SIRPB1C have been identified to be expressed as ligands among the Lepr+ MSCs, MSCs-Osteo, and Col-Osteo clusters, while the receptor CD47 is inferred to act as target on all granulocytes-neutrophils (Supplemental Table 5.2). SIRP is known as the 'don't eat me' pathway, targeting innate immune system cells to prevent phagocytosis of the organism's own tissues[282]. Meanwhile, it is mostly described as a pathway where SIRP is expressed among immune cells for immune regulation purposes. Only a handful of papers have described SIRP expression among BM stromal cells and osteoblasts, and how its activity induces osteoblastic differentiation[283,284], This SIRP-mediated interaction between bone and the immune system has not yet been studied, nor a possible role for SIRP signaling in mediating granulopoiesis can be identified.

To summarize, my imaging data indicated that Gr1+ cells proliferate preferentially near osteoblasts in a non-random manner, but not in direct contact with them. The CellChat analysis performed here failed to identify cell-cell contact mediated molecular pathways that could explain this spatial relationship. Therefore, proliferation of Gr1+ cells near osteoblasts is likely to be mediated by soluble factors or ECM molecules.

5.9.2 Molecular interactions between granulocyte progenitors and Gr1+ cells with the osteoblastic niche – secreted signaling

Following the findings and spatial patterns observed in Chapter 3. It is clear that the majority of Gr1+EdU+ cells are not in direct contact with their osteogenic niche. Therefore, regardless of the abundance of the ALP+ and PDPN+ niche population, the mechanisms that act primarily on Gr1+EdU+ cells depend on secreted signaling via soluble factors. In line with this idea, CellChat was able to identify and infer crosstalk dynamics based on secreted signaling. These interactions include most of the best-known HSCs and HSPCs inductive chemokines, which are responsible for inducing different hematopoietic effects (Supplemental Table 5.3).

The KIT pathways originate from the MSC-Osteo and Lepr MSCs clusters, which were identified as representing MSCs and mesenchymal cells undergoing osteoblast differentiation (Figure 4.12-B KIT). The *Kitl* (SCF) produced by the osteogenic niche, which exerts its effect upon hematopoiesis through the Kit receptor (c-Kit), is debated in terms of its specific mechanism of action. It has been determined that membrane-bound SCF (mSCF) is the particular form of SCF

required for hematopoiesis maintenance, given that soluble SCF is incapable of compensating for the effects of mSCF deficiency in mice[285,286]. Meanwhile, soluble SCF provides a transient stimulus on the Kit receptor compared to the sustained induction of mSCF[287]. Unfortunately, there is no clear way in which I can distinguish between these two SCF forms based solely on the transcriptomic competence, and the assumption of CellChat database that this factor only operates as a secreted factor. Nonetheless, given my data obtained in Chapter 3 and the literature, is possible to infer that the spatial proximity to the osteogenic niche can lead to differential effects of the SCF in myelopoiesis induction. However, given that SCF is essential for inducing S-phase entry into the cell cycle and that the Kit receptor is expressed at low levels in quiescent HSCs compared to the highest levels observed in GMPs, it is possible that extensive Kit receptor expression compensates for the transient effects of soluble SCF secreted by these osteogenic and Lepr+ cells widely available throughout the BM ecosystem [43,96,128,287]. This would enable active proliferation of Gr1+ cells even in the absence of contact with mSCF in the osteogenic niche[43,96,287].

The next relevant secreted pathway identified is the chemokine CXCL12, which is produced mostly by the MSCs Lepr+, MSCs Osteo, and to a lesser extent by MSC-chondro clusters and the MSCs subpopulation (Figure 4.12-B CXCL, and supplemental table 5.3). They target all granulocytes and neutrophils of interest by CXCR4 and ACKR3 receptors. Among the first factors known to induce hematopoiesis and form an inductive niche among the BM, its deletion of the CXCL12 or CXCR4 elements in the perinatal BM is known to disrupt the functions of myeloid progenitors through impairment of their main chemotactic migration[65,67,77].

CXCL12 is known to signal mostly through the CXCR4 receptor. This binding is assumed to be a mechanism that keeps maturing granulocytes, such as neutrophils, attached to their niche (neutrophil arrest); their further maturation reduces CXCR4 expression to the point of final detachment and release into circulation. Furthermore, this pathway is involved in chemotaxis[288]. Given its soluble and chemoattractant mechanisms and my results in Chapter 3, it is probable that CXCL12 stimuli acts at a distance from the osteogenic niche. However, further in situ exploration by means of IF on the spatial disposition and enrichment of CXCL12 among the Gr1+EdU+ niche is needed, as recent studies suggest that the availability of CXCL12 may enrich the niche in a more locally restricted-hotspots fashion especially among the TB[289].

In addition to the inferred cross-talk with CXCL12-CXCR4, CellChat identified the atypical chemokine receptor 3 (ACKR3) as an additional target (supplemental table 5.3). This receptor has recently been shown to have a stronger affinity for CXCL12 (a ten-fold higher affinity) and is mostly characterized as a scavenger receptor that aims to remove CXCL12 from the environment. This is because unlike the mechanism with CXCR4, ACKR3 receptor is recycled after binding, leading CXCL12 into lysosomal degradation[290–292]. Taken together, the literature on the functions of the CXCL12 ligand and the identified receptors, CXCR4 and ACKR3, makes it clear that the chemoattractant roles are necessary for granulocyte functions such as migration and release into circulation. However, other roles of CXCL12 in regulating myelopoiesis, especially by means of ACKR3 remain elusive and require further exploration.

Another interesting pathway inferred by CellChat was mediated by the Adipoq ligand, which targets both *Adipor1* and *Adipor2* receptors (Figure 4.12-B ADIPONECTIN, and supplemental table 5.3). This ligand is mainly expressed by the Lepr+ MSC cluster, followed to a lesser extent by the Osteo cluster. It also targets all the remaining osteo-chondro niche cells and granulocyte-neutrophils, suggesting broad BM function. Initially, this adipokine was described as a suppressor of granulopoiesis[293]. Its expression is not limited to mesenchymal stromal cells and adipocytes; low levels have been found to be expressed by lymphocytes and other non-hematopoietic cells, which is sufficient to suppress GMPs[293,294]. The anti-inflammatory properties of adiponectin were further explored, and it was confirmed that adiponectin-deficient and obese mice exhibit similar disrupted inflammation in the BM, suggesting that the presence of adipocytes alone does not necessarily produce appropriate anti-inflammatory signaling. Adipocytes have been shown to disrupt HSPC proliferation and the hematopoietic environment in the BM[294,295]. Hence, this pathway represents a negative regulator for proliferative GMPs-neutrophils, as its function involves suppression of the SOCS3 regulator of STAT3 signaling, with unclear evidence of being secreted by the osteogenic niche, suggesting contamination of some niche clusters with Lepr+ cells.

Other pathways, such as *Spp1* (osteopontin), which is produced by most osteogenic niche cells and target integrins and CD44 (Figure 4.12-B SPP1, and supplemental table 5.3), suggest further cell adhesion or migration functions. The literature characterizes *Spp1* to have an antagonistic function in the regulation of the HSPC pool size[44,296,297]. *Spp1* is described to be

also expressed by MSCs as well as mature stromal cells[44], however, OPN staining shows a more restricted expression to the bone matrix and mostly colocalized with Collagen type I[62]. *Spp1* in the context of MDS, and in tune to its regulatory functions, has been shown to be overexpressed in response to the perturbations induced by MDS-propagating cells of CD34+CD38− phenotype, suggesting an adaptive response aiming at antagonizing the myeloid inductive effects and not a granulopoietic function[298].

Further pathways, such as those involving IGF (insulin-like growth factor) and IGFBP (insulin-like growth factor binding protein) (Figure 4.12-B IGF, and supplemental table 5.3), may not directly impact granulopoiesis, as studies on IGF deficiency have not shown an effect on hematopoiesis, possibly given the redundancy among insulin-metabolic pathways acting upon similar receptors[299]. However, recent studies have explored the effects of ageing on the BM and found that, given the relevance of these pathways in the context of bone and osteogenesis, a reduction in IGF induces similar MSCs biased differentiation towards adipocytes inducing myeloid-biased hematopoiesis, linking osteogenesis dynamics to the proper regulation of myeloid progenitors, including granulocytes[93,300,301]. Hence, despite not having a direct role on the GMPs, it is relevant to explore further as the homeostasis maintenance of the osteogenic niche is crucial for proper hematopoietic-myeloid functions.

Finally, the Midkine (MDK) and Pleiotrophin (PTN) pathways are among those with the greatest number of similar receptors inferred to interact with both ligands (Figure 4.12-B MK, and supplemental table 5.3). Interestingly, the Midkine pathway is usually described as a regulator of bone formation and remodeling in bone. For example, MDK-deficient mice exhibit increased trabecular bone formation, increased bone anabolism in cortical bone and a protective effect against bone loss following ovariectomy. MDK deficiency also accelerates fracture healing when antagonized[302–304]. Meanwhile, PTN is mostly found among endothelial niche cells, where its deletion affects LT-HSCs[305,306]. Despite gaining attention in relation to dendritic cells and T cells, the effects of these two heparin-binding cytokines are still considered to be overall pleiotropic, so no granulopoiesis induction function could be corroborated and further research into their specific effects on GMPs is necessary.

5.9.3 Molecular interactions between Gr1+ cells and the osteoblastic niche – ECM-Receptor

In this case, the inferred crosstalk pathways do not imply proximity to the cell source, as is the case with cell-cell contact L-R pairs or conflicting literature regarding soluble and membrane-bound secreted elements. Rather, it analyzes the competence and role of the cell source producing the ECM components according to the expressed genes, as well as the cells with the competence to express receptors that are predicted to interact with such ECM.

The ECM of bone is complex and impressively dynamic, as it is constantly remodelled, recycled and formed de novo. Various types of ECM molecules exist in bone, including collagens (types I–XI and XXII), fibronectin, laminins, HSPGs, vitronectin, Bglap and MGP. Of those CellChat identified as acting upon granulocytes and neutrophils were laminins, THBS and fibronectin (Figure 4.13).

In the case of laminin, which in this case were identified as laminin subunit beta 1 (*Lamb1*), laminin subunit beta 2 (*Lamb2*) and laminin subunit gamma 1 (*Lamc1*), expressed by all osteochondral niche clusters (Figure 4.13-B LAMININ, and Supplemental table 5.4), are well characterized in the literature as bone matrix elements acting in osteogenesis dynamics, especially amidst mechanical stress[307]. However, for the specific purpose of myeloid and granulopoiesis induction, most of literature describe other laminins/subunits (such as *Lama4*-Laminin 421 and Integrin alpha9beta1) as being involve in the context of the vascular niche by influencing homing, vascular remodelling, quiescence exit among HSCs and granulopoiesis induction[308–310]. Hence, the laminins-integrins interactions here identified in the context of the osteogenic niche and granulopoiesis remained to be studied more thoroughly and no inductive effect could be found.

One of the most unexpected results concerns the THBS-mediated pathways involving the thrombospondin proteins (THBS1, THBS3 and THBS4), which mostly originate from the MSC-Chondro and MSC-Subpop clusters, and targets the rest of clusters by means of *Sdc1*, *Sdc4* and CD47 receptors (Figure 4.13-B THBS, and Supplemental table 5.4). THBS1 is expressed by MSC-Subpop cluster has mostly been described in relation to its function in wound healing mechanisms, suggesting a role in the recruitment of the innate immune system as a chemoattractant[311–314]. However, its functions beyond ECM components and its role in regulating processes such as angiogenesis and osteogenesis have also been explored, yielding interesting results. THBS1 deletion has recently been shown to reduce age-related myeloid-biased hematopoiesis in aged mice, which is associated with a further reduction in systemic inflammatory cytokines, reduced

adiposity and leptin levels[315]. THBS1 is found to be a modulatory ECM element that links the ECM to the cell surface rather than being a structural molecule. One of the receptors targeted for these functions is CD47, which affects several metabolic functions, such as glucose and fat metabolism, inflammatory signaling by cytokine activation and cell stress by ROS, leading to cell death in lymphoid cells[313,316]. Therefore, these pathways involving CD47 suggest a role in phagocytosis, although research into its effects on granulocyte progenitors is limited. CellChat inferred pathways involving granulocytes and neutrophils, which suggest that they have the transcriptomic competence to respond to BM THBS1 stimuli. This opens the door to further research into potential granulopoiesis functions.

Finally, given the distribution and functions of THBS3, THBS5/Comp in literature respectively[317,318], and THBS4 expression pattern which does not provide a strong enrichment among the Gr1+EdU+ niche in Chapter 3 (Figure 3.9 E). These THBS elements may not operate as a relevant niche component for the purpose of myelopoiesis-granulopoiesis.

5.9.4 Molecular interactions between Gr1+ cells and the osteoblastic niche – summary

In summary, the literature, my in situ results and the communication pathways inferred and explored here confirm that the osteogenic niche is relevant for Gr1+EdU+ cells via secreted elements rather than cell contact. Kit and CXCL12 are undoubtedly the major inductive elements crucial for cell cycle induction and cell migration-homing, as supported by the literature, while the remaining pathways (including secreted *Spp1* and *Mk*) support negative regulation. Cell to cell contact did not reveal proliferative inductive signaling, these pathways are reported as inflammatory reactive adhesion mechanisms and neutrophil-phagocytosis repression. Finally, ECM components such as laminins and the targeted receptors inferred by CellChat do not appear to have an inductive effect on granulopoiesis.

5.9.5 Molecular interactions between Gr1+ cells and the vascular niche – Cell-cell contact

When analyzing potential molecular interactions between Gr1+ cells and the vascular niche in terms of cell-cell contact, many of the same players identified for the osteoblastic niche were inferred by CellChat. However, given that my imaging showed that most of Gr1+EdU+ cells are in direct contact with CD31+ blood vessels, these inferred interactions should be considered more relevant.

The ICAM pathways were identified as being more prevalent among almost all vascular niche clusters, except for pericytes and sinusoidal ECs Subpopulation (Figure 4.14-B ICAM). These clusters take on the role of signal sender by means of ICAM-1 and ICAM-2, interacting with granulocyte progenitors and neutrophils through integrins (ITGAL, ITGB2 and ITGAM) (Supplemental table 5.2). ICAM-1 is the best-known of the two ICAM members, given that its deletion impacts HSC mobilization, leading to a higher myeloid-to-lymphoid cell ratio and impaired quiescence[275]. ICAM-1 is expressed at much higher levels in ECs, and following my findings and the literature, the vascular niche plays a more significant role in regulating the adhesion and migration of HSCs, thereby preventing them from entering the cell cycle and maintaining their stemness[275]. Hence, the quiescent-maintenance function of ICAM-1 does not represent a pathway in which GMPs are induced into cell cycle. Finally, ICAM-2, which is predominantly expressed in ECs, has been identified as inducing arrest/retention to the vascular niche by impeding neutrophil release until inflammatory stimuli[319] .

In the case of *Thy1*, the restricted pattern remains consistent within the vascular niche transcriptome, with expression limited to the pericyte cluster (Figure 4.14-B THY1). However, *Thy1* itself has not been described under the context of perivascular stimuli for hematopoiesis-myelopoiesis, where the focus is regarding CXCL12 mostly, and most recent studies favor the sinusoid niche for HSC maintenance[59,320,321]. Finally, considering the restricted spatial niche that SM22+ pericytes occupy among my in situ data, contrasting Coutu et al[62], further and more robust sections must be collected to elucidate a more consistent spatial peri-vascular/pericyte architecture.

A greater variety of ADGRG members appear to be involved in the vascular niche context, including *ADGRG1*, *ADGRG6* and *ADGRE5* (Figure 4.14-B ADGRG, Supplemental table 5.2). These originate from most vascular niche cells, targeting granulocyte progenitors, in a manner similar to the osteo-chondral niche. The only significant difference seems to be the repertoire of collagen molecules binding to them, including the *Col4a1* and *Col4a2* genes, two main components of the basement membrane of the BM vasculature[62] . However, no clear conclusion can be drawn about the induction of granulopoiesis based on these L-R pairs and the literature reviewed.

The interactions inferred by CD34 signaling are unique to the vascular niche. Here, CD34 is identified as a signaling ligand originating from ECs, CD34+ BMECs, and the clusters of

granulocyte progenitors, which target sinusoidal ECs and ECs by inferring binding to *Selp* receptor (Figure 4.14-B CD34, Supplemental table 5.2). Therefore, this crosstalk pattern indicates an influence that does not target the granulocytes-neutrophils of interest, or a biased interpretation of CellChat's database, based solely on transcriptomic competence.

The pathways inferred for E-selectin (SELE), whose expression is dominated by sinusoidal clusters and followed by endothelial cell (ECs) clusters (Figure 4.14-B SELE, and Supplemental table 5.2). These clusters interact with both neutrophil progenitor and basophil progenitor clusters via CD44 and *Glg*-gene receptors (which encode E-selectin ligand-1, ESL-1). Meanwhile selectins are known for their role in hematopoietic cells homing and extravasation into tissues by means of *Esl-1*, which includes myeloid progenitors, their functions rely on systemic inflammation signaling[322,323]. An indirect effect on HPSCs regulation relies on the negative regulation of *Esl-1* upon TGFβ, suggesting a more complex and context-dependent mechanism[324,325].

5.9.6 Molecular interactions between Gr1+ cells and the vascular niche – Secreted signaling

Once again, SCF and the c-Kit receptor are involved in one of the best-described mechanisms by which HSCs enter a proliferative state. The Kit pathway originates from expression of SCF by the ECs, CD34+BMECs and pericytes clusters, targeting granulocyte-progenitors expressing c-Kit (Figure 4.15-B KIT, and Supplemental table 5.3). Despite SCF being present in both the osteogenic and vascular niches, it has attracted most attention in the latter since the discovery that conditional deletion of SCF across ECs and Lepr cells depletes HSCs, in contrast to osteoblastic deletion of SCF[52]. Moreover, similar findings regarding mSCF gained relevance in the vascular context, as mSCF may act in coordination with other membrane-bound vascular ligands. These includes interaction with VCAM-1 to improve adhesion strength, HSC polarization, and protrusions in vitro[326]. Hence, cooperation with other niche-specific ligands prioritizes adhesion mechanisms over cell migration, which is a consistently relevant phenomenon observed among myeloid progenitors and further GMPs[285,326] . In contrast to the fact that a large proportion of Gr1+EdU+ cells are located in contact with CD31 vascular niches, the vast majority of them are found at a distance of <50μm. Hence, opposite to the osteogenic context, the vascular niche may rely heavily on the mSCF to exert the proliferative stimuli to Gr1+EdU+ cells while cooperating with other endothelial adhesion molecules.

The vascular niche revealed a transcriptomic program involving a greater diversity of CXC ligands-receptors interactions: CXCL12-CXCR4 and CXCL9/10 -ACKR1 (Figure 4.15-B CXCL, and Supplemental table 5.3). Similar mechanisms are at play, regarding the homeostatic function of the CXCL!2 whose interaction with CXCR4 is associated with the retention of progenitors and BM neutrophils, preventing their release into circulation, until the antagonist factor G-CSF interaction is sensed[97]. Deletion of either CXCL12 or CXCR4 directly disrupts the retention of CMPs[77,190,327], It is possible that these proliferative Gr1+ cells require the adhesive stimuli to maintain a homeostatic rate of pre-neutrophil pools among the BM, which, upon inflammation, could be rapidly release into circulation. Nonetheless, it is worth mentioning that recent IF imaging findings have provided conflicting results, as the imaging of CXCL12 across the BM reveals enrichment among the bone niche mostly, in a hotspot fashion, which does not strictly correlate the location of CAR-cells (CXCL12-GFP)[289]. Hence, further IF imaging by means of protein ligation of in situ endothelial-CXCL12 and niche enrichment is required to conciliate this disparity.

In the case of the remaining chemokines identified, CXCL9 and CXCL10, which share high similarities, these are related to inflammatory signaling and cell adhesion. CXCL10 is particularly relevant in relation to the self-renewal mechanisms of HSCs. However, the identified receptor, ACKR1, has not been shown to be involved in these hematopoietic functions beyond the characterization of the vascular recruitment of macrophages in pathological conditions[328–330].

Interestingly, *Adipoq* was also identified and inferred in the largest ECs cluster (Figure 4.15-B ADIPONECTIN, and Supplemental table 5.3). It is possible that these cells are CAR/Lepr- cells contaminating/embedded within the ECs cluster, particularly given that *Adipoq* expression is limited to a few cells within the cluster, overlapping with Lepr and CXCL12 gene expression pattern. Further strategies such as subclustering with more strict parameters to avoid these contaminations are necessary to improve the resolution of the integrated dataset.

Spp1 was also identified as part of the crosstalk between ECs, pericytes and granulocytes/neutrophils (Figure 4.15-B SPP1, and Supplemental table 5.3). *Spp1* has been identified as being expressed differentially in Type S vasculature, which is also the source of CXCL12 while lacking SCF expression, which is expressed in Type H vasculature[194]. Type H vasculature is located primarily in the epiphysis of 3-month-old mice, which is close to the age of the mice used in my experiments[194]. Moreover, unlike the osteogenic niche, expression of *Spp1* in

BM vasculature remains active and does not decrease with age[94]. *Spp1* targets and acts on HSCs and HPSCs via integrins and CD44 to arrest the cell cycle[297,331,332]. However, it is unclear why *Spp1* functions associated with the vasculature do not prevent myeloid bias with age. Under ageing conditions, OPN treatment attenuates HSC ageing and reduces CMP frequency to that observed in young mice[94]. In addition, IF staining of OPN is not present among the vasculature in the BM, meaning contradictory results, hence, optimization on the staining and available anti-OPN ABs are needed, in order to confirm its expression in Type S vasculature.

In the case of IGF1 and IGFBP3, which target the IGF1R and TMEM219 receptors respectively (Figure 4.15-B IGF, and Supplemental table 5.3), no clear direct effect on granulopoiesis seems to have been characterized in the literature. However, there are further clues specific to vascular niche cells that may indicate special interactions. Recently, insulin metabolism and IGF1 activity were described as regulatory agents of endothelial CXCR4[190]. Obese mouse models appear to upregulate CXCR4 and trigger leukocyte adhesion via CXCL12, an effect that is reversed by the induction of IGF1 signaling. Therefore, IGF1 may not directly interact with proliferation-inducing mechanisms but appears to be part of the endothelial CXCR4-neutrophil axis, which is known to be relevant to myeloid differentiation[190].

Finally, *Plau* (the gene that encodes plasminogen activator, urokinase uPA) seems to be a particularly restricted pathway between ECs in sinusoids and the Gr1+ neutrophil cluster (Figure 4.15-B PLAU, and Supplemental table 5.3). According to the literature, this pathway has a significant impact on HPSCs. The expression and action of uPA activates/breaks down other crucial secreted and membrane-bound factors, most notably membrane-bound SCF, VCAM1 and fibronectin, while binding to the uPAR receptor allowing cell mobilization[333–335]. Therefore, the vascular niche not only influences adhesion and mobility to induce further HSPC differentiation, but also proteolysis-induced remodeling of the niche stemming from sinusoidal ECs[336,337]. Considering that both the identified sinusoidal ECs1 cluster and the neutrophils express *Plau* (uPA) and its main receptor *PlauR* (uPAR), I suggest that this crosstalk may occur in a coordinated manner in feedback to induce neutrophil migration and vascular plasminogen activation for remodeling of a unique sinusoidal niche population specialized for Gr1+ cells.

5.9.7 Molecular interactions between Gr1+ cells and the vascular niche – ECM-Receptor signaling

In comparison to the osteochondral niche, the vascular niche presents a particular laminin isoform that is relevant to vascular-mediated hematopoietic induction: laminin alpha4, encoded by *Lama4* gene cluster (Figure 4.16-B LAMININ, and Supplemental table 5.4). This isoform is a component of the basement membrane of sinusoidal and large vessels[308,309]. Mice with a deletion of *Lama4* produce fewer short-term HPSCs and slower hematopoietic reconstitution, which is assumed to stem from slower progenitor cycling, though it does not interrupt myeloid-granulocyte differentiation downstream, probably due to compensating mechanism of other ECM components of the vascular niche[308]. The targeting of laminin alpha 4 to all granulocytes and neutrophils by integrins (ITGA1, ITGA6, ITGA7, ITGA9 and ITGB1), CD44 and *Dag1*; and its presence in all vascular niche clusters inferred by CellChat, may indicate a stochastic effect rather than the action of a specific proliferative agent, however, further functional assays are required to test granulopoiesis induction[333,338,339]. The remaining laminins do not appear to have any direct effects on granulocyte functions beyond adhesion.

Regarding the THBS mediated pathway, only THBS1 has been identified as playing a role in cell communication. Interestingly, this originates from Gr1+ neutrophils targeting all cell types (including autocrine signaling) by interacting with CD47 and CD36 receptors (Figure 4.16-B THBS, and Supplemental table 5.4). Nonetheless, as is the case with Vascular niche-CD34 pathways, its communication pattern does not involve niche stimulation towards GMPs-neutrophils.

Finally, *Vtn* (encoding gene for vitronectin) is here identified as being expressed by the pericyte cluster, which is also involved with the PlauR (uPAR) receptor, seen previously in section 5.9.5 (Figure 4.16-B VTN, and Supplemental table 5.4). This is consistent with the fact that vitronectin can act on PlauR cells (Gr1+ neutrophils in this case), especially when integrins are involved in complex signaling mechanisms. Therefore, vitronectin both in CellChat inference and references appears to interact specifically with integrin α5β1 in collaboration with the uPAR[340,341]. This gains relevance considering that integrin and vitronectin interactions are involved in some myeloid differentiation processes, including human monocyte-macrophage differentiation[342]. This may influence the maturation of Gr1+ neutrophils in mice too, as they are the only targeted cell cluster of interest among the granulocytes-neutrophils clusters.

5.9.8 Molecular interactions between Gr1+ cells and the vascular niche – summary

In summary, the cell-to-cell contact pathways described here did not reveal any clear granulopoietic proliferation inductive stimuli on which Gr1+EdU+ cells may rely to maintain their cell division features. Meanwhile, the c-Kit and SCF secreted pathways are the most well-described ligand-receptor in inducing GMPs cell cycle entry, although the mSCF form may be central to this pathway given the proximity of Gr1+EdU+ cells to the vascular niche. Therefore, a new understanding of vascular mSCF is necessary to differentiate osteogenic and vascular niche functions. Furthermore, conflicting views surround CXCL12, and the inconsistent presence of these factors and CAR-cells across the BM vasculature reported in previous studies jeopardizes the establishment of definitive mechanisms through which Gr1+EdU+ cells may bind to CXCR4. Additionally, PLAU suggests more intricate niche mechanisms that rely on vascular remodeling as potential effectors of myeloid-GMP mobilization and regulation. This suggests the need for further research into vascular remodeling events and their impact on GMPs niches. Finally, no ECM seems to directly induce a proliferation stimulus in Gr1+ cells.

5.10 Summary

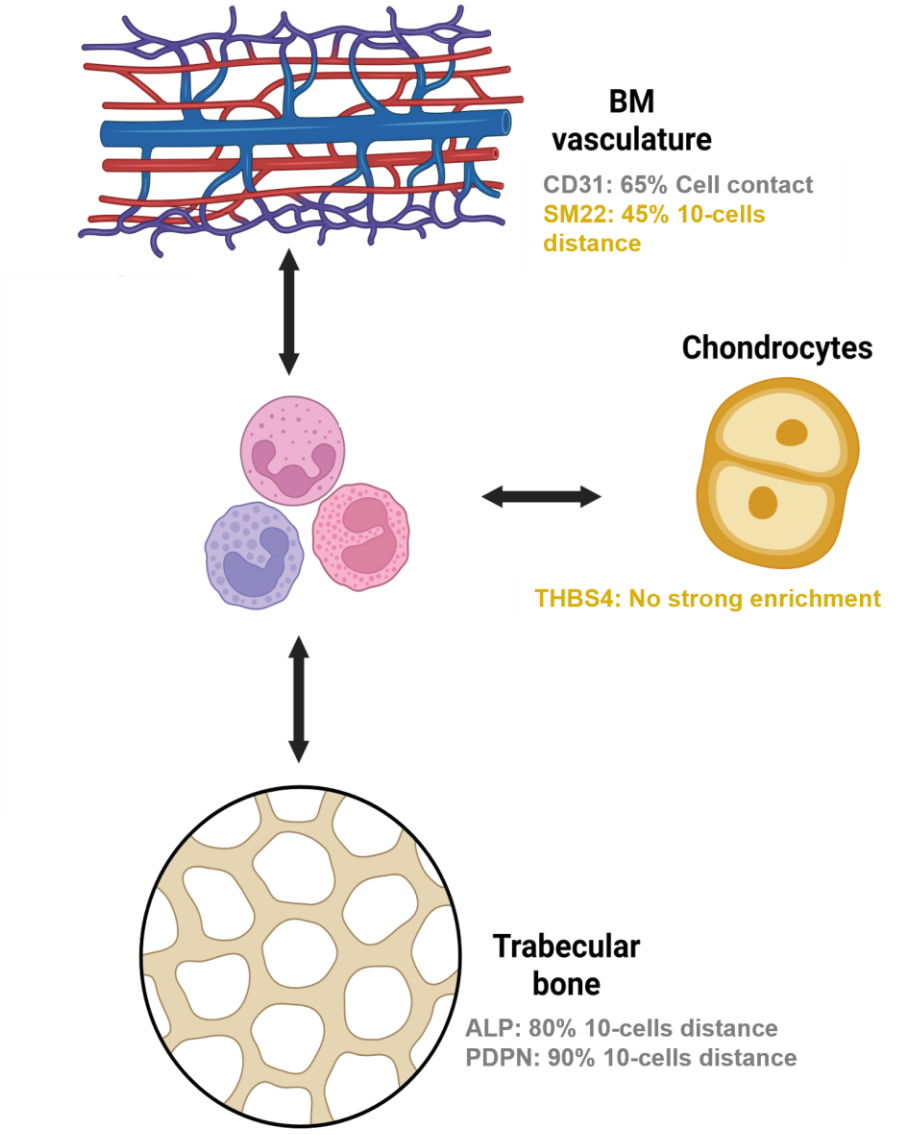

Figure 5.1 **Chapter 3 Findings summary.** The in situ mapping of the myeloid Gr1 proliferative niche in the femur of adult mice shows that the local enrichment is context specific depending on the niche component in question. The osteogenic niche of the distal epi/metaphysis is characterized by TB, and at a 10-cells distance they enrich the niche of the majority of Gr1+EdU+ cells in a non-random fashion. Meanwhile, the vascular niche of the distal epi/metaphysis is the most abundant niche component here analyzed, and it enriches the majority of Gr1+EdU+ at a cell-contact distance in a non-random fashion. The peri-vascular niche, in contrast, enriches almost half of Gr1+EdU+ cells at a 10-cells distance with a weak significance despite its restricted abundance in the epi/metaphysis. Finally, the chondrogenic niche mapped by its THBS4 ECM component did not represent a spatially relevant component of the Gr1+EdU+ environment.

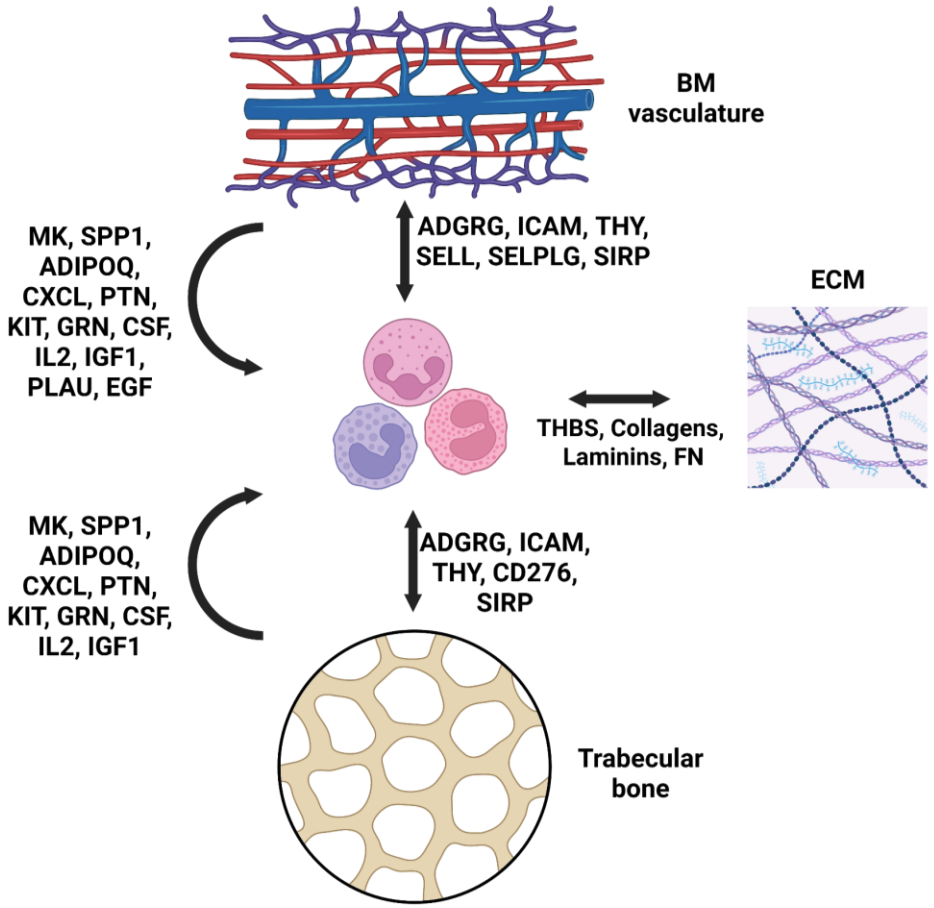

Figure 5.2 **Chapter 4 Findings summary.** Inferred communication pathways identified and explored based on CellChat analysis. GMPs (polymorphonuclear cells) in the BM ecosystem are preferentially located at a cell-contact distance from the vasculature; meanwhile, they remain mostly at a distance at 10 cells from the osteogenic component, which is mostly represented by bone trabeculae. Inferred cell-contact communication involves the ADGRG, ICAM, THY. SELL, SELPG and SIRP pathways; meanwhile ADGRG, ICAM, THY, CD276 and SIRP are involved with the osteogenic niche. ECM and receptor pathways are largely conserved in both niche contexts and involve THBS, collagen, laminins and fibronectin (FN). The most robust predictions identified were those mediated by secreted signaling: MK, SPP1, ADIPOQ, CXCL, PTN, KIT, GRN, CSF, IL2, IGF1 and EGF for the pathways through which the vascular niche may communicate with GMP-neutrophils. Finally, the osteogenic niche shows similar inferences mediated by MK, SPP1, ADIPOQ, CXCL, PTN, KIT, GRN, CSF, IL2 and IGF1.

The Immunofluorescent imaging efforts by means of 3D confocal microscopy is an effective and necessary tool for further mapping the bone and bone marrow ecosystem in relation to its niche functions in myelopoiesis, as proved here in Chapter 3, providing for the first time a robust mapping of proliferative GMPs-neutrophils. Meanwhile, proliferation labelling was effectively achieved by incorporation of the thymidine analogue EdU, representing a cost-friendly

and technically efficient option for exploring the in situ arrangement of proliferative cells in the BM, which follow particular hotspot patterns, especially among the bone trabeculae of the distal metaphysis and epiphysis of femurs.

Gr1+ cells, which represent GMPs-neutrophils, are proliferative and spatially accommodate preferably close to the BM vascularity, while remaining mostly at 10-cell distance to the bone niche in a non-random manner. This reveals for the first time among the reported references, a clear in situ proliferative-GMPs spatial niche architecture.

Moreover, the bioinformatics-neural network based SCVI model is an effective open-source tool useful for integrating single-cell transcriptomic libraries and identifying relevant heterogeneity, comprising thousands of cells and expressed genes discernable by their transcriptomic profiles while identifying shared biological signatures. Then, the cell communication inference tool CellChatv2 can provide insights into transcriptomic competence between cells of interest, with clear sender-receiver roles in three relevant communication contexts: cell-to-cell contact, secreted signaling, and ECM-receptor interaction. However, further updated/curated L-R databases are important to explore and account for the BM context. Most cell-to-cell contact pathways revealed negative regulatory pathways among the osteogenic and vascular niches. ECM-receptor pathways revealed the greatest variety of targeted receptors; however, no clear proliferation-inducing effects could be confirmed by the L-R genes identified. Finally, the secreted signaling context provided the most promising pathways for the direct induction of cell proliferation by SCF-Kit, the crucial cell attachment axis of the CXCR4-CXCL12 signaling pathway and further complex stimulus networks, which are mediated by insulin metabolism (IGF and IGFBP) and vascular proteolytic remodeling (PLAU); these require further in situ exploration and functional assays to explore further how they influence on granulopoiesis induction.

5.11 Supplemental data

Marker genes identified for relevant granulocyte-neutrophil cells	
Cluster	**Marker genes**
Neutro Prog	Mpo, Prtn3, Ctsg, Plac8, Pgam1
Neutro Prog1	Elane, Ms4a3, Prtn3, Ctsg, Alas1
Eo/Baso-Prog	Ms4a2, Cpa3, Csrp3, Fcer1a', Lmo4
Baso Prog	Lig1, Dctpp1, Hells, Stmn1, Dtl
Neutrophils	S100a8, S100a9, Lcn2, Camp, Ngp
Neutrophils1	Jchain, C1qc, Gzma, C1qb, Retnlg

Supplemental table 5.1. Clusters identified and annotated as the major granulocyte progenitor and neutrophil cells identities.

CellChat. Cell-Cell contact L-R genes			
Ligand (Osteo-Chondro Niche)	**Receptor (Granulocytes-Neutrophils)**	**Ligand (Vascular Niche)**	**Receptor (Granulocytes-Neutrophils)**
ICAM1	ITGAL_ITGB2	ICAM1	ITGAL_ITGB2
	ITGAM_ITGB2		ITGAM_ITGB2
	ITGAM_ITGB2L		ITGAM_ITGB2L
	SPN		SPN
	ITGAL		ITGAL
ICAM 2	ITGAL_ITGB2	ICAM2	ITGAL_ITGB2
	ITGAM_ITGB2		ITGAM_ITGB2
	ITGAM_ITGB2L		ITGAM_ITGB2L
COL3A1	ADGRG1	COL3A1	ADGRG1
TGM2		TGM2	
THY1	ADGRE	COL4A1	ADGRG6
	ITGAM_ITGB2	COL4A2	
SIRPB1A	CD47	THY1	ADGRE5
SIRPB1B	CD47		ITGAM_ITGB2
SIRPB1C	CD47	SIRPB1A	CD47
CD276	TREML2	SIRPB1B	CD47
		SIRPB1C	CD47
		SELL	CD34
		SELE	CD44
			GLG1
		CD34	SELP
		LAIR1	LILRB4A

Supplemental Table 5.2. Genes identified and inferred to interact through cell contact pathways between niche cells as signal senders and granulocytes-neutrophils as signal receivers.

CellChat. Secreted Signaling L-R genes			
Ligand (Osteo-Chondro Niche)	**Receptor (Granulocytes-Neutrophils)**	**Ligand (Vascular Niche)**	**Receptor (Granulocytes-Neutrophils)**
CXCL12	CXCR4	CXCL12	CXCR4
	ACKR3	CXCL9	ACKR1
KITL	KIT	CXCL10	ACKR1
ADIPOQ	ADIPOR1	KITL	KIT
	ADIPOR2	ADIPOQ	ADIPOR1
SPP1	CD44		ADIPOR1
	ITGAV_ITGB1	SPP1	ITGAV_ITGB1
	ITGAV_ITGB5		ITGA4_ITGB1
	ITGA4_ITGB1		ITGA9_ITGB1
IGF1	IGF1R		ITGA5_ITGB1
IGFBP3	TMEM219	IGFBP3	TMEM219
IL7	IL7R_IL2RG	IGF1	IGF1R
TSLP	IL7R_CRLF2	PLAU	PLAUR
MDK	SDC1		
	SDC2		
	SDC4		
	PTPRZ1		
	ITGA4_ITGB1		
	ITGA6_ITGB1		
	LRP1		
	NCL		

Supplemental Table 5.3. Genes identified and inferred to interact through secreted signaling pathways between niche cells as signal senders and granulocytes-neutrophils as signal receivers.

CellChat. ECM-Receptor L-R genes			
Ligand (Osteo-Chondro Niche)	**Receptor (Granulocytes-Neutrophils)**	**Ligand (Vascular Niche)**	**Receptor (Granulocytes-Neutrophils)**
THBS1	SDC1	THBS1	SDC1
	SDC4		SDC4
	CD47		CD36
THBS3	SDC1		CD47
	SDC4	LAMA4	ITGA1_ITGB1
	CD47		ITGA6_ITGB1
THBS4	SDC1		ITGA7_ITGB1
	SDC4		ITGA9_ITGB1
	CD47		CD44
COMP	SDC1		DAG1
	SDC4	LAMB1	ITGA1_ITGB1
	CD47		ITGA6_ITGB1
LAMB1	ITGA1_ITGB1		ITGA7_ITGB1
	ITGA6_ITGB1		ITGA9_ITGB1
	CD44		CD44
	DAG1		DAG1
LAMB2	ITGA1_ITGB1	LAMB2	ITGA1_ITGB1
	ITGA6_ITGB1		ITGA6_ITGB1
	CD44		ITGA7_ITGB1
	DAG1		ITGA9_ITGB1
LAMC1	ITGA1_ITGB1		CD44
	ITGA6_ITGB1		DAG1
	CD44	LAMC1	ITGA1_ITGB1
	DAG1		ITGA6_ITGB1
FN1	ITGA4_ITGB1		ITGA7_ITGB1
	ITGAV_ITGB1		ITGA9_ITGB1
	ITGA4_ITGB7		CD44
	CD44		DAG1
	SDC1	VTN	ITGAV_ITGB1
	SDC4		PLAUR

Supplemental Table 5.4. Genes identified and inferred to interact through ECM-Receptor pathways between niche cells as signal senders and granulocytes-neutrophils as signal receivers.

5.12 Limitations

The present project initially aimed to collect data on bone samples from both male and female mice in a triplicate design for purposes of comparison and potential identification of sexual dimorphism. However, due to technical difficulties and time constraints, it was not possible to produce triplicates for both sexes, and samples were pooled. Therefore, the current results do not address this issue, and the interpretation operates under the assumption that there are no significant differences between male and female mice. However, this assumption may not be accurate and requires further exploration in future studies.

The present project involved the immunofluorescent staining of granulocytes-neutrophils using an anti-Gr1 antibody. This staining strategy was the only one that produced images of myeloid lineage cells by confocal microscopy. Other antibodies targeting different myeloid lineages were tested, including Ter119 and CD271 (Glycophorin A), as well as CD117, CD11b and CD16, in order to identify erythroid cells, HSPCs and monocytes, respectively. However, despite using similar IF protocols, only Ter119 produced useful staining for identifying a wide spectrum of erythroblasts and erythrocytes. Therefore, despite the precise and extensive Gr1+ staining, the present results, which are based on Gr1+ staining only, lack further granulocyte lineage specificity. Following FACS protocols, a more comprehensive strategy usually requires combinations of cell surface markers to improve the specificity of the detected phenotype, as is the case for GMPs, which are considered to have an Sca-1+CD11b+Gr1+ phenotype. Several myeloid-granulocyte lineages remain to be characterised in terms of their spatial niche composition, as Gr1+ staining alone is insufficient to provide a complete picture of granulocyte-derived cells.

To identify the main elements of the niche available throughout the BM ecosystem, I used osteogenic (ALP, PDPN), endothelial (CD31) and peri-vascular (SM22) cell surface markers, and chondrogenic (THBS4) ECM marker. This staining strategy successfully identified most cell types reported to occupy and operate as specialized bone marrow niches. Nonetheless, the SM22+ produced a non-random enrichment worth exploring further with other cell-markers such as Sca-1 and CD90, to identify the pan-perivascular niche thoroughly. Moreover, this extensive pan-niche staining approach lacks the capacity to distinguish relevant heterogeneity among the cells described in the niches, particularly among BM stromal cells, which can be targeted using further staining markers such as CXCL12 and LepR. Therefore, the present results can only be

interpreted based on the single-cell transcriptomic competence data analysis regarding niche heterogeneity and its interaction with granulocyte-neutrophil cells of interest, without providing direct in situ spatial context for comparison.

For image cytometry purposes, I relied on the computation and analysis of spatial distance values, which are described here as '10-cell diameter distance', representing 50µm, and 'cell contact distance', representing <5µm. These values were arbitrarily selected based on the average size of GMPs reported in the literature and confirmed during the image segmentation process of Gr1+EdU+ cells, which had a consistent diameter of 5µm. This was used to generate and interpret the present results. However, more precise distance variables need to be implemented as these distances may not accurately depict the spatial enrichment and dynamics of different chemokine factors, such as CXCL12 or soluble/membrane-bound SCF. This would provide more detailed insights into disputed perspectives on the local vs. gradient distribution of key chemokines and address the question about how extensive or restricted can a niche be in the BM.

The datasets selected for the final integration of the scRNA-seq, as described and used in Chapter 4, are from a mix of female and male mice of different post-natal ages, ranging from 8 to 16 weeks. This means that despite the differences being only a few weeks, there may be induced biases that do not completely and accurately represent the interactions identified in Chapter 4 when compared with the in situ spatial data of 11–12 week-old mice used in Chapter 3.

Cell clusters were identified and manually annotated to produce a diverse transcriptomic view of heterogeneous HSCs, HSPCs, GMPs, immune cells and niche cells. Consistent marker genes were used to identify and recognize the cell type represented in each cluster, providing a degree of confidence. Cell communication inferences were possible with a wide variety of pathway patterns. However, due to time constraints during the project, I was unable to test these pathways using in vitro-in vivo functional assays, which limited these inferences to hypotheses forming conclusions.

5.13 Future directions

Further expansion and optimization of cell surface markers for in situ IF would improve the resolution of both myeloid-granulocyte and niche heterogeneity, driving more comprehensive data and results. This would distinguish spatial patterns more specific and particular lineages, such

as monocytes with CD11b, CD16 and CD115; megakaryocytes with CD9 and CD41; erythroid cells with GypA, Ter119 and Sca-1; BM stromal cells with MSCs properties with CXCL12 and LepR; sinusoids with Stab2; and pericytes with Sca-1 and CD90.

Future exploration should focus on more comprehensive and refined distance variables to account for the in situ spatial-dynamics of membrane-to-soluble factors, as well as inspecting the spatial tendencies of niche enrichment associated with each cell lineages. CXCL12 exploration already provided contrasting data, hence, other factors such as SCF with both soluble and membrane bound forms will clarify further the understanding on niches. Hence, PLA-IF staining is compulsory to clarify basic notions of the characteristics of the myeloid niche.

Single-cell transcriptomics is an unparalleled tool for exploring gene expression, distinguishing functional heterogeneity and inferring cell communication dynamics based on their competence to perform, send and recognize specific signaling. As previously mentioned, the major limitation of this technique is the lack of spatial context, which restricts the scope for interpreting the results. Therefore, it is essential to extend the resolution of the data into a spatially coherent context using spatial transcriptomics assays, which have already been explored by Baccin et al. By means of spatial-laser capture dissection (LCM-seq), who achieved functional spatial transcriptomics of cortical bone tissue in the mouse femur and tibia; a technique with potential to increase the robustness with 3D imaging. Nevertheless, optimization to enable effective BM spatial transcriptome analysis will be necessary.

Following the contrasts between in situ staining and transcriptome competence, the present project successfully overcame the limitations of each method. This is because the available data on gene expression cannot easily be extrapolated to the in situ composition without a reference point, in which case immunostaining becomes an invaluable tool. Hence, a greater number of replicates with the different staining markers are crucial to generate, in order to push the robustness of the Myeloid and GMPs-BM niches.

CellChat cell communication inference tool is a useful resource for generating hypotheses about pathway patterns to be investigated in future studies. However, so far, the inferred communication relies on a unidirectional signaling source-signaling receiver. This could bias the interpretation of pathways, failing to reflect the putative bidirectional feedback communication system taking place between the niche and the granulocytes. As discussed here regarding the IGF-

insulin dynamics, vascular niche cells express and react by means of CXCR4 stimulation. Meanwhile, some myeloid cells, such as monocytes, can express SDF-1 (CXCL12), and confirmed by the CXCL12 transcriptomic signature present among the neutrophil cluster. Therefore, feedback communication may play a significant role in determining how the niche responds to stimulation to induce further granulopoietic differentiation.

Finally, the implementation of functional assays using in vitro cell cultures and in vivo KO/cKO of the pathways inferred by CellChat is crucial to verify these conclusions and move them from the scope of forming hypotheses to real data, which could have an unknown impact on the induction of myelopoiesis. In particular, exploring the cKO of SCF in situ, targeting expression among osteoblasts and ECs, and performing further ligation-protein IF imaging has the potential to reveal which form of the ligand (soluble or membrane-bound) is expressed by either niche. It is also highly promising to explore whether mSCF is distributed by means of gradients or local hot spots. Meanwhile, exploring combinations of vascular adhesion/ECM molecules with the binding-induced effects of CXCL12 could provide further insight into whether this chemoattractant relies on cooperation with laminins or Vtn in vitro. Furthermore, the greater binding affinity of the ACKR3 receptor, which is proposed to perform CXCL12-scavenger functions, could be an interesting target for study by means of CXCR4-KO in vitro. Here, I could test whether incorporating doses of CXCL12 can induce a similar adhesive effect to that seen with CXCR4 binding, or if ACKR3 can compensate at some point this effect. Finally, further scRNA-seq libraries are necessary to capture whole BM and bone cellularity, as in the case of Baccin et al., to formalize and standardize a compendium of datasets without risking batch effects, while categorizing by the transcriptome by means of sex, age, and state (steady or perturbed).

5.14 Conclusions

Historically, the field of hematopoiesis and myelopoiesis is one of the most studied physiological systems, with roots stretching back centuries. Research on the BM has fed into the cell theory, leading to an understanding of stem cells and their unique self-renewal, proliferative and differentiation features. These features are at the core of regenerative medicine research.

The study of the BM and the conditions in which the myelopoietic system operates, regulates and coordinates has been of great interest for decades. The introduction of cell sorting and fluorescence-based assays has enabled the entire system to be immunophenotyped in detail.

However, one crucial component is still missing: The in situ spatial architecture of the adult BM and its inductive niches.

Considered the 'Holy Grail' of the field, understanding the niche composition and, by extension, the specific stimuli that coordinates the system is essential.

To this end, I present an analysis of the niche composition of proliferative Gr1+ cells, which represent the GMPs and neutrophils of the innate immune system.

This niche comprises the osteogenic and vascular components available in the BM, specifically among the trabeculae of the distal femur bone in adult mice. The niche composition enriches proliferative Gr1+ cells at different distances; the osteogenic component at 10 cells away and the vascular component by means of cell contact, forming the basic spatial architecture.

However, imaging approaches pose challenges and limitations that can be offset by the extensive data collected by single-cell transcriptomics techniques. Using this data, I was able to de novo identify the relevant cell types of interest for niche composition and GMP-neutrophils with great detail and heterogeneity. Using these cell types, I was able to employ cell communication inference tools to identify the putative crosstalk through which these cells communicate, which mostly depends on secreted signaling pathways.

Future research is needed on functional in vitro and in vivo assays to test the hypotheses formed by cell communication inference, while it is also crucial to continue generating robust spatial data mapping of such a complex tissue.

Ultimately, this work advances efforts in the field towards achieving the most desired goals of regenerative medicine, such as treating myeloid-related pathologies, ex vivo expansion of myeloid cells, and creating the ultimate atlas of the bone marrow and its functional niches.

References

1. Sawai CM, Babovic S, Upadhaya S, et al. Hematopoietic Stem Cells Are the Major Source of Multilineage Hematopoiesis in Adult Animals. *Immunity*. 2016;45(3). doi:10.1016/j.immuni.2016.08.007

2. Kiel MJ, Iwashita T, Yilmaz ÖH, Morrison SJ. Spatial differences in hematopoiesis but not in stem cells indicate a lack of regional patterning in definitive hematopoietic stem cells. *Dev Biol*. 2005;283(1). doi:10.1016/j.ydbio.2005.03.037

3. Dupard SJ, Grigoryan A, Farhat S, Coutu DL, Bourgine PE. Development of Humanized Ossicles: Bridging the Hematopoietic Gap. *Trends Mol Med*. 2020;26(6). doi:10.1016/j.molmed.2020.01.016

4. Lassailly F, Foster K, Lopez-Onieva L, Currie E, Bonnet D. Multimodal imaging reveals structural and functional heterogeneity in different bone marrow compartments: Functional implications on hematopoietic stem cells. *Blood*. 2013;122(10). doi:10.1182/blood-2012-11-467498

5. Metzger TA, Shudick JM, Seekell R, Zhu Y, Niebur GL. Rheological behavior of fresh bone marrow and the effects of storage. *J Mech Behav Biomed Mater*. 2014;40. doi:10.1016/j.jmbbm.2014.09.008

6. Jansen LE, Birch NP, Schiffman JD, Crosby AJ, Peyton SR. Mechanics of intact bone marrow. *J Mech Behav Biomed Mater*. 2015;50. doi:10.1016/j.jmbbm.2015.06.023

7. Zimmermann EA, Ritchie RO. Bone as a Structural Material. *Adv Healthc Mater*. 2015;4(9). doi:10.1002/adhm.201500070

8. Cordeiro Gomes A, Hara T, Lim VY, et al. Hematopoietic Stem Cell Niches Produce Lineage-Instructive Signals to Control Multipotent Progenitor Differentiation. *Immunity*. 2016;45(6). doi:10.1016/j.immuni.2016.11.004

9. Nombela-Arrieta C, Manz MG. Quantification and three-dimensional microanatomical organization of the bone marrow. *Blood Adv*. 2017;1(6). doi:10.1182/bloodadvances.2016003194

10. Mitroulis I, Kalafati L, Hajishengallis G, Chavakis T. Myelopoiesis in the Context of Innate Immunity. *J Innate Immun*. 2018;10(5-6). doi:10.1159/000489406

11. Pinho S, Frenette PS. Haematopoietic stem cell activity and interactions with the niche. *Nat Rev Mol Cell Biol*. 2019;20(5). doi:10.1038/s41580-019-0103-9

12. Mazzarello P. A unifying concept: The history of cell theory. *Nat Cell Biol*. 1999;1(1). doi:10.1038/8964

13. Neumann FE. Über die Bedeutung des Knochenmarks für die Blutbildung. *Zentralblatt für die medizinischen Wissenschaften*. Published online 1868.

14. TILL JE, McCULLOCH EA. A direct measurement of the radiation sensitivity of normal mouse bone marrow cells. *Radiat Res*. 1961;14. doi:10.2307/3570892

15. Becker AJ, McCulloch EA, Till JE. Cytological demonstration of the clonal nature of spleen colonies derived from transplanted mouse marrow cells. *Nature*. 1963;197(4866). doi:10.1038/197452a0

16. Spangrude GJ, Heimfeld S, Weissman IL. Purification and characterization of mouse hematopoietic stem cells. *Science (1979)*. 1988;241(4861). doi:10.1126/science.2898810

17. Dexter TM, Allen TD, Lajtha LG. Conditions controlling the proliferation of haemopoietic stem cells in vitro. *J Cell Physiol*. 1977;91(3):335-344. doi:10.1002/jcp.1040910303

18. Schofield R. The relationship between the spleen colony-forming cell and the haemopoietic stem cell. A hypothesis. *Blood Cells*. 1978;4(1-2).

19. Friedenstein AJ, Chailakhyan RK, Gerasimov U V. Bone marrow osteogenic stem cells: in vitro cultivation and transplantation in diffusion chambers. *Cell Prolif*. 1987;20(3). doi:10.1111/j.1365-2184.1987.tb01309.x

20. Mardon HJ, Bee J, von der Mark K, Owen ME. Development of osteogenic tissue in diffusion chambers from early precursor cells in bone marrow of adult rats. *Cell Tissue Res*. 1987;250(1). doi:10.1007/BF00214667

21. Pittenger MF, Mackay AM, Beck SC, et al. Multilineage potential of adult human mesenchymal stem cells. *Science (1979)*. 1999;284(5411). doi:10.1126/science.284.5411.143

22. Lord B, Testa N, Hendry J. The relative spatial distributions of CFUs and CFUc in the normal mouse femur. *Blood*. 1975;46(1). doi:10.1182/blood.v46.1.65.bloodjournal46165

23. Maloney M, Lamela R, Dorie M, Patt H. Concentration gradient of blood stem cells in mouse bone marrow--an open question. *Blood*. 1978;51(3). doi:10.1182/blood.v51.3.521.bloodjournal513521

24. Moore KA, Ema H, Lemischka IR. In vitro maintenance of highly purified, transplantable hematopoietic stem cells. *Blood*. 1997;89(12). doi:10.1182/blood.v89.12.4337

25. Lu LS, Wang SJ, Auerbach R. In vitro and in vivo differentiation into B cells, T cells, and myeloid cells of primitive yolk sac hematopoietic precursor cells expanded > 100-fold by coculture with a clonal yolk sac endothelial cell line. *Proc Natl Acad Sci U S A*. 1996;93(25). doi:10.1073/pnas.93.25.14782

26. Ohneda O, Fennie C, Zheng Z, et al. Hematopoietic stem cell maintenance and differentiation are supported by embryonic aorta-gonad-mesonephros region-derived endothelium. *Blood*. 1998;92(3). doi:10.1182/blood.v92.3.908

27. Wolf NS, Kone A, Priestley G V., Bartelmez SH. In vivo and in vitro characterization of long-term repopulating primitive hematopoietic cells isolated by sequential Hoechst 33342-rhodamine 123 FACS selection. *Exp Hematol*. 1993;21(5).

28. Kiel MJ, Yilmaz ÖH, Iwashita T, Yilmaz OH, Terhorst C, Morrison SJ. SLAM family receptors distinguish hematopoietic stem and progenitor cells and reveal endothelial niches for stem cells. *Cell*. 2005;121(7). doi:10.1016/j.cell.2005.05.026

29. Zhang J, Niu C, Ye L, et al. Identification of the haematopoietic stem cell niche and control of the niche size. *Nature*. 2003;425(6960). doi:10.1038/nature02041

30. Olsson A, Venkatasubramanian M, Chaudhri VK, et al. Single-cell analysis of mixed-lineage states leading to a binary cell fate choice. *Nature*. 2016;537(7622). doi:10.1038/nature19348

31. Nestorowa S, Hamey FK, Pijuan Sala B, et al. A single-cell resolution map of mouse hematopoietic stem and progenitor cell differentiation. *Blood*. 2016;128(8). doi:10.1182/blood-2016-05-716480

32. Tusi BK, Wolock SL, Weinreb C, et al. Population snapshots predict early haematopoietic and erythroid hierarchies. *Nature*. 2018;555(7694). doi:10.1038/nature25741

33. Sun J, Ramos A, Chapman B, et al. Clonal dynamics of native haematopoiesis. *Nature*. 2014;514(7522). doi:10.1038/nature13824

34. Busch K, Klapproth K, Barile M, et al. Fundamental properties of unperturbed haematopoiesis from stem cells in vivo. *Nature*. 2015;518(7540). doi:10.1038/nature14242

35. Upadhaya S, Sawai CM, Papalexi E, et al. Kinetics of adult hematopoietic stem cell differentiation in vivo. *Journal of Experimental Medicine*. 2018;215(11). doi:10.1084/jem.20180136

36. Tikhonova AN, Dolgalev I, Hu H, et al. The bone marrow microenvironment at single-cell resolution. *Nature*. 2019;569(7755). doi:10.1038/s41586-019-1104-8

37. Vassen L, Dührsen U, Kosan C, Zeng H, Möröy T. Growth factor independence 1 (Gfi1) regulates cell-fate decision of a bipotential granulocytic-monocytic precursor defined by expression of Gfi1 and CD48. *Am J Blood Res*. 2012;2(4).

38. Fraszczak J, Vadnais C, Rashkovan M, et al. Reduced expression but not deficiency of GFI1 causes a fatal myeloproliferative disease in mice. *Leukemia*. 2019;33(1). doi:10.1038/s41375-018-0166-1

39. Horman SR, Velu CS, Chaubey A, et al. Gfi1 integrates progenitor versus granulocytic transcriptional programming. *Blood*. 2009;113(22). doi:10.1182/blood-2008-09-179747

40. Sugiyama T, Kohara H, Noda M, Nagasawa T. Maintenance of the Hematopoietic Stem Cell Pool by CXCL12-CXCR4 Chemokine Signaling in Bone Marrow Stromal Cell Niches. *Immunity*. 2006;25(6). doi:10.1016/j.immuni.2006.10.016

41. Tzeng YS, Li H, Kang YL, Chen WG, Cheng W, Lai DM. Loss of Cxcl12/Sdf-1 in adult mice decreases the quiescent state of hematopoietic stem/progenitor cells and alters the

pattern of hematopoietic regeneration after myelosuppression. *Blood*. 2011;117(2). doi:10.1182/blood-2010-01-266833

42. Xu C, Gao X, Wei Q, et al. Stem cell factor is selectively secreted by arterial endothelial cells in bone marrow. *Nat Commun*. 2018;9(1). doi:10.1038/s41467-018-04726-3

43. Doran MR, Markway BD, Aird IA, et al. Surface-bound stem cell factor and the promotion of hematopoietic cell expansion. *Biomaterials*. 2009;30(25). doi:10.1016/j.biomaterials.2009.04.043

44. Nilsson SK, Johnston HM, Whitty GA, et al. Osteopontin, a key component of the hematopoietic stem cell niche and regulator of primitive hematopoietic progenitor cells. *Blood*. 2005;106(4). doi:10.1182/blood-2004-11-4422

45. Muller-Sieburg CE, Cho RH, Karlsson L, Huang JF, Sieburg HB. Myeloid-biased hematopoietic stem cells have extensive self-renewal capacity but generate diminished lymphoid progeny with impaired IL-7 responsiveness. *Blood*. 2004;103(11). doi:10.1182/blood-2003-10-3448

46. Taichman RS, Reilly MJ, Emerson SG. Human osteoblasts support human hematopoietic progenitor cells in in vitro bone marrow cultures. *Blood*. 1996;87(2). doi:10.1182/blood.v87.2.518.bloodjournal872518

47. Calvi LM, Adams GB, Weibrecht KW, et al. Osteoblastic cells regulate the haematopoietic stem cell niche. *Nature*. 2003;425(6960). doi:10.1038/nature02040

48. Xue Y, Merchant S, Reyes A, Luo M, Morrison SJ. Leptin Receptor+ Stromal Cells Create a Perisinusoidal Niche for Thrombopoiesis in the Bone Marrow By Synthesizing Cxcl14. *Blood*. 2024;144(Supplement 1). doi:10.1182/blood-2024-205682

49. Zhang Y, Sun J, Greenblatt M, Lucas-Alcaraz D. Bone and region-specific targeting of SCF and CXCL12 in stromal niche cells reveals local and lineage-specific regulation of terminal hematopoiesis. *Blood*. 2025;146(Supplement 1):430-430. doi:10.1182/blood-2025-430

50. Omatsu Y, Sugiyama T, Kohara H, et al. The Essential Functions of Adipo-osteogenic Progenitors as the Hematopoietic Stem and Progenitor Cell Niche. *Immunity*. 2010;33(3). doi:10.1016/j.immuni.2010.08.017

51. Yue R, Zhou BO, Shimada IS, Zhao Z, Morrison SJ. Leptin Receptor Promotes Adipogenesis and Reduces Osteogenesis by Regulating Mesenchymal Stromal Cells in Adult Bone Marrow. *Cell Stem Cell*. 2016;18(6). doi:10.1016/j.stem.2016.02.015

52. Ding L, Saunders TL, Enikolopov G, Morrison SJ. Endothelial and perivascular cells maintain haematopoietic stem cells. *Nature*. 2012;481(7382):457-462. doi:10.1038/nature10783

53. Heil J, Olsavszky V, Busch K, et al. Bone marrow sinusoidal endothelium controls terminal erythroid differentiation and reticulocyte maturation. *Nat Commun*. 2021;12(1). doi:10.1038/s41467-021-27161-3

54. Yamazaki S, Ema H, Karlsson G, et al. Nonmyelinating schwann cells maintain hematopoietic stem cell hibernation in the bone marrow niche. *Cell*. 2011;147(5). doi:10.1016/j.cell.2011.09.053

55. Winkler IG, Sims NA, Pettit AR, et al. Bone marrow macrophages maintain hematopoietic stem cell (HSC) niches and their depletion mobilizes HSCs. *Blood*. 2010;116(23). doi:10.1182/blood-2009-11-253534

56. Nombela-Arrieta C, Pivarnik G, Winkel B, et al. Quantitative imaging of haematopoietic stem and progenitor cell localization and hypoxic status in the bone marrow microenvironment. *Nat Cell Biol*. 2013;15(5). doi:10.1038/ncb2730

57. Lo Celso C, Fleming HE, Wu JW, et al. Live-animal tracking of individual haematopoietic stem/progenitor cells in their niche. *Nature*. 2009;457(7225). doi:10.1038/nature07434

58. Kiel MJ, Acar M, Radice GL, Morrison SJ. Hematopoietic Stem Cells Do Not Depend on N-Cadherin to Regulate Their Maintenance. *Cell Stem Cell*. 2009;4(2). doi:10.1016/j.stem.2008.10.005

59. Kunisaki Y, Bruns I, Scheiermann C, et al. Arteriolar niches maintain haematopoietic stem cell quiescence. *Nature*. 2013;502(7473). doi:10.1038/nature12612

60. Gomariz A, Helbling PM, Isringhausen S, et al. Quantitative spatial analysis of haematopoiesis-regulating stromal cells in the bone marrow microenvironment by 3D microscopy. *Nat Commun*. 2018;9(1). doi:10.1038/s41467-018-04770-z

61. Rafii S, Butler JM, Ding B Sen. Angiocrine functions of organ-specific endothelial cells. *Nature*. 2016;529(7586). doi:10.1038/nature17040

62. Coutu DL, Kokkaliaris KD, Kunz L, Schroeder T. Three-dimensional map of nonhematopoietic bone and bone-marrow cells and molecules. *Nat Biotechnol*. 2017;35(12):1202-1210. doi:10.1038/nbt.4006

63. Kokkaliaris KD, Kunz L, Cabezas-Wallscheid N, et al. Adult blood stem cell localization reflects the abundance of reported bone marrow niche cell types and their combinations. *Blood*. 2020;136(20). doi:10.1182/BLOOD.2020006574

64. Zhou BO, Yue R, Murphy MM, Peyer JG, Morrison SJ. Leptin-receptor-expressing mesenchymal stromal cells represent the main source of bone formed by adult bone marrow. *Cell Stem Cell*. 2014;15(2):154-168. doi:10.1016/j.stem.2014.06.008

65. Ma Q, Jones D, Borghesani PR, et al. Impaired B-lymphopoiesis, myelopoiesis, and derailed cerebellar neuron migration in CXCR4- and SDF-1-deficient mice. *Proc Natl Acad Sci U S A*. 1998;95(16). doi:10.1073/pnas.95.16.9448

66. Barreda DR, Hanington PC, Belosevic M. Regulation of myeloid development and function by colony stimulating factors. *Dev Comp Immunol*. 2004;28(5). doi:10.1016/j.dci.2003.09.010

67. Nagasawa T, Hirota S, Tachibana K, et al. Defects of B-cell lymphopoiesis and bone-marrow myelopoiesis in mice lacking the CXC chemokine PBSF/SDF-1. *Nature*. 1996;382(6592). doi:10.1038/382635a0

68. Karsunky H, Zeng H, Schmidt T, et al. Inflammatory reactions and severe neutropenia in mice lacking the transcriptional repressor GFi1. *Nat Genet*. 2002;30(3). doi:10.1038/ng831

69. Fulzele K, Krause DS, Panaroni C, et al. Myelopoiesis is regulated by osteocytes through Gsα-dependent signaling. *Blood*. 2013;121(6). doi:10.1182/blood-2012-06-437160

70. Zhang J, Wu Q, Johnson CB, et al. In situ mapping identifies distinct vascular niches for myelopoiesis. *Nature*. 2021;590(7846). doi:10.1038/s41586-021-03201-2

71. Panopoulos AD, Watowich SS. Granulocyte colony-stimulating factor: Molecular mechanisms of action during steady state and “emergency” hematopoiesis. *Cytokine*. 2008;42(3). doi:10.1016/j.cyto.2008.03.002

72. Zhang D, Chen G, Manwani D, et al. Neutrophil ageing is regulated by the microbiome. *Nature*. 2015;525(7570). doi:10.1038/nature15367

73. Metcalf D. The colony-stimulating factors and cancer. *Cancer Immunol Res*. 2013;1(6). doi:10.1158/2326-6066.CIR-13-0151

74. Baryawno N, Przybylski D, Kowalczyk MS, et al. A Cellular Taxonomy of the Bone Marrow Stroma in Homeostasis and Leukemia. *Cell*. 2019;177(7). doi:10.1016/j.cell.2019.04.040

75. Dolgalev I, Tikhonova AN. Connecting the Dots: Resolving the Bone Marrow Niche Heterogeneity. *Front Cell Dev Biol*. 2021;9. doi:10.3389/fcell.2021.622519

76. Kwak H, Salvucci O, Weigert R, et al. Sinusoidal ephrin receptor EPHB4 controls hematopoietic progenitor cell mobilization from bone marrow. *Journal of Clinical Investigation*. 2016;126(12). doi:10.1172/JCI87848

77. Qing M, Jones D, Springer TA. The chemokine receptor CXCR4 is required for the retention of B lineage and granulocytic precursors within the bone marrow microenvironment. *Immunity*. 1999;10(4). doi:10.1016/S1074-7613(00)80046-1

78. Raaijmakers MHGP, Mukherjee S, Guo S, et al. Bone progenitor dysfunction induces myelodysplasia and secondary leukaemia. *Nature*. 2010;464(7290). doi:10.1038/nature08851

79. Duarte D, Hawkins ED, Akinduro O, et al. Inhibition of Endosteal Vascular Niche Remodeling Rescues Hematopoietic Stem Cell Loss in AML. *Cell Stem Cell*. 2018;22(1). doi:10.1016/j.stem.2017.11.006

80. Krevvata M, Silva BC, Manavalan JS, et al. Inhibition of leukemia cell engraftment and disease progression in mice by osteoblasts. *Blood*. 2014;124(18). doi:10.1182/blood-2013-07-517219

81. Hanoun M, Zhang D, Mizoguchi T, et al. Acute myelogenous leukemia-induced sympathetic neuropathy promotes malignancy in an altered hematopoietic stem cell Niche. *Cell Stem Cell*. 2014;15(3). doi:10.1016/j.stem.2014.06.020

82. Passaro D, Di Tullio A, Abarrategi A, et al. Increased Vascular Permeability in the Bone Marrow Microenvironment Contributes to Disease Progression and Drug Response in Acute Myeloid Leukemia. *Cancer Cell*. 2017;32(3). doi:10.1016/j.ccell.2017.08.001

83. Moser-Katz T, Joseph NS, Dhodapkar M V., Lee KP, Boise LH. Game of Bones: How Myeloma Manipulates Its Microenvironment. *Front Oncol*. 2021;10. doi:10.3389/fonc.2020.625199

84. Agarwal P, Isringhausen S, Li H, et al. Mesenchymal Niche-Specific Expression of Cxcl12 Controls Quiescence of Treatment-Resistant Leukemia Stem Cells. *Cell Stem Cell*. 2019;24(5). doi:10.1016/j.stem.2019.02.018

85. Zhang B, Ho YW, Huang Q, et al. Altered Microenvironmental Regulation of Leukemic and Normal Stem Cells in Chronic Myelogenous Leukemia. *Cancer Cell*. 2012;21(4). doi:10.1016/j.ccr.2012.02.018

86. Kumar B, Garcia M, Weng L, et al. Acute myeloid leukemia transforms the bone marrow niche into a leukemia-permissive microenvironment through exosome secretion. *Leukemia*. 2018;32(3). doi:10.1038/leu.2017.259

87. Kusumbe AP, Ramasamy SK, Adams RH. Coupling of angiogenesis and osteogenesis by a specific vessel subtype in bone. *Nature*. 2014;507(7492). doi:10.1038/nature13145

88. Gnani D, Crippa S, della Volpe L, et al. An early-senescence state in aged mesenchymal stromal cells contributes to hematopoietic stem and progenitor cell clonogenic impairment through the activation of a pro-inflammatory program. *Aging Cell*. 2019;18(3). doi:10.1111/acel.12933

89. Maryanovich M, Zahalka AH, Pierce H, et al. Adrenergic nerve degeneration in bone marrow drives aging of the hematopoietic stem cell niche. *Nat Med*. 2018;24(6). doi:10.1038/s41591-018-0030-x

90. Kato Y, Hou LB, Miyagi S, et al. Bmi1 restricts the adipogenic differentiation of bone marrow stromal cells to maintain the integrity of the hematopoietic stem cell niche. *Exp Hematol*. 2019;76. doi:10.1016/j.exphem.2019.07.006

91. Pioli PD, Casero D, Montecino-Rodriguez E, Morrison SL, Dorshkind K. Plasma Cells Are Obligate Effectors of Enhanced Myelopoiesis in Aging Bone Marrow. *Immunity*. 2019;51(2). doi:10.1016/j.immuni.2019.06.006

92. Ju Z, Jiang H, Jaworski M, et al. Telomere dysfunction induces environmental alterations limiting hematopoietic stem cell function and engraftment. *Nat Med*. 2007;13(6). doi:10.1038/nm1578

93. Young K, Eudy E, Bell R, et al. Decline in IGF1 in the bone marrow microenvironment initiates hematopoietic stem cell aging. *Cell Stem Cell*. 2021;28(8). doi:10.1016/j.stem.2021.03.017

94. Guidi N, Sacma M, Ständker L, et al. Osteopontin attenuates aging-associated phenotypes of hematopoietic stem cells. *EMBO J*. 2017;36(7). doi:10.15252/embj.201694969

95. Ergen A V., Boles NC, Goodell MA. Rantes/Ccl5 influences hematopoietic stem cell subtypes and causes myeloid skewing. *Blood*. 2012;119(11). doi:10.1182/blood-2011-11-391730

96. Katayama N, Shih J, Nishikawa S, Kina T, Clark S, Ogawa M. Stage-specific expression of c-kit protein by murine hematopoietic progenitors. *Blood*. 1993;82(8). doi:10.1182/blood.v82.8.2353.bloodjournal8282353

97. Hyun KK, De La Luz Sierra M, Williams CK, Gulino AV, Tosato G. G-CSF down-regulation of CXCR4 expression identified as a mechanism for mobilization of myeloid cells. *Blood*. 2006;108(3). doi:10.1182/blood-2005-10-4162

98. Militi S, Riccioni R, Parolini I, et al. Expression of interleukin 3 and granulocyte-macrophage colony-stimulating factor receptor common chain βc, βIT in normal haematopoiesis: Lineage specificity and proliferation-independent induction. *Br J Haematol*. 2000;111(2). doi:10.1111/j.1365-2141.2000.02348.x

99. Metcalf D. Clonal analysis of proliferation and differentiation of paired daughter cells: Action of granulocyte-macrophage colony-stimulating factor on granulocyte-macrophage precursors. *Proc Natl Acad Sci U S A*. 1980;77(9 II). doi:10.1073/pnas.77.9.5327

100. Lieschke G, Grail D, Hodgson G, et al. Mice lacking granulocyte colony-stimulating factor have chronic neutropenia, granulocyte and macrophage progenitor cell deficiency, and impaired neutrophil mobilization. *Blood*. 1994;84(6). doi:10.1182/blood.v84.6.1737.bloodjournal8461737

101. Stark MA, Huo Y, Burcin TL, Morris MA, Olson TS, Ley K. Phagocytosis of apoptotic neutrophils regulates granulopoiesis via IL-23 and IL-17. *Immunity*. 2005;22(3). doi:10.1016/j.immuni.2005.01.011

102. Balmer ML, Schürch CM, Saito Y, et al. Microbiota-Derived Compounds Drive Steady-State Granulopoiesis via MyD88/TICAM Signaling. *The Journal of Immunology*. 2014;193(10). doi:10.4049/jimmunol.1400762

103. Seymour JF, Lieschke GJ, Grail D, Quilici C, Hodgson G, Dunn AR. Mice lacking both granulocyte colony-stimulating factor (CSF) and granulocyte-macrophage CSF have impaired reproductive capacity, perturbed neonatal granulopoiesis. Lung disease, amyloidosis, and reduced long-term survival. *Blood*. 1997;90(8). doi:10.1182/blood.v90.8.3037

104. Radin MJ, Wellman ML. Granulopoiesis. In: *Schalm's Veterinary Hematology*. Wiley; 2022:323-332. doi:10.1002/9781119500537.ch41

105. Rørvig S, Østergaard O, Heegaard NHH, Borregaard N. Proteome profiling of human neutrophil granule subsets, secretory vesicles, and cell membrane: correlation with transcriptome profiling of neutrophil precursors. *J Leukoc Biol*. 2013;94(4). doi:10.1189/jlb.1212619

106. Uhm TG, Kim BS, Chung Y. Eosinophil development, regulation of eosinophil-specific genes, and role of eosinophils in the pathogenesis of asthma. *Allergy Asthma Immunol Res*. 2012;4(2). doi:10.4168/aair.2012.4.2.68

107. Franco CB, Chen CC, Drukker M, Weissman IL, Galli SJ. Distinguishing Mast Cell and Granulocyte Differentiation at the Single-Cell Level. *Cell Stem Cell*. 2010;6(4). doi:10.1016/j.stem.2010.02.013

108. Arinobu Y, Iwasaki H, Gurish MF, et al. Developmental checkpoints of the basophil/mast cell lineages in adult murine hematopoiesis. *Proc Natl Acad Sci U S A*. 2005;102(50). doi:10.1073/pnas.0509148102

109. Sasaki H, Kurotaki D, Osato N, et al. Transcription factor IRF8 plays a critical role in the development of murine basophils and mast cells. *Blood*. 2015;125(2). doi:10.1182/blood-2014-02-557983

110. Qi X, Hong J, Chaves L, et al. Antagonistic Regulation by the Transcription Factors C/EBPα and MITF Specifies Basophil and Mast Cell Fates. *Immunity*. 2013;39(1). doi:10.1016/j.immuni.2013.06.012

111. Siracusa MC, Saenz SA, Hill DA, et al. TSLP promotes interleukin-3-independent basophil haematopoiesis and type 2 inflammation. *Nature*. 2011;477(7363). doi:10.1038/nature10329

112. Jacob AM, Lindemann AF, Wagenpfeil J, et al. Autofluorescence-based tissue characterization enhances clinical prospects of light-sheet-microscopy. *Sci Rep*. 2024;14(1). doi:10.1038/s41598-024-67366-2

113. Beerman I, Luis TC, Singbrant S, Lo Celso C, Méndez-Ferrer S. The evolving view of the hematopoietic stem cell niche. *Exp Hematol*. 2017;50. doi:10.1016/j.exphem.2017.01.008

114. Acar M, Kocherlakota KS, Murphy MM, et al. Deep imaging of bone marrow shows non-dividing stem cells are mainly perisinusoidal. *Nature*. 2015;526(7571). doi:10.1038/nature15250

115. Kunz L, Coutu DL. Multicolor 3D Confocal Imaging of Thick Tissue Sections. In: *Methods in Molecular Biology*. Vol 2350. 2021. doi:10.1007/978-1-0716-1593-5_7

116. Coutu DL, Kokkaliaris KD, Kunz L, Schroeder T. Multicolor quantitative confocal imaging cytometry. *Nat Methods*. 2018;15(1):39-46. doi:10.1038/nmeth.4503

117. Coutu DL, Kokkaliaris KD, Kunz L, Schroeder T. Multicolor quantitative confocal imaging cytometry. *Nat Methods*. 2018;15(1):39-46. doi:10.1038/nmeth.4503

118. Fleming TJ, Fleming ML, Malek TR. Selective expression of Ly-6G on myeloid lineage cells in mouse bone marrow. RB6-8C5 mAb to granulocyte-differentiation antigen (Gr-1) detects members of the Ly-6 family. *The Journal of Immunology*. 1993;151(5). doi:10.4049/jimmunol.151.5.2399

119. Yáñez A, Coetzee SG, Olsson A, et al. Granulocyte-Monocyte Progenitors and Monocyte-Dendritic Cell Progenitors Independently Produce Functionally Distinct Monocytes. *Immunity*. 2017;47(5). doi:10.1016/j.immuni.2017.10.021

120. Kwok I, Becht E, Xia Y, et al. Combinatorial Single-Cell Analyses of Granulocyte-Monocyte Progenitor Heterogeneity Reveals an Early Uni-potent Neutrophil Progenitor. *Immunity*. 2020;53(2). doi:10.1016/j.immuni.2020.06.005

121. Grieshaber-Bouyer R, Radtke FA, Cunin P, et al. The neutrotime transcriptional signature defines a single continuum of neutrophils across biological compartments. *Nat Commun*. 2021;12(1). doi:10.1038/s41467-021-22973-9

122. Muir A, Bennett A, Smith H, et al. The wild mouse bone marrow has a unique myeloid and lymphoid composition and phenotype. *Discovery Immunology*. 2023;2(1). doi:10.1093/discim/kyad005

123. Pu S, Qin B, He H, et al. Identification of early myeloid progenitors as immunosuppressive cells. *Sci Rep*. 2016;6. doi:10.1038/srep23115

124. Lu YC, Xavier-Ferrucio J, Wang L, et al. The Molecular Signature of Megakaryocyte-Erythroid Progenitors Reveals a Role for the Cell Cycle in Fate Specification. *Cell Rep*. 2018;25(8). doi:10.1016/j.celrep.2018.10.084

125. Wu R, Salehi F, Redecke V, et al. Murine hematopoietic progenitor cell lines with erythroid and megakaryocyte potential. *Nature Communications* . 2025;16(1). doi:10.1038/s41467-025-62668-z

126. Hallett SA, Ono W, Ono N. Growth plate chondrocytes: Skeletal development, growth and beyond. *Int J Mol Sci*. 2019;20(23). doi:10.3390/ijms20236009

127. Ono N, Ono W, Nagasawa T, Kronenberg HM. A subset of chondrogenic cells provides early mesenchymal progenitors in growing bones. *Nat Cell Biol*. 2014;16(12):1157-1167. doi:10.1038/ncb3067

128. Comazzetto S, Murphy MM, Berto S, Jeffery E, Zhao Z, Morrison SJ. Restricted Hematopoietic Progenitors and Erythropoiesis Require SCF from Leptin Receptor+ Niche Cells in the Bone Marrow. *Cell Stem Cell*. 2019;24(3). doi:10.1016/j.stem.2018.11.022

129. Volk SW, Shah SR, Cohen AJ, et al. Type III collagen regulates osteoblastogenesis and the quantity of trabecular bone. *Calcif Tissue Int*. 2014;94(6). doi:10.1007/s00223-014-9843-x

130. Müller AM, Hermanns MI, Skrzynski C, Nesslinger M, Müller KM, Kirkpatrick CJ. Expression of the endothelial markers PECAM-1, vWF, and CD34 in Vivo and in Vitro. *Exp Mol Pathol*. 2002;72(3). doi:10.1006/exmp.2002.2424

131. van der Wath RC, Wilson A, Laurenti E, Trumpp A, Liò P. Estimating dormant and active hematopoietic stem cell kinetics through extensive modeling of bromodeoxyuridine label-retaining cell dynamics. *PLoS One*. 2009;4(9). doi:10.1371/journal.pone.0006972

132. Nowakowski RS, Lewin SB, Miller MW. Bromodeoxyuridine immunohistochemical determination of the lengths of the cell cycle and the DNA-synthetic phase for an anatomically defined population. *J Neurocytol*. 1989;18(3). doi:10.1007/BF01190834

133. Denoth-Lippuner A, Jaeger BN, Liang T, et al. Visualization of individual cell division history in complex tissues using iCOUNT. *Cell Stem Cell*. 2021;28(11). doi:10.1016/j.stem.2021.08.012

134. Hwang B, Lee JH, Bang D. Single-cell RNA sequencing technologies and bioinformatics pipelines. *Exp Mol Med*. 2018;50(8). doi:10.1038/s12276-018-0071-8

135. Jovic D, Liang X, Zeng H, Lin L, Xu F, Luo Y. Single-cell RNA sequencing technologies and applications: A brief overview. *Clin Transl Med*. 2022;12(3). doi:10.1002/ctm2.694

136. Macosko EZ, Basu A, Satija R, et al. Highly parallel genome-wide expression profiling of individual cells using nanoliter droplets. *Cell*. 2015;161(5). doi:10.1016/j.cell.2015.05.002

137. Klein AM, Mazutis L, Akartuna I, et al. Droplet barcoding for single-cell transcriptomics applied to embryonic stem cells. *Cell*. 2015;161(5). doi:10.1016/j.cell.2015.04.044

138. Zheng GXY, Terry JM, Belgrader P, et al. Massively parallel digital transcriptional profiling of single cells. *Nat Commun*. 2017;8. doi:10.1038/ncomms14049

139. Picelli S, Björklund ÅK, Faridani OR, Sagasser S, Winberg G, Sandberg R. Smart-seq2 for sensitive full-length transcriptome profiling in single cells. *Nat Methods*. 2013;10(11). doi:10.1038/nmeth.2639

140. Longo SK, Guo MG, Ji AL, Khavari PA. Integrating single-cell and spatial transcriptomics to elucidate intercellular tissue dynamics. *Nat Rev Genet*. 2021;22(10). doi:10.1038/s41576-021-00370-8

141. Stegle O, Teichmann SA, Marioni JC. Computational and analytical challenges in single-cell transcriptomics. *Nat Rev Genet*. 2015;16(3). doi:10.1038/nrg3833

142. Baccin C, Al-Sabah J, Velten L, et al. Combined single-cell and spatial transcriptomics reveal the molecular, cellular and spatial bone marrow niche organization. *Nat Cell Biol*. 2020;22(1). doi:10.1038/s41556-019-0439-6

143. Kucinski I, Campos J, Barile M, et al. A time- and single-cell-resolved model of murine bone marrow hematopoiesis. *Cell Stem Cell*. 2024;31(2). doi:10.1016/j.stem.2023.12.001

144. Hamey FK, Lau WWY, Kucinski I, et al. Single-cell molecular profiling provides a high-resolution map of basophil and mast cell development. *Allergy: European Journal of Allergy and Clinical Immunology*. 2021;76(6). doi:10.1111/all.14633

145. Gayoso A, Lopez R, Xing G, et al. A Python library for probabilistic analysis of single-cell omics data. *Nat Biotechnol*. 2022;40(2). doi:10.1038/s41587-021-01206-w

146. Jin S, Plikus M V., Nie Q. CellChat for systematic analysis of cell–cell communication from single-cell transcriptomics. *Nat Protoc*. 2025;20(1):180-219. doi:10.1038/S41596-024-01045-4;SUBJMETA=114,2391,2694,553,631,794;KWRD=CELLULAR+SIGNALLING+NETWORKS,MULTICELLULAR+SYSTEMS,SOFTWARE

147. Xu C, Lopez R, Mehlman E, Regier J, Jordan MI, Yosef N. Probabilistic harmonization and annotation of single-cell transcriptomics data with deep generative models. *Mol Syst Biol*. 2021;17(1). doi:10.15252/msb.20209620

148. Jin S, Guerrero-Juarez CF, Zhang L, et al. Inference and analysis of cell-cell communication using CellChat. *Nat Commun*. 2021;12(1). doi:10.1038/s41467-021-21246-9

149. Badia-I-Mompel P, Vélez Santiago J, Braunger J, et al. decoupleR: ensemble of computational methods to infer biological activities from omics data. *Bioinformatics Advances*. 2022;2(1). doi:10.1093/bioadv/vbac016

150. Domínguez Conde C, Xu C, Jarvis LB, et al. Cross-tissue immune cell analysis reveals tissue-specific features in humans. *Science (1979)*. 2022;376(6594). doi:10.1126/science.abl5197

151. Lv Z, Liu Y, Jing Y, et al. Impaired proliferation of growth plate chondrocytes in a model of osteogenesis imperfecta. *Biochem Biophys Res Commun*. 2022;613. doi:10.1016/j.bbrc.2022.04.138

152. Karnik SJ, Gulbronson C, Jordan PC, et al. Multiplex imaging of murine bone marrow using Phenocycler 2.0™. *Leukemia*. 2025;39(6). doi:10.1038/s41375-025-02596-5

153. Dzierzak E, Philipsen S. Erythropoiesis: Development and differentiation. *Cold Spring Harb Perspect Med*. 2013;3(4). doi:10.1101/cshperspect.a011601

154. May A, Forrester LM. The erythroblastic island niche: modeling in health, stress, and disease. *Exp Hematol*. 2020;91. doi:10.1016/j.exphem.2020.09.185

155. Shainer R, Kram V, Kilts TM, et al. Biglycan regulates bone development and regeneration. *Front Physiol*. 2023;14. doi:10.3389/fphys.2023.1119368

156. Farhat S, Tilouche B, Short S, et al. Self-renewing Sox9+ osteochondral stem cells in the postnatal skeleton. Preprint posted online December 8, 2023. doi:10.1101/2023.12.07.570646

157. Angelozzi M, de Charleroy CR, Lefebvre V. EdU-Based Assay of Cell Proliferation and Stem Cell Quiescence in Skeletal Tissue Sections. In: *Methods in Molecular Biology*. Vol 2230. 2021. doi:10.1007/978-1-0716-1028-2_21

158. Crippen TL, Jones IM. Cell proliferation in the bone marrow, thymus and spleen of mice studied by continuous, in vivo bromodeoxycytidine labelling and flow cytometric analysis. *Cell Prolif*. 1989;22(3). doi:10.1111/j.1365-2184.1989.tb00206.x

159. Ashhurst TM, Cox DA, Smith AL, King NJC. Analysis of the murine bone marrow hematopoietic system using mass and flow cytometry. In: *Methods in Molecular Biology*. Vol 1989. 2019. doi:10.1007/978-1-4939-9454-0_12

160. Shih CH, Whalen BA, Goto Y, Hogg JC, Van Eeden SF. Flow cytometric method for enumeration and characterization of newly released polymorphonuclear leukocytes from the bone marrow using 5′-bromo-2′-deoxyuridine. *Am J Physiol Cell Physiol*. 2005;289(3 58-3). doi:10.1152/ajpcell.00589.2004

161. Kiel MJ, He S, Ashkenazi R, et al. Haematopoietic stem cells do not asymmetrically segregate chromosomes or retain BrdU. *Nature*. 2007;449(7159). doi:10.1038/nature06115

162. Basu S, Hodgson G, Katz M, Dunn AR. Evaluation of role of G-CSF in the production, survival, and release of neutrophils from bone marrow into circulation. *Blood*. 2002;100(3). doi:10.1182/blood.V100.3.854

163. Knudsen E, Iversen PO, Bøyum A, Seierstad T, Nicolaysen G, Benestad HB. G-CSF enhances the proliferation and mobilization, but not the maturation rate, of murine myeloid cells. *Eur J Haematol*. 2011;87(4). doi:10.1111/j.1600-0609.2011.01658.x

164. Sugimoto Y, Katayama N, Masuya M, et al. Differential cell division history between neutrophils and macrophages in their development from granulocyte-macrophage progenitors. *Br J Haematol*. 2006;135(5). doi:10.1111/j.1365-2141.2006.06367.x

165. Wilson A, Laurenti E, Oser G, et al. Hematopoietic Stem Cells Reversibly Switch from Dormancy to Self-Renewal during Homeostasis and Repair. *Cell*. 2008;135(6). doi:10.1016/j.cell.2008.10.048

166. Morcos MNF, Zerjatke T, Glauche I, et al. Continuous mitotic activity of primitive hematopoietic stem cells in adult mice. *Journal of Experimental Medicine*. 2020;217(6). doi:10.1084/jem.20191284

167. Sugimura R, He XC, Venkatraman A, et al. Noncanonical Wnt signaling maintains hematopoietic stem cells in the niche. *Cell*. 2012;150(2). doi:10.1016/j.cell.2012.05.041

168. Bernitz JM, Kim HS, MacArthur B, Sieburg H, Moore K. Hematopoietic Stem Cells Count and Remember Self-Renewal Divisions. *Cell*. 2016;167(5). doi:10.1016/j.cell.2016.10.022

169. Evrard M, Kwok IWH, Chong SZ, et al. Developmental Analysis of Bone Marrow Neutrophils Reveals Populations Specialized in Expansion, Trafficking, and Effector Functions. *Immunity*. 2018;48(2). doi:10.1016/j.immuni.2018.02.002

170. Lian JB, Stein GS. Development of the osteoblast phenotype: molecular mechanisms mediating osteoblast growth and differentiation. *Iowa Orthop J*. 1995;15.

171. Kalajzic Z, Liu P, Kalajzic I, et al. Directing the expression of a green fluorescent protein transgene in differentiated osteoblasts: Comparison between rat type I collagen and rat osteocalcin promoters. *Bone*. 2002;31(6). doi:10.1016/S8756-3282(02)00912-2

172. Mizoguchi T, Pinho S, Ahmed J, et al. Osterix marks distinct waves of primitive and definitive stromal progenitors during bone marrow development. *Dev Cell*. 2014;29(3):340-349. doi:10.1016/j.devcel.2014.03.013

173. Maes C, Kobayashi T, Selig MK, et al. Osteoblast precursors, but not mature osteoblasts, move into developing and fractured bones along with invading blood vessels. *Dev Cell*. 2010;19(2):329-344. doi:10.1016/j.devcel.2010.07.010

174. Golub EE, Boesze-Battaglia K. The role of alkaline phosphatase in mineralization. *Curr Opin Orthop*. 2007;18(5). doi:10.1097/BCO.0b013e3282630851

175. Chaudhary SC, Kuzynski M, Bottini M, et al. Phosphate induces formation of matrix vesicles during odontoblast-initiated mineralization in vitro. *Matrix Biology*. 2016;52-54. doi:10.1016/j.matbio.2016.02.003

176. Martín-Villar E, Megías D, Castel S, Yurrita MM, Vilaró S, Quintanilla M. Podoplanin binds ERM proteins to activate RhoA and promote epithelial-mesenchymal transition. *J Cell Sci*. 2006;119(21). doi:10.1242/jcs.03218

177. Acton SE, Astarita JL, Malhotra D, et al. Podoplanin-Rich Stromal Networks Induce Dendritic Cell Motility via Activation of the C-type Lectin Receptor CLEC-2. *Immunity*. 2012;37(2). doi:10.1016/j.immuni.2012.05.022

178. Osada M, Inoue O, Ding G, et al. Platelet activation receptor CLEC-2 regulates blood/lymphatic vessel separation by inhibiting proliferation, migration, and tube formation of lymphatic endothelial cells. *Journal of Biological Chemistry*. 2012;287(26). doi:10.1074/jbc.M111.329987

179. Smith SM, Melrose J. Podoplanin is expressed by a sub-population of human foetal rib and knee joint rudiment chondrocytes. *Tissue Cell*. 2011;43(1). doi:10.1016/j.tice.2010.11.003

180. Chan CKF, Gulati GS, Sinha R, et al. Identification of the Human Skeletal Stem Cell. *Cell*. 2018;175(1). doi:10.1016/j.cell.2018.07.029

181. Zhang K, Barragan-Adjemian C, Ye L, et al. E11/gp38 Selective Expression in Osteocytes: Regulation by Mechanical Strain and Role in Dendrite Elongation. *Mol Cell Biol*. 2006;26(12). doi:10.1128/mcb.02120-05

182. Mizuhashi K, Ono W, Matsushita Y, et al. Resting zone of the growth plate houses a unique class of skeletal stem cells. *Nature*. 2018;563(7730). doi:10.1038/s41586-018-0662-5

183. Lauing KL, Cortes M, Domowicz MS, Henry JG, Baria AT, Schwartz NB. Aggrecan is required for growth plate cytoarchitecture and differentiation. *Dev Biol*. 2014;396(2). doi:10.1016/j.ydbio.2014.10.005

184. Massengale M, Massengale JL, Benson CR, et al. Adult Prg4+ progenitors repair long-term articular cartilage wounds in vivo. *JCI Insight*. 2023;8(17). doi:10.1172/jci.insight.167858

185. Jeschke A, Bonitz M, Simon M, et al. Deficiency of Thrombospondin-4 in Mice Does Not Affect Skeletal Growth or Bone Mass Acquisition, but Causes a Transient Reduction of Articular Cartilage Thickness. *PLoS One*. 2015;10(12). doi:10.1371/journal.pone.0144272

186. Song S, Fan J, Ding G, et al. Descendants of hypertrophic chondrocytes promote angiogenesis by secreting THBS4 during bone growth and injury repair. *Bone Res*. 2025;13(1):92. doi:10.1038/s41413-025-00469-2

187. Baek SH, Maiorino E, Kim H, Glass K, Raby BA, Yuan K. Single Cell Transcriptomic Analysis Reveals Organ Specific Pericyte Markers and Identities. *Front Cardiovasc Med*. 2022;9. doi:10.3389/fcvm.2022.876591

188. Debnath S, Yallowitz AR, McCormick J, et al. Discovery of a periosteal stem cell mediating intramembranous bone formation. *Nature*. 2018;562(7725):133-139. doi:10.1038/s41586-018-0554-8

189. Hooper AT, Butler JM, Nolan DJ, et al. Engraftment and Reconstitution of Hematopoiesis Is Dependent on VEGFR2-Mediated Regeneration of Sinusoidal Endothelial Cells. *Cell Stem Cell*. 2009;4(3). doi:10.1016/j.stem.2009.01.006

190. Rathjen T, Kunkemoeller B, Cederquist CT, et al. Endothelial Cell Insulin Signaling Regulates CXCR4 (C-X-C Motif Chemokine Receptor 4) and Limits Leukocyte Adhesion to Endothelium. *Arterioscler Thromb Vasc Biol*. 2022;42(7). doi:10.1161/ATVBAHA.122.317476

191. Yokota T, Oritani K, Butz S, et al. The endothelial antigen ESAM marks primitive hematopoietic progenitors throughout life in mice. *Blood*. 2009;113(13). doi:10.1182/blood-2008-07-167106

192. Sipkins DA, Wei X, Wu JW, et al. In vivo imaging of specialized bone marrow endothelial microdomains for tumour engraftment. *Nature*. 2005;435(7044). doi:10.1038/nature03703

193. Yang J, Ii M, Kamei N, et al. CD34+ cells represent highly functional endothelial progenitor cells in murine bone marrow. *PLoS One*. 2011;6(5). doi:10.1371/journal.pone.0020219

194. Iga T, Kobayashi H, Kusumoto D, et al. Spatial heterogeneity of bone marrow endothelial cells unveils a distinct subtype in the epiphysis. *Nat Cell Biol*. 2023;25(10). doi:10.1038/s41556-023-01240-7

195. Liu H, Xia X, Li B. Mesenchymal stem cell aging: Mechanisms and influences on skeletal and non-skeletal tissues. *Exp Biol Med*. 2015;240(8). doi:10.1177/1535370215591828

196. Mendelson A, Frenette PS. Hematopoietic stem cell niche maintenance during homeostasis and regeneration. *Nat Med*. 2014;20(8). doi:10.1038/nm.3647

197. Kim HN, Chang J, Shao L, et al. DNA damage and senescence in osteoprogenitors expressing Osx1 may cause their decrease with age. *Aging Cell*. 2017;16(4). doi:10.1111/acel.12597

198. Kuranda K, Vargaftig J, de la Rochere P, et al. Age-related changes in human hematopoietic stem/progenitor cells. *Aging Cell*. 2011;10(3). doi:10.1111/j.1474-9726.2011.00675.x

199. Nishikawa K, Nakashima T, Takeda S, et al. Maf promotes osteoblast differentiation in mice by mediating the age-related switch in mesenchymal cell differentiation. *Journal of Clinical Investigation*. 2010;120(10). doi:10.1172/JCI42528

200. Moore SG, Dawson KL. Red and yellow marrow in the femur: Age-related changes in appearance at MR imaging. *Radiology*. 1990;175(1). doi:10.1148/radiology.175.1.2315484

201. Vande Berg BC, Lecouvet FE, Moysan P, Maldague B, Jamart J, Malghem J. MR assessment of red marrow distribution and composition in the proximal femur: Correlation with clinical and laboratory parameters. *Skeletal Radiol*. 1997;26(10). doi:10.1007/s002560050291

202. Yu B, Huo L, Liu Y, et al. PGC-1α Controls Skeletal Stem Cell Fate and Bone-Fat Balance in Osteoporosis and Skeletal Aging by Inducing TAZ. *Cell Stem Cell*. 2018;23(2). doi:10.1016/j.stem.2018.06.009

203. Rossi DJ, Bryder D, Zahn JM, et al. Cell intrinsic alterations underlie hematopoietic stem cell aging. *Proc Natl Acad Sci U S A*. 2005;102(26). doi:10.1073/pnas.0503280102

204. Pang WW, Price EA, Sahoo D, et al. Human bone marrow hematopoietic stem cells are increased in frequency and myeloid-biased with age. *Proc Natl Acad Sci U S A*. 2011;108(50). doi:10.1073/pnas.1116110108

205. Liang Y, Van Zant G, Szilvassy SJ. Effects of aging on the homing and engraftment of murine hematopoietic stem and progenitor cells. *Blood*. 2005;106(4). doi:10.1182/blood-2004-11-4282

206. Lacava G, Laus F, Amaroli A, et al. P62 deficiency shifts mesenchymal/stromal stem cell commitment toward adipogenesis and disrupts bone marrow homeostasis in aged mice. *J Cell Physiol*. 2019;234(9). doi:10.1002/jcp.28299

207. Baumann CI, Bailey AS, Li W, Ferkowicz MJ, Yoder MC, Fleming WH. PECAM-1 is expressed on hematopoietic stem cells throughout ontogeny and identifies a population of erythroid progenitors. *Blood*. 2004;104(4). doi:10.1182/blood-2004-03-0989

208. Paul F, Arkin Y, Giladi A, et al. Transcriptional Heterogeneity and Lineage Commitment in Myeloid Progenitors. *Cell*. 2015;163(7). doi:10.1016/j.cell.2015.11.013

209. Hao Y, Stuart T, Kowalski MH, et al. Dictionary learning for integrative, multimodal and scalable single-cell analysis. *Nat Biotechnol*. 2024;42(2). doi:10.1038/s41587-023-01767-y

210. Lopez R, Regier J, Cole MB, Jordan MI, Yosef N. Deep generative modeling for single-cell transcriptomics. *Nat Methods*. 2018;15(12). doi:10.1038/s41592-018-0229-2

211. Papayannopoulos V. Neutrophil extracellular traps in immunity and disease. *Nat Rev Immunol*. 2018;18(2). doi:10.1038/nri.2017.105

212. Sollberger G, Brenes AJ, Warner J, Arthur JSC, Howden AJM. Quantitative proteomics reveals tissue-specific, infection-induced and species-specific neutrophil protein signatures. *Sci Rep*. 2024;14(1). doi:10.1038/s41598-024-56163-6

213. Burn GL, Raisch T, Tacke S, et al. Myeloperoxidase transforms chromatin into neutrophil extracellular traps. *Nature*. 2025;647(8090). doi:10.1038/s41586-025-09523-9

214. Karatepe K, Zhu H, Zhang X, et al. Proteinase 3 Limits the Number of Hematopoietic Stem and Progenitor Cells in Murine Bone Marrow. *Stem Cell Reports*. 2018;11(5). doi:10.1016/j.stemcr.2018.10.004

215. von Richthofen HJ, Westerlaken GHA, Gollnast D, et al. Soluble Signal Inhibitory Receptor on Leukocytes-1 Is Released from Activated Neutrophils by Proteinase 3 Cleavage. *The Journal of Immunology*. 2023;210(4). doi:10.4049/jimmunol.2200169

216. Liu H, Sun L, Zhao H, et al. Proteinase 3 depletion attenuates leukemia by promoting myeloid differentiation. *Cell Death Differ*. 2024;31(6). doi:10.1038/s41418-024-01288-4

217. Aghdassi AA, John DS, Sendler M, et al. Absence of the neutrophil serine protease cathepsin G decreases neutrophil granulocyte infiltration but does not change the severity of acute pancreatitis. *Sci Rep*. 2019;9(1). doi:10.1038/s41598-019-53293-0

218. Ledford JG, Kovarova M, Koller BH. Impaired Host Defense in Mice Lacking ONZIN. *The Journal of Immunology*. 2007;178(8). doi:10.4049/jimmunol.178.8.5132

219. Cai ML, Gui L, Huang H, et al. Proteomic Analyses Reveal Higher Levels of Neutrophil Activation in Men Than in Women With Systemic Lupus Erythematosus. *Front Immunol*. 2022;13. doi:10.3389/fimmu.2022.911997

220. Nasri M, Ritter M, Mir P, et al. CRISPR/Cas9-mediated ELANE knockout enables neutrophilic maturation of primary hematopoietic stem and progenitor cells and induced pluripotent stem cells of severe congenital neutropenia patients. *Haematologica*. 2020;105(3). doi:10.3324/haematol.2019.221804

221. Horwitz MS, Corey SJ, Grimes HL, Tidwell T. ELANE Mutations in Cyclic and Severe Congenital Neutropenia. Genetics and Pathophysiology. *Hematol Oncol Clin North Am*. 2013;27(1). doi:10.1016/j.hoc.2012.10.004

222. Liu Z, Gu Y, Chakarov S, et al. Fate Mapping via Ms4a3-Expression History Traces Monocyte-Derived Cells. *Cell*. 2019;178(6). doi:10.1016/j.cell.2019.08.009

223. van Wijk K, Nakajima O. From Deficiency to Therapy: Systemic Consequences of ALAS1 Disruption and the Protective Role of 5-ALA. 2025;15(8). doi:10.3390/life15081259

224. Saitoh S, Takeda Y, Araki A, et al. 5-Aminolevulinic Acid (5-ALA) Plays an Important Role in the Function of Innate Immune Cells. *Inflammation*. 2025;48(4). doi:10.1007/s10753-024-02212-1

225. Matsumura T, Totani H, Gunji Y, et al. A Myb enhancer-guided analysis of basophil and mast cell differentiation. *Nat Commun*. 2022;13(1). doi:10.1038/s41467-022-34906-1

226. Lilla JN, Chen CG, Mukai K, et al. Reduced mast cell and basophil numbers and function in Cpa3-Cre; Mcl-1 fl/fl mice. *Blood*. 2011;118(26). doi:10.1182/blood-2011-03-343962

227. Voehringer D, Shinkai K, Locksley RM. Type 2 immunity reflects orchestrated recruitment of cells committed to IL-4 production. *Immunity*. 2004;20(3). doi:10.1016/S1074-7613(04)00026-3

228. Dahlin JS, Hamey FK, Pijuan-Sala B, et al. A single-cell hematopoietic landscape resolves 8 lineage trajectories and defects in Kit mutant mice. *Blood*. 2018;131(21). doi:10.1182/blood-2017-12-821413

229. Drissen R, Buza-Vidas N, Woll P, et al. Distinct myeloid progenitor-differentiation pathways identified through single-cell RNA sequencing. *Nat Immunol*. 2016;17(6). doi:10.1038/ni.3412

230. Ziouzenkova O, Plutzky J. Retinoid metabolism and nuclear receptor responses: New insights into coordinated regulation of the PPAR-RXR complex. *FEBS Lett*. 2008;582(1). doi:10.1016/j.febslet.2007.11.081

231. Niederreither K, Subbarayan V, Dollé P, Chambon P. Embryonic retinoic acid synthesis is essential for early mouse post- implantation development. *Nat Genet*. 1999;21(4). doi:10.1038/7788

232. Zhang W, Tu G, Lv C, Long J, Cong L, Han Y. Matrix metalloproteinase-9 is up-regulated by CCL19/CCR7 interaction via PI3K/Akt pathway and is involved in CCL19-driven BMSCs migration. *Biochem Biophys Res Commun*. 2014;451(2). doi:10.1016/j.bbrc.2014.07.112

233. Schaniel C, Sirabella D, Qiu J, Niu X, Lemischka IR, Moore KA. Wnt-inhibitory factor 1 dysregulation of the bone marrow niche exhausts hematopoietic stem cells. *Blood*. 2011;118(9). doi:10.1182/blood-2010-09-305664

234. Stickens D, Behonick DJ, Ortega N, et al. Altered endochondral bone development in matrix metalloproteinase 13-deficient mice. *Development*. 2004;131(23). doi:10.1242/dev.01461

235. Jiang Y, Liu L, Deng YX, et al. MMP13 promotes the osteogenic potential of BMP9 by enhancing Wnt/β-catenin signaling via HIF-1α upregulation in mouse embryonic

fibroblasts. *International Journal of Biochemistry and Cell Biology*. 2023;164. doi:10.1016/j.biocel.2023.106476

236. Wang JS, Kamath T, Mazur CM, et al. Control of osteocyte dendrite formation by Sp7 and its target gene osteocrin. *Nat Commun*. 2021;12(1). doi:10.1038/s41467-021-26571-7

237. Liu F, Malaval L, Aubin JE. The mature osteoblast phenotype is characterized by extensive plasticity. *Exp Cell Res*. 1997;232(1). doi:10.1006/excr.1997.3501

238. Shi Z, Yang F, Du T, et al. Analysis of the CPZ/Wnt4 osteogenic pathway for high-bonding-strength composite-coated magnesium scaffolds through transcriptomics. *Mater Today Bio*. 2024;28. doi:10.1016/j.mtbio.2024.101234

239. Marom R, Song IW, Busse EC, et al. The IFITM5 mutation in osteogenesis imperfecta type V is associated with an ERK/SOX9-dependent osteoprogenitor differentiation defect. *Journal of Clinical Investigation*. 2024;134(15). doi:10.1172/JCI170369

240. Zhao W, Wiedemann P, Wölfel EM, et al. Decreased trabecular bone mass in Col22a1-deficient mice. *Cells*. 2021;10(11). doi:10.3390/cells10113020

241. O'Keefe RJ, Puzas JE, Loveys L, Hicks DG, Rosier RN. Analysis of type II and type X collagen synthesis in cultured growth plate chondrocytes by in situ hybridization: Rapid induction of type X collagen in culture. *Journal of Bone and Mineral Research*. 1994;9(11). doi:10.1002/jbmr.5650091107

242. Zaucke F, Dinser R, Maurer P, Paulsson M. Cartilage oligomeric matrix protein (COMP) and collagen IX are sensitive markers for the differentiation state of articular primary chondrocytes. *Biochemical Journal*. 2001;358(1). doi:10.1042/0264-6021:3580017

243. Tscheudschilsuren G, Bosserhoff AK, Schlegel J, et al. Regulation of mesenchymal stem cell and chondrocyte differentiation by MIA. *Exp Cell Res*. 2006;312(1). doi:10.1016/j.yexcr.2005.09.017

244. Wang W, Li F, Wang K, Cheng B, Guo X. PAPSS2 promotes alkaline phosphates activity and mineralization of osteoblastic MC3T3-E1 cells by crosstalk and smads signal pathways. *PLoS One*. 2012;7(8). doi:10.1371/journal.pone.0043475

245. Zhou X, von der Mark K, Henry S, Norton W, Adams H, de Crombrugghe B. Chondrocytes Transdifferentiate into Osteoblasts in Endochondral Bone during Development, Postnatal Growth and Fracture Healing in Mice. *PLoS Genet*. 2014;10(12). doi:10.1371/journal.pgen.1004820

246. Lo WC, Chiou JF, Gelovani JG, et al. Transplantation of embryonic fibroblasts treated with platelet-rich plasma induces osteogenesis in SAMP8 mice monitored by molecular imaging. *Journal of Nuclear Medicine*. 2009;50(5). doi:10.2967/jnumed.108.057372

247. Cayami FK, Claeys L, de Ruiter R, et al. Osteogenic transdifferentiation of primary human fibroblasts to osteoblast-like cells with human platelet lysate. *Sci Rep*. 2022;12(1). doi:10.1038/s41598-022-18512-1

248. Pihlström S, Määttä K, Öhman T, et al. A multi-omics study to characterize the transdifferentiation of human dermal fibroblasts to osteoblast-like cells. *Front Mol Biosci*. 2022;9. doi:10.3389/fmolb.2022.1032026

249. Bandyopadhyay S, Duffy M, Ahn KJ, et al. Mapping the Cellular Biogeography of Human Bone Marrow Niches Using Single-Cell Transcriptomics and Proteomic Imaging. *Blood*. 2023;142(Supplement 1). doi:10.1182/blood-2023-179280

250. Zhong L, Yao L, Tower RJ, et al. Single cell transcriptomics identifies a unique adipose lineage cell population that regulates bone marrow environment. *Elife*. 2020;9. doi:10.7554/eLife.54695

251. Zhang T, Li H, Sun S, et al. Microfibrillar-associated protein 5 suppresses adipogenesis by inhibiting essential coactivator of PPARγ. *Sci Rep*. 2023;13(1). doi:10.1038/s41598-023-32868-y

252. Higaki K, Aiba S, Shimoyama T, Omatsu Y, Nagasawa T. Universal fibroblasts across tissues can differentiate into niche cells for hematopoietic stem cells. *Cell Rep*. 2025;44(5). doi:10.1016/j.celrep.2025.115620

253. Jeon HJ, Park J, Shin JH, Chang MS. Insulin-like growth factor binding protein-6 released from human mesenchymal stem cells confers neuronal protection through IGF-1R-mediated signaling. *Int J Mol Med*. 2017;40(6). doi:10.3892/ijmm.2017.3173

254. Gabbitas B, Canalis E. Growth factor regulation of insulin-like growth factor binding protein- 6 expression in osteoblasts. *J Cell Biochem*. 1997;66(1). doi:10.1002/(SICI)1097-4644(19970701)66:1<77::AID-JCB9>3.0.CO;2-V

255. Futrega K, Robey PG, Klein TJ, Crawford RW, Doran MR. A single day of TGF-β1 exposure activates chondrogenic and hypertrophic differentiation pathways in bone marrow-derived stromal cells. *Commun Biol*. 2021;4(1). doi:10.1038/s42003-020-01520-0

256. Liang T, Li P, Liang A, et al. Identifying the key genes regulating mesenchymal stem cells chondrogenic differentiation: an in vitro study. *BMC Musculoskelet Disord*. 2022;23(1). doi:10.1186/s12891-022-05958-7

257. Méndez-Ferrer S, Michurina T V., Ferraro F, et al. Mesenchymal and haematopoietic stem cells form a unique bone marrow niche. *Nature*. 2010;466(7308). doi:10.1038/nature09262

258. Tormin A, Brune JC, Olsson E, et al. Characterization of bone marrow-derived mesenchymal stromal cells (MSC) based on gene expression profiling of functionally defined MSC subsets. *Cytotherapy*. 2009;11(2). doi:10.1080/14653240802716590

259. Li CS, Yang P, Ting K, et al. Fibromodulin reprogrammed cells: A novel cell source for bone regeneration. *Biomaterials*. 2016;83. doi:10.1016/j.biomaterials.2016.01.013

260. Kanazawa S, Okada H, Hojo H, et al. Mesenchymal stromal cells in the bone marrow niche consist of multi-populations with distinct transcriptional and epigenetic properties. *Sci Rep*. 2021;11(1). doi:10.1038/s41598-021-94186-5

261. Freeman BT, Jung JP, Ogle BM. Single-cell RNA-Seq of bone marrow-derived mesenchymal stem cells reveals unique profiles of lineage priming. *PLoS One*. 2015;10(9). doi:10.1371/journal.pone.0136199

262. Ying Z, Lyu L, Xu X, et al. Resident vascular Sca1+ progenitors differentiate into endothelial cells in vascular remodeling via miR-145-5p/ERG signaling pathway. *iScience*. 2024;27(6). doi:10.1016/j.isci.2024.110080

263. Copland I, Sharma K, Lejeune L, et al. CD34 expression on murine marrow-derived mesenchymal stromal cells: impact on neovascularization. *Exp Hematol*. 2008;36(1). doi:10.1016/j.exphem.2007.08.032

264. Schledzewski K, Géraud C, Arnold B, et al. Deficiency of liver sinusoidal scavenger receptors stabilin-1 and -2 in mice causes glomerulofibrotic nephropathy via impaired hepatic clearance of noxious blood factors. *Journal of Clinical Investigation*. 2011;121(2). doi:10.1172/JCI44740

265. Jardine L, Webb S, Goh I, et al. Blood and immune development in human fetal bone marrow and Down syndrome. *Nature*. 2021;598(7880). doi:10.1038/s41586-021-03929-x

266. Desterke C, Petit L, Sella N, et al. Inferring Gene Networks in Bone Marrow Hematopoietic Stem Cell-Supporting Stromal Niche Populations. *iScience*. 2020;23(6). doi:10.1016/j.isci.2020.101222

267. Sivaraj KK, Dharmalingam B, Mohanakrishnan V, et al. YAP1 and TAZ negatively control bone angiogenesis by limiting hypoxia-inducible factor signaling in endothelial cells. *Elife*. 2020;9. doi:10.7554/eLife.50770

268. Fu R, Lv WC, Xu Y, et al. Endothelial ZEB1 promotes angiogenesis-dependent bone formation and reverses osteoporosis. *Nat Commun*. 2020;11(1). doi:10.1038/s41467-019-14076-3

269. Gadomski S, Singh SK, Singh S, et al. Id1 and Id3 Maintain Steady-State Hematopoiesis by Promoting Sinusoidal Endothelial Cell Survival and Regeneration. *Cell Rep*. 2020;31(4). doi:10.1016/j.celrep.2020.107572

270. Hyung CS, Ji M, Gooya J, Lee M, Klarmann KD, Keller JR. Cell-nonautonomous function of Id1 in the hematopoietic progenitor cell niche. *Blood*. 2009;114(6). doi:10.1182/blood-2008-09-179788

271. Tanaka A, Itoh F, Nishiyama K, et al. Inhibition of endothelial cell activation by bHLH protein E2-2 and its impairment of angiogenesis. *Blood*. 2010;115(20). doi:10.1182/blood-2009-05-223057

272. Khurana S, Melacarne A, Yadak R, et al. SMAD signaling regulates CXCL12 expression in the bone marrow niche, affecting homing and mobilization of hematopoietic progenitors. *Stem Cells*. 2014;32(11). doi:10.1002/stem.1794

273. Lang A, Benn A, Wolter A, et al. Endothelial SMAD1/5 signaling couples angiogenesis to osteogenesis during long bone growth. *bioRxiv*. Published online 2023. doi:10.1101/2023.01.07.522994

274. Diamond MS, Staunton DE, De Fougerolles AR, et al. ICAM-1 (CD54): A counter-receptor for Mac-1 (CD11b/CD18). *Journal of Cell Biology*. 1990;111(6 PART 2). doi:10.1083/jcb.111.6.3129

275. Liu Y feng, Zhang S ying, Chen Y ying, et al. ICAM-1 Deficiency in the Bone Marrow Niche Impairs Quiescence and Repopulation of Hematopoietic Stem Cells. *Stem Cell Reports*. 2018;11(1). doi:10.1016/j.stemcr.2018.05.016

276. Picke AK, Campbell GM, Blüher M, et al. Thy-1 (CD90) promotes bone formation and protects against obesity. *Sci Transl Med*. 2018;10(453). doi:10.1126/scitranslmed.aao6806

277. Wang T, Tian L, Haino M, et al. Improved antibacterial host defense and altered peripheral granulocyte homeostasis in mice lacking the adhesion class G protein receptor CD97. *Infect Immun*. 2007;75(3). doi:10.1128/IAI.00869-06

278. Miedel EL, Brisson BK, Hamilton T, et al. Type III collagen modulates fracture callus bone formation and early remodeling. *Journal of Orthopaedic Research*. 2015;33(5). doi:10.1002/jor.22838

279. Ebrahimi Samani S, Kaartinen MT. Increased Osteoclastogenesis in Absence of TG2 Is Reversed by Transglutaminase Inhibition—Evidence for the Role for TG1 in Osteoclast Formation. *Cells*. 2023;12(17). doi:10.3390/cells12172139

280. King RG, Herrin BR, Justement LB. Trem-Like Transcript 2 Is Expressed on Cells of the Myeloid/Granuloid and B Lymphoid Lineage and Is Up-Regulated in Response to Inflammation. *The Journal of Immunology*. 2006;176(10). doi:10.4049/jimmunol.176.10.6012

281. Leitner J, Klauser C, Pickl WF, et al. B7-H3 is a potent inhibitor of human T-cell activation: No evidence for B7-H3 and TREML2 interaction. *Eur J Immunol*. 2009;39(7). doi:10.1002/eji.200839028

282. Barclay AN, Van Den Berg TK. The interaction between signal regulatory protein alpha (SIRPα) and CD47: Structure, function, and therapeutic target. *Annu Rev Immunol*. 2014;32. doi:10.1146/annurev-immunol-032713-120142

283. Holm CK, Engman S, Sulniute R, Matozaki T, Oldenborg PA, Lundberg P. Lack of SIRPα phosphorylation and concomitantly reduced SHP-2–PI3K–Akt2 signaling decrease osteoblast differentiation. *Biochem Biophys Res Commun*. 2016;478(1). doi:10.1016/j.bbrc.2016.07.048

284. Koskinen C, Persson E, Baldock P, et al. Lack of CD47 impairs bone cell differentiation and results in an osteopenic phenotype in vivo due to impaired signal regulatory protein α (SIRPα) signaling. *Journal of Biological Chemistry*. 2013;288(41):29333-29344. doi:10.1074/jbc.M113.494591

285. Broudy VC. Stem cell factor and hematopoiesis. *Blood*. 1997;90(4). doi:10.1182/blood.v90.4.1345

286. McCarthy KF, Ledney GD, Mitchell R. A DEFICIENCY OF HEMATOPOIETIC STEM CELLS IN STEEL MICE. *Cell Prolif*. 1977;10(2). doi:10.1111/j.1365-2184.1977.tb00137.x

287. Miyazawa K, Williams DA, Gotoh A, Nishimaki J, Broxmeyer HE, Toyama K. Membrane-bound steel factor induces more persistent tyrosine kinase activation and longer life span of c-kit gene-encoded protein than its soluble form. *Blood*. 1995;85(3). doi:10.1182/blood.v85.3.641.bloodjournal853641

288. Gouwy M, Struyf S, Catusse J, Proost P, Van Damme J. Synergy between proinflammatory ligands of G protein-coupled receptors in neutrophil activation and migration. *J Leukoc Biol*. 2004;76(1). doi:10.1189/jlb.1003479

289. Kunz L, Schroeder T. A 3D Tissue-wide Digital Imaging Pipeline for Quantitation of Secreted Molecules Shows Absence of CXCL12 Gradients in Bone Marrow. *Cell Stem Cell*. 2019;25(6). doi:10.1016/j.stem.2019.10.003

290. Yen YC, Schafer CT, Gustavsson M, et al. Structures of atypical chemokine receptor 3 reveal the basis for its promiscuity and signaling bias. *Sci Adv*. 2022;8(28). doi:10.1126/sciadv.abn8063

291. Balabanian K, Lagane B, Infantino S, et al. The chemokine SDF-1/CXCL12 binds to and signals through the orphan receptor RDC1 in T lymphocytes. *Journal of Biological Chemistry*. 2005;280(42). doi:10.1074/jbc.M508234200

292. Naumann U, Cameroni E, Pruenster M, et al. CXCR7 functions as a scavenger for CXCL12 and CXCL11. *PLoS One*. 2010;5(2). doi:10.1371/journal.pone.0009175

293. Crawford LJA, Peake R, Price S, Morris TCM, Irvine AE. Adiponectin is produced by lymphocytes and is a negative regulator of granulopoiesis. *J Leukoc Biol*. 2010;88(4). doi:10.1189/jlb.1109723

294. Masamoto Y, Arai S, Sato T, et al. Adiponectin Enhances Antibacterial Activity of Hematopoietic Cells by Suppressing Bone Marrow Inflammation. *Immunity*. 2016;44(6). doi:10.1016/j.immuni.2016.05.010

295. Naveiras O, Nardi V, Wenzel PL, Hauschka P V., Fahey F, Daley GQ. Bone-marrow adipocytes as negative regulators of the haematopoietic microenvironment. *Nature*. 2009;460(7252). doi:10.1038/nature08099

296. Wei Q, Nakahara F, Asada N, et al. Snai2 Maintains Bone Marrow Niche Cells by Repressing Osteopontin Expression. *Dev Cell*. 2020;53(5). doi:10.1016/j.devcel.2020.04.012

297. Stier S, Ko Y, Forkert R, et al. Osteopontin is a hematopoietic stem cell niche component that negatively regulates stem cell pool size. *Journal of Experimental Medicine*. 2005;201(11). doi:10.1084/jem.20041992

298. Kfoury YS, Ji F, Jain E, et al. The bone marrow stroma in human myelodysplastic syndrome reveals alterations that regulate disease progression. *Blood Adv*. 2023;7(21). doi:10.1182/bloodadvances.2022008268

299. Sharma Y, Flurkey K, Astle CM, Harrison DE. Mice severely deficient in growth hormone have normal hematopoiesis. *Exp Hematol*. 2005;33(7). doi:10.1016/j.exphem.2005.04.003

300. Young K, Borikar S, Bell R, Kuffler L, Philip V, Trowbridge JJ. Progressive alterations in multipotent hematopoietic progenitors underlie lymphoid cell loss in aging. *Journal of Experimental Medicine*. 2016;213(11). doi:10.1084/jem.20160168

301. Gekas C, Graf T. CD41 expression marks myeloid-biased adult hematopoietic stem cells and increases with age. *Blood*. 2013;121(22). doi:10.1182/blood-2012-09-457929

302. Liedert A, Mattausch L, Röntgen V, et al. Midkine-deficiency increases the anabolic response of cortical bone to mechanical loading. *Bone*. 2011;48(4). doi:10.1016/j.bone.2010.12.019

303. Neunaber C, Catala-Lehnen P, Beil FT, et al. Increased trabecular bone formation in mice lacking the growth factor midkine. *Journal of Bone and Mineral Research*. 2010;25(8). doi:10.1002/jbmr.75

304. Haffner-Luntzer M, Heilmann A, Rapp AE, et al. Antagonizing midkine accelerates fracture healing in mice by enhanced bone formation in the fracture callus. *Br J Pharmacol*. Published online 2016. doi:10.1111/bph.13503

305. Himburg HA, Muramoto GG, Daher P, et al. Pleiotrophin regulates the expansion and regeneration of hematopoietic stem cells. *Nat Med*. 2010;16(4). doi:10.1038/nm.2119

306. Himburg HA, Harris JR, Ito T, et al. Pleiotrophin Regulates the Retention and Self-Renewal of Hematopoietic Stem Cells in the Bone Marrow Vascular Niche. *Cell Rep*. 2012;2(4). doi:10.1016/j.celrep.2012.09.002

307. Guo P, Zhou Y, Jin Z, Zhou Y, Tan W song. Fluid shear stress promotes osteogenesis of bone mesenchymal stem cells at early matrix maturity phase through Lamin A/ METTL3 signal axis. *Biochem Eng J*. 2022;188. doi:10.1016/j.bej.2022.108685

308. Susek KH, Korpos E, Huppert J, et al. Bone marrow laminins influence hematopoietic stem and progenitor cell cycling and homing to the bone marrow. *Matrix Biology*. 2018;67. doi:10.1016/j.matbio.2018.01.007

309. Thyboll J, Kortesmaa J, Cao R, et al. Deletion of the Laminin α4 Chain Leads to Impaired Microvessel Maturation. *Mol Cell Biol*. 2002;22(4). doi:10.1128/mcb.22.4.1194-1202.2002

310. Chen C, Huang X, Atakilit A, Zhu QS, Corey SJ, Sheppard D. The Integrin α9β1 Contributes to Granulopoiesis by Enhancing Granulocyte Colony-Stimulating Factor Receptor Signaling. *Immunity*. 2006;25(6). doi:10.1016/j.immuni.2006.10.013

311. Agah A, Kyriakides TR, Lawler J, Bornstein P. The lack of thrombospondin-1 (TSP1) dictates the course of wound healing in double-TSP1/TSP2-null mice. *American Journal of Pathology*. 2002;161(3). doi:10.1016/S0002-9440(10)64243-5

312. Shingu T, Bornstein P. Overlapping Egr-1 and Sp1 sites function in the regulation of transcription of the mouse thrombospondin 1 gene. *Journal of Biological Chemistry*. 1994;269(51). doi:10.1016/s0021-9258(18)31669-7

313. Bergström SE, Uzunel M, Talme T, Bergdahl E, Sundqvist KG. Antigen-induced regulation of T-cell motility, interaction with antigen-presenting cells and activation through endogenous thrombospondin-1 and its receptors. *Immunology*. 2015;144(4). doi:10.1111/imm.12424

314. Kirsch T, Woywodt A, Klose J, et al. Endothelial-derived thrombospondin-1 promotes macrophage recruitment and apoptotic cell clearance. *J Cell Mol Med*. 2010;14(7). doi:10.1111/j.1582-4934.2009.00799.x

315. Ramalingam P, Gutkin MC, Poulos MG, et al. Suppression of thrombospondin-1–mediated inflammaging prolongs hematopoietic health span. *Sci Immunol*. 2025;10(103). doi:10.1126/sciimmunol.ads1556

316. Manna PP, Frazier WA. The Mechanism of CD47-Dependent Killing of T Cells: Heterotrimeric Gi-Dependent Inhibition of Protein Kinase A. *The Journal of Immunology*. 2003;170(7). doi:10.4049/jimmunol.170.7.3544

317. Hankenson KD, Hormuzdi SG, Meganck JA, Bornstein P. Mice with a Disruption of the Thrombospondin 3 Gene Differ in Geometric and Biomechanical Properties of Bone and Have Accelerated Development of the Femoral Head. *Mol Cell Biol*. 2005;25(13). doi:10.1128/mcb.25.13.5599-5606.2005

318. Posey KL, Hankenson K, Veerisetty AC, Bornstein P, Lawler J, Hecht JT. Skeletal abnormalities in mice lacking extracellular matrix proteins, thrombospondin-1,

thrombospondin-3, thrombospondin-5, and type IX collagen. *American Journal of Pathology*. 2008;172(6). doi:10.2353/ajpath.2008.071094

319. Halai K, Whiteford J, Ma B, Nourshargh S, Woodfin A. ICAM-2 facilitates luminal interactions between neutrophils and endothelial cells in vivo. *J Cell Sci*. 2014;127(3). doi:10.1242/jcs.137463

320. Upadhaya S, Krichevsky O, Akhmetzyanova I, Sawai CM, Fooksman DR, Reizis B. Intravital Imaging Reveals Motility of Adult Hematopoietic Stem Cells in the Bone Marrow Niche. *Cell Stem Cell*. 2020;27(2). doi:10.1016/j.stem.2020.06.003

321. Silva WN, Costa AC, Picoli CC, et al. Hematopoietic stem cell stretches and moves in its bone marrow niche. *Crit Rev Oncol Hematol*. 2021;163. doi:10.1016/j.critrevonc.2021.103368

322. Winkler IG, Barbier V, Nowlan B, et al. Vascular niche E-selectin regulates hematopoietic stem cell dormancy, self renewal and chemoresistance. *Nat Med*. 2012;18(11). doi:10.1038/nm.2969

323. Sreeramkumar V, Leiva M, Stadtmann A, et al. Coordinated and unique functions of the E-selectin ligand ESL-1 during inflammatory and hematopoietic recruitment in mice. *Blood*. 2013;122(24). doi:10.1182/blood-2013-07-514497

324. Leiva M, Quintana JA, Ligos JM, Hidalgo A. Haematopoietic ESL-1 enables stem cell proliferation in the bone marrow by limiting TGFβ availability. *Nat Commun*. 2016;7. doi:10.1038/ncomms10222

325. Javier J, Hinge A, Bartram J, Xu J, Filippi MD. Transforming growth factor-β signaling modifies the hematopoietic acute inflammatory response to drive bone marrow failure. *Haematologica*. 2021;107(6):1323-1334. doi:10.3324/haematol.2020.273292

326. Hao J, Zhou H, Nemes K, et al. Membrane-bound SCF and VCAM-1 synergistically regulate the morphology of hematopoietic stem cells. *Journal of Cell Biology*. 2021;220(10). doi:10.1083/jcb.202010118

327. Eash KJ, Greenbaum AM, Gopalan PK, Link DC. CXCR2 and CXCR4 antagonistically regulate neutrophil trafficking from murine bone marrow. *Journal of Clinical Investigation*. 2010;120(7). doi:10.1172/JCI41649

328. Jinquan T, Quan S, Jacobi HH, et al. CXC chemokine receptor 3 expression on CD34+ hematopoietic progenitors from human cord blood induced by granulocyte-macrophage colony-stimulating factor: Chemotaxis and adhesion induced by its ligands, interferon γ-inducible protein 10 and monokine induced by interferon γ. *Blood*. 2000;96(4). doi:10.1182/blood.v96.4.1230

329. Sun B, Xun Z, Zhou Z, et al. Single-cell transcriptomic analysis deciphers the inflammatory microenvironment characterized by CXCL9+ fibroblasts and ACKR1+ endothelial cells in immune-related myocarditis. *J Transl Med*. 2025;23(1). doi:10.1186/s12967-025-06551-x

330. Liu F, Sun X, Deng S, et al. Cxcl10 and Cxcr3 regulate self-renewal and differentiation of hematopoietic stem cells. *Stem Cell Res Ther*. 2024;15(1). doi:10.1186/s13287-024-03861-7

331. Cao H, Heazlewood SY, Williams B, et al. The role of CD44 in fetal and adult hematopoietic stem cell regulation. *Haematologica*. 2016;101(1). doi:10.3324/haematol.2015.135921

332. Lesley J, English NM, Gál I, Mikecz K, Day AJ, Hyman R. Hyaluronan binding properties of a CD44 chimera containing the link module of TSG-6. *Journal of Biological Chemistry*. 2002;277(29). doi:10.1074/jbc.M201068200

333. Scott LM, Priestley G V., Papayannopoulou T. Deletion of α4 Integrins from Adult Hematopoietic Cells Reveals Roles in Homeostasis, Regeneration, and Homing. *Mol Cell Biol*. 2003;23(24). doi:10.1128/mcb.23.24.9349-9360.2003

334. Collen D. Ham-Wasserman lecture: role of the plasminogen system in fibrin-homeostasis and tissue remodeling. *Hematology / the Education Program of the American Society of Hematology American Society of Hematology Education Program*. Preprint posted online 2001. doi:10.1182/asheducation-2001.1.1

335. Tjwa M, Sidenius N, Moura R, et al. Membrane-anchored uPAR regulates the proliferation, marrow pool size, engraftment, and mobilization of mouse hematopoietic stem/progenitor cells. *Journal of Clinical Investigation*. 2009;119(4). doi:10.1172/JCI36010

336. Tjwa M, Moura R, Moons L, et al. Fibrinolysis-independent role of plasmin and its activators in the haematopoietic recovery after myeloablation. *J Cell Mol Med*. 2009;13(11-12). doi:10.1111/j.1582-4934.2008.00521.x

337. Pepper MS. Role of the matrix metalloproteinase and plasminogen activator-plasmin systems in angiogenesis. *Arterioscler Thromb Vasc Biol*. 2001;21(7). doi:10.1161/hq0701.093685

338. Bungartz G, Stiller S, Bauer M, et al. Adult murine hematopoiesis can proceed without β1 and β7 integrins. *Blood*. 2006;108(6). doi:10.1182/blood-2005-10-007658

339. Arroyo AG, Yang JT, Rayburn H, Hynes RO. α4 integrins regulate the proliferation/differentiation balance of multilineage hematopoietic progenitors in vivo. *Immunity*. 1999;11(5). doi:10.1016/S1074-7613(00)80131-4

340. Waltz DA, Chapman HA. Reversible cellular adhesion to vitronectin linked to urokinase receptor occupancy. *Journal of Biological Chemistry*. 1994;269(20). doi:10.1016/s0021-9258(17)36688-7

341. Wei Y, Lukashev M, Simon DI, et al. Regulation of integrin function by the urokinase receptor. *Science (1979)*. 1996;273(5281). doi:10.1126/science.273.5281.1551

342. Nusrat AR, Chapman HA. An autocrine role for urokinase in phorbol ester-mediated differentiation of myeloid cell lines. *Journal of Clinical Investigation*. 1991;87(3). doi:10.1172/jci115070